Data-Driven Control of Refrigeration System

Vinther, Kasper

Publication date:
2014

Document Version
Peer reviewed version

Kasper Vinther

Data-Driven Control of Refrigeration Systems

AALBORG UNIVERSITY
DENMARK

Ph.D. thesis:
Data-Driven Control of Refrigeration Systems

Ph.D. student:
Kasper Vinther

Supervisors:
Professor Jakob Stoustrup
External Lecturer Henrik Rasmussen
External Lecturer Roozbeh Izadi-Zamanabadi

ISBN: 978-87-7152-032-3
March 2014

List of publications:

- K. Vinther, C. H. Lyhne, E. B. Sørensen, and H. Rasmussen. Evaporator Superheat Control with One Temperature Sensor using Qualitative System Knowledge. American Control Conference, Montreal, Canada, pp. 374–379, June 2012.
- K. Vinther, H. Rasmussen, R. Izadi-Zamanabadi, and J. Stoustrup. Utilization of Excitation Signal Harmonics for Control of Nonlinear Systems. IEEE Multiconference on Systems and Control, Dubrovnik, Croatia, pp. 1627–1632, October 2012.
- K. Vinther, H. Rasmussen, R. Izadi-Zamanabadi, and J. Stoustrup. Single Temperature Sensor Based Evaporator Filling Control Using Excitation Signal Harmonics. IEEE Multi-conference on Systems and Control, Dubrovnik, Croatia, pp. 757–763, October 2012.
- K. Vinther, H. Rasmussen, R. Izadi-Zamanabadi, and J. Stoustrup. Single temperature sensor superheat control using a novel maximum slope-seeking method. International Journal of Refrigeration, vol. 36, issue 3, pp. 1118–1129, May 2013.
- K. Vinther, R. Izadi-Zamanabadi, H. Rasmussen, and J. Stoustrup. A Fault Tolerant Superheat Control Strategy for Supermarket Refrigeration Systems. International Conference on Control and Fault-Tolerant Systems, Nice, France, pp. 426–431, October 2013.
- K. Vinther, H. Rasmussen, R. Izadi-Zamanabadi, and J. Stoustrup. Control of a Class of Nonlinear Systems using a Maximum Slope-seeking Method. Submitted for publication, 2013.
- K. Vinther, V. Chandan, and A. G. Alleyne. Learning/Repetitive Control for Building Systems with Nearly Periodic Disturbances. European Control Conference, Zürich, Switzerland, pp. 1198–1203, July 2013.
- K. Vinther, H. Rasmussen, R. Izadi-Zamanabadi, J. Stoustrup, and A. G. Alleyne. A Learning Based Precool Algorithm for Utilization of Foodstuff as Thermal Energy Storage. IEEE Multi-conference on Systems and Control, Hyderabad, India, pp. 314–321, August 2013.
- K. Vinther, H. Rasmussen, R. Izadi-Zamanabadi, J. Stoustrup, and A. G. Alleyne. Learning-Based Precool Algorithms for Exploiting Foodstuff as Thermal Energy Reserve on Hot Days. Submitted for publication, 2013.

This thesis has been submitted for assessment in partial fulfillment of the PhD degree. The thesis is based on the submitted or published scientific papers which are listed above. Parts of the papers are used directly or indirectly in the extended summary of the thesis. As part of the assessment, co-author statements have been made available to the assessment committee and are also available at the Faculty. The thesis is not in its present form acceptable for open publication but only in limited and closed circulation as copyright may not be ensured.

Contents

Preface and Acknowledgements

This thesis is submitted as a collection of papers in partial fulfillment of the requirements for the degree of Doctor of Philosophy at the Section of Automation and Control, Department of Electronic Systems, Aalborg University, Denmark. The work has been carried out in the period from November 2010 to November 2013 under the supervision of Professor Jakob Stoustrup and Associate Professor Henrik Rasmussen.

The work was financially supported by the Faculty of Engineering and Science at Aalborg University, the Danish Council for Independent Research - Technology and Production Sciences, and Danfoss A/S.

I would like to thank my colleagues at the Section of Automation and Control for an inspiring and joyful working environment and especially my supervisors Jakob Stoustrup and Henrik Rasmussen for sharing their profound knowledge within control theory, their insight in application of such, and thoughtful criticism, which have significantly improved the quality of my research. Thanks also goes to Seyed Ehsan Shafiei for constructive discussions on modeling and control of supermarket refrigeration systems and to Rasmus Pedersen for sharing supermarket refrigeration system test facility data.

My deepest thanks also goes to industrial co-supervisor Roozbeh Izadi-Zamanabadi for his feedback, support, countless ideas, and help with maturing of the control solutions towards industrial use. I would also like to thank Honglian Deng, Torben Green, and Tommy Friis Jensen for their technical support during my stays at Danfoss A/S in Nordborg. Furthermore, I would like to thank participants in the ESO2 project for sharing data from a Danish supermarket.

During the course of the project I have had the opportunity to visit the Department of Mechanical Science and Engineering at the University of Illinois, Urbana, USA. I would like to thank professor Andrew Alleyne for welcoming me and for invaluable feedback. I was amazed by the high scientific level there. I would also like to extend my thanks to the inspiring and helpful people in the Alleyne Research Group with a special thank to Vikas Chandan and Justin Koeln for our fruitful collaboration.

Last but not least, I would like to express my gratitude to my family for encouragement and my wife Anne Sofie for her patience, loving support, our countless hours of insightful discussions, and help with LaTeX.

Abstract

Refrigeration is used in a wide range of applications, e.g., for storage of food at low temperatures to prolong shelf life and in air conditioning for occupancy comfort. The main focus of this thesis is control of supermarket refrigeration systems. This market is very competitive and it is important to keep the variable costs at a minimum and, if possible, offer products which have higher robustness, performance, and functionality than similar products from competitors. However, the multitude of different system configurations, system complexity, component wear, and changing operating conditions make optimal tuning of controllers a difficult and time consuming task. These are also some of the challenges which make advanced model-based control difficult, and a model-based controller will often be tailored to a specific system. The focus in this thesis is therefore instead on development of data-driven control strategies with a higher plug and play potential.

One of the main control challenges in refrigeration systems is proper control of superheat for efficient and safe operation of the system. This task can be performed by an electronic expansion valve and requires two sensors, which traditionally are a pressure and a temperature sensor. In this thesis, a novel maximum slope-seeking (MSS) control method is developed. This has resulted in a control implementation, which successfully has been able to control the evaporator superheat in four widely different refrigeration system test facilities without using a pressure sensor. A single-sensor solution is thus provided, which either reduces the variable costs or increases the robustness of the system by not relying on pressure measurements. MSS is an example of data-driven control and can be applied to a broad class of nonlinear control problems. The method utilizes the qualitative nonlinearity in the system and harmonic analysis of a perturbation signal to reach an unknown, but suitable, operating point.

Another important control task in refrigeration systems is to maintain the temperature of the refrigerated space or foodstuff within the desired/legislative requirement, e.g., to prevent possible deterioration of the foodstuff. Refrigeration systems are often dimensioned to be able to cope with the highest possible loads and the hottest temperatures during the year, while also taking into account extreme weather conditions. Overdimensioning is expensive, both in terms of the variable cost, but also due to possibly higher peak energy consumption costs. Further, load patterns could have some degree of repeatability on a daily basis, and the possible use of repetitive control and iterative learning control are therefore investigated in this thesis. As a result, learning-based precool strategies are proposed, which utilize the thermal storage capability in foodstuff to shift some of the peak load to less loaded hours. The precool time and period can continuously be updated based on data from previous days and the data-driven solutions are not based on models of the system, prior knowledge of load patterns, or weather forecasts and can therefore easily be added to existing systems.

Synopsis

Køling bruges i en lang række applikationer eksempelvis til opbevaring af fødevarer ved lave temperaturer for at forlænge holdbarheden og i klimaanlæg til forbedring af indeklima. Denne afhandling fokuserer hovedsageligt på regulering af køleanlæg i supermarkeder. Dette er et meget konkurrencepræget marked og det er derfor vigtigt at holde de variable omkostninger på et minimum og hvis det er muligt tilbyde produkter, som har højere robusthed, ydeevne og funktionalitet sammenlignet med konkurrenternes produkter. Men de mange forskellige systemkonfigurationer, kompleksiteten af systemerne, komponentslid, og skiftende driftsbetingelser gør optimal tuning af regulatorer en vanskelig og tidskrævende opgave. Dette er også nogle af de udfordringer, der gør avanceret modelbaseret regulering vanskelig og en modelbaseret regulator vil ofte være skræddersyet til et specifikt system. Fokus i denne afhandling er derfor i stedet på at udvikle datadrevne reguleringsstrategier med et større plug and play potentiale.

En af hovedudfordringerne ifm. regulering af kølesystemer er passende styring af overhedning for effektiv og sikker drift. Dette kan gøres med en elektronisk ekspansionsventil og kræver to følere, der traditionelt er en tryk- og en temperaturføler. I denne afhandling er en ny "maximum slope-seeking"(MSS) reguleringsmetode udviklet. Det har udmyntet sig i en reguleringsimplementation, som med succes har været i stand til at styre fordamperoverhedningen i fire vidt forskellige kølesystemstestanlæg uden brug af tryksensor. En én-sensor løsning er derved fundet, som enten kan reducere de variable omkostninger eller øge robustheden ved ikke at være afhængig af trykmålinger. MSS er et eksempel på datadreven regulering og kan anvendes i en bred klasse af ulineære reguleringsproblemer. Metoden udnytter den kvalitative ulinearitet i systemet og harmonisk analyse af et perturbationssignal til at nå et ukendt men passende driftspunkt.

En anden vigtig reguleringsopgave i kølesystemer er at holde temperaturen af det afkølede rum eller fødevarerne inden for det ønskede/lovmæssige krav, fx for at forhindre eventuel forringelse af fødevarerne. Køleanlæg er ofte dimensionerede til at kunne klare de størst tænkelige belastninger og de varmeste temperaturer i løbet af året, mens der også tages hensyn til ekstreme vejrforhold. Overdimensioning er dyrt, både hvad angår de variable omkostninger, men også på grund af eventuelt højere omkostsninger ifm. spidsbelastninger. Endvidere kan belastningsmønstre have en vis grad af repeterbarhed på daglig basis og mulig brug af "repetetive control"og "iterative learning control"er derfor blevet undersøgt. På baggrund heraf foreslås i denne afhandling læringsbaserede forkølingsstrategier, som kan udnytte den termiske lagerkapacitet, der er i fødevarer, til at flytte noget af spidsbelastningen til mindre belastede timer. Den anvendte forkølingstid og periode kan opdateres løbende baseret på data fra foregående dage og de datadrevne løsninger er ikke baserede på modeller af systemet, forudgående kendskab til belastningsmønstre, eller vejrudsigter og kan derfor nemt tilføjes til eksisterende systemer.

1 | Introduction

This chapter first provides the project background and a description of a typical refrigeration system based on the most common vapor compression cycle (VCC) principle, which is the type of refrigeration considered in this thesis. Then, the motivation and objectives for this research is given, which is followed by a review of the state-of-the-art within these objectives and an outline of the research challenges. Finally, an outline of the remainder of the thesis is given.

1.1 Background and Motivation

This project was proposed in collaboration with Danfoss A/S and their Automatic Control department, which is now a part of the Electronic Control & Services department under the Refrigeration & Air Conditioning Controls division. Danfoss is a leading company within refrigeration and their range of services and products include areas such as refrigeration of food, air conditioning, building heating, district heating, solar inverters, and electrical motor control. This thesis is mainly focused on supermarket refrigeration systems control, which is one of the major markets for Danfoss. A general description of a supermarket refrigeration system is given in the following subsection before going into detail in the typical control challenges and the research objectives. Extension of the developed concepts to areas such as air conditioning and water chillers have also been made in this project as the basic refrigeration system behind is very similar.

1.1.1 Description of a Typical Supermarket Refrigeration System

Refrigeration systems are required in order to maintain a high quality and shelf life of foodstuff, which is achieved by keeping the food at low temperatures. Supermarket refrigeration systems have multiple fridge and freezer display cases each equipped with local control of the air temperature inside the display case. Fig. 1.1 shows typical display cases in a Danish Supermarket.

A refrigerant is circulated to ensure transport of heat from one medium to another. This heat transfer is achieved by proper control of pressures and mass flows inside the refrigeration system using compressors, valves, and fans. A simplified schematic of a typical supermarket refrigeration system is shown in Fig. 1.2 and the state of the refrigerant in the vapor compression type refrigeration cycle is illustrated using a pressure-enthalpy diagram in Fig. 1.3. The states are marked with light blue numbers in the figures and there

Figure 1.1: Supermarket display cases. Freezer gondolas are located in the front and open shelf type fridges are located in the back.

are in general four processes in the vapor compression refrigeration cycle; compression, condensation, expansion, and evaporation.

Compression (State 1-2): If we start at State 1, then a gaseous refrigerant is compressed by the compressor rack consisting of multiple compressors in parallel depending on the capacity needs of the system. The compression results in an increase in pressure from $P_{cp,mt}$ to P_c at State 2 and a corresponding temperature increase of the refrigerant (isobaric condensation process assumed). Two compression stages, with two separate compressor racks, are used when the refrigeration system both services freezers at a low temperature (LT) and fridges at a medium temperature (MT). The LT compressor rack takes the refrigerant at State 1' with pressure $P_{cp,lt}$ to State 2' with pressure $P_{cp,mt}$. The work performed on the refrigerant by the compressors can be computed as

$$\dot{W}_{cp,mt} = \dot{m}_{rcp,mt} \left(h_{cp,o,mt} - h_{cp,i,mt} \right), \tag{1.1}$$

$$\dot{W}_{cp,lt} = \dot{m}_{rcp,lt} \left(h_{cp,o,lt} - h_{cp,i,lt} \right), \tag{1.2}$$

where $\dot{W}_{cp,mt}$ and $\dot{W}_{cp,lt}$ are the work performed by the MT and LT compressor racks, $\dot{m}_{rcp}$ is refrigerant mass flow through the compressor rack, and $h_{cp,o}$ and $h_{cp,i}$ are the specific enthalpy out of and into the compressor rack. Equation (1.1) and (1.2) assume a steady state process with a steady flow and are derived based on the first law of thermodynamics. The specific enthalpy cannot be measured, but can be calculated based on pressure and temperature measurements and refrigerant property tables included in software packages such as RefEqns [Skovrup, 2000].

Condensation (State 2-3): The refrigerant is then directed to a condenser unit located outside, which circulates colder air across the refrigerant piping to transfer heat to the surroundings. This lowers the temperature of the refrigerant, which starts to condensate. The temperature of the refrigerant is constant during condensation (liquid/gas mixture) and a requirement for proper heat transfer is that the outside air temperature $T_{air,o}$ is lower than the saturation temperature T_c of the refrigerant, which is determined by the

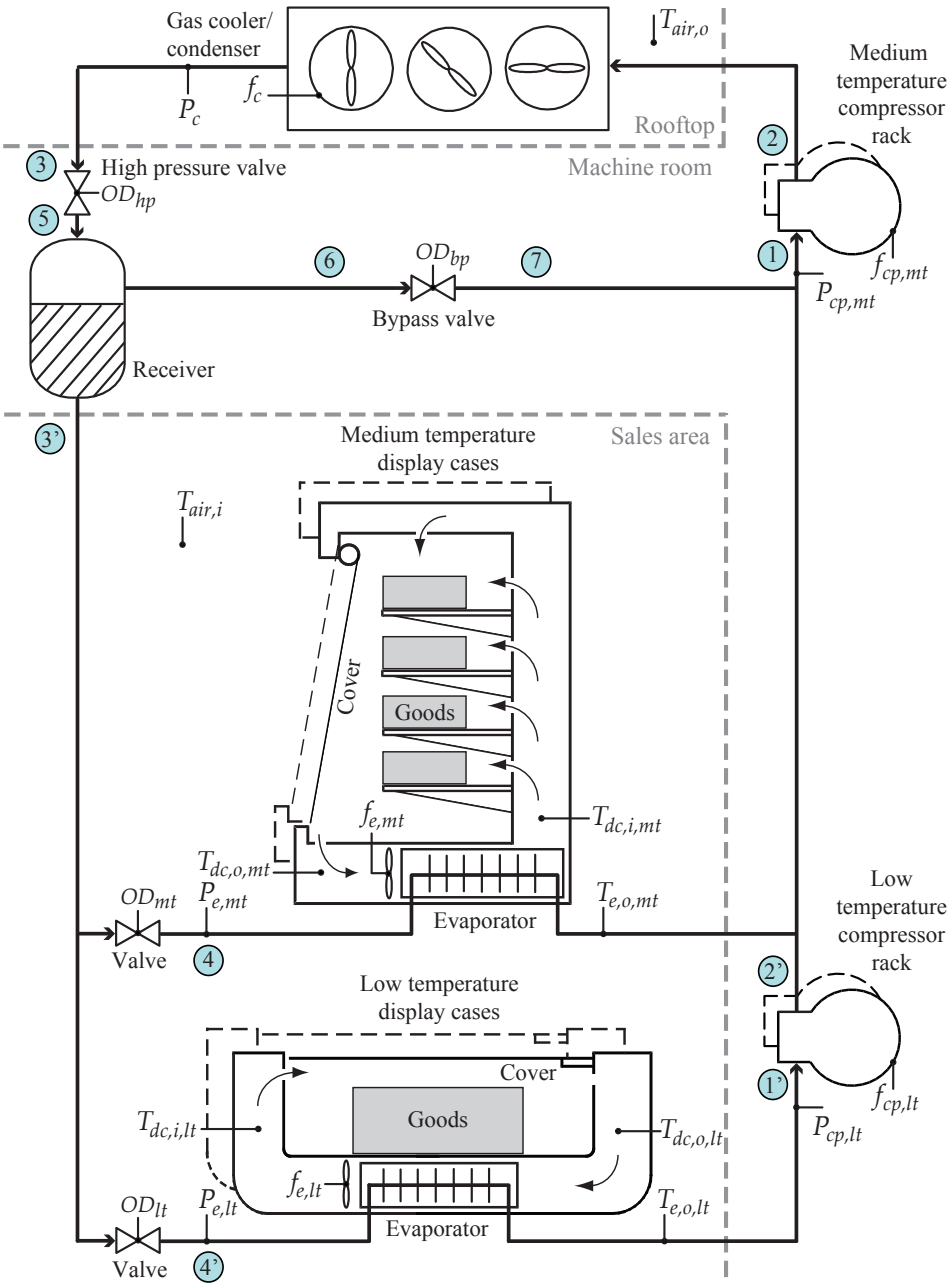

Figure 1.2: Simplified schematic of a supermarket refrigeration system with multiple medium and low temperature type of display cases (the cross-sectional area of only one of each display case is shown). Numbers marked with light blue are references to the corresponding state in the pressure-enthalpy diagram shown in Fig. 1.3.

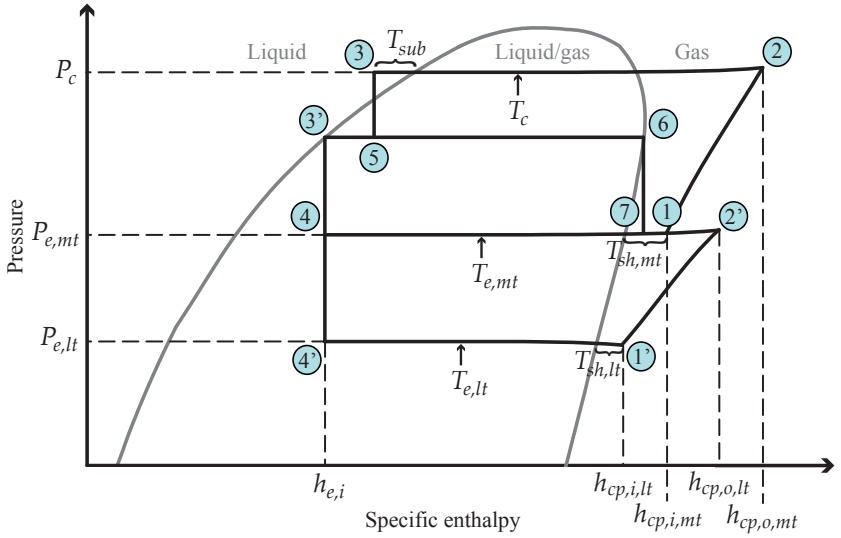

Figure 1.3: Pressure-enthalpy diagram showing the state of the refrigerant in the vapor compression type refrigeration cycle.

refrigerant type and the pressure P_c. At State 3 the refrigerant is slightly subcooled and liquefied. The condenser unit is called a gas cooler if the high pressure side of the vapor compression cycle is operated in the supercritical region.

Expansion (State 3-4): Some refrigeration systems have a high pressure and a bypass expansion valve in connection with a receiver. The high pressure valve lowers the pressure by expanding the refrigerant to State 5, which ensures a smaller pressure difference across each valve in the system. The bypass valve takes gas from the receiver at State 6 and bypasses it to the suction line before the compressor at State 7. This can be used to create an artificial load on the system and can reduce the number of compressor on/off switches especially at low load conditions. The bypassed gaseous refrigerant will also increase the suction pressure and temperature and can help prevent frosting. Liquid refrigerant is then directed from the receiver at State 3' to the individual display cases and cold storage rooms, each installed with an evaporator and an expansion valve. The valve maintains a pressure difference and the opening degree OD of the valve determines the refrigerant flow individually depending on the required cooling capacity of each evaporator. All refrigerant expansion processes can be assumed to be isenthalpic with no heat transfer to or from the surroundings and thus having equal enthalpy.

Evaporation (State 4-1): The refrigerant then evaporates in the evaporators due to circulation of hotter air across the evaporator fins. This gives a heat transfer from the air in the cold storage to the refrigerant. A requirement for proper heat transfer is that the evaporation temperature $T_{e,mt}$ or $T_{e,lt}$ is below the desired temperature in the cold storage. Again, by using the first law of thermodynamics, the steady state heat transfer rate out of the cold storages can be computed as

$$\dot{Q}_{e,mt} = \dot{m}_{re,mt} \left(h_{e,o,mt} - h_{e,i,mt} \right), \tag{1.3}$$

$$\dot{Q}_{e,lt} = \dot{m}_{re,lt} \left(h_{e,o,lt} - h_{e,i,lt} \right), \tag{1.4}$$

where $\dot{Q}_{e,mt}$ and $\dot{Q}_{e,lt}$ are the total heat transfer rates out of the MT and LT sections of evaporators, $\dot{m}_{re}$ is the total refrigerant mass flow through the section, and $h_{e,o}$ and $h_{e,i}$ are the specific enthalpy out of and into the section. The refrigerant mass flow through the LT evaporators $\dot{m}_{re,lt}$ is equal to $\dot{m}_{rcp,lt}$ in steady state, and $h_{e,o}$ and $h_{cp,i}$ are almost equivalent if the pipes between the evaporator and compressor rack are well insulated. The evaporation process can also be assumed isobaric, since the pressure drop in most cases is negligible. When all the refrigerant is evaporated into gas form it starts to superheat. The difference in temperature between evaporation temperature T_e and the temperature at the inlet of the compressor at State 1 or 1' is called superheat T_{sh}.

For further details on supermarket refrigeration systems see, for example, [Larsen, 2005, Petersen et al., 2012, Shafiei et al., 2013b]. Additionally, note that water chillers and air conditioning systems are very similar in construction using the same basic vapor compression cycle to either cool air or water depending on the configuration.

1.1.2 Supermarket Refrigeration System Control

The most important task of the refrigeration system is to ensure that the temperature of the foodstuff is maintained at the right temperature in each of the cold storages, e.g., display cases, to maintain high food quality and shelf life. The heat transfer rate out of the individual cold storages (cooling) should therefore in average match the heat transfer rate into the cold storage (load). It is not possible to measure the heat transfer rates directly and not practical to measure the foodstuff temperature, since this means that the shop owner would need to place thermocouples on the foodstuff. The display case air temperature coming out of the display case into the evaporator $T_{dc,o}$ and/or the air coming back to the display case $T_{dc,i}$ is instead measured and typically controlled with an on/off hysteretic feedback loop. This controller switches the valve on when the temperature is above an upper limit, which generates a refrigerant flow and thus cooling, and off again when it is below a lower limit. The evaporator fan speed f_e could also be varied according to the required cooling demand. However, this fan is mostly operated at constant speed in supermarket refrigeration systems.

There exist legislative temperature thresholds for different types of refrigerated foodstuff and the supermarket refrigeration system should maintain the temperature within these thresholds. In Denmark the Danish Veterinary and Food Administration (DVFA) is responsible for conducting yearly checks of the supermarkets to ensure that the regulative is met and that self checks have been performed. The inspection rules and thresholds for different foodstuffs can be found in [Danish Veterinary and Food Administration, 2005, Danish Veterinary and Food Administration, 2013]. Freezers should typically be operated below -18$^\circ C$ and fridges should be operated between 0 and 5$^\circ C$, but it also depends on the type of food. If some of the foodstuff has been maintained outside the limits during self checks or a DVFA inspection, then that could consequently result in discarded foodstuff and possibly a penalty fine to the shop owner depending on the severity. Health hazards could also arise due to increased bacteria growth in the foodstuff. DVFA usually inspects the temperature in supermarkets using an infrared temperature measurement device, which measures the product surface temperature. If there is a problem, a thermometer is inserted in the display case to measure the air temperature or placed on the

product itself [Danish Veterinary and Food Administration, 2013]. The Danish legislation on the allowed temperature is actually on the air temperature. However, by ensuring that the product is within the bound, then it is less likely that the air temperature is measured. The $5°C$ limit for some fridge products is chosen because most bacterial growth stops below this temperature [Danish Veterinary and Food Administration, 2005].

Apart from maintaining the foodstuff at the right temperature it is also important to operate the refrigeration system as optimal as possible. The coefficient of performance COP is a measure of how well the system operates as it gives the relation between the energy put into the system versus the amount of cooling obtained. A high number thus indicates a well operated system and the total COP can be defined as

$$COP = \frac{\dot{Q}_{e,mt} + \dot{Q}_{e,lt}}{\frac{\dot{W}_{cp,mt}}{\eta_{mt}} + \frac{\dot{W}_{cp,lt}}{\eta_{lt}} + \sum_{i=1}^{N} \dot{W}_{f,i}}, \tag{1.5}$$

where $\eta_{mt} \in]0,1[$ and $\eta_{lt} \in]0,1[$ represent the efficiency when going from consumed electrical power to actual work performed on the refrigerant by the MT or LT compressor racks. $\dot{W}_{f,i}$ is the electrical power consumption of fan i out of N (evaporator and condenser fans). Valve power consumption is negligible and not included. Note here that there also exist other more simple approximations of the COP, e.g., which do not include the fans as they typically only account for roughly 10% of the total power consumption.

The work of the compressor racks were expressed in Eq. (1.1) and (1.2). The mass flow matches the required cooling. This means that the difference in enthalpy should be minimized to optimize the system performance. The difference in enthalpy is determined by the efficiency of the compressor rack, which is a mechanical optimization task, and the pressure difference between the high and low pressure side. The system can therefore be optimized by increasing the suction pressures $P_{e,lt}$ and $P_{e,mt}$ while lowering the condenser pressure P_c. The suction pressures are typically controlled by the compressor racks and the setpoints have to be low enough to make the evaporation temperature lower than the desired temperature of the air in the display case. The condenser pressure is controlled by the condenser fan speed f_c, which is increased if the pressure gets too high. The resulting increase in air flow gives a higher heat transfer and faster condensation, which lowers the pressure. The condenser pressure setpoint has to be high enough to get the condensation temperature above the outside air temperature $T_{air,o}$ and can thus be set to follow this temperature with a fixed offset. The pressure difference can therefore not be made smaller than what the surrounding temperatures allow.

A high heat transfer in the evaporators is obtained by having a high liquid to gas ratio of refrigerant in the evaporator. However, all the refrigerant should be evaporated before the compressor rack in order to reduce the wear on the compressors and the risk of damaging them. An important control task in the refrigeration system is thus to maintain suitable levels of superheat $T_{sh,mt}$ and $T_{sh,lt}$, since zero superheat is an indication of possible flooding of the compressors and too high superheat gives a low utilization of the evaporator cooling capacity. The superheat is controlled by regulating the mass flow into the evaporator with the valve and the setpoint is typically between 6-12^oC.

It is also important to control the level of subcooling T_{sub}. This is mostly because even small gas bubbles in the liquid refrigerant drastically lowers the mass flow through the valve, which will cause a drop in the obtainable cooling capacity. There is also an operating point dependent energy optimal level of subcooling different from zero [Pottker

& Hrnjak, 2012], which can be obtained by the condenser fan, the high pressure valve, and the bypass valve.

Due to safety reasons and system performance it is also necessary to include fault detection and isolation (FDI) and possibly fault handling or fault tolerant control (FTC). This is typically done on a higher supervisory level in a hierarchical control structure. Some of the issues could be refrigerant leakage, heat exchanger fouling, critical low/high pressures, or pressure sensor "freezing". The first two problems affect the system performance and manifest themselves on a longer term, which can make them harder to detect. An exception is fouling due to frost build up on the evaporator fins, which have to be defrosted once to several times a day. Defrost is performed using an electrical heater and/or a temporary shutdown of refrigerant flow and it is either scheduled or based on measurements from an extra temperature sensor placed on top of the fins. Safety limits on pressures are usually maintained with pressostats, limits on operating ranges, or proper shutdown mechanisms. A combination of impurities/dirt and oil might also block the passage to pressure sensors, which can result in that the measurement signal "freezes". This can eventually lead to evaporator flooding, liquid in the compressor, and compressor damage, since pressure sensors are used to calculate the evaporation temperature and thus the superheat temperature.

Another problem that might occur in refrigeration systems with multiple evaporators is synchronization of the temperature hysteresis controlled on/off valves. This is mostly a problem if the display cases are homogeneous and it can lead to large fluctuations in mass flow. The requested compressor rack capacity will as a result vary a lot giving an increase in on/off compressor switches and increased variability in power grid consumption [Larsen et al., 2007b].

A way to significantly reduce the heat transfer rate (load) on the display cases are to use night covers. Some systems have automatic covers, which roll down during closed hours and some older systems have to be manually covered with foam plates. This covering and uncovering gives big changes in system load, which gives an additional control challenge. The effect is enforced by increased customer and employee activity, when the supermarket is open.

Finally, the large thermal energy storage capability of the foodstuff provides load shifting and cost optimization possibilities. Cost optimization can be achieved by cooling more when the energy price are low and/or when it is more favorable during nighttime where the system COP is higher, due to lower outside temperatures. Supermarkets could therefore provide ancillary services to the grid by shifting power consumption according to power production. Another potential is to utilize the thermal storage capability to better cope with hot summer days by, e.g., precooling the foodstuff in advance during the night.

1.1.3 Control Challenges and Overall Objectives

The research presented in this thesis addresses a part of the extensive amount of control problems mentioned in Subsection 1.1.2. These control problems have been categorized in Fig. 1.4 into essential lower level decentralized control tasks and higher level supervisory control challenges meant to make the system more robust, cost optimal, and energy efficient.

The main objective of the supermarket refrigeration system is to maintain the temperature in the display cases within the legislative requirements due to health issues and to

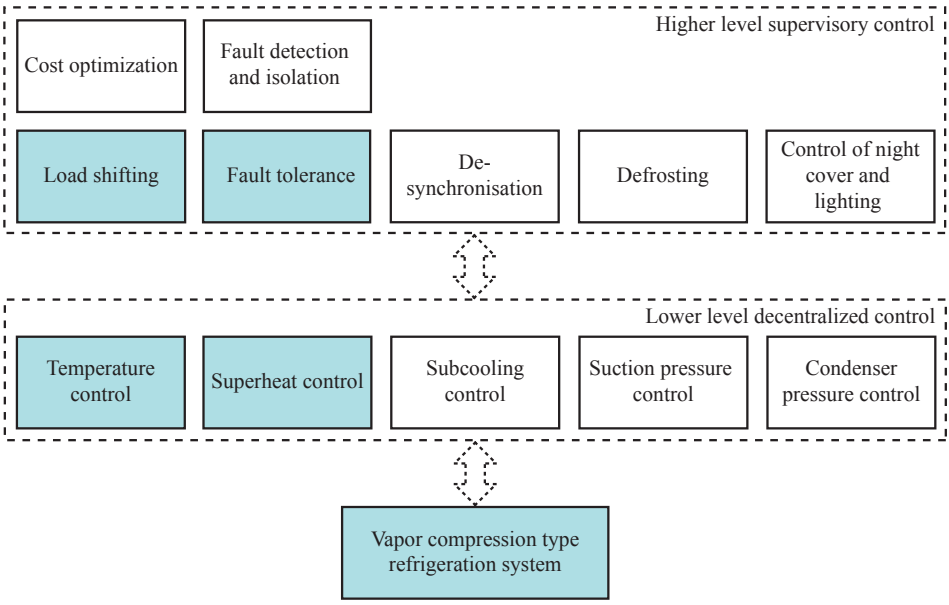

Figure 1.4: Overview of typical control challenges in supermarket refrigeration systems. Light blue boxes indicate the focus of this thesis.

ensure high foodstuff shelf life. Furthermore, as stated in Subsection 1.1.2, if some of the foodstuff has been maintained outside the limits during self checks or a DVFA inspection, then that could consequently result in discarded foodstuff and possibly a penalty fine to the shop owner depending on the severity. Dimensioning a refrigeration system to also meet the highest possible load condition is costly (e.g., hottest summer day with highest customer activity). Fig. 1.5 shows the filtered total estimated compressor rack work applied to the refrigerant in a representative medium sized Danish supermarket during three days. The estimate is calculated based on Eq. (1.1) and (1.2). Note the variability in

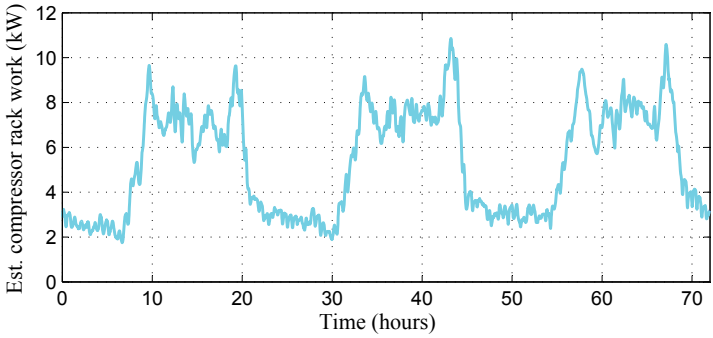

Figure 1.5: Filtered total estimated compressor rack work during three days in a medium sized Danish supermarket.

the load during the day and the high load during the opening hours of the supermarket with customer activity and higher outdoor temperature. Furthermore, an overdimensioned system will also have a higher peak power demand, which could result in an additional cost in terms of larger transformers or extensions of transmission lines for large systems. Finally, additional display cases might be added later, which puts further stress on the system. An alternative to overdimensioning the system could be to utilize the thermal storage capability of foodstuff and store energy in terms of "coldness" for later use. Some of the peak load and required cooling capacity could possibly be shifted temporally by precooling the foodstuff in lightly loaded hours during the night or early morning. Load shifting could also add robustness towards component wear and degradation during the refrigeration systems lifetime.

The second most important control challenge, after maintaining the display case temperature within the requirements, is to maintain a suitable superheat level and thus to ensure the integrity of the compressor rack, while meeting the required cooling demand. A typical Danfoss evaporator superheat control setup requires a control unit, an electronic expansion valve (EEV), a temperature sensor, and a pressure sensor. The setup is illustrated in Fig. 1.6. The sensors provide the evaporator outlet temperature $T_{e,o}$ and the evaporation temperature T_e (through the pressure P_e and refrigerant property tables). The difference in these temperatures is defined as the superheat T_{sh}. Each evaporator (display case) is equipped with this control setup and approximately one third of the total cost of these components is the pressure sensor. In this example it is assumed that the control unit and valve cost is halved, since these components are also necessary for display case air temperature control. The pressure sensor also costs approximately three times as much as the temperature sensor and is not as reliable, since impurities and oil can clutter the sensor and because it is more sensible to mechanical and electrical stress. Alternative superheat control is therefore investigated in this thesis, which does not require a pressure sensor and can function as a fallback strategy in case of pressure sensor malfunction.

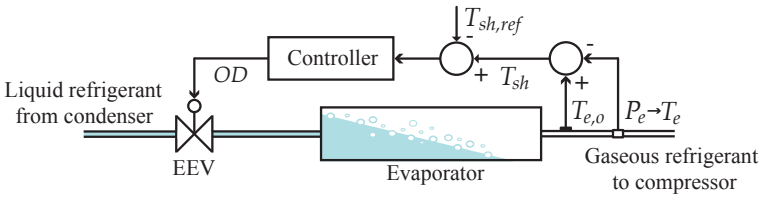

Figure 1.6: Evaporator superheat control setup.

Denmark roughly has 4500 supermarkets[1] and their refrigeration systems are seldom completely similar, since each supermarket is different in size and needs. This means that there exist thousands of different system configurations worldwide. Changes in operating conditions and load patterns will also occur during the day and during the year due to seasonal weather changes. Finally, system parameters can change due to component wear, heat exchanger fouling, ice buildup, reduction in refrigerant charge, changes in foodstuff type and amount, etc. These are some of the challenges, which make advanced model-based control solutions difficult and a solution will therefore often be tailored to a

[1] http://ing.dk/artikel/supermarkeder-kan-gore-store-maengder-kulkraft-overflodige-103015

specific system and have some form of adaptation mechanism. Another challenge is the nonlinearity of some of the control problems and the cross coupling between the lower level controllers. An example is the characteristic of the relationship between the evaporator valve opening degree and the superheat, which is very flat until the evaporator is almost filled with liquid refrigerant. At this point the superheat drops fast and then flattens out again at zero when the evaporator is flooded. Making a controller that gets the opening degree to a level that gives a small non-zero superheat fast without suffering from valve hunting (instability) at the desired operating point is difficult [Lim et al., 2009]. The controllers could often be tuned more optimally. However, this results in an additional investment. The multitude of different system configurations and changing operating conditions also make tuning difficult. These challenges justifies an effort to incorporate more intelligence and adaptation and a move towards control strategies with a higher degree of plug and play potential. Furthermore, model-based control approaches often lack flexibility, modularity, and robustness towards changes.

The focus of the research presented in this thesis has therefore been to improving the tolerance of superheat control towards potential pressure sensor problems by making this sensor obsolete and to improve the robustness of foodstuff temperature control towards saturation situations through "intelligent" load shifting. Additionally, emphasis has been on non model-based solutions with a high plug and play potential, in order to reduce the commissioning costs, which is also in the interest of the industrial partner Danfoss. The other control challenges summarized in Fig. 1.4 are mostly energy optimization related. The broad objectives are in short:

- To derive single-sensor superheat control solutions, which do not require a pressure sensor.
- To improve the robustness of foodstuff temperature control towards saturation situations.
- To find non model-based solutions with a high degree of plug and play potential.

1.2 State-of-the-Art

An overview of the existing literature is first given, before outlining the research challenges and hypotheses. The overview includes a discussion of existing superheat and foodstuff temperature control strategies, together with a discussion of key control methods related to the proposed solutions and the broad objectives outlined in Subsection 1.1.3.

1.2.1 Superheat Control

Transfer of heat from a medium (cooling), in vapor compression cycle systems, is carried out by evaporation of liquid refrigerant in an evaporator at a temperature below the temperature of the surrounding medium. When all the refrigerant is evaporated it starts to superheat. If liquid or a two-phase mixture of refrigerant is allowed to leave the evaporator and enter the compressor (zero superheat situation), it can potentially cause increased wear on the compressor or in the worst case damage it. The most common reasons for

compressor failure are [Danfoss, 2009]; refrigerant flood back, flooded starts, liquid slugging, overheating, and lack of lubrication. These failures can in most cases be avoided by maintaining a proper level of superheat. It is also important not to have too high superheat, since the vaporization process accounts for the majority of the heat transfer and a low superheat is thus required for maximum cooling capacity of the system [Outtagarts et al., 1997, Elliott et al., 2011].

Modeling of Evaporator Dynamics

Different approaches for modeling of evaporator dynamics are first covered, before going into detail with the superheat control strategies. A thorough review on this subject is given in [Rasmussen, 2012a]. The approaches include data-based, moving boundary (MB), switched moving boundary (SMB), and fixed control volume (FCV) modeling, which usually have increasing complexity and computational needs in that order.

The evaporator is essentially a distributed parameter system described by balance equations [Gruhle & Isermann, 1985, Rasmussen, 2012a] and the FCV approach can give a detailed approximation of the evaporator dynamics. However, the simpler lumped parameter MB approach has been widely used in the literature (e.g., see [Wedekind et al., 1978, Broersen & van der Jagt, 1980, Grald & MacArthur, 1992, He et al., 1997, Willatzen et al., 1998, He & Asada, 2003, Schurt et al., 2009, Rasmussen & Larsen, 2011]), which models the evaporator with a two-phase fluid and a superheated vapor zone having a time-varying boundary. The number of zones can be varied to also model start-up and shut-down situations using SMB models [McKinley & Alleyne, 2008, Li & Alleyne, 2010].

The modeling choice should in general reflect the level of detail required in the analysis and data-based modeling can provide an even simpler approach to describe the important evaporator dynamics. The use of linear first and second order dynamics, Hammerstein, autoregressive-moving-average (ARMA), neural networks, and linear parameter varying (LPV) models are briefly discussed in [Rasmussen, 2012a]. In [Elliott & Rasmussen, 2010], second-order models are utilized to capture EEV-superheat and EEV-pressure dynamics. Identification of first order plus dead time (FOPDT) model at high and low load are used for control of an EEV-evaporator loop in [Finn & Doyle, 2000] and linear parameter varying (LPV) FOPDT and second order models are similarly used in [Outtagarts et al., 1997] to describe mass flow to superheat dynamics. Furthermore, second-order Padé approximations of FOPDT models in one nominal and four extreme conditions are used in [Lim et al., 2009], to derive a suitable proportional-integral (PI) superheat controller for the different operating conditions in question.

Superheat Control Strategies

Thermostatic expansion valves (TEV) provide a simple and cheap way to control superheat. They work by having a sensing bulb, placed at the evaporator outlet, which is filled with two-phase refrigerant. The pressure in the sensing bulb is affected by the temperature at the evaporator outlet, which is determined by the amount of superheat. When the superheat is high, the sensing bulb pressure increases, which acts on a diaphragm that creates a force on a spring system that opens up the valve more. When the superheat decreases, the valve opening decreases again accordingly. TEVs are purely mechanical and do not require sensors or an electronic controller, which is the case with EEVs. However,

EEVs can offer improved performance under nonlinear operating conditions and transients by having higher control freedom [Finn & Doyle, 2000]. EEVs usually either have a stepper motor that controls the opening degree or use pulse width modulation (PWM) with a frequency that is much faster than the evaporator dynamics.

A problem that often occurs in TEV operation (and also EEV) is valve hunting, where the length of the two-phase flow and the superheat in the evaporator start to oscillate. [Broersen & van der Jagt, 1980] used an evaporator model to show that the interaction between the evaporator dynamics and TEV can cause valve hunting. According to [Chen et al., 2002] there are many beliefs on why hunting exists and they show through experiments that valve hunting is primarily caused by changes in heat transfer mechanism and not just control problems. A change between convective and nucleate boiling at low temperature gradients causes a change in heat transfer coefficient and flow type, which leads to valve hunting. This indicates that the superheat setpoint should not be too low whatever the choice of valve and the critical point is also called minimum stable superheat. With EEVs it is possible to operate closer to the minimum stable superheat by adapting the reference setpoint and, e.g., variance-based adaptation of the reference is used in Danfoss EEV solutions [Danfoss, 2008].

Most of the systems today with EEV valves use simple variations of proportional-integral-derivative (PID) control. A PID controller is tested in [Outtagarts et al., 1997] and both P, PI, and PID control is tested in [Finn & Doyle, 2000] with increasing performance. However, there are still some performance issues, since the system dynamics change considerable under different conditions (e.g., low flow versus high flow). The PI(D) type control should be tuned conservatively to be stable for all operating conditions, which also means that performance requirements might not always be fulfilled. This issue is well described in [Lim et al., 2009] and a pattern recognition adaptive controller is proposed in [Seem, 1998], where a PI controller is retuned each time a step change in setpoint is made. Furthermore, [Finn & Doyle, 2000] suggests an adaptive scheme that updates the control parameters based on the surrounding temperature and model-based gain scheduling is applied to a PID controller in [Rasmussen et al., 2006a].

The simple PI(D) superheat control solution without adaptation still requires initial tuning. Different auto-tuning or self-tuning approaches exist in the literature (e.g., see [Åström & Hägglund, 1988, Åström & Hägglund, 1995, Yu, 2006]). Low-order modeling from relay feedback is also described in [Shen et al., 1996, Wang et al., 1997] and [Bi et al., 2000] uses relay feedback and step tests to tune of PID control loops in heating, ventilation, and air conditioning (HVAC) systems. The control can either be tuned in nominal operating conditions or in a critical operating point such as low temperature and low flow where the system gain is high [Lim et al., 2009]. Self-tuning plug&control for temperature control, or in general low order models, is presented in [Pfeiffer, 2000, Visioli, 2003], where PI(D) control loops are tuned in closed-loop based on the first step change in setpoint and therefore provide a faster tuning alternative to relay feedback. However, a conservative control parameter start guess is instead required.

There are also more advanced alternatives to the standard PI(D) EEV superheat control, which seek to handle larger ranges of operating conditions better. Model-based gain scheduling is, e.g., applied to a PID superheat controller in [Rasmussen et al., 2006a]. Another example of more advanced control is given in [He & Asada, 2003] where feedback linearization is used to make PI design straightforward and [Rasmussen et al., 2006b] suggests converting superheat to a referred variable leading to control of a linear sys-

tem independent of the operating point. The backstepping approach can also be used to compensate for the nonlinearity [Rasmussen & Larsen, 2009b] and cascaded superheat control structures are proposed in, e.g., [Elliott & Rasmussen, 2010, Elliott et al., 2011], where an inner loop controls the pressure with the EEV and an outer loop changes the pressure setpoint based on the superheat error.

EEV technology is also becoming more complex. A hybrid expansion valve (HEV) design is presented in [Elliott et al., 2009], which uses a diaphragm as in TEVs for fast regulation of flow and a stepper motor and spring to adjust the pressure on the diaphragm. The stepper motor position is governed by a slow superheat regulator. This gives better performance compared with TEV operation and HEVs also have better motor lifetime than stepper motor EEVs. As another example, Danfoss offers a new EcoFlow valve that can have individual opening degrees for each tube in the evaporator, which can provide a way to balance the filling across the evaporator [Danfoss, 2011]. This also makes it possible to defrost each individual section of the evaporator individually and, thus, does not require dedicated defrost heaters.

An alternative to EEV superheat control is to use the compressors for superheat control and then use the EEV for capacity control. However, the compressor frequency and superheat relationship is highly nonlinear. Nonlinear control such as backstepping is used in [Rasmussen, 2008, Rasmussen & Larsen, 2009a, Rasmussen & Larsen, 2011] to solve this problem. The ability to control the superheat with multiple inputs is also an indicator of the high cross coupling in the refrigeration system. This cross-coupling is shown in [He et al., 1997] using relative gain array, and a linear quadratic Gaussian (LQG)-based multiple-input multiple-output (MIMO) control strategy with gain scheduling is proposed in [He et al., 1998] using a linearized model of the refrigeration system. LQG-based MIMO control is also presented in [Schurt et al., 2009] with the inclusion of a Kalman state observer. Decoupling can also be achieved using alternatively chosen SISO loops. [Jain & Alleyne, 2009, Jain et al., 2010] show that controlling the average system pressure with the EEV, the differential pressure with the compressor, and the average evaporator temperature with the evaporator fan can result in better reference tracking. However, the strategy is only shown for single evaporator systems with one EEV and not for supermarket refrigeration systems with multiple EEVs.

Pressure Sensor Malfunction and Potential Solutions

Most EEV superheat control setups use a pressure and a temperature sensor to calculate the superheat and a fixed PI(D) controller to ensure that the superheat tracks the reference superheat despite the potential performance benefit of more advanced controllers. This is mainly because of the widespread use of PI(D) control, the intuitive operation of decentralized control loops, the low complexity, and the high flexibility/modularity (each evaporator has its own superheat control, which does not rely on information from other parts of the system). More advanced control also often relies on good model knowledge and deriving such a model can be a significant undertaking. However, an alternative strategy is needed if the pressure sensor fails in order to be able to continue operation and maintain the correct temperature without compromising the compressors.

A possible solution is to replace the pressure sensor with a temperature sensor placed on the outside of the evaporator inlet tube after the EEV, which approximately have the same temperature as the evaporation temperature. This gives a two-temperature-sensor

superheat control solution as in [Finn & Doyle, 2000, Chen et al., 2002]. However, pressure sensors are still used despite that temperature sensors are cheaper and possibly more reliable. The pressure sensor does give a faster and better measure of the evaporation temperature than a temperature sensor, due to the slower dynamics and low-pass characteristics of the tube wall. Replacing pressure sensors with temperature sensors in existing systems also imposes an added cost in terms of new sensors, installation cost, and tuning.

The increased closed-loop variance close to the minimum stable superheat can be used to adapt the superheat reference as described in [Danfoss, 2008]. Here the reference is lowered until the variance exceeds a limit, and the possibility of using this principle, when the pressure measurement is not available, is investigated in this thesis. This solution is also closely related to automatic variance control concepts, e.g., see [Moir, 2001].

The qualitative behavior of the evaporator outlet temperature as a function of the EEV opening degree is also nonlinear. The evaporator input/output (I/O) relationship is almost flat at low opening degrees and then suddenly drops close to the minimum stable superheat and then flattens out again when the evaporator is flooded. This qualitative behavior is illustrated in Fig. 1.7, and the system gain therefore has a maximum close to the minimum stable superheat. The exact relationship will of course depend on the operating conditions and the system. Note, that the typical lumped parameter model used in the literature does not have a smooth s-shape, but rather a sharp corner when $T_{e,o}$ reaches T_e. However, actual evaporator behavior does not exhibit sharp corners because of refrigerant spray, sensor dynamics, superposition of separate evaporator sections (investigated in [Lyhne & Sørensen, 2011]), and because it is a distributed parameter system.

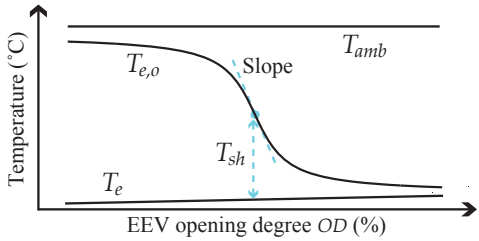

Figure 1.7: Qualitative nonlinear relationship between evaporator outlet temperature $T_{e,o}$ and valve opening degree OD.

The increase in gain could be detected using a dedicated perturbation signal, which could provide the missing information for superheat control in case of pressure sensor malfunction. The general idea of detecting the system gain with a perturbation signal and utilizing the increase in gain near a low superheat to develop a single-sensor superheat controller has been proposed in [Izadi-Zamanabadi et al., 2012a]. The idea therein is to make a large step up in input and then detect the extremum in system gain by continuous calculation of the rate of change of the evaporator outlet temperature. When an extremum is detected then the lowest encountered evaporator outlet temperature could be used as zero superheat reference. However, this temperature might change over time and the step test would have to be performed either continuously or with a given interval. One of the main aims of the research presented in this thesis has been to further investigate the possibility of developing a perturbation-based single-sensor superheat control.

1.2.2 Perturbation-Based Control

The perturbation principle is used in the non model-based extremum-seeking (ES) and slope-seeking (SS) control schemes, where a sinusoidal signal is applied to the system input. These methods use the perturbation of the nonlinear system to estimate the gradient and feedback control then ensures convergence toward the zero slope point in the I/O-map (extremum) or a certain slope (other than zero) corresponding to a suitable operating point. The first appearance of ES control is believed to be [Leblanc, 1922], while a resurgence of interest was sparked with more rigorous assessment of stability in [Wang & Krstić, 2000] using singular perturbation and averaging analysis. Later, non-local stability properties where derived in [Tan et al., 2006]. A thorough coverage of the subject is provided in books such as [Ariyur & Krstić, 2003, Zhang & Ordóñez, 2012] and a literature review on ES is given in, e.g., [Tan et al., 2010]. [Henning et al., 2008] investigates the use of an extended Kalman filter for gradient estimation in SS control and possible adaptation of the perturbation amplitude to limit the impact of perturbation on the system output. Observers are also used in [Moase et al., 2010, Bishop et al., 2011] for ES control and [Bishop et al., 2011] provides an analytic way to find an upper bound in the feedback gain. [Moase & Manzie, 2011] also suggests adaptation of the control parameters in real-time to make a fast ES controller and [Haring et al., 2013] suggests an alternative gradient estimator using a periodic finite impulse response (FIR) filter, which extracts first harmonic information and effectively filter out other harmonics and, thus, showing better performance than the traditional infinite impulse response (IIR) filters used in ES and SS.

The use of ES control in optimization of refrigeration processes is already beginning to emerge. An example is given in [Li et al., 2005], where ES is used to optimize a tunable thermoacoustic cooler. The chilled water setpoint temperature can also be optimized using ES in cooling towers, because the total power consumption of the chiller compressors and cooling tower fans is a convex function of the water temperature (these components are the main power consumers these HVAC systems) [Tyagi et al., 2006, Sane et al., 2006]. The main benefit of ES is that a model of the chiller and cooling tower is not required. The same strategy is used in [Li et al., 2012] except that the fan speed is perturbed instead of the water temperature. [Li et al., 2010] also investigates the use of ES control in HVAC control for optimization of outdoor air damper opening in air-side economizers. Optimization of the total power consumption of the compressor and evaporator fan, in a vapor compression cycle system, can also be performed using ES control by perturbing the fan speed [Burns & Laughman, 2012]. Furthermore, the optimal subcooling in vapor compression cycle air conditioning systems is shown to be non-zero and highly dependent on the operating conditions in [Koeln & Alleyne, 2013] and a non model-based control method using ES control is presented for optimization of the subcooling.

The qualitative nonlinear I/O-relationship illustrated in Fig. 1.7 indicates the potential use of SS control. A discrete ES/SS control setup, using the filter proposed in [Haring et al., 2013], is shown in Fig. 1.8 for an example Hammerstein system with an s-shaped nonlinearity. The objective in ES/SS is to drive the input offset $\bar{u}(k)$ towards u^* and u^* denotes the input at the desired reference slope f'_{ref}. The Gain/gradient/slope of the system in the current operating point $\bar{u}(k)$ can be extracted using the gradient estimator filter and a perturbation signal $A_{ex}\sin(\omega_{ex}k)$, with amplitude A_{ex} and period ω_{ex}. The gradient estimator basically extracts the amplitude of the first harmonic in the output and relates it to the amplitude of the input. The variable N_ϕ can be used to compensate for

any potential phase shift in the dynamics $f_o(t)$ and a function $r(f'_{ref})$ can be used to offset the error signal $\xi(k)$ according to the desired reference slope f'_{ref}. The scheme is ES control if $r(f'_{ref}) = 0$. However, ES control would not make sense on the s-shaped nonlinearity as it would converge to $\bar{u}(k) = \pm\infty$.

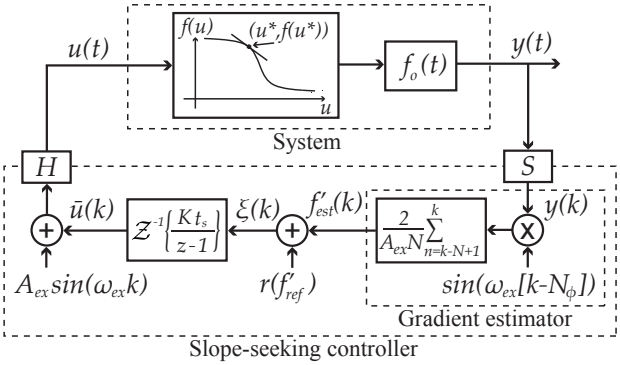

Figure 1.8: ES/SS control scheme. Sample and hold on the system is denoted (S/H).

A suitable operating point for the evaporator system could be to control the opening degree of the EEV to a level where the I/O-map experiences a maximum in the slope, which is close to the minimum stable superheat. A problem with SS control is that the maximum slope point is not a possible operating point, because the gradient decreases in both directions leading to instability. Global convergence to the desired operating point using a reference slope to either side of the maximum slope would also not be possible, see Fig. 1.9. Furthermore, estimation of a good reference slope is also difficult, if not practically impossible, for a time-varying s-shaped I/O-map (the evaporator I/O gain variation due to changes in operating conditions is shown in [Lim et al., 2009, Elliott & Rasmussen, 2010]). An alternative maximum slope seeking (MSS) control scheme inspired by ES/SS control, which does not require specification of a reference slope, is therefore investigated in this thesis. MSS could potentially eliminate the need for a pressure sensor or provide fault tolerance in existing systems, without additional hardware and very limited system knowledge. Note also that no other non model-based single-sensor superheat control strategy has been found in the literature.

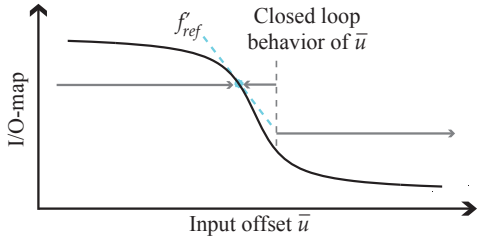

Figure 1.9: Convergence direction with SS control using a reference slope close to the maximum slope point.

1.2.3 Temperature Control and Load Shifting

The purpose of refrigeration systems is to maintain the temperature of spaces or products within specified bounds. For example, in supermarkets it is important to maintain the temperature of the foodstuff within legislative requirements, in buildings it is important to obtain thermal comfort for the occupants, and in pharmaceutical or food processing facilities it might be important to track the right setpoint temperature during production. Different temperature control strategies and load shifting possibilities are outlined in the following.

Conventional Temperature Control

The most common temperature control strategies in HVAC systems are on/off hysteretic control and PI(D) control, e.g., see [Seem, 1998, Underwood, 1999, Bi et al., 2000, Lim et al., 2009]. On/off hysteretic control is mostly used in supermarkets for control of the temperature in the display cases, e.g., see [Larsen, 2005, Sonntag et al., 2008, Sarabia et al., 2009, Hovgaard et al., 2012a, Shafiei et al., 2013b]. These strategies are widely used due to their simple implementations, but hysteretic control can give large fluctuations in the suction pressure, due to the on/off operation of the EEVs, resulting in frequent compressor switches and increased wear. However, the fluctuations will average out if there are many evaporators and care is taken to desynchronize them so that they do not turn on and off at the same time [Larsen et al., 2007b]. There are some studies of continuous valve opening temperature control for supermarket display cases. An example could be to control the superheat in an inner loop as usual and then set the superheat reference in an outer loop dependent on the air temperature in the display case. This gives a lower filling of the evaporator, when less cooling is required and a much more steady suction pressure [Petersen et al., 2012]. However, an advantage with on/off hysteretic control is that it does not require any tuning and it can be used in conjunction with TEVs, which is not possible in the cascaded control structure. A positive side effect of on/off operation is also that less ice builds up on the evaporator and the ice is more dense giving a better heat transfer. Further, operating with a low filling can give a nonhomogenous temperature distribution in the display case, which can impact the food quality [Sarabia et al., 2009].

Advanced Temperature Control and Load Shifting Strategies

Knowledge of variations in weather, occupancy in buildings, restocking times in supermarkets, energy prices, and opening hours can be included in the refrigeration system temperature control problem to improve performance, reduce running costs, and/or to better handle potential out of capacity situations. This, e.g., involves precooling during the night and early morning to utilize a higher system efficiency due to lower outdoor temperatures and potentially lower energy prices. The additional cost associated with a higher heat loss due to a lower temperature should then not exceed the savings obtained by precooling. Precool can also help prepare the system to meet peak loads if capacity limits will be reached or in general reduce peak loads to give a more flat demand.

Significant energy cost savings are demonstrated in [Braun, 2003], where building thermal mass is used for load shifting and reduction of peak cooling loads. Braun estimates the savings to be in the range from 0 to 35%, depending upon utility rates, type of equipment, accuracy of occupancy schedules, climate, building construction, and control

strategy. Based on simulations in [Hovgaard et al., 2011] it is similarly estimated that 20% of the capacity in supermarket refrigeration systems can be offered as regulating power, which can cover a significant part of the total primary reserve needs in Denmark. Furthermore, [S. Goli & Olsen, 2011] states that the load from refrigerated warehouses located in California was 360 MW in 2008 and that the potential demand response capability of these warehouses is somewhere between 45-90 MW (12.5-25%).

There are in general two control strategies being employed for cost optimization and load shifting. The simplest is a fixed schedule for the setpoints in the system or a schedule derived based on day ahead expectations/predictions. The second strategy is to use some variation of model predictive control (MPC). In MPC a cost function over a receding prediction horizon is minimized to find an optimal set of inputs to the system under certain constraints (e.g., actuator and temperature limits). This makes MPC an ideal candidate for load shifting and temperature control, since economical incentives can be optimized while temperatures are guaranteed to stay within the constraints.

Examples of using a fixed schedule compared with energy/demand optimization control (MPC) is provided in [Braun, 2003] for large buildings. Other examples of advanced model-based temperature control in buildings focused on energy savings and occupancy comfort are given in [Prívara et al., 2011, Castilla et al., 2011, Oldewurtel et al., 2012, Goyal et al., 2012, Álvarez et al., 2013b]. The strategies therein use a combination of occupancy estimation, weather forecasts, and energy prices to compute optimal settings for the HVAC system.

Demand response opportunities have been investigated for nine refrigerated warehouses in [S. Goli & Olsen, 2011]. Using a day-ahead demand response scheme, where a central server asked the warehouses for demand response services to help reduce peak loads, showed good results. One site was able to shift 36% of its load in a 2-4 hour period when compared with the baseline by shutting off some of the equipment and adjusting the setpoints in a pre-set hierarchy. Models of four low temperature warehouses located in the North Central U.S. have also been used to simulate different predefined load-shifting schedules in [Altwies & Reindl, 2002]. The first strategy cools for 10 hours and then turns off for 14 hours, which could save up to 53% of the total cooling cost. However, this would also require investment in larger refrigerators big enough to apply all the necessary cooling within the 10 hours. The second strategy was to always maintain the same cooling load during 24 hours, which reduces the electricity fluctuations and peak load. The last strategy was a mix.

MPC load shifting strategies are also beginning to emerge for supermarket refrigeration systems. An economic-optimizing nonlinear MPC scheme using weather and energy prices and thermal storage capabilities in supermarket display cases is presented in [Hovgaard et al., 2011, Hovgaard et al., 2012a]. The scheme reduces operating costs and provides 15 min up/down regulating services to the grid and simulations show significant savings of up to approximately 30%. A linear MPC scheme is similarly proposed in [Shafiei et al., 2013a, Shafiei et al., 2013c] showing approximately the same savings. A linear scheme is possible due to a separate optimization algorithm for the suction pressure. A virtual power plant setup with MPC, which tries to minimize grid power overproduction using refrigeration systems as flexible consumers, is demonstrated in [Pedersen et al., 2013]. Each node is approximated by a simple flexibility model describing their current energy level, dain rate, fill rate, and constraints on the energy level. A test using three simulated nodes and a water chiller system shows the potential use of thermal systems as

"blowoff" valves in cases with electricity overproduction. In [Cai et al., 2008], a model of a display case is also used to demonstrate that MPC can be used to handle potential capacity limitations in refrigeration systems by precooling the foodstoff in an antisipatory manner on hot summer days.

Installation of thermal energy storage (TES) tanks, called active storages, can also help solve capacity limitations, give additional demand response capabilities, and/or provide the possibility of downscaling the refrigeration system. Examples of the use of TES in buildings using MPC or fixed precool schedules are given in, e.g., [Henze & Krati, 1998, Ma et al., 2012, Powell et al., 2013]. A combination of the utilization of TES and building thermal mass (passive storage) is also demonstrated in [Zhou et al., 2005] with optimal control to shift electrical loads to off-peak hours at night and in the weekend. The study on a large three story office building modeled in EnergyPlus [U.S. Department of Energy, 2013] shows big potential savings when compared with only fixed precool of TES during nighttime. However, a considerable additional capital investment is also associated with installation of TES. Investigations in [Vrettos et al., 2013] on buildings with photovoltaics, electric water heat, slap cooling, heat pump, and battery storage additionally showed that using batteries as storage element is not economically tractible as the payback time is approximately 20 year and the expected lifetime of batteries are between 5-15 year and almost the same demand response was possible without the battery.

Precooling and Food Quality

Storing thermal energy in foodstuff in terms of "coldness" by precooling it can potentially affect the quality and shelf life negatively due to the higher fluctuations in temperature. The advantages of precooling in terms of demand response capabilities, reduced peak demand, or higher shelf life due to lower average/maximum temperature should therefore exceed the disadvantages.

Results from different studies on foodstuff quality have been compiled in [Altwies & Reindl, 2002]. The studies included food products such as cauliflower, spinach, peas, strawberries, etc. and showed that storage temperature fluctuations over the ranges of interest had little to no effect on frozen foods. However, significant quality loss is observed when fluctuations included freeze/thaw cycles. A study also indicated that nutrient retention can be expected to remain the same or even improve, due to a lower average storage temperature with precooling. Different frozen food products (salmon, mackerel, pork, ice cream, pizza, brocolli, etc.) were also studied in [Gormley et al., 2002], which showed that the fluctuations in temperature for most of the products had minimal effect on color, texture, water-holding capacity, and drip loss on thawing. However, parameters such as peroxide and free fatty acid were affected on a longer term in products containing fat. Additionally, most bacteria growth in non frozen foods stops below 5°C [Danish Veterinary and Food Administration, 2005], which indicate that upper temperature limits are probably more important than fluctuating temperatures. The potential quality loss caused by cycling temperatures due to precooling is less critical, when precooling is applied to handle capacity limitation situations, since quality and shelf life is mainly affected by bacteria growth, which increase with higher temperatures. The shop owner also risks having to discard all the foodstuff if legislative temperature requirements are not maintained. Furthermore, an accumulated quality loss model for foodstuffs is derived in [Cai, 2007]. This model is based on the foodstuff temperature sensitivity and quality loss time

constant, where higher accumulated quality loss occurs with higher temperature.

The potential for thermal energy storage in different refrigerated foodstuffs is predominantly determined by the mass, specific heat capacity, exposed surface area A, and surface heat transfer coefficient U. Another important factor is the Biot number B, which indicates if a lumped or non-lumped temperature analysis is appropriate;

$$B = \frac{U\frac{V}{A}}{k}, \tag{1.6}$$

where k is the thermal conductivity and V is the volume [Ash, 2005]. The Biot number can also be seen as the ratio of internal temperature difference required to move energy within a product compared with the difference required at the surface to add or remove the same amount of energy and a lumped temperature analysis can be applied if the Biot number is small ($B < 0.1$). The storage capability of different foodstuffs was experimentally studied in [Hovgaard et al., 2012b], where most of the obtained Biot numbers were above 0.1. However, a lumped temperature analysis is often performed despite of the high Biot numbers, since this approach does not involve solving complex multidimensional partial differential equations. Additionally, it might not be important to distinguish between the exterior and the interior of the foodstuff during a precool phase if it ensured that enough precool time is applied to activate the entire mass. Refrigeration system saturation, due to increasing outside temperatures, might also happen slow enough to allow a lumped analysis. The study in [Hovgaard et al., 2012b] also showed that products such as milk almost have a 12-hour load shifting potential.

Simulation Benchmarks

A simulation benchmark model provides a way to evaluate different control strategies under the exact same load conditions, which would not be possible otherwise. Performance can also quickly be evaluated for longer periods of time (weeks, months, or years) and introducing saturation in buildings and supermarket refrigeration systems is often not practically feasible.

Different advanced simulation tools for buildings exist such as EnergyPlus [U.S. Department of Energy, 2013] aimed at estimating the energy usage of a building while taking all the building materials into account. Lumped resistive-capacitive networks is a simpler and more commonly used method for modeling of the zone/room and wall temperature dynamics in buildings for control purposes (e.g., see [Lorenz & Masy, 1982, Hudson & Underwood, 1999, Gouda et al., 2002, Oldewurtel et al., 2012, Ma et al., 2012]). Each zone is typically modeled by a capacitance and each wall is modeled by three resistors and two capacitors also referred to as the 3R2C modeling approach illustrated in Fig. 1.10. The states in the model are the temperatures of the inner and outer wall surfaces $T_{wi,i}$ and $T_{wo,i}$, respectively, and the temperature of the ambient $T_{ai,i}$ and $T_{ao,i}$, which could be zone temperature, outside air temperature, or ground temperature. The parameters of the model are the heat resistances and thermal capacitances of all the i walls included in the model ($R_{wi,i}$, $R_{wo,i}$, $R_{ww,i}$, $C_{w,i}$, and $C_{wo,i}$).

A detailed study on modeling of vapor compression cycles is given in [Rasmussen, 2012a, Rasmussen, 2012b] and different available tools for simulation of supermarket refrigeration systems also exist. Thermosys [CU Aerospace, 2013] is an example of such a tool, which can simulate complete dynamic vapor compression cycles with transient be-

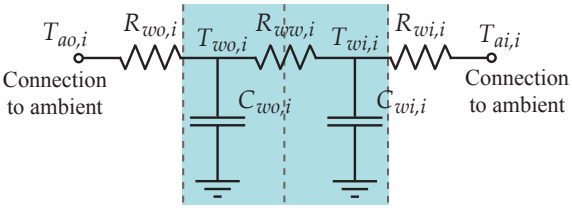

Figure 1.10: 3R2C lumped resistive-capacitive network model of a wall.

havior and shut-down and start-up operation. However, Thermosys is relatively slow and the model detail should in general match the particular problem. Simpler models might suffice for simulations focused on slow air and foodstuff temperatures dynamics. Individual models for the compressor rack, suction manifold, display cases, and condenser are typically used and [Larsen, 2005] demonstrated such a model, which is accepted for firsthand verification of new controllers at Danfoss. The model has also been used in slightly modified versions in, e.g., [Larsen et al., 2007a, Sonntag et al., 2008, Sarabia et al., 2009, Yang et al., 2011, Petersen et al., 2012, Shafiei et al., 2013b]. A supermarket simulation benchmark with three display cases is also presented in [Hovgaard et al., 2011, Hovgaard et al., 2012a] using parameters based on data from supermarkets. However, the air temperature is not part of this model. Estimation of refrigeration system parameters, based on supermarket data, is also presented in [Petersen et al., 2012, Shafiei et al., 2013b].

Utilization of Repetitiveness in Load Disturbances

The study in [Braun, 2003] shows that there is a tremendous potential for utilization of thermal mass for reduction of peak demand and on-peak energy consumption. However, the potential is also sensitive to uncertainty in building and refrigeration system characteristics, utility rates, weather forecasts, and occupancy schedules. [Braun, 2003] also shows the total cooling load profile during six days on two chiller units, which exhibit a very repeatable pattern (except during the weekend where the load profile is different). Furthermore, there is a much larger load in the occupancy hours. The high degree of repetitiveness in load disturbances is also visible in the data from a Danish medium sized supermarket refrigeration system presented in [Petersen et al., 2012]. The load behavior in these refrigeration systems is dependent on a combination of customer and employee activity, energy loss through insulation at the cooling sites, the temperature and humidity in the supermarket, the temperature thresholds used in the display cases, evaporator fan heat, heat from lighting, defrost cycles, and air infiltration to the display cases. Knowledge or prediction of the load pattern is required in model-based control such as MPC to be able to predict the required cooling. Kalman filters, as proposed in [Petersen et al., 2012], can be used to estimate the load, which has to be observable. Deriving such filters can be quite cumbersome especially in large systems and considering the multitude of different configurations of refrigeration systems. The observed repetitiveness in the load could instead be utilized in data-driven learning-based control schemes as an alternative to model-based approaches. The necessary precooling of foodstuff or building thermal mass, required to prevent cooling capacity saturation, due to repetitive peak loads that

might exceed system capacity, could be learned based on the saturation in previous days. A learning-based approach is an interesting alternative, since it does not require a model or adaptation of such, weather forecasts, occupancy schedules, or knowledge of supermarket opening hours.

1.2.4 Iterative Learning and Repetitive Control

Well established examples of learning-based control are iterative learning control (ILC) and repetitive control (RC). These methods are often used when a task is repeated, such as in batch processes, e.g., robot manipulation tasks that have to be repeated with high precision or if the disturbance repeats itself. The primary role of learning-based control is to improve the performance of an already stabilized system. There are in general two configurations; a parallel structure where a feedforward signal for the next repetition is learned and a serial structure where a reference modifying signal is learned. The parallel setup is also sometimes called a direct approach, and the serial setup is an indirect approach or a plug-in type learning controller (it just modifies the reference to an already existing closed-loop system). Fig. 1.11 illustrates ILC applied to a closed-loop system described by the controller C and the system G, where the reference vector $\mathbf{y}_r$ and/or the disturbance vector $\mathbf{d}$ has a repeatable pattern. A widely used learning algorithm is [Bristow et al., 2006]

$$\mathbf{f}_{j+1} = Q\left(\mathbf{f}_j + L\mathbf{e}_j\right), \tag{1.7}$$

where $\mathbf{f}_j$ is a vector of reference/error modifiers (serial setup) or feedforward signals (parallel setup) for repetition/trial j, $\mathbf{e}_j$ is a vector of tracking errors, and L and Q are learning functions. When trial j ends, a new batch or vector $\mathbf{f}$, to be used in trial $j+1$, is calculated based on the errors in the previous trial j. An approximate representation of the ILC system in the z-domain can be given as [Bristow et al., 2006]

$$F_{j+1}(z) = Q(z)\left(F_j(z) + zL(z)E_j(z)\right), \tag{1.8}$$

where $F(z)$ and $E(z)$ are z-transformations of the signals. The error is shifted forward in time by z in Eq. (1.8), which corresponds to a plant delay of one time step (should

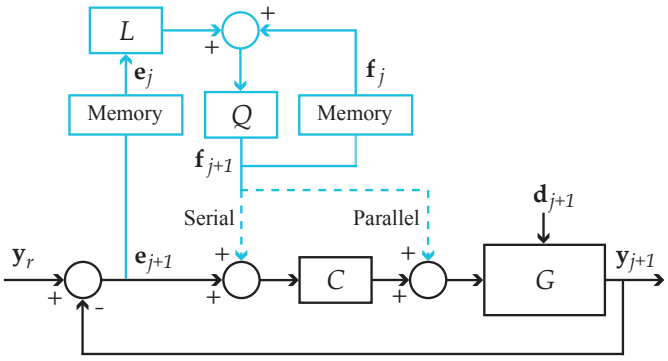

Figure 1.11: ILC (light blue) applied to a closed-loop system (black). Both serial and parallel ILC structure are shown.

in general match the particular system and the applied sample time). A well-known condition for stability and monotonic error convergence ($||\mathbf{e}_\infty - \mathbf{e}_{j+1}||_2 < ||\mathbf{e}_\infty - \mathbf{e}_j||_2$ for $j \in [1, 2, ...]$) in the ILC system is [Bristow et al., 2006]

$$||Q(z)\,(1 - zL(z)P(z))\,||_\infty < 1, \tag{1.9}$$

where $P(z)$ is the complementary sensitivity function ($P(z) = (1+G(z)C(z))^{-1}G(z)C(z)$ for the serial structure). If $L(z)$ is chosen to be the inverse of the complementary sensitivity function and $Q(z) = 1$, then zero tracking error can be achieved after one trial with perfect model knowledge and repeatability. However, this choice is sensitive to model errors, and performance can be traded for robustness with $Q(z)$, which in most cases is designed as a low-pass filter. This choice is made because the model is usually well known for low frequencies and because the repeatable part of the disturbances are mostly contained in the low frequency range, and it is also desirable to attenuate high frequency noise. An alternative design approach is to produce Bode plots of the feedback control system and base the ILC design on this system description [Longman, 2000].

The simplest implementation of Eq. (1.7) is obtained when Q and L are diagonal matrices. The learning transfer functions $Q(z)$ and $L(z)$ can also be implemented as zero-phase noncausal filters to avoid phase lag [Longman, 2000, Bristow et al., 2006], and in general, when filters are used, it is necessary to extend the vectors to be filtered in both ends to avoid filter transients. There are also more advanced ILC schemes such as including a derivative term in the learning algorithm, higher order ILC, and time-varying ILC and different design techniques such as frequency domain, lifted framework, optimal, and robust methods [Bristow et al., 2006]. An interesting ILC design technique is proposed in [Helfrich et al., 2008] using calculations of repeatable-to-nonrepeatable ratios (RNR) for all frequencies contained in tracking error data from previous trials without ILC implemented. These values are calculated as

$$RNR(\omega) = 20log\left(\frac{|FFT\,[\bar{\mathbf{e}}]|^2}{\frac{1}{N_t}\sum_{j=1}^{N_t}|FFT\,[\bar{\mathbf{e}} - \mathbf{e}_j]|^2}\right), \tag{1.10}$$

where FFT denotes the fast Fourier transform, N_t is the number of trials in the analysis, and the repeatable error $\bar{\mathbf{e}}$ is given as

$$\bar{\mathbf{e}} = \frac{1}{N_t}\sum_{j=1}^{N_t}\mathbf{e}_j. \tag{1.11}$$

$RNR(\omega)$ is also the power of the repeatable signal versus the power of the nonrepeatable signal in dB. If it is larger than 0 at some frequencies, then there is potential for improvement of the closed-loop system, and the learning filter could be applied to these frequencies using, e.g., low- or band-pass filters.

A comparison of ILC and RC is made in [Longman, 2000]. Here it is shown that serial ILC and serial RC are essentially equivalent mathematically and that the stability condition given in Eq. (1.9) can be applied in both cases. However, there is an important difference in that ILC calculations are performed once at the end of each trial, whereas RC calculates the reference modifier in real time at each time step k. Some of the previous publications on discrete-time RC include [Tomizuka et al., 1989, Kempf et al., 1993]

where different designs of the serial type RC are discussed. The equivalence of the methods are also highlighted in [Wang et al., 2009] together with an ILC/RC literature survey and guidelines for choice of method. The outline of ILC and RC given above is not exhaustive. For further detail see [Longman, 2000, Bristow et al., 2006, Wang et al., 2009] and the references therein.

Simple PI(D) temperature controllers in buildings seldom perform well at all possible operating conditions because the system response is not linear, and the control is typically tuned only for a selected nominal situation or conservatively based on the worst case operating conditions; also the control parameters might have been reused from a similar system and not tuned properly in the first place [Underwood, 1999, Bi et al., 2000, Lim et al., 2009]. It is therefore investigated in this thesis if the potential use of the plug-in type serial ILC/RC can help improve the existing temperature control by utilization of the potential repetitiveness in load disturbances. Furthermore, the RNR calculation could help to design the learning-based control in a data-driven way rather than deriving complex models. Using a serial ILC/RC structure also means that the existing control is left unchanged and if the performance of ILC/RC is not living up to expectations, then it can easily be deactivated. Additionally, no modifications are necessary in the existing system, because it is only the setpoints that are changed. These proposed applications of learning-based control are outside the typical application areas and use of ILC/RC to improve temperature control in buildings or in supermarket refrigeration system has not been found in the literature. However, application of RC in building systems have been pursued in [Álvarez et al., 2013a], parallel to the work presented in this thesis. Here PI control is used to control the thermal comfort in a building quantified using the predicted mean vote (PMV). The controller and a model of the PMV is used to design a learning filter using the internal model principle. The results are very promising and indicate the hidden potential of utilization of learning-based control in buildings. However, the results are achieved with perfect repeatability in occupancy on a daily basis and it would be interesting to see the performance under more realistic load patterns.

Another potential use of learning-based control theory is to handle refrigeration system saturation, when the system is not dimensioned to cope with hot days. The idea is that yearly weather variations happens slowly and a learning control implementation could start to apply precool in the early colder hours of the day, to better cope with capacity limitations later in the hot hours of the day, based on the level of saturation in previous days. This could potentially provide a non model-based alternative to MPC. [Mishra et al., 2011] proposes an optimization-based constrained ILC scheme for constrained linear systems. However, this method only ensures that the ILC converges to the optimum within the imposed constraints. Changing the reference signal in an already saturated system does not help and the reference has to be altered in an anticipatory manner (precool). A learning law with a noncausal compensator (an upper triangular learning matrix L) could give precool before the error occurs. However, this precool would also be seen as an error causing stability issues. A tailored learning law for the precool problem is thus required.

1.3 Research Challenges and Hypotheses

In conclusion, non model-based single temperature sensor superheat control could involve utilization of increased variance close the the minimum stable superheat or the qualitative

s-shaped characteristic of the nonlinear relationship between valve opening degree and evaporator outlet temperature. Derivation of a general control method for systems having similar I/O-maps, where the maximum slope point is a suitable operating point, is additionally investigated in this thesis. Learning-based control utilizing repeatability in load disturbances could also provide a non model-based approach to application of precool in refrigeration systems to reduce potential saturation during peak loads or in general to improve performance of conventional PI and on/off hysteretic temperature control.

The broad objectives and the above discussion lead to the following six hypotheses:

1. The superheat in refrigeration system evaporators can be controlled using only a single temperature sensor with similar performance as existing controllers.

2. The proposed superheat control can be implemented on existing systems in a plug and play fashion without a priori system knowledge.

3. A general non model-based control solution can be derived for systems where the nonlinearity in the I/O-map has s-shaped characteristics and where the maximum slope point is a suitable operating point.

4. Repetitiveness in load disturbances can be utilized to improve the temperature tracking performance of refrigeration systems.

5. The potential risk of deterioration of refrigerated foodstuff during hot summer days can be minimized by precooling the foodstuff in an anticipatory manner before the refrigeration system capacity goes into saturation.

6. The tracking performance improvement and precooling can be performed without additional hardware, predefined schedules, or system models using learning-based approaches.

1.4 Outline of the Thesis

The background, motivation, state-of-the-art, and research challenges are presented in Sections 1.1-1.3. Based on this, a division of the research work into two subject areas is made in the following two chapters. The subjects are; single temperature sensor superheat control using qualitative system knowledge (Hypothesis 1-3) and improvement of refrigeration system temperature control by utilization of daily repetitiveness (Hypothesis 4-6). A summary of the results and findings within these two research areas is provided in Chapter 2, which also contains a condensed list of contributions with reference to published and submitted papers. A conclusion on the work is then drawn in Chapter 3, which is followed by an outline of perspectives and recommendations. The thesis is written as a collection of papers, which are located in the contributions part. However, Chapter 2 can be read without having access to the papers. A short abstract of each paper is provided in the following to give an overview of the publications.

Paper A [Vinther et al., 2012a]

In this paper, a single temperature sensor superheat control is derived. The solution uses an inner loop to control the evaporator outlet temperature, while an outer loop

adjusts the reference by estimation of suction pressure and calculation of the sample variance, which increases at the minimum stable superheat. A startup tuning procedure is additionally proposed and tests are conducted on an air conditioning system and a water chiller system.

Paper B [Vinther et al., 2012c]
In this paper, a perturbation-based maximum slope-seeking (MSS) control method is proposed for a class of nonlinear systems having sigmoid function properties. The control is based on a harmonic analysis and adaptation of the perturbation amplitude is also proposed. The performance is compared with a basic slope-seeking controller through simulation on a Hammerstein system model.

Paper C [Vinther et al., 2012b]
In this paper, the proposed MSS control is applied to an air conditioning system and a water chiller system. Safety logic for fast detection of flooding is provided and results from 8 hour tests on the two system are presented, which include large disturbance steps and operation under different conditions.

Paper D [Vinther et al., 2013d]
In this paper, a general tuning procedure for the MSS controller is proposed and tested on the same systems as in Paper C, with the addition of a supermarket refrigeration system test setup. The obtained superheat with MSS control is also compared with conventional two-sensor control and TEV control. On/off hysteretic display case air temperature is also tested together with MSS superheat control.

Paper E [Vinther et al., 2013b]
In this paper, the tuning procedure from Paper D is fully automated and tests are performed on another supermarket refrigeration system using CO_2 as refrigerant.

Paper F [Vinther et al., 2013c]
In this paper, focus has been put on stating more rigorous assumptions about the class of systems MSS is intended for and stability and convergence conditions are derived. A method to find an upper estimate on the feedback gain is also provided and Monte Carlo simulations on different models with parameter uncertainty are used to demonstrate the robustness of the control method.

Paper G [Vinther et al., 2013a]
In this paper, a serial repetitive controller is added to the existing temperature control in an example office building simulation to improve the tracking performance. The repetitive controller is tuned based on calculation of repeatable-to-nonrepeatable ratios for each frequency in past data.

Paper H [Vinther et al., 2013e]
In this paper, a learning-based precool strategy is proposed to reduce the level of saturation in supermarket refrigeration systems when peak demands exceed the capacity. Tuning guidelines are also proposed and a suitable simulation benchmark is presented. The benchmark is then used to compare the performance with and without precool of foodstuff in a yearlong simulation.

Paper I [Vinther et al., 2013f]

In this paper, an extension of the results in Paper H is made. The repetitiveness of the refrigeration system load is demonstrated using data from a real supermarket and an additional precool strategy is proposed, where precooling is applied to the freezer section instead of the individual medium temperature display cases.

2 | Summary of Contributions

This chapter provides a summary of the contributions and results published or submitted in the nine referenced papers. Each research area is treated separately in Section 2.1 and 2.2 and a condensed list of contributions are finally given in Section 2.3.

2.1 Single Temperature Sensor Superheat Control Using Qualitative System Knowledge

Evaporator superheat can potentially be controlled with a single sensor by utilizing the qualitative system behavior. This section is based on Papers A-F and a short description of the different refrigeration system test facilities is first provided for reference when presenting results. Then variance-based superheat control is discussed, which is followed by presentation of MSS control and perturbation-based superheat control.

2.1.1 Description of Test Facilities

Four different refrigeration system test facilities have been used for test of superheat control methods; an air conditioning system (located at Aalborg University), a water chiller system (located at Aalborg University), a supermarket refrigeration system using R404A as refrigerant (located at Danfoss), and another supermarket refrigeration system using CO_2 (located at Danfoss). These systems therefore constitute a wide variety of setups.

A simplified schematic of the residential air conditioning system is shown in Fig. 2.1. The maximum cooling capacity is approximately 11 kW and a corresponding load can be applied to the cold room with electrical heaters. The system use refrigerant R410A and has a finned tube evaporator, a Danfoss Ecoflow valve (PWM controlled with a 10 second period), a scroll compressor, and a microchannel condenser unit.

A similar simplified schematic of the water chiller system is shown in Fig. 2.2. This system has an approximate maximum cooling capacity of 4 kW and water is circulated on the secondary side of the evaporator in a circuit with a 60 liter water tank, a pump, and a heater. The refrigerant is R134a and the system also consists of a scroll compressor, a condenser unit, and interchangeable expansion valves; either a stepper motor EEV or a thermostatic expansion valve (TEV).

The supermarket refrigeration system using refrigerant R404A is shown in Fig. 2.3. This system has a compressor rack with three compressors, a condenser unit, and four display cases; two open shelfs and two open gondolas. Each display case has a finned

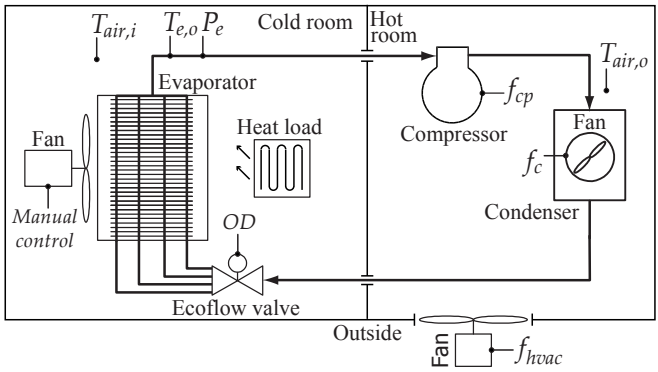

Figure 2.1: Simplified schematic of the air conditioning system using refrigerant R410A.

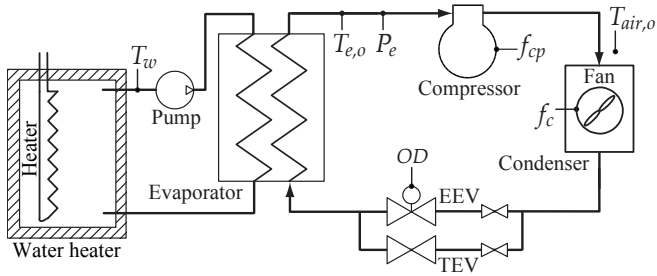

Figure 2.2: Simplified schematic of the water chiller system using refrigerant R134a.

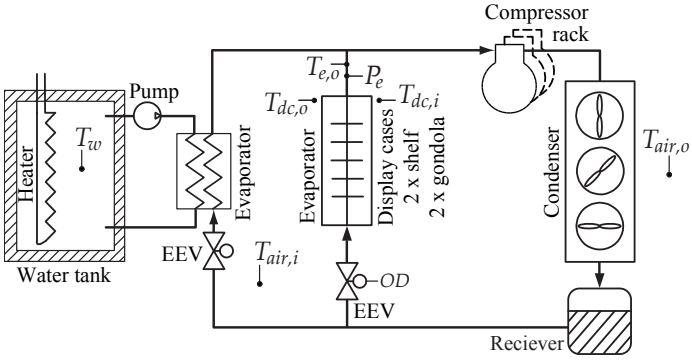

Figure 2.3: Simplified schematic of the supermarket refrigeration system using refrigerant R404A.

tube evaporator, an EEV valve (PWM controlled with 6 second period), a defrost heater, and a night cover/curtain. An additional water chiller load system can also be connected.

A simplified schematic of the CO_2 supermarket refrigeration system is shown in Fig. 2.3. This system has 2 medium temperature (MT) and 2 low temperature (LT) compressor units; one in each section is controlled by a frequency converter. The system also consists

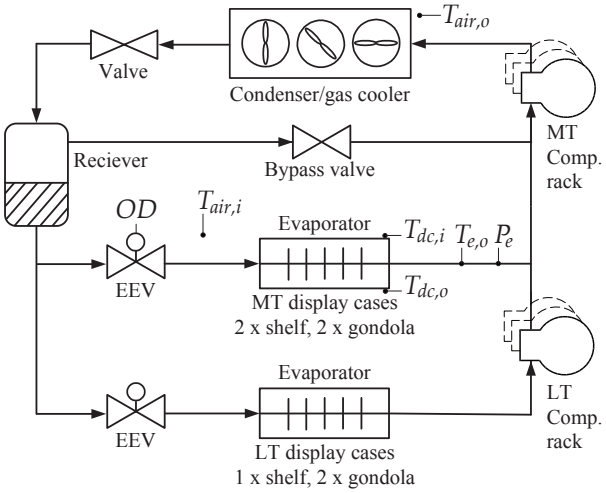

Figure 2.4: Simplified schematic of the supermarket refrigeration system using refrigerant R744 (CO_2).

of 7 display cases; 2 MT open shelfing units, 1 MT open gondola, 1 MT closed gondola, 1 LT closed shelfing unit, 1 LT closed gondola, and 1 LT open gondola. The thermal mass in the display cases is provided by ethylene- and propylene-glycol containers and foodstuff is emulated by blocks of tylose, with temperature sensors placed in the middle and on the surface, see Fig. 2.5.

Figure 2.5: MT open shelfing units with ethylene- and propylene-glycol containers (left) and tylose block with temperature sensors (right).

The air conditioning and water chiller systems are monitored and controlled with the Matlab XPC toolbox and the two supermarket refrigeration systems use MiniLog Software. Only some of the available sensors and control inputs are visualized in the figures. The sensors related to superheat control are sampled at 1 Hz and for further information see the individual papers or visit `www.es.aau.dk/projects/refrigeration/test-facilities/`.

2.1.2 Variance-Based Superheat Control

The proposed variance-based superheat control setup is illustrated in Fig. 2.6. A PI controller in an inner loop tracks a reference setpoint for the evaporator outlet temperature $T_{e,o}$ and the reference setpoint $T_{e,o,ref}$ is adapted in an outer loop. A logic block continuously lowers the superheat reference $T_{sh,ref}$ using a ramp until the variance in $T_{e,o}$ exceeds an upper threshold σ^2_{high}. The superheat reference is then stepped back and ramped down again when the variance goes below a lower threshold σ^2_{low}. A step back in superheat reference is also made if the superheat reference goes below $1°C$. The evaporation pressure is simultaneously estimated by the opening degree OD and a linear gain c, which is adapted with the MIT rule each time the upper variance threshold is reached. The bottom graph in Fig. 2.6 also shows how the level of variance increases as the opening degree is slowly increased in an open-loop experiment. The highest variance is close to a low superheat (minimum stable superheat). The variance thresholds can be determined based on this open-loop experiment and a step test can be used to tune the PI controller.

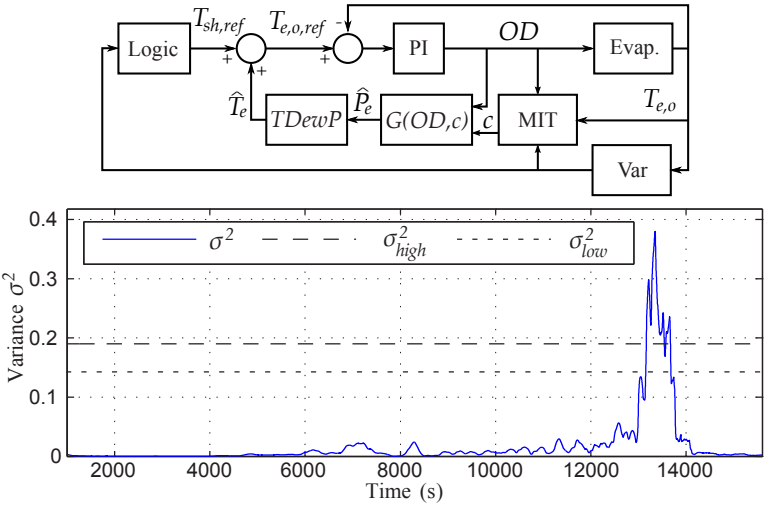

Figure 2.6: Variance-based superheat control (top) and calculated variance for different opening degrees based on an open-loop experiment (bottom).

Fig. 2.7 shows how the estimated superheat $\hat{T}_{sh}$ follows the measured superheat T_{sh} and how the superheat reference $T_{sh,ref}$ is continuously ramped down and stepped back, thus, effectively maintaining a low non-zero superheat in the evaporator. The first 1000 seconds is the initial startup phase and a disturbance in the room temperature $T_{air,i}$ is introduced at approximately 4000 seconds. For further detail see Paper A [Vinther et al., 2012a], which also contains results from the water chiller test facility.

The proposed solution is a simplification of the first observer based solution presented in [Lyhne & Sørensen, 2011], which also contains additional test results. An even simpler implementation has also been tested on the air conditioning and water chiller systems. This approach modifies the evaporator outlet temperature directly and does not estimate the pressure. One of the tests on the water chiller system is shown in Fig. 2.8. The con-

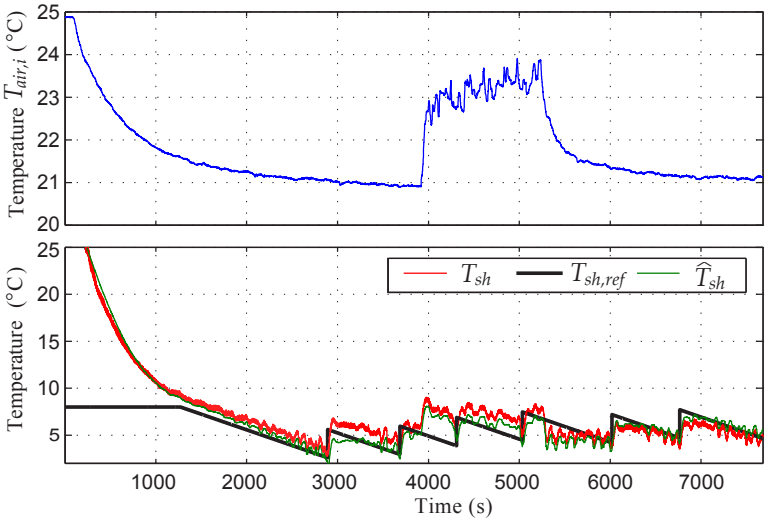

Figure 2.7: Closed-loop test on the air conditioning system using variance-based superheat control.

troller maintains the evaporator outlet temperature $T_{e,o}$ in between the surrounding water temperature T_w and the evaporation temperature T_e, without knowing these temperatures. The reference $T_{e,o,ref}$ is stepped back each time the variance exceed the threshold.

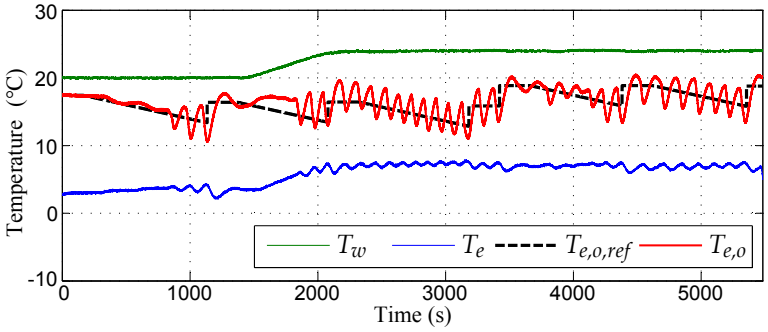

Figure 2.8: Closed-loop test on the water chiller system using variance-based outlet temperature control.

All the variance based controllers have shown to work close to the nominal operating conditions. However, the variance also depends on the amount and size of disturbances and the system gain, which varies with operating conditions. This means that it is difficult to determine a suitable variance threshold for all operating conditions. More advanced estimation of the pressure would also require additional knowledge such as compressor frequency and load. A more robust single-sensor superheat control solution is therefore needed, which has led to the development of the maximum slope-seeking (MSS) control scheme.

2.1.3 Maximum Slope-Seeking Control

Preliminary System Assumptions

System assumptions are outlined in the following, before going into detail with the MSS control. To simplify the analysis, only SISO systems are considered, which can be represented with a Hammerstein model structure given as

$$y(t) = (f_o \star f(u(\cdot)))(t) \tag{2.1}$$

where u is the input to the system, y is the output, $f(\cdot)$ is the static nonlinear function, $f_o(\cdot)$ is the function describing the output dynamics (having the Laplace domain transfer function $F_o(s) = \mathcal{L}\{f_o(t)\}$), and $\star$ is the convolution operator. The Hammerstein model structure is also illustrated in Fig. 2.9. Additionally, it is assumed that $f(\cdot)$ is either monotonically decreasing or increasing, time-invariant, smooth, and bounded within the input set $u \in U \subset \mathbb{R}$ under consideration. The first three derivatives with respect to u are also bounded and continuous, and f' is either non-negative or non-positive bell shaped with a unique extremum $(u^*, f(u^*))$ (maximum slope point) defined within U. The second derivative f'' therefore has a unique zero crossing. These are also sigmoid function properties and a monotonic decreasing I/O-map example is illustrated in Fig. 2.10. It is not strictly required that $f(\cdot)$ is time-invariant and smooth, but it is assumed here for simplicity. Finally, it is assumed that the output dynamics (described by $F_o(s)$) are linear, time-invariant, and asymptotically stable.

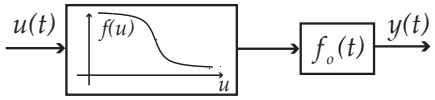

Figure 2.9: Hammerstein model structure.

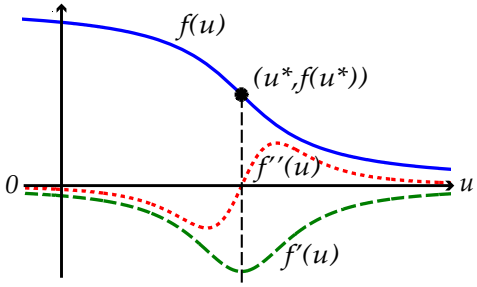

Figure 2.10: Qualitative I/O-relationship for a monotonically decreasing nonlinearity.

MSS Control Problem and Design

The proposed MSS control scheme is illustrated in Fig. 2.11 and it is intended for systems where the maximum slope point $(u^*, f(u^*))$ is a suitable operating point. The objective is therefore to make $\lim_{k\to\infty} \bar{u}(k) = u^*$, while only knowing that the system is qualitatively

defined by the assumptions given above. The unknown operating point $(u^*, f(u^*))$ is reached by continuous perturbation of the system using a sinusoidal signal $A_{ex}\sin(\omega_{ex}k)$, with amplitude A_{ex} and period defined by ω_{ex}. Curvature information is then extracted by sampling the output y using sample and hold (S/H) and a periodic FIR filter with the output

$$\xi(k) = \frac{2}{N}\sum_{n=k-N+1}^{k} y(n)\cos\left(2\omega_{ex}\left(n - N_\phi\right)\right), \tag{2.2}$$

where N_ϕ is an optional phase shift compensation given in samples and $N = \frac{T_{ex}}{t_s}$ is the number of samples in one perturbation period with sample time t_s (assumed sufficiently small compared to perturbation period).

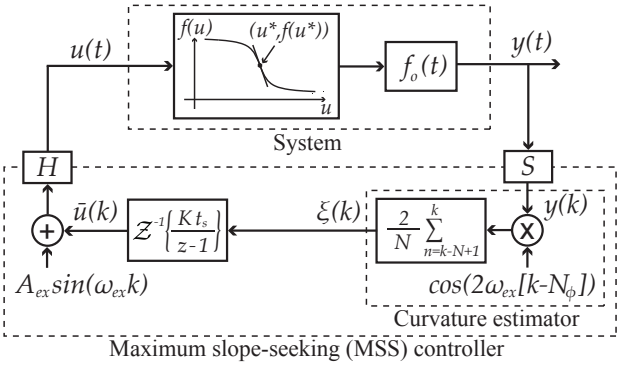

Figure 2.11: MSS control applied on a Hammerstein system.

The output y contains a steady state term and multiple harmonics of the perturbation signal due to the distortion caused by the system nonlinearity. Multiplication with a cosine term with the second harmonic frequency and summing over one period gives a filter magnitude response of zero for all the harmonics and only leaves a DC term. It has been shown in Paper F [Vinther et al., 2013c] that, for sufficiently small A_{ex} and K, the error signal approximately becomes

$$\xi(k) \approx -\frac{c_2 A_{ex}^2 f''(\bar{u})}{4}\cos(\phi - \phi_2), \tag{2.3}$$

where c_2 and ϕ_2 are the gain and phase shift caused by $F_o(s)$ at the second harmonic frequency and ϕ is given by the phase shift compensation N_ϕ. For a monotonic decreasing I/O-map ($f'(u) < 0$ for all $u \in U$, $c_2 > 0$) we have

$$\xi(k) = 0 \text{ for } f''(\bar{u} = u^*), \tag{2.4}$$

$$\xi(k) > 0 \text{ for } f''(\bar{u} < u^*), \tag{2.5}$$

$$\xi(k) < 0 \text{ for } f''(\bar{u} > u^*), \tag{2.6}$$

if we can ensure that the phase shift satisfies $|\phi - \phi_2| < \frac{\pi}{2}$ (can be achieved by picking ω_{ex} sufficiently small, i.e., slow perturbation compared to system dynamics). If the phase shift ϕ_2 is known it is also possible to compensate for it using N_ϕ.

Distortion of the perturbation is illustrated for a simple static system in Fig. 2.12. The open-loop frequency content is calculated in three operating points using FFT analysis and it shows that the second harmonic disappears at the maximum slope point, where there is zero mean curvature (see also Paper B [Vinther et al., 2012c]). The properties of the error signal $\xi(k)$ given in Eq. (2.4)-(2.6) are also illustrated in Fig. 2.12.

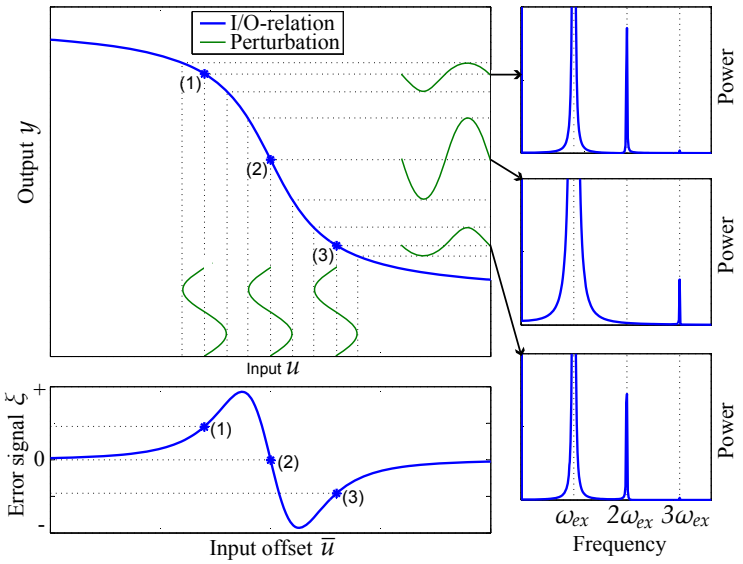

Figure 2.12: Distortion of the input signal in three operating points and error signal ξ for different input offsets $\bar{u}$.

The error signal $\xi(k)$ in Eq. (2.3) is a good estimate of the curvature if $\phi \approx \phi_2$ and if it is scaled by $-\frac{4}{c_2 A_{ex}^2}$. However, we are only interested in the sign change of $\xi(k)$ in MSS control and a discrete integrator $C(z) = \frac{Kt_s}{z-1}$ is added in the feedback loop to drive the input offset $\bar{u}(k)$ towards u^*. Low frequency content is added to the input signal when $\bar{u}(k)$ is changed in closed-loop. However, this low frequency content will be filtered away by curvature estimator if it is well separated from $2\omega_{ex}$. This can be ensured by choosing a sufficiently small feedback gain K and the sign of K should also match the system under consideration. A positive K is required in the example given above with a monotonic decreasing static nonlinearity and $c_2 > 0$. Finally, note that MSS control will converge to the zero mean curvature point, which will be offset from the maximum slope point if the I/O-map is not symmetric around this point. However, the offset is limited by the amplitude of the perturbation A_{ex}, which can be chosen small (but should be large enough to overcome noise). Additional detail on stability and convergence can be found in Paper F [Vinther et al., 2013c].

Upper Bound Estimate on the Integral Gain

The above analysis only states that a stabilizing feedback gain K exists. A method to get an estimate of the upper bound on K is therefore derived in Paper F [Vinther et al.,

2013c]. An outline of the result is that the FIR filter is periodic and that stability can be analyzed by deriving a monodromy matrix $\Psi_A(k)$ for the closed-loop system for one period T defined as

$$\Psi_A(k) = \mathbf{A}(k+T-1)\mathbf{A}(k+T-2)...\mathbf{A}(k), \tag{2.7}$$

where $\mathbf{A}(k) \in \mathbb{R}^{n\times n}$ is the state transition matrix at time index k. A well known result for such systems is that the eigenvalues of the monodromy matrix do not depend on k and that the system is stable if and only if the characteristic multipliers (eigenvalues) of the monodromy matrix are contained within the open unit disc [Bittanti & Colaneri, 2000]. Furthermore, marginal stability is in general obtained if and only if the eigenvalues are contained within the closed unit disc, and further, any eigenvalue on the unit circle is semi-simple [Horn & Johnson, 1985].

Since the desired operating point $(u^*, f(u^*))$ is where the gain in the system is highest (critical point), we can eliminate the static nonlinearity by replacing it with the maximum gain. A requirement is then that $\bar{u}(0) = \bar{u}(k) = u^* \ \forall k > 0$ in the closed-loop system with the perturbation set to zero ($A_{ex} = 0$). This can be satisfied by choosing a K where all the eigenvalues of the monodromy matrix are contained within the unit disc. A higher K with eigenvalues outside the unit disc is not stable, when the perturbation amplitude is small, and limit cycles will occur since the system gain decreases away from u^*.

Simulation Examples

Convergence to the maximum slope point is shown in Fig. 2.13 using an example system with FOPDT dynamics. The input offset $\bar{u}$ converges to u^* and the response in the I/O-map ends up circling around the maximum slope point due to the continuous and intentional perturbation (with amplitude $A_{ex} = 2$). The chosen feedback gain K is just below the upper limit found with the monodromy matrix.

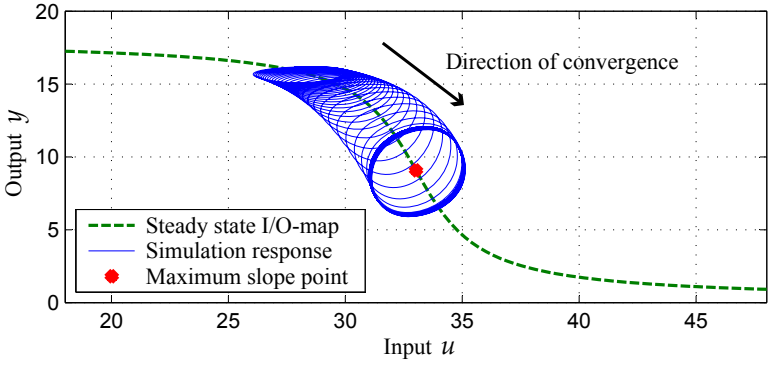

Figure 2.13: Convergence in an example system illustrated with an I/O-map.

Fig. 2.14 shows how limit cycles occur if the feedback gain K is chosen too large for the same system as in Fig. 2.13. The figure also shows how the input offset $\bar{u}$ jumps away from the maximum slope point in the unstable situation and that it does not converge back when the system is not perturbed ($A_{ex} = 0$).

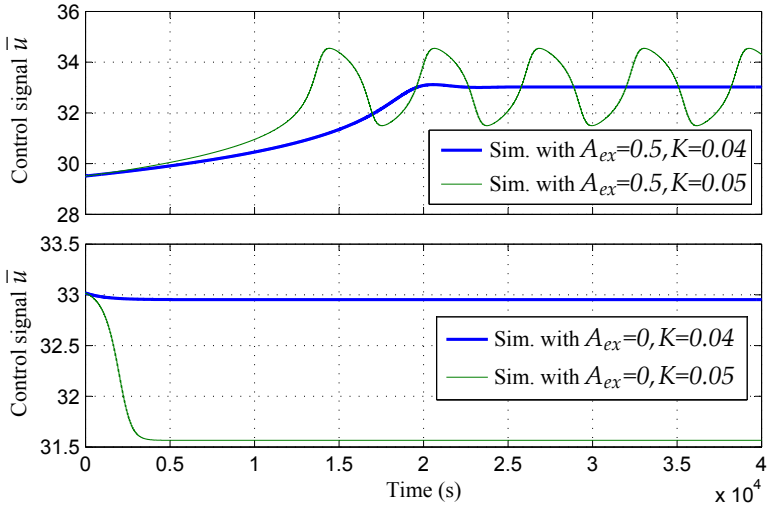

Figure 2.14: Response of the input offset $\bar{u}$ in a stable and an unstable situation.

Modified MSS for Systems with Dynamics

An uncompensated phase shift larger than 90 degrees will flip the sign properties of the feedback error signal $\xi(k)$ and cause divergence from the desired operating point. Choosing a slow perturbation and compensating with N_ϕ can help guarantee that this does not happen. However, the phase shift might not be known exactly and could be time-varying. Further, a conservatively chosen perturbation frequency will make the feedback loop slow. A modified MSS control setup is therefore introduced and shown in Fig. 2.15. The cross product between the first two harmonics is instead taken. The harmonics $H_p(k)$

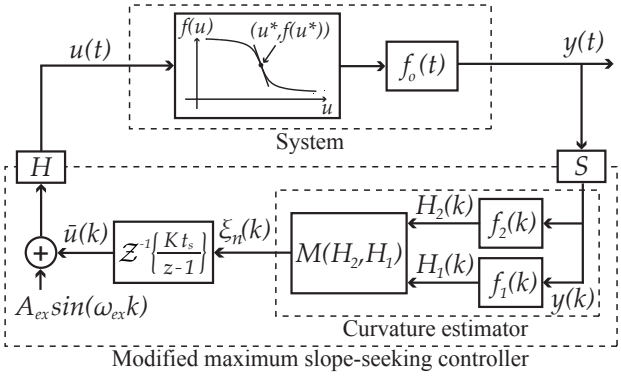

Figure 2.15: Modified MSS control applied to a Hammerstein system.

are calculated using periodic FIR filters as in Eq. 2.2;

$$\begin{aligned} H_p(k) =& \frac{2}{N} \sum_{n=k-N+1}^{k} \left(\cos\left(p\omega_{ex}\left(n-N_\phi\right)\right) - j\sin\left(p\omega_{ex}\left(n-N_\phi\right)\right) y(n)\right), \\ \equiv& a_p(k) - jb_p(k), \end{aligned} \tag{2.8}$$

with $p = \{1, 2\}$ being the number of the harmonic. The cross product is then defined as

$$M(H_1, H_2) = \frac{a_1(k)b_2(k) - a_2(k)b_1(k)}{\eta} = \frac{|H_1|\,|H_2|\sin(\theta_{12})}{\eta}, \tag{2.9}$$

where the angle from the first harmonic to the second is denoted θ_{12} and η is an optional normalization function. A similar expression as given in Eq. (2.3) can be derived for the modified MSS controller when A_{ex} and K are sufficiently small (see also Paper F [Vinther et al., 2013c]);

$$\xi_n(k) \approx \frac{c_1 c_2 A_{ex}^3 f'(\bar{u}) f''(\bar{u})}{4\eta} \cos(\phi_1 - \phi_2 + \phi), \tag{2.10}$$

where c_p and ϕ_p are the gain and phase shift at the harmonic in question caused by the output dynamics. The sign properties of $\xi_n(k)$ are the same as given in Eq. (2.4)-(2.6) for a monotonic decreasing I/O-map ($f'(u) < 0$ for all $u \in U$, $c_1 > 0$, $c_2 > 0$). The cross product ensures that only the uncompensated phase shift difference between the first and second harmonic needs to be less than ± 90 degrees. This is easier to fulfill, since these frequencies are only an octave apart, and the modified MSS control is therefore a more robust solution for systems with dynamics when compared with the implementation shown in Fig. 2.11.

The normalization η is optional, but gives a way to compensate for changes in system gain. The error signal in open-loop with different normalizations ($\eta_0 = 1$, $\eta_2 = |H_1(k)|^2$, $\eta_3 = |H_1(k)|^3$) is shown in Fig. 2.16 using the same simulation parameters as in Fig. 2.13. η_3 gives an almost linear relationship. However, tests have shown that η_2 works better in refrigeration systems as it weights the error signal less when the amplitude of the harmonics becomes small and thus better reflects the trust that can be put in the Fourier analysis, when noise and disturbances become significant compared with the output due to perturbation.

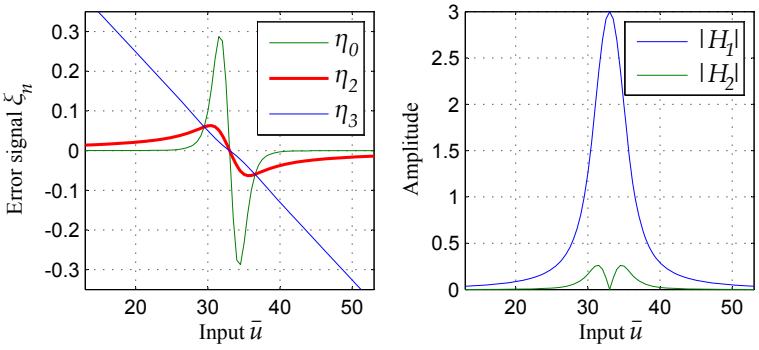

Figure 2.16: Normalized error and amplitude of harmonics as a function of input $\bar{u}$.

2.1.4 Perturbation-Based Superheat Control

MSS control can be used in a broad class of nonlinear systems that have I/O-maps with sigmoid function properties (s-shaped) and where the maximum slope point is a suitable operating point. It is originally intended as a solution to the single-sensor superheat control problem in refrigeration systems and the proposed implementation for superheat control is illustrated in Fig. 2.17. The method exploits the qualitative characteristic of the I/O-map between input opening degree OD and evaporator outlet temperature $T_{e,o}$, which slowly decreases when OD is increased and then suddenly drops fast and then flattens out when the evaporator floods. The fast drop happens near the minimum stable superheat, which also corresponds to a good utilization of the evaporator (good amount of liquid refrigerant in the evaporator). The modified MSS controller shown in Fig. 2.15 is therefore used to drive the input offset $\bar{u}$ towards the maximum slope point without knowing its location. Anti-windup is added to the integrator, since the opening degree OD is limited between 0-100%, and it is also important to act fast if the evaporator suddenly floods due to large disturbances. Safety logic is therefore proposed, which uses the amplitude of the first harmonic to detect if the perturbation signal suddenly becomes very small in the output, which could indicate a flooding situation.

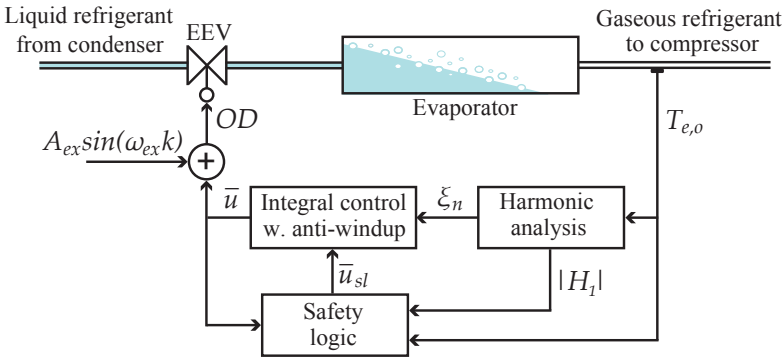

Figure 2.17: Proposed single-sensor evaporator superheat control setup.

The results within single-sensor superheat control are summarized in the following, which include analysis of the evaporator characteristics, automatic tuning of the MSS control, safety logic for fast flooding detection, and test results obtained from the four test facilities described in Subsection 2.1.1. Additional detail and test results can be found in Papers C-E [Vinther et al., 2012b, Vinther et al., 2013d, Vinther et al., 2013b].

Automatic Tuning of MSS Control

Fig. 2.18 shows the relation between input OD and output $T_{e,o}$ in the evaporator for three of the test facilities. The fitted sigmoid function indicates that all the evaporators qualitatively have the same behavior of the outlet temperature $T_{e,o}$; there are two horizontal asymptotes determined by the ambient temperatures and the evaporation temperature T_e, and a point where the temperature decreases fastest (maximum system gain). The exact shape of the I/O-map is dependent on the system operating conditions, e.g., the temperature of the asymptotes, and the fit shown in Fig. 2.18 is not valid for other operating

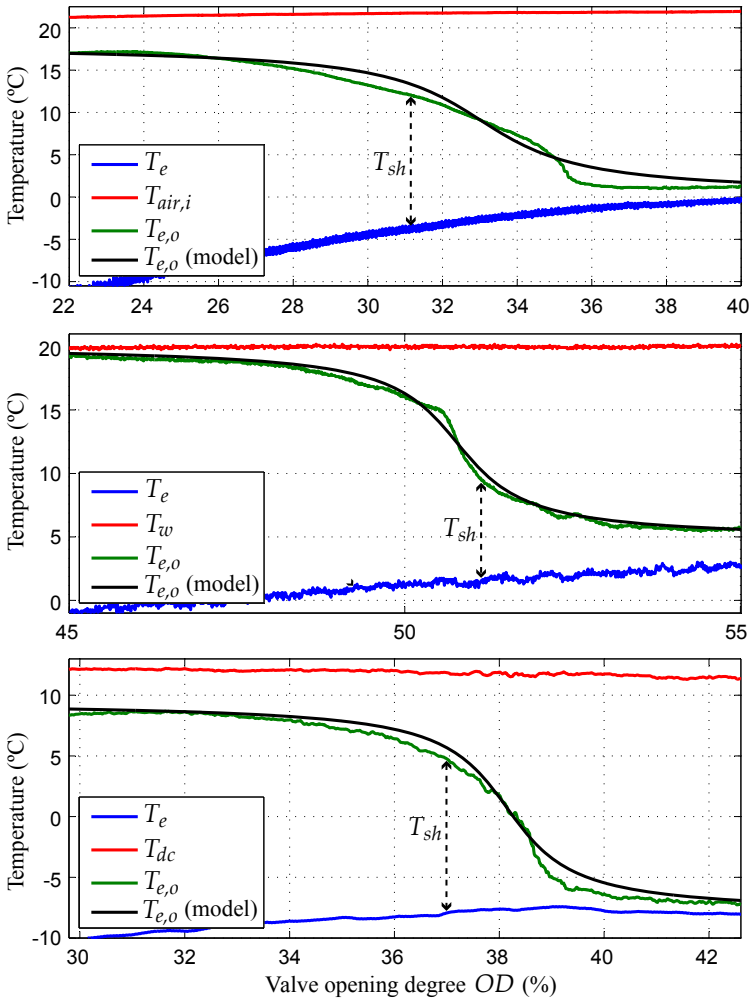

Figure 2.18: Temperature during a slow input sweep from low OD to high OD on the air conditioning system (top), water chiller system (middle), and a MT open shelf type display case in the supermarket refrigeration system using R404A (bottom). A sigmoid function is fitted to the $T_{e,o}$ measurements using a 2-norm.

conditions. However, the qualitative s-shaped relationship remains the same, which can be exploited with MSS control. Furthermore, system dynamics are not revealed in the OD-sweep tests and, as discussed in Subsection 1.2.1 and 1.2.2, the exact evaporator dynamics are quite complex, but can approximated by simpler FOPDT models depending on the level of detail required (see also [Izadi-Zamanabadi et al., 2012b]).

Test experience have shown that the Hammerstein model structure, with a static nonlinearity describing the changes in gain and a FOPDT describing the dynamics, can be used to derive a representative model of the response from OD to $T_{e,o}$ for tuning of the MSS controller. Automatic approaches to identifying this model are described in Paper

D and E [Vinther et al., 2013d, Vinther et al., 2013b] and outlined in the following.

The Hammerstein model is parameterized by a static nonlinearity

$$T_{e,o} = -k_1 atan\left(k_2\left(OD + OD^*\right)\right) + T_{e,o}^* \tag{2.11}$$

and FOPDT dynamic

$$F_o(s) = \frac{1}{(T_{sys}s + 1)} e^{-sT_d}, \tag{2.12}$$

where the gains k_1 and k_2, the maximum slope point (OD^*,$T_{e,o}^*$), the time constant T_{sys}, and the delay T_d can be identified using a simple ramp test and a biased relay feedback test. This procedure is shown in Fig. 2.19, which also shows the individual identified models described by Eq. (2.11) and (2.12). Further, a comparison between the combined Hammerstein model and the sinusoidal response close to the maximum slope point is shown in Fig. 2.20, which indicates a good model fit.

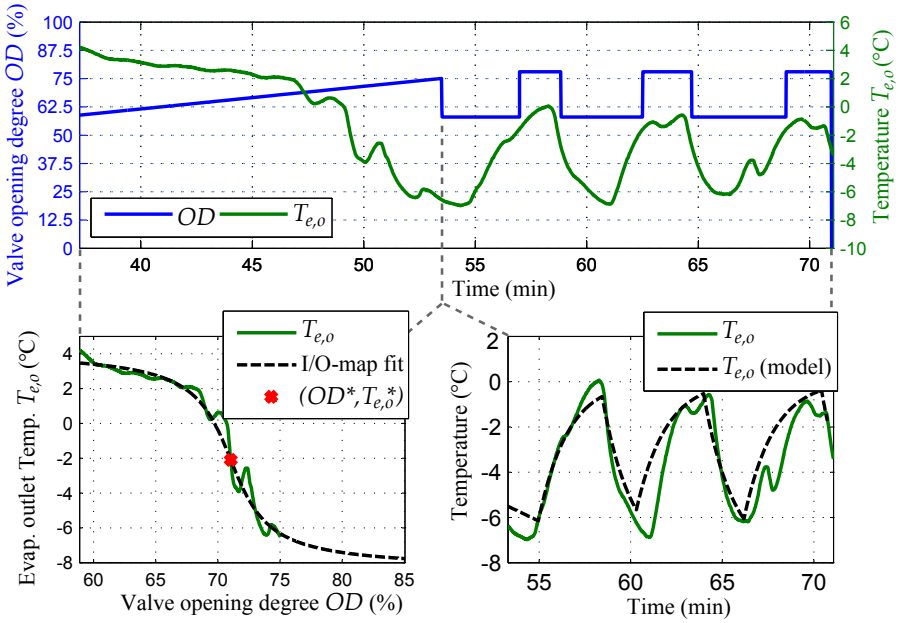

Figure 2.19: Ramp and relay feedback test on a MT open shelf type display case in the CO_2 supermarket refrigeration system.

More advanced identification of Hammerstein models for nonlinear systems can be found in, e.g., [Eskinat et al., 1991, Crama & Schoukens, 2001, Tan et al., 2012], and could involve the Matlab system identification toolbox and the $nlhw$ function. [Eskinat et al., 1991] also gives an example with a heat exhanger. However, only a rough parameter estimate is needed for tuning.

Ramp and relay feedback tests performed on the four refrigeration systems described in Subsection 2.1.1 have provided the model parameters presented in Table 2.1. Note that

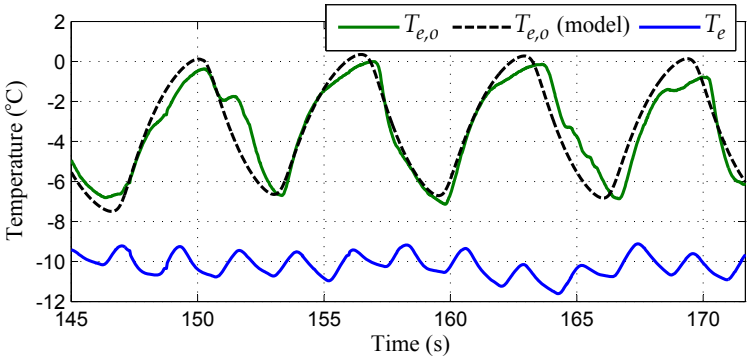

Figure 2.20: Measured and modeled evaporator outlet temperature $T_{e,o}$ with a sine input. The evaporation temperature T_e is also shown.

Parameter	Air con.	Water chiller	Display case (R404A)	Display case (R744)
k_1	5.68	4.89	5.59	4.02
k_2	0.50	1.31	1.07	0.44
OD^*	33.02	50.78	38.15	71.04
$T^*_{e,o}$	9.08	12.41	0.71	-2.10
T_{sys}	23.07	31.51	59.52	96.95
T_d	15	26	29	87

Table 2.1: Identified evaporator model parameters for the air conditioning system, water chiller system, and a display case in each of the supermarket refrigeration systems.

identification of OD^* and $T^*_{e,o}$ is only used to initialize the relay feedback test and not used in tuning of the MSS controller.

The parameters in MSS control are the perturbation period T_{ex}, the amplitude A_{ex}, the phase shift compensation N_ϕ, and the integral gain K. The perturbation signal should in general be slower than the system dynamics and a good choice of T_{ex}, based on test experience from different refrigeration systems, is between 3-5 times the system time constant T_{sys}, in order to also account for variation in parameters and model uncertainty. The choice of amplitude A_{ex} is not highly critical, but should in general give adequate perturbation of the output compared with the average noise level and disturbances. The identified model could be used to find an amplitude that approximately gives the desired perturbation near the maximum slope point. The phase shift compensation N_ϕ can be set to match the system delay T_d, which is relatively large in refrigeration systems and, if left uncompensated, would introduce a large difference in phase shift between the harmonics. N_ϕ could also include the phase shift caused by the first order dynamics. Finally, a suitable integral gain K can be determined based on the system model and the already chosen parameters (T_{ex}, A_{ex}, and N_ϕ). This can be done by iterating K in simulation until a prespecified performance criteria is met, e.g., overshoot less than 10%. Tuning is also discussed in Paper D and E [Vinther et al., 2013d, Vinther et al., 2013b] and the control parameters used in the tests are summarized in Table 2.2.

Parameter	Air con.	Water chiller	Display case (R404A)	Display case (R744)
N_ϕ	15	26	29	87
T_{ex}	120	130	180	388
A_{ex}	8.5	10.8	8.0	10
K	0.079	0.067	0.042	0.0285

Table 2.2: MSS Control parameters used in the tests presented in this subsection.

Exact knowledge of system parameters for controller tuning is not critical, which is illustrated using Monto Carlo simulations, see Fig. 2.21. The model parameters k_1, k_2, T_{sys}, and T_d have been varied randomly in a range of $\pm 50\%$ from the nominal values given in Table 2.1 in 100 simulations (same variation in dynamics is also suggested in [Izadi-Zamanabadi et al., 2012b]). All simulations, starting from random initial $\bar{u}$, conververged to the maximum slope point using the same control parameters in all tests. For further detail see Paper F [Vinther et al., 2013c].

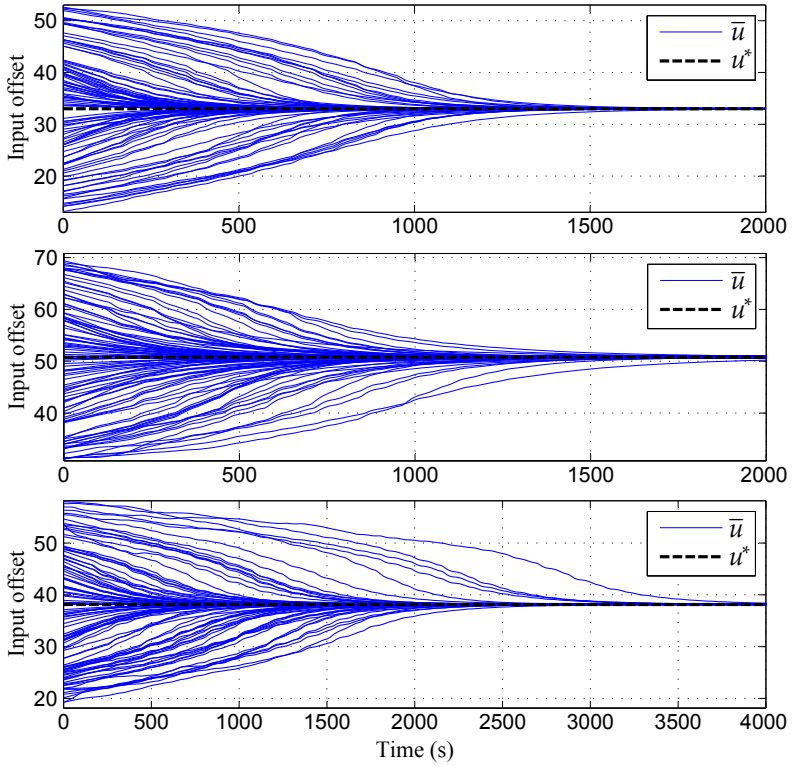

Figure 2.21: Time evolution of the input offset $\bar{u}$ in 100 individual simulations on the air conditioning system model (top), water chiller system model (middle), and display case model (R404A) (bottom).

Safety Logic for Fast Flooding Detection

The proposed safety logic for fast detection of flooding (overflow) situations in the evaporator is described using a flowchart in Fig. 2.22. The amplitude of the first harmonic $|H_1|$ is used as an indicator of healthy/unhealthy situations. If the amplitude is consistently low (e.g., for the duration of a perturbation period T_{ex}), then action should be taken and the opening degree is stepped back for safety reasons. A check is then made to see if the low amplitude was caused by a low flow (very high superheat) or an overflow situation (very low superheat) in the evaporator, which determines where the input offset $\bar{u}$ should start ramping up from. The amplitude $|H_1|$ will eventually become large as $\bar{u}$ increases and a switch back to MSS is then made.

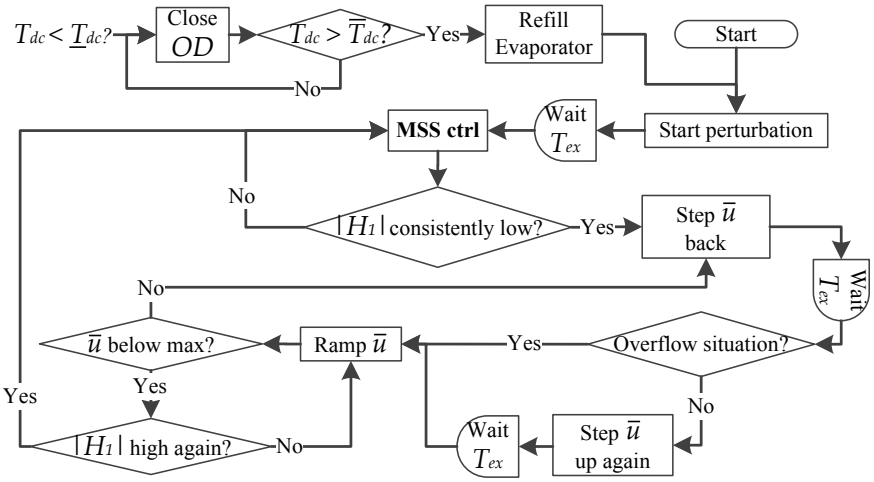

Figure 2.22: Flowchart describing the safety logic.

The air temperature in display cases T_{dc} is also maintained within a lower bound $\underline{T}_{dc}$ and an upper bound $\overline{T}_{dc}$ using hysteretic on/off control on the valve. This control overrides the superheat control and is shown in Fig. 2.22 as an interrupt. An additional algorithm is proposed after the off period (closed OD), which quickly refills the evaporator before MSS starts. More detail on the refill algorithm can be found in Paper E [Vinther et al., 2013b] and the safety logic is further described in Papers D and E [Vinther et al., 2013d, Vinther et al., 2013b].

Test Results

The single-sensor superheat control setup based on MSS, shown in Fig. 2.17, has been tested on four different refrigeration systems. Some of the test results, presented in Papers C-F [Vinther et al., 2012b, Vinther et al., 2013d, Vinther et al., 2013b, Vinther et al., 2013c], are highlighted in the following.

Fig. 2.23 shows a part of the result from a test conducted on a MT display case in the CO_2 supermarket system (see Fig. 2.5). Some of the data is also presented in Fig. 2.20 and the full test is presented in Paper E [Vinther et al., 2013b]. MSS control is started after an evaporator refill procedure and the evaporator outlet temperature $T_{e,o}$

quickly drops down to a too low value, due to a too high initial OD. The error signal ξ_n then becomes negative and the OD offset $\bar{u}$ is integrated down and stabilizes close to the maximum slope point at an average superheat of $7°C$.

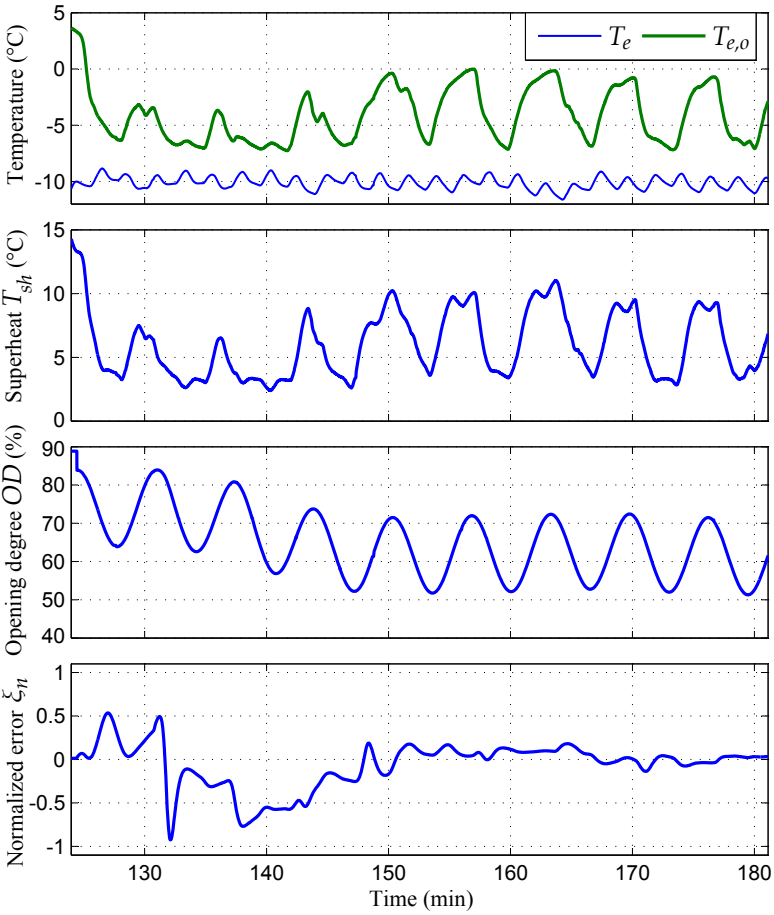

Figure 2.23: Single-sensor superheat control test result from a MT display case in the CO_2 supermarket system. The evaporation temperature T_e and superheat T_{sh} are not available in the control, but shown for verification purposes.

Fig. 2.24 shows the first 3.5 hours of a 8.33 hour test, presented in Paper D [Vinther et al., 2013d], conducted on the water chiller refrigeration system. The compressor frequency and heat load were varied according to the benchmark described in [Izadi-Zamanabadi et al., 2012b], in order to test disturbance rejection and operation under different conditions. The initial OD is too low and this is correctly detected as a low flow situation by the safety logic. OD is then ramped up and MSS control takes over after approximately 20 minutes. This convergence time is higher than what can be achieved with a TXV valve or conventional two-sensor control. However, it was done using only the evaporator outlet temperature measurement and, thus, without a pressure sensor. The

average superheat during the entire 8.33 hour test was 12.9°C (12.2°C without the first 20 minutes) with single-sensor MSS control and 12.68°C with the TXV valve (a lower average superheat setting with the TXV valve would give excessive valve hunting). The slightly higher superheat is due to the higher superheat during initialization and activation of the safety logic, which approximately gives a 15 minute period with higher superheat. An example of safety logic taking over is shown 1.5 hour into the test, which is caused by a step down in load followed by a large step down in compressor frequency. This results in a low superheat and $\bar{u}$ is stepped back for safety reasons and ramped back up.

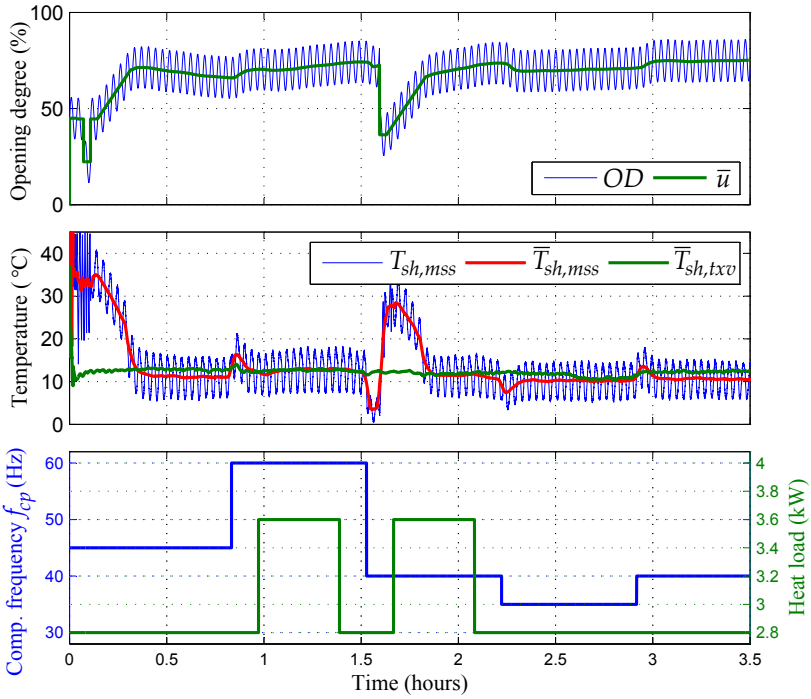

Figure 2.24: Single-sensor superheat control test result from the water chiller system. The superheat, compressor frequency, and heat load are not available in the MSS control and the obtained superheat from a separate test using a TXV valve is shown for comparison.

Fig. 2.25 shows two 2.5 hour tests conducted on a MT display case in the R404A supermarket refrigeration system. Both tests were conducted under approximately the same operating conditions and with the same initial conditions to be able to compare the superheat obtained with MSS control and with conventional two-sensor control. Furthermore, the night cover was up the first 1.5 hours and lowered from 1.5 to 2.5 hours. The conventional two-sensor control adapts the superheat reference based on the variance level as described in [Danfoss, 2008]. Two-sensor control therefore operates just above the minimum stable superheat, whereas the MSS control operates with an average superheat $\bar{T}_{sh,mss}$ close to the maximum slope point at a lower superheat, which gives a higher utilization of the evaporator. For further detail see Paper D [Vinther et al., 2013d].

MSS single-sensor superheat control combined with hysteretic on/off display case air

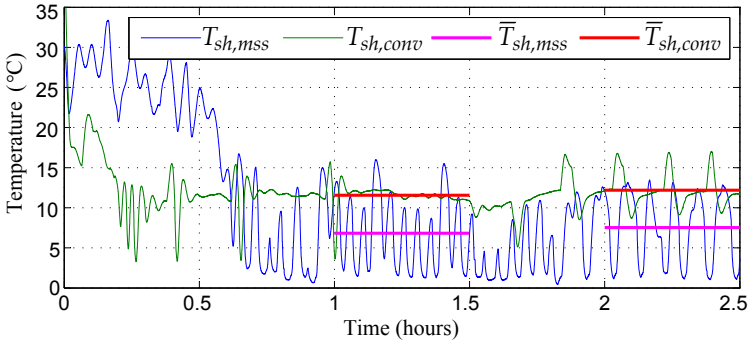

Figure 2.25: Obtained superheat using MSS control $T_{sh,mss}$ and conventional two-sensor control $T_{sh,conv}$ on the MT display case in the R404A supermarket refrigeration system. The two control methods have been tested separately with almost similar operating conditions and the results are overlayed sharing the same time axis.

temperature control is shown in Fig. 2.26. The display case air temperature T_{dc} is taken from an initial temperature of approximately $15°C$ to between the hysteresis limits of 0 and $5°C$ during the 4 hour test. The average superheat will be relatively high due to the on/off operation of the valve, but it is optimized during the on period. For further detail see Paper D [Vinther et al., 2013d].

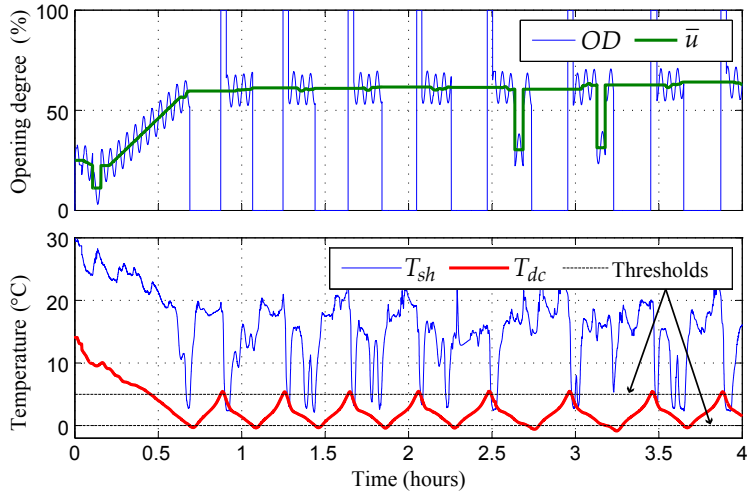

Figure 2.26: Combined superheat and air temperature control on a MT display case in the R404A supermarket refrigeration system.

In summary, the tests demonstrate that single-sensor evaporator superheat control based on MSS is possible and that the average obtained superheat is comparable or even lower than what can be achieved with conventional two-sensor control. However, the single-sensor solution is not as fast during initial startup and require continuous perturba-

tion of the system.

2.2 Improvement of Refrigeration System Temperature Control by Utilization of Daily Repetitiveness

Repetitiveness in load patterns and learning based control can potentially be utilized to improve the existing temperature control in refrigeration systems. Two different cases are investigated in this thesis; repetitive control for building HVAC systems and learning-based precool strategies for supermarket refrigeration systems. The contributions and obtained results within these subjects, presented in Papers G-I [Vinther et al., 2013a, Vinther et al., 2013e, Vinther et al., 2013f], are summarized in the following.

2.2.1 Repetitive Control in Building HVAC Systems

Building Simulation Model

An example single-zone office building simulation model is derived in Paper G [Vinther et al., 2013a], to be able to evaluate and compare the performance of the designed controllers under the same operating conditions over longer periods of time (e.g., a year). The model is based on the 3R2C modeling framework, see Fig. 1.10, and has the discrete state space model representation

$$\begin{bmatrix}\mathbf{T}_w \\ T_z\end{bmatrix}(k+1) = \begin{bmatrix}\mathbf{A}_{ww} & \mathbf{A}_{wz} \\ \mathbf{A}_{zw} & A_{zz}\end{bmatrix}\begin{bmatrix}\mathbf{T}_w \\ T_z\end{bmatrix}(k) + \begin{bmatrix}\mathbf{0} \\ B_z\end{bmatrix}\dot{Q}_{hvac}(k) + \begin{bmatrix}\mathbf{B}_{air} & \mathbf{B}_{gnd} & \mathbf{B}_{dw} & \mathbf{0} \\ 0 & 0 & \mathbf{0} & B_{dz}\end{bmatrix}\begin{bmatrix}T_{air,o} \\ T_{gnd} \\ \mathbf{d}_w \\ d_z\end{bmatrix}(k), \tag{2.13}$$

where $\mathbf{T}_w$ is a vector with the inner and outer wall surface temperatures, T_z is the zone temperature, $T_{air,o}$ is the outside air temperature, T_{gnd} is the ground temperature, $\dot{Q}_{hvac}$ is the HVAC heat transfer rate, $\mathbf{d}_w$ is a vector of lumped Long Wave Radiation (LWR) and Short Wave Radiation (SWR) heat transfers affecting each wall, and d_z is the thermal load on the zone. Finally, the matrices $\mathbf{A}_{ww}$, $\mathbf{A}_{wz}$, $\mathbf{A}_{zw}$, A_{zz}, B_z, $\mathbf{B}_{air}$, $\mathbf{B}_{gnd}$, $\mathbf{B}_{dw}$, and B_{dz} are derived from the resistances and capacitances in the 3R2C networks.

The disturbance inputs $T_{air,o}$, T_{gnd}, and $\mathbf{d}_w$ are derived for an entire year based on typical meteorological year 2 (TMY2) weather data for Phoenix, Arizona. This hot location requires mostly cooling, but also some heating during the winter months, and the weather profile has repeatability on a daily basis and changes seasonally. The disturbance load d_z on the $\approx$6000 m^3 office zone comes from body heat, appliances, and lighting. It is randomly generated each day based on five Gaussian probability density functions (PDF) governing how many people arrive for work, how many hours each person works, when each person works, when each person has lunch, and how long that person's lunch is. Furthermore, it is assumed that each person contributes with 0.6 kW heating when occupying the zone and 0.3 kW when the person is at lunch (the numbers include body heat together with each persons share of the total heat from appliances and lighting). The values are close to 0.63 and 0.37 kW used in [Zhou et al., 2005] and Fig. 2.27 shows d_z during four days in the simulation.

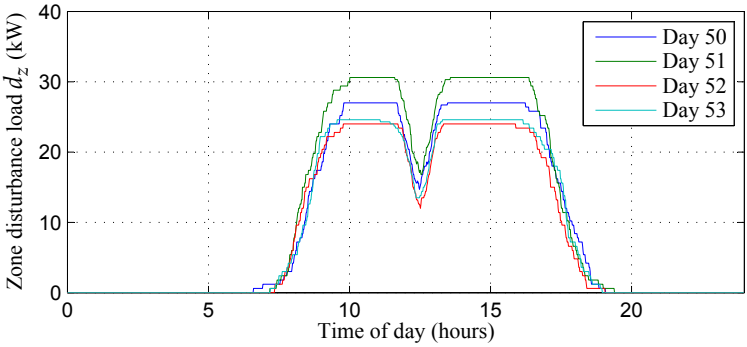

Figure 2.27: Randomly generated zone load during four days in the simulation.

The controllable input to the model is the HVAC heat transfer rate $\dot{Q}_{hvac}$, which is limited to the interval -35 to 17.5 kW. The zone temperature sample time and control update rate is set to 5 minutes, where typical values are between 1 to 15 minutes in buildings. This update rate is faster than the open-loop zone air temperature constant of about 27 minutes (wall temperatures are much slower) and assumed slow enough to allow the HVAC system to meet the desired heating/cooling demand before it is changed again. The objective is to maintain the zone air temperature T_z at a reference temperature $T_{z,r}$ by controlling $\dot{Q}_{hvac}$ and a PI feedback controller with anti-windup is therefore designed and added to the system. PI control is common in building system due to the intuitive and simple implementation. However, a fixed gain PI control will not work optimally in all operating conditions, because the extreme high and low load situations will determine how aggressively the control can be tuned.

Repetitiveness in Tracking Error Data

The described single-zone building model with zone temperature control is simulated for a year from 1st of January to 31st of December. The daily tracking error and repeatable-to-nonrepeatable ratio (RNR), calculated based on Eq. (1.10), are shown in Fig. 2.28. Large tracking errors occur when there is a quick change in load, e.g., when people meet for work, go to lunch, come back from lunch, and go home. The RNR also indicates that there is repeatability in the low frequency range. The frequency at the first two peaks in RNR correspond to the first and third harmonic of a square signal with a period of approximately 18 hours, which fit with the shape of the disturbance load. A few days also have a tracking error between 13 to 17 hours, which is caused by slight saturation of the HVAC system during the hottest days in the summer period. The repeatable pattern seen in the tracking error motivates the development of a learning/repetitive type control for improvement of the tracking performance.

Serial Repetitive Control Implementation

The proposed addition of reference modifying serial repetitive control (RC) to the existing feedback controlled zone temperature is shown in Fig. 2.29. The basic idea is to modify the reference/error seen by the inner controller C to get better closed-loop performance

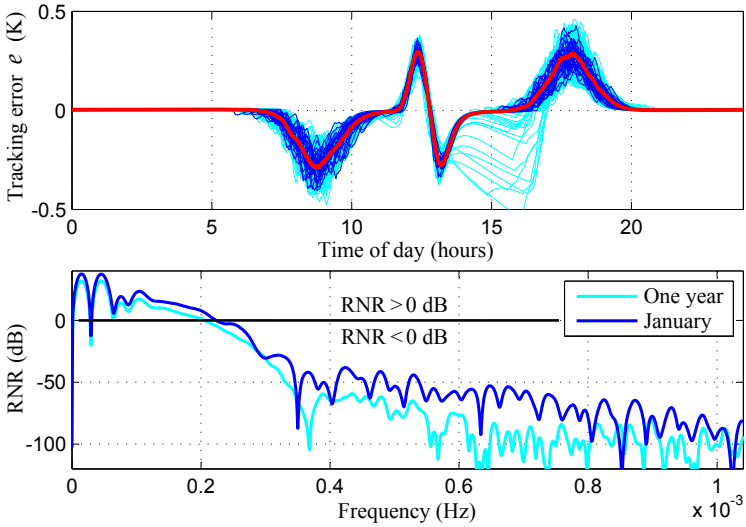

Figure 2.28: The top graph shows the daily tracking error e during January (blue), the repeatable error calculated with Eq. (1.11) for January (red), and the daily error for an entire year (cyan). The bottom graph shows the RNR based on January tracking errors (blue) and the entire year (cyan).

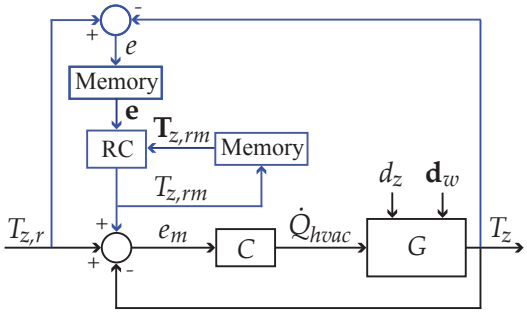

Figure 2.29: Proposed addition of serial RC (blue) to the existing temperature controller and system (black).

of the original error e. This is achieved by modifying the zone temperature reference $T_{z,r}$ with the RC block using a vector of past errors $\mathbf{e} = [e(k-2N+2), ..., e(k-1), e(k)]$, a vector of past reference modifiers $\mathbf{T}_{z,rm} = [T_{z,rm}(k-2N+1), ..., T_{z,rm}(k-2), T_{z,rm}(k-1)]$, and learning filters L and Q. The output of the RC block for the next time step k is defined as

$$\hat{\mathbf{T}}_{z,rm} = Q(\mathbf{T}_{z,rm} + L\mathbf{e}), \tag{2.14}$$

$$\hat{\mathbf{T}}_{z,rm} = [\hat{T}_{z,rm}(1), \hat{T}_{z,rm}(2), ..., \hat{T}_{z,rm}(2N-1)], \tag{2.15}$$

$$T_{z,rm}(k+1) = \hat{T}_{z,rm}(N+1), \tag{2.16}$$

where $T_{z,rm}(k+1)$ is the updated version of the reference modifier used in the last trial/day (N samples back in time) to be applied in the next time step. $T_{z,rm}(k+1)$ is then saved in memory, and the error e goes to zero as the number of trials/days go to infinity if there is enough repetitiveness. Furthermore, vectors are used in the calculations because of the learning filters L and Q, which can be causal/noncausal filters with low-pass, band-pass, or high-pass characteristics depending on the frequencies where repeatability occurs.

Based on past tracking error data and the RNR calculations, e.g., from January, it is possible to choose an appropriate filter type and cutoff frequency for the learning filter L. Here, a noncausal low-pass filter implementation is used and designed based on the Matlab functions $butter$ and $filtfilt$. The Q filter can then be chosen to satisfy Eq. (1.9). This means that even though the learning-based approach is non model-based, a model is still needed in order to check for stability. However, it might be possible to base the analysis on identification of a simple generic FOPDT model. Modifying the reference is also not as critical as directly introducing a feedforward signal between the controller and the system using a parallel RC structure, as the inner closed-loop is already assumed to be asymptotically stable. For further detail on the proposed serial RC implementation and tuning see Paper G [Vinther et al., 2013a].

One Year Simulation Case Study

Data from January is used to tune the learning filter and the performance during the rest of the year is compared with control without RC in the following. Fig. 2.30 first indicates how the reference is modified by RC and continuously updated each day. Note how the shape of the modified reference is similar to the repeatable error in Fig. 2.28. Fig. 2.31 additionally shows the zone temperature for each day in March both with and without RC. The deviation from the reference $T_{z,r} = 22.5°\text{C}$ has been reduced with RC and the summed error using different norms, the total energy consumption, and the total energy charge in U.S. $ using a time-of-use tariff are outlined in Table 2.3. The total sum of the error is reduced by 52-67% depending on the norm with almost no change in energy charge cost and no additional hardware. The obtained result will of course depend on how

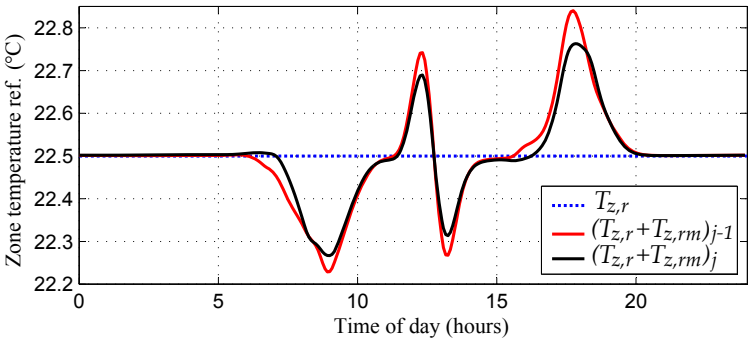

Figure 2.30: Original temperature reference $T_{z,r}$ and modified temperature reference $T_{z,r} + T_{z,rm}$ during the last two days/trials in the simulation (j denotes the trial number).

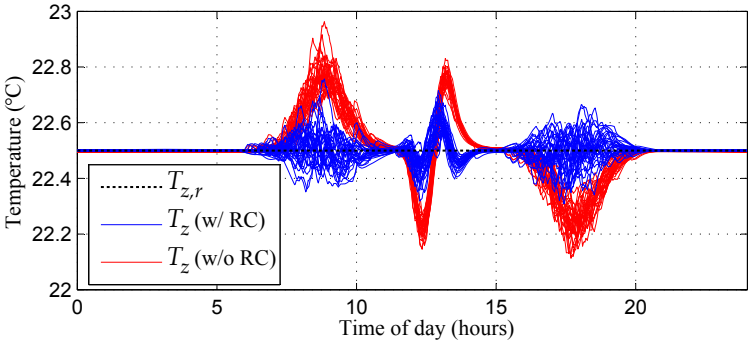

Figure 2.31: Zone temperature for each day in March with and without RC.

Table 2.3: Comparison of control with and without RC, based on simulation data from 1st of February to the 31st of December.

quantity	without RC	with RC	% improvement
$\sum_{j=1}^{334} \|\mathbf{e}_j\|_\infty$	115.28	55.43	51.91
$\sum_{j=1}^{334} \|\mathbf{e}_j\|_2$	1357.70	475.87	64.95
$\sum_{j=1}^{334} \|\mathbf{e}_j\|_1$	29037.42	9584.77	66.99
Total energy (kWh)	50612	50450	0.32
Total energy charge (U.S. $)	2926.31	2915.54	0.37

well the initial PI control is tuned, but RNR calculations, using past tracking error data, can be used to evaluate, if there is potential for improvement with learning-based control.

The few days with saturation during the summer period are still saturated. Modifying the reference does not help if the system is already saturated and shifting the error to base the modification of the reference on future errors in order to precool the system will give oscillatory behavior, since the precool period will also be seen as an error and introduce modification of the reference even earlier in the opposite direction and so forth. Alternative learning-based strategies are therefore required in order to handle saturation in refrigeration system capacity better using precooling to shift the peak load.

2.2.2 Learning-Based Precool Strategies

Repetitiveness in Supermarket Refrigeration System Load

The repetitiveness in the load has been investigated using data from a medium sized Danish supermarket refrigeration system. This system is similar to the CO_2 supermarket refrigeration test facility described in Subsection 2.1.1 and the main components of the refrigeration system are seven medium temperature (MT) storage evaporators, four low temperature (LT) storage evaporators, two compressors for the MT storages, two compressors for the LT storages, a bypass valve (BP), a gas cooler/condenser, and a receiver. The supermarket is open every day between 8 am and 9 pm and data is sampled every 60 seconds. Filtered compressor work $\dot{W}_{cp}$, cooling load $\dot{Q}$, and valve opening OD from

six consecutive days from 18th of September 2011 are shown in Fig. 2.32. A high in-

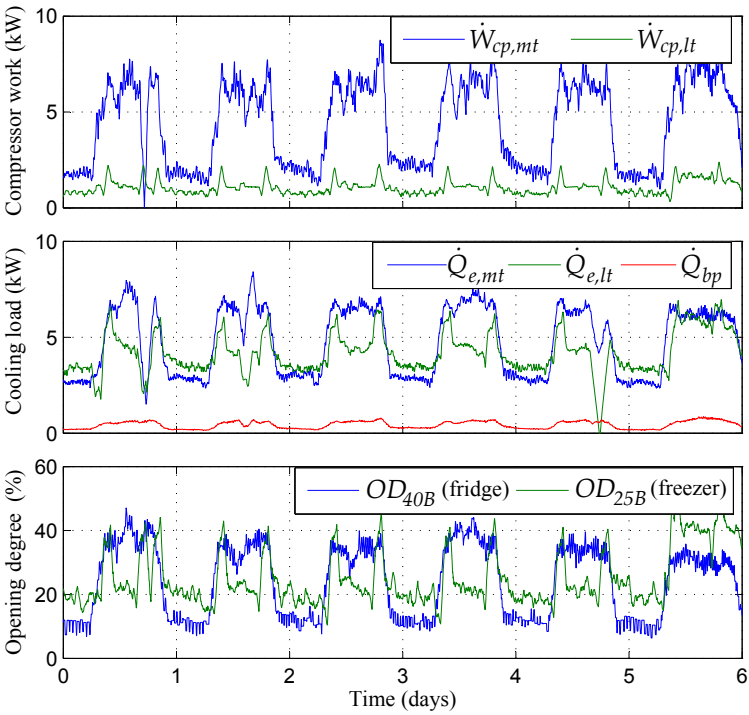

Figure 2.32: Low-pass filtered data from a medium sized supermarket showing the estimated work of the compressor racks (top), the estimated cooling loads (middle), and the opening degree OD of a fridge and a freezer display case (bottom).

crease in load is seen during the opening hours of the supermarket, which results in a repeatable pattern on a daily basis. The MT fridge section with four open shelf type display cases shows the highest repeatability and if the refrigeration system saturates, it will most likely occur during the opening hours in the middle of the day on hot summer days. Further detail can be found in Paper I [Vinther et al., 2013f].

Supermarket Refrigeration System Simulation Model

A supermarket refrigeration system simulation model is presented in Paper H [Vinther et al., 2013e]. The purpose of the model is to simulate the dynamics of the air and foodstuff temperature in display cases and potential saturation of the compressor racks due to high cooling loads and outdoor air temperature. The model therefore provides a benchmark to compare different precool strategies.

The model simulates four MT storages with hysteretic control on the air temperature T_{dc}, a suction manifold that connects all the mass flows, and a MT compressor rack that controls the suction pressure. The temperature corresponding to the condensation pressure is set five degrees above the outdoor temperature and it is assumed that the condenser dynamics and condenser pressure control are fast and negligible compared with

the rest of the system. Compressor capacity limitations and yearlong TMY2 weather data are then used to simulate hot days with high condenser pressure and corresponding higher load on the compressors. An increased load during the supermarket opening hours, where the night covers are up and customer activity is higher, is simulated by increasing the overall heat transfer coefficient between the air in the supermarket $T_{air,i}$ and the average display case air temperature $T_{dc} = \frac{1}{2}T_{dc,i} + \frac{1}{2}T_{dc,o}$. The resulting cooling load $\dot{Q}_{e,mt}$ is approximately twice as high during the opening hours, which is comparable with the supermarket data shown in Fig. 2.32.

Fig. 2.33 shows the air and foodstuff temperature in the second MT display case with hysteretic control using the simulation parameters given in Paper H [Vinther et al., 2013e]. The valve is turned on when $T_{dc,2}$ reaches an upper threshold $\overline{T}_{dc,2}$ and turned off again when $T_{dc,2}$ goes below a lower threshold $\underline{T}_{dc,2}$. The dynamics of the foodstuff temperature are much slower than the air temperature dynamics and by lowering the thresholds it is possible to save thermal energy in the foodstuff in terms of "coldness".

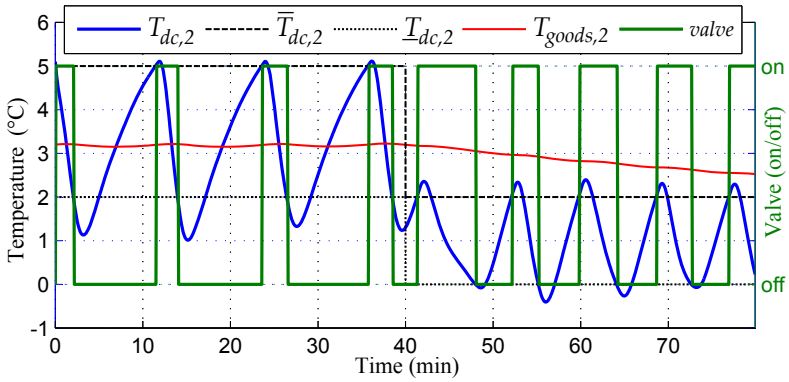

Figure 2.33: Display Case 2 air temperature controlled with hysteretic on/off control. A shift in temperature thresholds is made after 40 minutes.

The thermal storage potential in each display case will mainly depend on the type of food, the amount, and how it is packed. Different combinations of heat transfer coefficient and mass times specific heat are therefore simulated in each of the four cold storages. A step in the air temperature T_{dc} from 3.5 to 1°C is simulated and the time it takes the foodstuff temperature T_{goods} to reach 90% of the step is 166 minutes, for Display Case 1, 250 minutes for Display Case 2, 500 minutes for Display Case 3, and 300 minutes for the cold storage room. This is roughly the time it takes to precool each individual cold storage, and Fig. 2.34 shows average display case air temperature and foodstuff temperatures from a similar step test conducted on a MT open shelf type display case in the CO_2 supermarket refrigeration system test facility. The time it takes the foodstuff surface temperature $T_{goods,surf}$ to reach 90% of the step is roughly 350 minutes and the foodstuff core temperature $T_{goods,core}$ initially drops slower, but reaches 90% of the step in roughly the same time. The precool times in the simulation are chosen to be both faster and slower than this to simulate different situtions. The precool time for a closed MT gondola display case in the test facility was similarly identified to be approximately 475 minutes and a closed LT gondola display case had a precool time of 900 minutes.

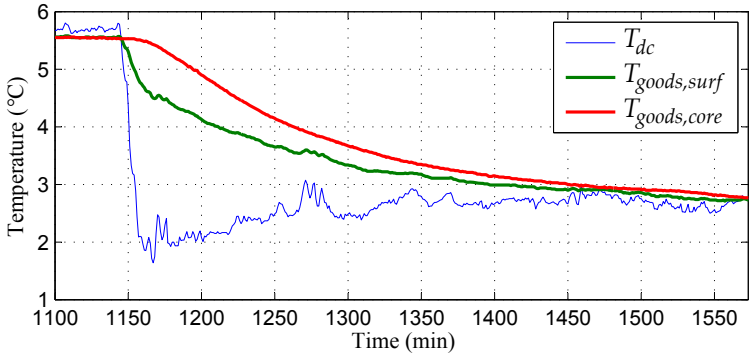

Figure 2.34: Display case food temperatures during a step in the air temperature on the CO_2 supermarket refrigeration system test facility. Temperature sensors on a tylose block are used to get the foodstuff temperatures, see Fig. 2.5.

Simulation of MT open shelf type display cases are thus considered to be the worst case scenario in terms of thermal storage potential.

Proposed Learning-Based Precool Strategies

The proposed learning-based precool strategy for hysteretic controlled display cases is illustrated in Fig. 2.35 using a trial domain notation, where j denotes the trial number.

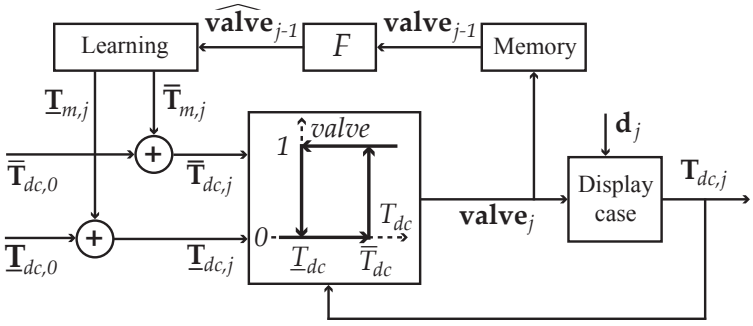

Figure 2.35: Proposed addition of learning-based precooling to hysteretic temperature control in display cases.

Each trial starts at midnight (or when the load is low) and lasts a day in the supermarket refrigeration system case. The objective is then to lower the baseline display case air temperature thresholds $\overline{T}_{dc,0}$ and $\underline{T}_{dc,0}$ when precooling is needed in an anticipatory manner based on the saturation in previous days. The saturation can be detected by low-pass filtering the vector of valve signals from the previous trial $\mathbf{valve}_{j-1}$ saved in memory to get $\widehat{\mathbf{valve}}_{j-1}$. If $||\widehat{\mathbf{valve}}_{j-1}||_\infty$ exceeds an upper threshold $\widehat{valve}$, then more precooling is needed to shift more of the peak load to less loaded hours. The precool time Δ is

recalculated for each trial and defined as

$$\Delta_j = \Delta_{j-1} + \delta_{j-1}, \tag{2.17}$$

$$\delta_{j-1} = \begin{cases} l_1\overline{\Delta} & \text{if } \left|\left|\widehat{\mathbf{valve}}_{j-1}\right|\right|_\infty \geq \overline{\widehat{valve}} \\ l_2\overline{\Delta} & \text{otherwise,} \end{cases} \tag{2.18}$$

where δ is the update to the precool time, $l_1 =]0, 1]$ is the learning gain, $l_2 = [-1, 0[$ is the de-learning gain, and $\overline{\Delta}$ is the maximum allowed precooling time. Further, the precool time is limited between 0 and $\overline{\Delta}$ and is

$$\Delta_j = \begin{cases} \overline{\Delta} & \text{if } \Delta_j > \overline{\Delta} \\ 0 & \text{if } \Delta_j < 0 \\ \Delta_j & \text{otherwise.} \end{cases} \tag{2.19}$$

The time when the precool should be applied during the day is parameterized by t_{end}, which can be the start of the longest saturation period in $\widehat{\mathbf{valve}}$. An alternative could also be to set t_{end} manually based on the supermarket opening hours, a time-of-use energy charge tariff, experience, etc. The threshold modifying vectors $\overline{\mathbf{T}}_m$ and $\underline{\mathbf{T}}_m$ are then set to zero outside the period of precool parameterized by Δ and t_{end} and to predefined precool thresholds $\overline{T}_m$ and $\underline{T}_m$ inside the precool period. $\underline{T}_m$ must be chosen so that $\underline{T}_{dc}$ is still above the hard constraints on the air temperature in the display case (e.g., 0 degree in MT display case). The full procedure is described in `ALGORITHM_1`.

Initialize $\Delta = 0$, $n = 0$, $\overline{\mathbf{T}}_m = \mathbf{0}$, $\underline{\mathbf{T}}_m = \mathbf{0}$, $t_{end} = 0$
Wait until midnight (start of new trial)
function ALGORITHM_1($valve$)
    if n has reached 24 hours of data **then**
        Reset n
        Filter **valve** to get $\widehat{\mathbf{valve}}$
        Find longest saturation period in $\widehat{\mathbf{valve}}$
        if system is saturated **then**
            Set t_{end} at start of long saturation period
        end if
        Update Δ according to Eq. (2.17), (2.18), and (2.19)
        Set $\overline{\mathbf{T}}_m = \mathbf{0}$ and $\underline{\mathbf{T}}_m = \mathbf{0}$
        Insert precool in $\overline{\mathbf{T}}_m$, $\underline{\mathbf{T}}_m$ using Δ, t_{end}, $\overline{T}_m$, $\underline{T}_m$
        Extend precool to include saturation period
    else
        Increment n
    end if
    Set new temperature thresholds in fridge display case: $\overline{T}_{dc} = \overline{\mathbf{T}}_{dc,0}(n) + \overline{\mathbf{T}}_m(n)$, $\overline{T}_{dc} = \overline{\mathbf{T}}_{dc,0}(n) + \overline{\mathbf{T}}_m(n)$
    Save **valve**$(n) = valve$
end function

The precool is extended to include the saturation period in order to keep the temperature in the display case low for as long as possible. Further detail on the proposed precool algorithms and tuning guidelines are provided in Papers H and I [Vinther et al., 2013e, Vinther et al., 2013f].

One Year Simulation Case Study

Three strategies have been simulated on the supermarket refrigeration system in Paper H [Vinther et al., 2013e]. The first strategy is simply to precool all the cold storages constantly by always having the air temperature thresholds on the low settings. The compressor rack has been dimensioned to exactly be able to keep the foodstuff temperature below the upper limit during the entire year using this strategy. The second strategy is not to precool at all. The third strategy is to use `ALGORITHM_1` in each of the cold storages to apply precooling more intelligently compared with constant precooling. Table 2.4 summarizes the results with the three strategies. The foodstuff temperature in Display Case 1 and 2 violated the upper temperature constraint in five and four days, respectively, if the foodstuff is not precooled. Further, a slightly lower average temperature in the display cases due to precooling also slows down bacteria growth. The energy charge cost based on the simulated compressor power and a time-of-use energy tariff showed an increase of 4.24% using constant precooling and only 1.21% using the precool algorithm. The kWh numbers are rough estimates, but the strategies are compared under the same conditions and the differences do indicate the advantage of the precool algorithm.

Table 2.4: Summary of case study results for simulation from 1st of January to the 31st of December with and without precool locally in each fridge.

Quantity	No precool	Variable precool	Constant precool
$T_{goods,1}$ above lim. (days)	5	0	0
$T_{goods,2}$ above lim. (days)	4	0	0
$T_{goods,3}$ above lim. (days)	0	0	0
$T_{goods,cs}$ above lim. (days)	0	0	0
Total energy (kWh)	54742	55401	57235
Energy charge (U.S. $)	3089	3126	3220

Fig. 2.36 shows foodstuff temperature in Display Case 2 with and without the precool algorithm during four hot summer days. The MT compressor capacity quickly saturates when the supermarket opens. This results in an increased suction pressure and the inability of the refrigeration system to keep the air temperature down. The increased air temperature affects the foodstuff, which as a result goes above the upper limit of 5°C. The foodstuff temperature is kept lower during the day when precool is applied, which shifts some of the load in the saturated period to the non saturated earlier hours. The maximum precool time is activated in the presented days, which brings the foodstuff temperature down to 1°C before the system saturates. The precool time Δ for each day in the simulation with variable precool is shown in Fig. 2.37. Maximum precooling is applied during the summer period as expected and removed again during the winter. Remark that the learning-based precool algorithm does not have a system model and does not know the weather, but continuously tries to find the least amount of precool that removes system saturation, just based on the saturation in the past days.

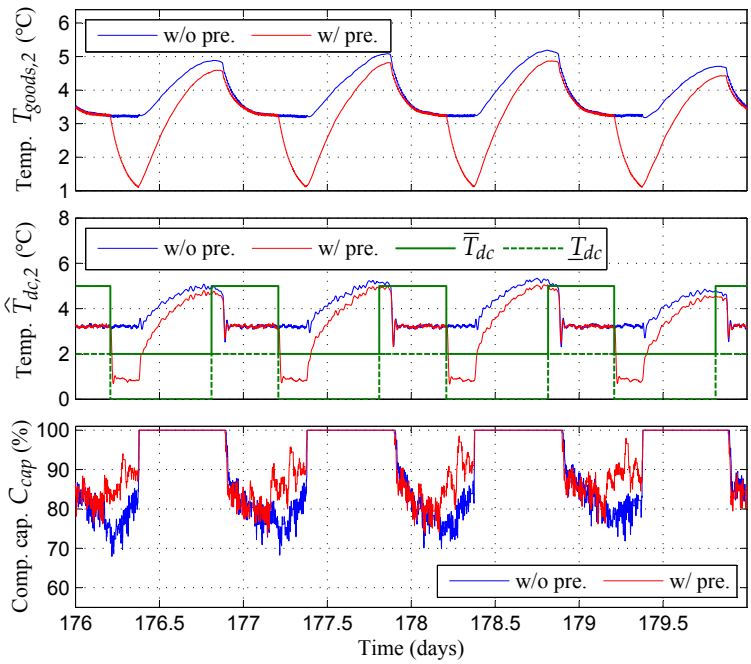

Figure 2.36: Foodstuff temperature and low-pass filtered air temperature in Display Case 2, together with MT compressor capacity, during four saturated summer days in the simulations without and with variable precool applied locally.

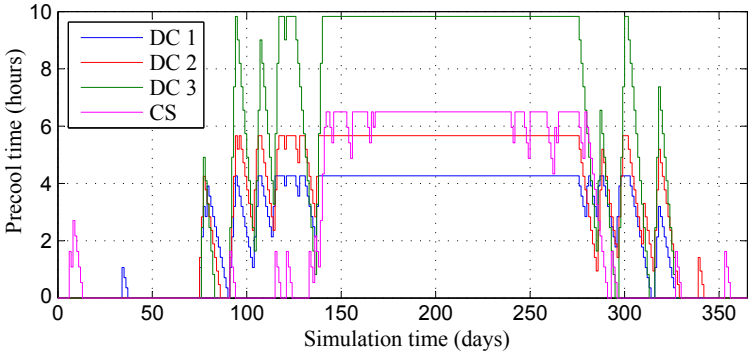

Figure 2.37: Precool time applied in the three display cases and in the cold storage room for each day in the simulation.

An alternative precool algorithm has been simulated in Paper I [Vinther et al., 2013f] where saturation in any MT cold storage results in precool in the LT freezer section instead. The precool period is not extended into the saturation period in this algorithm as the stored thermal energy in the frozen food should be "released" when the MT compressor rack saturation starts. Fig. 2.38 shows how the freezer foodstuff temperature $T_{goods,fr}$ is

lowered before the compressor rack saturates, which results in less saturation and lower maximum temperature in the MT display case.

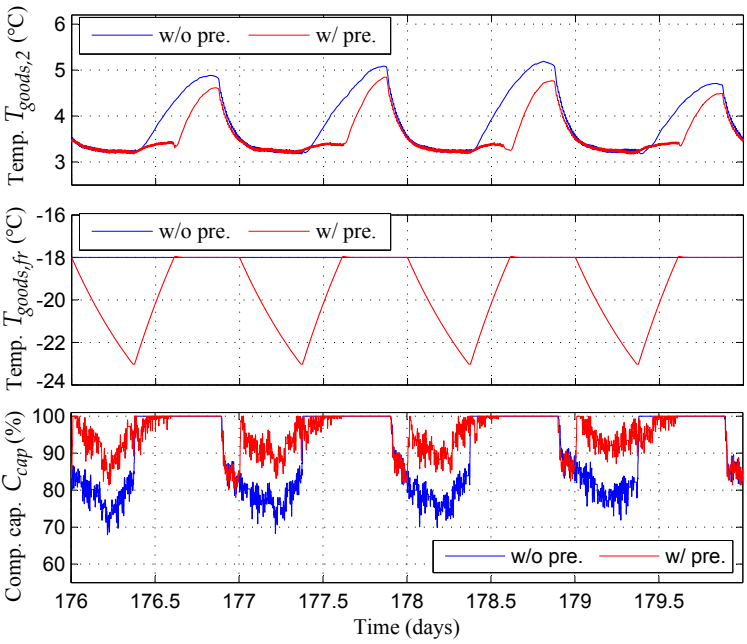

Figure 2.38: Foodstuff temperature in Display Case 2 and in freezers, together with MT compressor capacity, during four saturated summer days without and with variable precool.

Similar performance in terms of keeping the foodstuff temperature in the MT cold storages below the upper threshold is achieved with this precool strategy during the simulated year. Further, the result can be obtained with a relatively fast LT freezer section precool time of 420 minutes, which also means low capability of storing thermal energy for longer periods of time. In comparison, data from a LT freezer gondola in the CO_2 supermarket refrigeration system show a 900 minute precool time, which therefore has even higher thermal storage potential than the simulated case. Additionally, the simulation shows that reducing the refrigerant demand from the LT section during the saturation period, by precooling it before the saturation, can also reduce the load on the MT compressor rack in the saturation period and therefore potentially prevent violation of the upper temperature threshold in the MT display cases during hot summer days. The mass of the foodstuff in the MT and LT sections were similar in the presented case study, and the potential of this precool strategy will of course depend on the relative size of the MT and LT sections.

2.3 Paper Contributions

A short summary of the contributions, within the two research areas presented in this thesis, is given in the following with reference to the individual publications.

2.3.1 Single Temperature Sensor Superheat Control Using Qualitative System Knowledge

Contribution 1: Single-sensor superheat control

Single temperature sensor superheat control was first demonstrated in Paper A [Vinther et al., 2012a], where it is shown how measurement variance can be used to gain the missing information for control. Tests on two refrigeration systems also show the applicability of the method. However, the method relies on identification of a variance threshold, which can be sensitive to large changes in operating conditions, as the level of variance also changes. An alternative perturbation-based control scheme has therefore been developed (see Contribution 2), which utilizes the observed s-shaped qualitative behavior of the evaporator I/O-map. Additional safety logic for fast detection of flooding is derived in Paper C [Vinther et al., 2012b]. Multiple tests on four widely different refrigeration systems, presented in Papers C, D, and E [Vinther et al., 2012b, Vinther et al., 2013d, Vinther et al., 2013b], show the applicability of the method and the possibility of controlling the superheat without a pressure sensor. Tests presented in Paper D [Vinther et al., 2013d] demonstrate that a lower average superheat can be maintained compared with conventional superheat control with two sensors due to operation closer to the minimum stable superheat.

Contribution 2: MSS control

A novel MSS method for control of a general class of nonlinear systems has been developed. The method is inspired by slope-seeking control and relies on continuous perturbation of the system. Harmonic analysis is then used to drive the input offset towards the maximum slope point in the I/O-map and the method does not require specification of the maximum slope and can adapt to changes in the I/O-map. MSS was first presented in Paper B [Vinther et al., 2012c] and analysis of stability and convergence for Hammerstein systems is provided in Paper F [Vinther et al., 2013c].

Contribution 3: Plug and play solution

Methods to automatically tune the MSS-based single temperature sensor superheat control are proposed and successfully tested in Papers D and E [Vinther et al., 2013d, Vinther et al., 2013b]. The tuning procedure uses a simple ramp test and a relay feedback test to identify the important characteristics of the particular evaporator. Paper E [Vinther et al., 2013b] demonstrates that the code can be added to an existing system, in a plug and play sense, without a priori system knowledge.

2.3.2 Improvement of Refrigeration System Temperature Control by Utilization of Daily Repetitiveness

Contribution 4: Repetitiveness in refrigeration systems

Analysis of data from a medium size Danish supermarket in Paper I [Vinther et al., 2013f] demonstrate that there can be a high degree of repetitiveness in the load on the refrigeration system and that it is mainly caused by opening and closing of the supermarket. Simulations of a temperature controlled building in Paper G [Vinther et al., 2013a] also indicate that calculation of a repeatable-to-nonrepeatable ratio

for each frequency contained in past tracking error data can be used to reveal if there is potential for learning-based control.

Contribution 5: Repetitive control in building systems

A serial repetitive control scheme for improvement of temperature control in buildings is given in Paper G [Vinther et al., 2013a]. The non model-based method utilizes any potential repetitiveness in tracking error and simulations on a building model demonstrate that significant improvements in tracking error can be obtained. A tuning procedure is also outlined and the serial structure of the repetitive control allows implementation without modification of the existing control loops.

Contribution 6: Learning-based precool strategies

A learning-based precool strategy for display cases is proposed in Paper H [Vinther et al., 2013e]. Here, EEV valve saturation in previous days lead to precool of the foodstuff in an anticipatory manner. This reduces the potential risk of violation of temperature limits and deterioration of the foodstuff. Simulations show that precool is only applied if needed (e.g., during hot summer months) and the solution provides a more intelligent alternative to fixed precool schedules and does not require a system model or load estimation as in MPC solutions. Another strategy is also demonstrated in Paper I [Vinther et al., 2013f], where precool is applied to the freezers, due to their slower dynamics and better thermal storage capabilities, instead of locally in each medium temperature display case.

3 | Conclusions and Perspectives

3.1 Conclusions

The aim of the research presented in this thesis has been to find alternative data-driven control strategies for vapor compression cycle refrigeration systems that can improve the robustness and performance of the conventional decentralized control loops in these systems. Further, a focal point has been to provide solutions with a high plug and play potential and to keep the variable costs at a minimum. Finally, superheat control is the most critical control challenge in refrigeration systems, and temperature control is the main reason for having a refrigeration system. This has therefore resulted in research in single-sensor evaporator superheat control using qualitative system knowledge and learning-based improvement of temperature control by utilization of daily repetitiveness.

Tests have shown that the static relationship between expansion valve opening degree and evaporator outlet temperature has a nonlinear s-shaped curve with two horizontal asymptotes and a maximum gain/slope near the minimum stable superheat. The maximum slope point also corresponds to a high refrigerant filling in the evaporator and a suitable superheat level. This qualitative characteristic can be utilized for control purposes, and a novel maximum slope-seeking (MSS) control method has therefore been developed. The MSS method relies on continuous perturbation of the system. This generates higher harmonics in the output due to the curvature of the nonlinear I/O-map. Filters are then used to extract the harmonics, which can be used to drive the input offset towards the maximum slope point, where the mean curvature is zero. Conditions for stability and convergence have been provided for Hammerstein systems. Further, MSS could be seen as an extension to the general slope-seeking (SS) control method for systems where the maximum slope is a suitable operating point; SS will not be stable in this situation as the slope decreases on both sides of the maximum slope, and MSS does not require a reference slope setpoint as in SS.

Multiple tests with changing operating conditions on four widely different refrigeration systems have demonstrated that it is possible to control the superheat of the evaporator to a suitable level, using only a single temperature measurement combined with an electronic expansion valve. Further, this was achieved in all the systems with the same non model-based control implementation based on MSS. A comparison with conventional two-sensor control and with control with a thermostatic expansion valve have also shown that similar or even slightly lower average superheat can be maintained with MSS control due to operation closer to the minimum stable superheat. However, the MSS controller is slower than conventional control, because it relies on continuous perturbation of the

system, which should be slower than the system dynamics. Safety logic has therefore been implemented which can ensure fast reaction in case of evaporator overflow or low flow situations caused by large and abrupt changes in operating conditions. MSS is a non model-based control method, but does require initial tuning. Automatic tuning procedures have therefore been proposed for refrigeration systems based on identification of a simple Hammerstein model and has been tested on the four test facilities. Additionally, simulations are used to demonstrate the robustness of the control towards uncertainty in model parameter estimates. The proposed solution therefore introduces the possibility of reducing the variable costs or provides a fallback strategy in case of pressure sensor malfunction, thus, increasing the robustness.

On the topic of improvement of existing temperature control, it has been demonstrated that refrigeration systems could experience daily repetitiveness in load disturbances and temperature tracking error due to the repetitive nature of weather conditions, occupancy, opening hours, etc. A reference modifying serial repetitive control (RC) implementation on a simulated building has demonstrated the potential of learning-based control and provided a temperature tracking performance improvement of more than 50%. However, the gained improvement depends on the situation and on the limitations of the underlying refrigeration system, e.g., its ability to suppress quick changes in load. Calculation of the repeatable-to-nonrepeatable ratio (RNR) of the tracking error for each frequency can reveal how repetitive the error is, it can reveal if there is potential for learning-based control, and it can help tune the learning filters. The reference modifying serial setup also allows easy implementation in existing systems compared with adding feedforward signals directly between the existing control and the system. The RC implementation will also automatically adapt to seasonal weather changes, changes in occupancy patterns, and changes in reference setpoint and does not need knowledge of any of these. The potential use of learning-based control could, e.g., be extended to include processing facilities where tight temperature tracking might be even more important or where the tracking improvement can allow operation closer to an upper temperature constaint, which could save electricity costs by requiring less cooling.

Finally, hot summer days and higher load during opening hours might saturate the refrigeration system in supermarkets, which can lead to violation of temperature thresholds. Learning-based precool algorithms have therefore been developed. The idea is to use the repetitiveness in the load pattern and then precool the foodstuff in an anticipatory manner based on the saturation during the previous days. This can temporally shift some of the peak load by utilization of the thermal storage capability of foodstuff. The proposed algorithms adapts to changes in component performance, weather, customer behavior, and to some extend to component failure (compressor out for maintenance will start to trigger precooling in the following days if it causes saturation). Further, the algorithms could also provide an alternative to expensive overdimensioning of the refrigeration system and could provide an easier implementable alternative to model predictive control (MPC), which would require models of the specific system and load pattern. The simulation case study presented in this thesis demonstrated that upper temperature threshold violation could be avoided with precooling, and that the algorithm only applied precooling during the hot summer period. However, note that the precool algorithm only reduces the saturation and cannot guarantee that upper temperature thresholds are not violated in case of extreme saturation, but it is considerably better than not doing anything. Potential use of the precool algorithm could also extend to ice production, warehouses, refrigerated

transports, building air conditioning, etc. if there is sufficient repeatability in the load pattern.

In summary, and in line with the hypotheses, it has been demonstrated that superheat in refrigeration systems can be controlled with only a single sensor and a novel MSS control method has been developed for this purpose. Further, repetitiveness in load is seen in many refrigeration systems, and realistic simulations have demonstrated that learning-based control can potentially be utilized to improve temperature tracking performance and to reduce system saturation. Finally, both the proposed MSS control and the proposed learning-based control implementations are examples of data-driven control with a high potential for plug and play, since they can be implemented with very limited knowledge of the underlying system and do not require a system model for control or additional hardware.

3.2 Perspectives and Recommendations

Perspectives and recommendations on single-sensor superheat control and MSS:

- Preliminary tests have indicated that the proposed single-sensor superheat control and conventional two-sensor control are comparable in terms of COP. However, longer tests in a climate controlled chamber with power measurements would be required, before a conclusion can be made about any long term economic difference in the two methods. This would help determine if single-sensor control has potential as a replacement for conventional control or if it is more suited as a fall-back strategy in case of pressure sensor malfunction.

- Improvement of the periodic FIR filters in MSS for better extraction of harmonics could be investigated. This would possibly allow faster perturbation of the system, faster convergence, and faster detection of evaporator overflow situations. The MSS method could also be used as a building block for development of a more advanced single-sensor superheat control setup using both evaporator outlet temperature and the information provided by the air temperature sensor located in display cases. Further, the air temperature sensor could also be used to provide a faster and more precise automatic startup tuning procedure, as it can help reveal if the display case is cold or hot, when the tuning procedure is started.

- Conditions for stability and convergence are provided for MSS control applied to Hammerstein systems. It could be interesting to simulate MSS on more detailed evaporator models and expand the class of systems that can be controlled by MSS. In general, MSS could possibly be applied to other control loops in the refrigeration system if a monotonically increasing or decreasing s-shaped I/O-map can be identified.

Perspectives and recommendations on learning-based improvement of temperature control by utilization of daily repetitiveness:

- The design of the RC implementation could potentially be based only on previous tracking error data, i.e., without a model of the system. However, the stability check requires the complementary sensitivity function for the existing closed-loop

system. A stability check could alternatively be based on a simple generic model if the RC loop is tuned conservatively. Fast convergence in the trial domain is also typically not important when reference modifying serial type RC is used for improvement of an existing stable closed-loop system.

- Buildings might be used less during the weekend and supermarkets can have different opening hours in the weekend. This gives a different load pattern in weekdays compared with weekends. Individual learning algorithms could therefore be activated for weekdays and weekends, which would require development of appropriate switching.
- Analysis of the foodstuff quality and shelf life using precooling compared to letting the temperature exceed thresholds could be investigated further. A lower temperature due to precooling decreases bacteria growth, but might have a negative effect on water content, texture, color, etc.
- The time it takes to precool the foodstuff in each display case is individual and the maximum allowed precool time should be identified either based on experience or experiments. The foodstuff temperature is not measured directly, but the precool time can be revealed, when a step down in air temperature is made, by monitoring how long it takes the valve duty cycle to settle after the step, since this duty cycle first settles when the temperature of the foodstuff has settled. This could either be performed during initial startup or each day based on the previous precool cycle.
- Finally, it would be interesting to test the learning-based precool algorithms on some of the refrigeration system test facilities, e.g., by comparing the performance with and without precool in a situation with compressor saturation.

References

[Ash, 2005] (2005). *ASHRAE Handbook - Fundamentals (SI Edition)*. American Society of Heating, Refrigeration and Air-conditioning Engineers, Inc.

[Altwies & Reindl, 2002] Altwies, J. E. & Reindl, D. T. (2002). Passive thermal energy storage in refrigerated warehouses. *International Journal of refrigeration*, 25(1), 149–157.

[Álvarez et al., 2013a] Álvarez, J., Costa-Castelló, R., Castilla, M., & Camacho, E. F. (2013a). Repetitive Control to Counteract the Effect of People on Thermal Comfort Control. In *European Control Conference* (pp. 1187–1191). Zürich, Switzerland.

[Álvarez et al., 2013b] Álvarez, J., Redondo, J. L., Camponogara, E., Normey-Rico, J., Berenguel, M., & Ortigosa, P. M. (2013b). Optimizing building comfort temperature regulation via model predictive control. *Energy and Buildings*, 57, 361–372.

[Ariyur & Krstić, 2003] Ariyur, K. B. & Krstić, M. (2003). *Real-Time Optimization by Extremum-Seeking Control*. Wiley-Interscience.

[Åström & Hägglund, 1988] Åström, K. J. & Hägglund, T. (1988). *Automatic Tuning of PID Controllers*. Instrument Society of America.

[Åström & Hägglund, 1995] Åström, K. J. & Hägglund, T. (1995). *PID Controllers: Theory, Design, and Tuning*. Instrument Society of America, 2nd edition.

[Bi et al., 2000] Bi, Q., Cai, W., Wang, Q., Hang, C., Lee, E., Sun, Y., Liu, K., Zhang, Y., & Zou, B. (2000). Advanced controller auto-tuning and its application in HVAC systems. *Control Engineering Practice*, 8(6), 633–644.

[Bishop et al., 2011] Bishop, B. J., Moase, W. H., & Manzie, C. (2011). Gain Selection in Observer-based Extremum Seeking Schemes. In *18th IFAC World Congress* (pp. 114–119). Milan, Italy.

[Bittanti & Colaneri, 2000] Bittanti, S. & Colaneri, P. (2000). Invariant representations of discrete-time periodic systems. *Automatica*, 36(12), 1777–1793.

[Braun, 2003] Braun, J. E. (2003). Load Control Using Building Thermal Mass. *Journal of Solar Energy Enginering*, 125(3), 292–301.

[Bristow et al., 2006] Bristow, D. A., Tharayil, M., & Alleyne, A. G. (2006). A survey of iterative learning control. *IEEE Control Systems Magazine*, 26(3), 96–114.

[Broersen & van der Jagt, 1980] Broersen, P. M. T. & van der Jagt, M. F. G. (1980). Hunting of Evaporators Controlled by a Thermostatic Expansion Valve. *ASME Journal of Dynamic Systems, Measurement, and Control*, 102(2).

[Burns & Laughman, 2012] Burns, D. J. & Laughman, C. (2012). Extremum Seeking Control for Energy Optimization of Vapor Compression Systems. In *International Refrigeration and Air Conditioning Conference* Purdue, USA.

[Cai, 2007] Cai, J. (2007). *Control of Refrigeration Systems for Trade-off between Energy Consumption and Food Quality Loss*. PhD thesis, Section of Automation and Control, Department of Electronic Systems, Aalborg University.

[Cai et al., 2008] Cai, J., Stoustrup, J., & Joergensen, J. B. (2008). Preventing Refrigerated Foodstuffs in Supermarkets from Being Discarded on Hot Days by MPC. In *17th IFAC World Congr.* (pp. 11092–11097). Seoul, Korea.

[Castilla et al., 2011] Castilla, M., Álvarez, J., Berenguel, M., Rodriguez, F., Guzmán, J. L., & Pérez, M. (2011). A comparison of thermal comfort predictive control strategies. *Energy and Buildings*, 43(10), 2737–2746.

[Chen et al., 2002] Chen, W., Zhijiu, C., Ruiqi, Z., & Yezheng, W. (2002). Experimental investigation of a minimum stable superheat control system of an evaporator. *International Journal of Refrigeration*, 25(8), 1137–1142.

[Crama & Schoukens, 2001] Crama, P. & Schoukens, J. (2001). First Estimates of Wiener and Hammerstein Systems Using Multisine Excitation. In *IEEE Instrumentation and Measurement Technology Conference* (pp. 1365–1369). Budapest, Hungary.

[CU Aerospace, 2013] CU Aerospace (2013). Thermosys. `http://www.thermosys.us/`.

[Danfoss, 2008] Danfoss (2008). *Electronic Expansion Valves - Fitters Notes (Part 8)*. Technical report, RA Marketing.

[Danfoss, 2009] Danfoss (2009). *Why Compressors Fail: Part 1 - Refrigerant Flood Back*. Technical report, Refrigeration and Air Conditioning.

[Danfoss, 2011] Danfoss (2011). *Most valves expand your refrigerant - EcoFlow expands your options*. Technical report, Advertising.

[Danish Veterinary and Food Administration, 2005] Danish Veterinary and Food Administration (2005). *Fakta om fødevarehygiejne - Tilberedning*. Technical report, Ministry of Food, Agriculture and Fisheries. In Danish.

[Danish Veterinary and Food Administration, 2013] Danish Veterinary and Food Administration (2013). How we control. `http://www.foedevarestyrelsen.dk/english/Inspection/`.

[Elliott et al., 2011] Elliott, M. S., Estrada, C., & Rasmussen, B. P. (2011). Cascaded Superheat Control with a Multiple Evaporator Refrigeration System. In *American Control Conference* (pp. 2065–2070). San Francisco, CA, USA.

[Elliott & Rasmussen, 2010] Elliott, M. S. & Rasmussen, B. P. (2010). On reducing evaporator superheat nonlinearity with control architecture. *International Journal of Refrigeration*, 33(3), 607–614.

[Elliott et al., 2009] Elliott, M. S., Walton, Z., Bolding, B., & Rasmussen, B. P. (2009). Superheat Control: A Hybrid Approach. *HVAC&R Research*, 15(6), 1021–1043.

[Eskinat et al., 1991] Eskinat, E., Johnson, S. H., & Luyben, W. L. (1991). Use of Hammerstein Models in Identification of Nonlinear Systems. *AIChE Journal*, 37(2), 255–268.

[Finn & Doyle, 2000] Finn, D. P. & Doyle, C. J. (2000). Control and optimization issues associated with algorithm-controlled refrigerant throttling devices. *ASHRAE Transactions*, 106(1), 524–533.

[Gormley et al., 2002] Gormley, R., Walshe, T., Hussey, K., & Butler, F. (2002). The Effect of Fluctuating vs. Constant Frozen Storage Temperature Regimes on Some Quality Parameters of Selected Food Products. *LWT - Food Science and Technology*, 35(2), 190–200.

[Gouda et al., 2002] Gouda, M., Danaher, S., & Underwood, C. (2002). Building thermal model reduction using nonlinear constrained optimization. *Building and Environment*, 37(12), 1255–1265.

[Goyal et al., 2012] Goyal, S., Ingley, H. A., & Barooah, P. (2012). Zone-Level Control Algorithms Based on Occupancy Information for Energy Efficient Buildings. In *American Control Conference* (pp. 3063–3068). Montréal, Canada.

[Grald & MacArthur, 1992] Grald, E. W. & MacArthur, J. W. (1992). A moving-boundary formulation for modeling time-dependent two-phase flows. *International Journal of Heat and Fluid Flow*, 13(3), 266–272.

[Gruhle & Isermann, 1985] Gruhle, W. D. & Isermann, R. (1985). Modeling and Control of a Refrigerant Evaporator. In *American Control Conference* (pp. 287–292). Boston, MA, USA.

[Haring et al., 2013] Haring, M., van de Wouw, N., & Nešić, D. (2013). Extremum-seeking control for nonlinear systems with periodic steady-state outputs. *Automatica*, 49(6), 1883–1891.

[He & Asada, 2003] He, X.-D. & Asada, H. (2003). A New Feedback Linearization Approach to Advanced Control of Multi-Unit HVAC Systems. In *American Control Conference* (pp. 2311–2316). Denver, CO, USA.

[He et al., 1997] He, X.-D., Liu, S., & Asada, H. H. (1997). Modeling of Vapor Compression Cycles for Multivariable Feedback Control of HVAC Systems. *ASME journal of Dynamic Systems, Measurement, and Control*, 119(2), 183–191.

[He et al., 1998] He, X.-D., Liu, S., Asada, H. H., & Itoh, H. (1998). Multivariable Control of Vapor Compression Systems. *HVAC&R Research*, 4(3), 205–230.

[Helfrich et al., 2008] Helfrich, B. E., Lee, C., Bristow, D. A., Xiao, X. H., Dong, J., Alleyne, A. G., Salapaka, S. M., & Ferreira, P. M. (2008). Combined H_∞-Feedback and Iterative Learning Control Design with Application to Nanopositioning Systems. In *American Control Conference* (pp. 3983–3900). Seattle, Washington, USA.

[Henning et al., 2008] Henning, L., Becker, R., Feuerbach, G., Muminovic, R., King, R., Brunn, A., & Nitsche, W. (2008). Extensions of adaptive slope-seeking for active flow control. *Proceedings of the Institution of Mechanical Engineers, Part I: Journal of Systems and Control Engineering*, 222(5), 309–322.

[Henze & Krati, 1998] Henze, G. P. & Krati, M. (1998). Ice Storage System Controls for the Reduction of Operating Cost and Energy Use. *Journal of Solar Energy Enginering*, 120(4), 275–281.

[Horn & Johnson, 1985] Horn, R. A. & Johnson, C. R. (1985). *Matrix Analysis*. Cambridge University Press.

[Hovgaard et al., 2012a] Hovgaard, T. G., Larsen, L. F. S., Edlund, K., & Jørgensen, J. B. (2012a). Model predictive control technologies for efficient and flexible power consumption in refrigeration systems. *Energy*, 44(1), 105–116.

[Hovgaard et al., 2011] Hovgaard, T. G., Larsen, L. F. S., & Jørgensen, J. B. (2011). Flexible and Cost Efficient Power Consumption using Economic MPC - A Supermarket Refrigeration Benchmark. In *IEEE Conference on Decision and Control and European Control Conference* (pp. 848–854). Orlando, Florida.

[Hovgaard et al., 2012b] Hovgaard, T. G., Larsen, L. F. S., & Skovrup, M. J. (2012b). Analyzing Control Challenges for Thermal Energy Storage in Foodstuffs. In *IEEE Multi-conference on Systems and Control* (pp. 956–961). Dubrovnik, Croatia.

[Hudson & Underwood, 1999] Hudson, G. & Underwood, C. P. (1999). A simple building modelling procedure for MATLAB/SIMULINK. In *IBPSA Building Simulation Conference* (pp. 776–783). Kyoto, Japan.

[Izadi-Zamanabadi et al., 2012a] Izadi-Zamanabadi, R., Larsen, L. F. S., & Thybo, C. (2012a). A METHOD FOR CONTROLLING A SUPPLY OF REFRIGERANT TO AN EVAPORATOR. Patent no: WO 2012/052019.

[Izadi-Zamanabadi et al., 2012b] Izadi-Zamanabadi, R., Vinther, K., Mojallali, H., Rasmussen, H., & Stoustrup, J. (2012b). Evaporator unit as a benchmark for Plug and Play and fault tolerant control. In *8th IFAC Symposium on Fault Detection, Supervision and Safety of Technical Processes* (pp. 701–706). Mexico City, Mexico.

[Jain & Alleyne, 2009] Jain, N. & Alleyne, A. G. (2009). Comparison of SISO and MIMO Control Techniques for a Diagonally Dominant Vapor Compression System. In *American Control Conference* (pp. 1580–1585). St. Louis, MO, USA.

[Jain et al., 2010] Jain, N., Li, B., Keir, M., Hencey, B., & Alleyne, A. (2010). Decentralized Feedback Structures of a Vapor Compression Cycle System. *IEEE Transactions on Control Systems Technology*, 18(1), 185–193.

[Kempf et al., 1993] Kempf, C., Messner, W., Tomizuka, M., & Horowitz, R. (1993). Comparison of Four Discrete-Time Repetitive Control Algorithms. *IEEE Control Systems*, 13(6), 48–54.

[Koeln & Alleyne, 2013] Koeln, J. & Alleyne, A. G. (2013). Optimal Subcooling in Vapor Compression Systems Via Extremum Seeking Control. In *6th Annual Dynamic Systems and Control Conference* Palo Alto, CA, USA.

[Larsen, 2005] Larsen, L. F. S. (2005). *Model Based Control of Refrigeration Systems*. PhD thesis, Section of Automation and Control, Department of Electronic Systems, Aalborg University.

[Larsen et al., 2007a] Larsen, L. F. S., Izadi-Zamanabadi, R., & Wisniewski, R. (2007a). Supermarket Refrigeration System - Benchmark for Hybrid System Control. In *European Control Conference* Kos, Greece.

[Larsen et al., 2007b] Larsen, L. F. S., Thybo, C., Wisniewski, R., & Izadi-Zamanabadi, R. (2007b). Synchronization and desynchronizing control scheme for supermarket refrigeration systems. In *IEEE Multi-conference on Systems and Control* (pp. 1414–1419). Singapore.

[Leblanc, 1922] Leblanc, M. (1922). Sur l'électrification des chemins de fer au moyen de courants alternatifs de fréquence élevée. *Revue Générale de l'Electricité*.

[Li & Alleyne, 2010] Li, B. & Alleyne, A. G. (2010). A dynamic model of a vapor compression cycle with shut-down and start-up operations. *International Journal of Refrigeration*, 3(33), 538–552.

[Li et al., 2010] Li, P., Li, Y., & Seem, J. E. (2010). Efficient Operation of Air-Side Economizer Using Extremum Seeking Control. *Journal of Dynamic Systems, Measurement, and Control*, 132(3), 031009 (10 pages).

[Li et al., 2012] Li, X., Li, Y., Seem, J. E., & Li, P. (2012). Extremum Seeking Control of Cooling Tower for Self-Optimizing Efficient Operation of Chilled Water Systems. In *American Control Conference* (pp. 3396–3401). Montreal, Canada.

[Li et al., 2005] Li, Y., Rotea, M. A., Chiu, G. T.-C., Mongeau, L. G., & Paek, I.-S. (2005). Extremum Seeking Control of a Tunable Thermoacoustic Cooler. *IEEE Transactions on Control Systems Technology*, 13(4), 527–Ű536.

[Lim et al., 2009] Lim, D., Rasmussen, B. P., & Swaroop, D. (2009). Selecting PID Control Gains for Nonlinear HVAC&R Systems. *HVAC&R Research*, 15(6), 991–1019.

[Longman, 2000] Longman, R. W. (2000). Iterative learning control and repetitive control for engineering practice. *International Journal of Control*, 73(10), 930–954.

[Lorenz & Masy, 1982] Lorenz, F. & Masy, G. (1982). Méthode d'évaluation de l'économie d'énergie apportée par l'intermittence de chauffage dans les bâtiments. *Traitement par differences finies d'un model a deux constantes de temps, Report No. GM820130-01. Faculte des Sciences Appliquees, University de Liege, Liege, Belgium.* (in French).

[Lyhne & Sørensen, 2011] Lyhne, C. H. & Sørensen, E. B. (2011). Generic Superheat Control of Evaporators using One Sensor and One Actuator. Aalborg University, Denmark. Master thesis.

[Ma et al., 2012] Ma, Y., Kelman, A., Daly, A., & Borrelli, F. (2012). Predictive Control for Energy Efficient Buildings with Thermal Storage: Modeling, Simulation, and Experiments. *IEEE Control Systems Magazine*, 32(1), 44–64.

[McKinley & Alleyne, 2008] McKinley, T. L. & Alleyne, A. G. (2008). An advanced nonlinear switched heat exchanger model for vapor compression cycles using the moving-boundary method. *International Journal of Refrigeration*, 31(7), 1253–124.

[Mishra et al., 2011] Mishra, S., Topcu, U., & Tomizuka, M. (2011). Optimization-Based Constrained Iterative Learning Control. *IEEE Transactions on Control Systems Technology*, 19(6), 1613–1621.

[Moase & Manzie, 2011] Moase, W. H. & Manzie, C. (2011). Fast extremum-seeking on Hammerstein plants. In *18th IFAC World Congress* (pp. 108–113). Milan, Italy.

[Moase et al., 2010] Moase, W. H., Manzie, C., & Brear, M. J. (2010). Newton-Like Extremum-Seeking for the Control of Thermoacoustic Instability. *IEEE Transactions on Automatic Control*, 55(9), 2094–2105.

[Moir, 2001] Moir, T. J. (2001). Automatic Variance Control and Variance Estimation Loops. *Circuits Syst. Signal Process*, 20(1), 1–10.

[Oldewurtel et al., 2012] Oldewurtel, F., Parisio, A., Jones, C. N., Gyalistras, D., Gwerder, M., Stauch, V., Lehmann, B., & Morari, M. (2012). Use of model predictive control and weather forecasts for energy efficient building climate control. *Energy and Buildings*, 45, 15–27.

[Outtagarts et al., 1997] Outtagarts, A., Haberschill, P., & Lallemand, M. (1997). The Transient Response of an Evaporator Fed Through an Electronic Expansion Valve. *International Journal of Energy Research*, 21(9), 793–807.

[Pedersen et al., 2013] Pedersen, R., Schwensen, J., Sivabalan, S., Corazzol, C., Shafiei, S. E., Vinther, K., & Stoustrup, J. (2013). Direct Control Implementation of a Refrigeration System in Smart Grid. In *American Control Conference* Washington, USA.

[Petersen et al., 2012] Petersen, L. N., Madsen, H., & Heerup, C. (2012). *ESO2 Optimization of Supermarket Refrigeration Systems : Mixed Integer MPC and System Performance*. Technical report, Tech. University of Denmark.

[Pfeiffer, 2000] Pfeiffer, B.-M. (2000). Towards 'plug and control': self-tuning temperature controller for PLC. *International Journal of Adaptive Control and Signal Processing*, 14(5), 519–532.

[Pottker & Hrnjak, 2012] Pottker, G. & Hrnjak, P. S. (2012). Effect of Condenser Subcooling of the Performance of Vapor Compression Systems: Experimental and Numerical Investigation. In *International Refrigeration and Air Conditioning Conference* Purdue, USA.

[Powell et al., 2013] Powell, K. M., Cole, W. J., Ekarika, U. F., & Edgar, T. F. (2013). Dynamic Optimization of a Campus Cooling System with Thermal Storage. In *European Control Conference* (pp. 4077–4082). Zürich, Switzerland.

[Prívara et al., 2011] Prívara, S., Vána, Z., Cigler, J., Oldewurtel, F., & Komárek, J. (2011). Role of MPC in Building Climate Control. In *21st European Symposium on Computer Aided Process Engineering* (pp. 728–732). Chalkidiki, Greece.

[Rasmussen, 2012a] Rasmussen, B. P. (2012a). Dynamic modeling for vapor compression systems - Part I: Literature review. *HVAC&R Research*, 18(5), 934–955.

[Rasmussen, 2012b] Rasmussen, B. P. (2012b). Dynamic modeling for vapor compression systems - Part II: Simulation tutorial. *HVAC&R Research*, 18(5), 956–973.

[Rasmussen, 2008] Rasmussen, H. (2008). Adaptive Superheat Control of a Refrigeration Plant using Backstepping. In *International Conference on Control, Automation and Systems* (pp. 653–658). Seoul, Korea.

[Rasmussen & Larsen, 2009a] Rasmussen, H. & Larsen, L. F. (2009a). Energy efficient control of a refrigeration plant. In *IEEE International Conference on Control Applications* (pp. 1495–1500). Saint Petersburg, Russia.

[Rasmussen & Larsen, 2009b] Rasmussen, H. & Larsen, L. F. S. (2009b). Nonlinear superheat and capacity control of a refrigeration plant. In *Mediterranean Conference on Control & Automation* (pp. 1072–1077). Thessaloniki, Greece.

[Rasmussen & Larsen, 2011] Rasmussen, H. & Larsen, L. F. S. (2011). Non-linear and adaptive control of a refrigeration system. *IET Control Theory and Applications*, 5(2), 364–378.

[Rasmussen et al., 2006a] Rasmussen, H., Thybo, C., & Larsen, L. F. S. (2006a). Automatic Tuning of the Superheat Controller in a Refrigeration Plant. In *Portuguese Conference on Automatic Control* Lisboa, Portugal.

[Rasmussen et al., 2006b] Rasmussen, H., Thybo, C., & Larsen, L. F. S. (2006b). Nonlinear Superheat and Evaporation Temperature control of a Refrigeration Plant. In *IFAC ESC'06: Energy Saving Control in Plants and Buildings* (pp. 252–254). Bansko, Bulgaria.

[S. Goli & Olsen, 2011] S. Goli, A. M. & Olsen, D. (2011). Demand response opportunities in industrial refrigerated warehouses in California. In *ACEEE Summer Study on Energy Efficiency in Industry* Niagara Falls, NY, USA.

[Sane et al., 2006] Sane, H. S., Haugstetter, C., & Bortoff, S. A. (2006). Building HVAC Control Systems - Role of Controls and Optimization. In *American Control Conference* (pp. 1121–1126). Minneapolis, Minn., USA.

[Sarabia et al., 2009] Sarabia, D., Capraro, F., Larsen, L. F. S., & de Prada, C. (2009). Hybrid NMPC of supermarket display cases. *Control Engineering Practice*, 17(4), 428–441.

[Schurt et al., 2009] Schurt, L. C., Hermes, C. J., & Neto, A. T. (2009). A model-driven multivariable controller for vapor compression refrigeration systems. *International Journal of Refrigeration*, 32(7), 1672–1682.

[Seem, 1998] Seem, J. E. (1998). A New Pattern Recognition Adaptive Controller with Application to HVAC Systems. *Automatica*, 34(8), 969–982.

[Shafiei et al., 2013a] Shafiei, S. E., Rasmussen, H., & Stoustrup, J. (2013a). Model Predictive Control for a Thermostatic Controlled System. In *European Control Conference* (pp. 1559–1564). Zürich, Switzerland.

[Shafiei et al., 2013b] Shafiei, S. E., Rasmussen, H., & Stoustrup, J. (2013b). Modeling Supermarket Refrigeration Systems for Demand-Side Management. *Energies*, 6(2), 900–920.

[Shafiei et al., 2013c] Shafiei, S. E., Stoustrup, J., & Rasmussen, H. (2013c). A supervisory control approach in economic MPC design for refrigeration systems. In *European Control Conference* (pp. 1565–1570). Zürich, Switzerland.

[Shen et al., 1996] Shen, S.-H., Wu, J.-S., & Yu, C.-C. (1996). Use of Biased-Relay Feedback for System Identification. *AIChE Journal*, 42(4), 1174–1180.

[Skovrup, 2000] Skovrup, M. (2000). *Thermodynamic and thermophysical properties of refrigerants - software package in borland delphi*. Technical report, Technical University of Denmark.

[Sonntag et al., 2008] Sonntag, C., Devanathan, A., & Engell, S. (2008). Hybrid NMPC of a Supermarket Refrigeration System using Sequential Optimization. In *17th IFAC World Congress* (pp. 13901–13906). Seoul, Korea.

[Tan et al., 2012] Tan, A. H., Wong, H. K., & Godfrey, K. (2012). Identification of a Wiener-Hammerstein system using an incremental nonlinear optimisation technique. *Control Engineering Practice*, 20(11), 1140–1148.

[Tan et al., 2010] Tan, Y., Moase, W., Manzie, C., Nešić, D., & Mareels, I. (2010). Extremum Seeking From 1922 To 2010. In *Proceedings of the 29th Chinese Control Conference* (pp. 14–26). Beijing, China.

[Tan et al., 2006] Tan, Y., Nešić, D., & Mareels, I. (2006). On non-local stability properties of extremum seeking control. *Automatica*, 42(6), 889–903.

[Tomizuka et al., 1989] Tomizuka, M., Tsao, T., & Chew, K. (1989). Analysis and Synthesis of Discrete-Time Repetitive Controllers. *Journal of Dynamic Systems, Measurement, and Control*, 111, 353–358.

[Tyagi et al., 2006] Tyagi, V., Sane, H., & Darbha, S. (2006). An Extremum Seeking Algorithm for Determining the Set Point Temperature for Condensed Water in a Cooling Tower. In *American Control Conference* (pp. 1127–1131). Minneapolis, Minn., USA.

[Underwood, 1999] Underwood, C. P. (1999). *HVAC Control Systems: Modelling, Analysis and Design*. Spon Press.

[U.S. Department of Energy, 2013] U.S. Department of Energy (2013). Energyplus energy simulation software. `http://apps1.eere.energy.gov/buildings/energyplus/`.

[Vinther et al., 2013a] Vinther, K., Chandan, V., & Alleyne, A. G. (2013a). Learning/Repetitive Control for Building Systems with Nearly Periodic Disturbances. In *European Control Conference* (pp. 1198–1203). Zürich, Switzerland.

[Vinther et al., 2012a] Vinther, K., Lyhne, C. H., Sørensen, E. B., & Rasmussen, H. (2012a). Evaporator Superheat Control with One Temperature Sensor using Qualitative System Knowledge. In *American Control Conference* (pp. 374–379). Montreal, Canada.

[Vinther et al., 2012b] Vinther, K., Rasmussen, H., Izadi-Zamanabadi, R., & Stoustrup, J. (2012b). Single Temperature Sensor based Evaporator Filling Control using Excitation Signal Harmonics. In *IEEE Multi-Conference on Systems and Control* (pp. 757–763). Dubrovnik, Croatia.

[Vinther et al., 2012c] Vinther, K., Rasmussen, H., Izadi-Zamanabadi, R., & Stoustrup, J. (2012c). Utilization of Excitation Signal Harmonics for Control of Nonlinear Systems. In *IEEE Multi-Conference on Systems and Control* (pp. 1627–1632). Dubrovnik, Croatia.

[Vinther et al., 2013b] Vinther, K., Rasmussen, H., Izadi-Zamanabadi, R., & Stoustrup, J. (2013b). A Fault Tolerant Superheat Control Strategy for Supermarket Refrigeration Systems. In *International Conference on Control and Fault-Tolerant Systems (SysTol)* (pp. 426–431). Nice, France.

[Vinther et al., 2013c] Vinther, K., Rasmussen, H., Izadi-Zamanabadi, R., & Stoustrup, J. (2013c). Control of a Class of Nonlinear Systems using a Maximum Slope-seeking Method. . Submitted for publication.

[Vinther et al., 2013d] Vinther, K., Rasmussen, H., Izadi-Zamanabadi, R., & Stoustrup, J. (2013d). Single temperature sensor superheat control using a novel maximum slope-seeking method. *International Journal of Refrigeration*, 36(3), 1118–1129.

[Vinther et al., 2013e] Vinther, K., Rasmussen, H., Izadi-Zamanabadi, R., Stoustrup, J., & Alleyne, A. G. (2013e). A Learning Based Precool Algorithm for Utilization of Foodstuff as Thermal Energy Storage. In *IEEE Multi-Conference on Systems and Control* (pp. 314–321). Hyderabad, India.

[Vinther et al., 2013f] Vinther, K., Rasmussen, H., Izadi-Zamanabadi, R., Stoustrup, J., & Alleyne, A. G. (2013f). Learning Based Precool Algorithms for Exploiting Foodstuff as Thermal Energy Reserve. . Submitted for publication.

[Visioli, 2003] Visioli, A. (2003). Time-optimal plug&control for integrating and FOPDT processes. *Journal of Process Control*, 13(3), 195–202.

[Vrettos et al., 2013] Vrettos, E., Lai, K., Oldewurtel, F., & Andersson, G. (2013). Predictive Control of Buildings for Demand Response with Dynamic Day-ahead and Real-time Prices. In *European Control Conference* (pp. 2527–2534). Zürich, Switzerland.

[Wang & Krstić, 2000] Wang, H.-H. & Krstić, M. (2000). Extremum seeking for limit cycle minimization. *IEEE Transactions on Automatic Control*, 45(12), 2432–Ű2437.

[Wang et al., 1997] Wang, Q.-G., Hang, C.-C., & Zou, B. (1997). Low-Order Modeling from Relay Feedback. *Ind. Eng. Chem. Res.*, 36(2), 375–381.

[Wang et al., 2009] Wang, Y., Gao, F., & Doyle, F. J. (2009). Survey on iterative learning control, repetitive control, and run-to-run control. *Journal of Process Control*, 19(10), 1589–1600.

[Wedekind et al., 1978] Wedekind, G. L., Bhatt, B. L., & Beck, B. T. (1978). A system mean void fraction model for predicting various transient phenomena associated with two-phase evaporating and condensing flows. *International Journal of Multiphase Flow*, 4(1), 97–114.

[Willatzen et al., 1998] Willatzen, M., Pettit, N. B. O. L., & Ploug-Sørensen, L. (1998). A general dynamic simulation model for evaporators and condensers in refrigeration. Part I: moving-boundary formulation of two-phase flows with heat exchange. *International Journal of Refrigeration*, 21(5), 398–403.

[Yang et al., 2011] Yang, Z., Rasmussen, K. B., Kieu, A. T., & Izadi-Zamanabadi, R. (2011). Fault Detection and Isolation for a Supermarket Refrigeration System - Part One: Kalman-Filter-Based. In *18th IFAC World Congress* (pp. 13233–13238). Milano, Italy.

[Yu, 2006] Yu, C.-C. (2006). *Autotuning of PID Controllers: A Relay Feedback Approach*. Springer, 2nd edition.

[Zhang & Ordóñez, 2012] Zhang, C. & Ordóñez, R. (2012). *Extremum-Seeking Control and Applications: A Numerical Optimization-Based Approach*. Advances in Industrial Control. Springer.

[Zhou et al., 2005] Zhou, G., Krati, M., & Henze, G. P. (2005). Parametric Analysis of Active and Passive Building Thermal Storage Utilization. *Journal of Solar Energy Enginering*, 127(1), 37–46.

Contributions

Paper A

Evaporator Superheat Control With One Temperature Sensor Using Qualitative System Knowledge

Kasper Vinther, Casper Hillerup Lyhne, Erik Baasch Sørensen, and Henrik Rasmussen

This appendix is based on a paper published in:
The proceedings of the American Control Conference (ACC), June 2012

Abstract

This paper proposes a novel method for superheat control using only a single temperature sensor at the outlet of the evaporator, while eliminating the need for a pressure sensor. An inner loop controls the outlet temperature and an outer control loop provides a reference setpoint, which is based on estimation of the evaporation pressure and suitable reference logic. The pressure is approximated as being linear and proportional to the opening degree of the expansion valve. This gain and the reference logic is based on calculation of the variance in the outlet temperature, which have shown to increase at low superheat. The parameters in the proposed controller structure can automatically be chosen based on two open-loop tests. Results from tests on two different refrigeration systems indicate that the proposed controller can control the evaporator superheat to a low level giving close to optimal filling of the evaporator, with only one temperature sensor. No a priori model knowledge was used and it is anticipated that the method is applicable on a wide variety of refrigeration systems.

1 Introduction

Refrigeration systems normally operate by continuous vaporization and compression of refrigerant. This process is maintained by a valve, an evaporator, a compressor and a condenser, and this setup remains to a considerable extent the same in most refrigeration systems. The details of the vapor compression type refrigeration process are not given here, but can be found in e.g. [1].

Refrigeration systems are typically controlled by decentralized control loops and evaporator superheat is controlled in one of these loops. Superheat control can be achieved by regulating the opening degree (OD) of the expansion valve. Superheating of the refrigerant beyond the evaporation temperature is important, since no superheat means that two-phase refrigerant will enter the compressor and increase the power comsumption and wear. This means that the flow through the valve must be kept a level, where all the refrigerant is evaporated before it reaches the compressor. At the same time, it is important to have as much two-phase refrigerant in the evaporator as possible, to increase the heat transfer and thus optimize the refrigeration process. So a key variable, which greatly effects the efficiency of a refrigeration system, is the superheat, which again is an indirect measure of the filling of the evaporator.

The heating, ventilating and air conditioning (HVAC) industry commonly use some variant of proportional-integral (PI) feedback control [2]. These controllers have traditionally been tuned by refrigeration and control specialists, due to the complexity and nonlinearity of the refrigeration process and the large number of different refrigeration system designs available. The problem is that the human operator often copies parameter values from any previous system in the hope that the new refrigeration system will work with these settings. However, each system is associated with different optimal working point conditions, sensor/actuator configurations and cooling demands. Furthermore, the tuning process can be time consuming and there is a risk of system damage, if the operator is not cautious. It is therefore desirable to automate the tuning process of controllers for refrigeration systems and/or implement adaptive algorithms.

Automatic tuning of PI/PID controllers have been treated in many books, see e.g. [3] and [4]. The relay method is used in [5] to obtain the ultimate frequency and gain, which

is used to find PID controller parameters based on model knowledge. These parameters are compared with Zeigler-Nichols tuned parameters and model-based gain scheduling is additionally employed to cope with the operating point dependent system gain. In [6], auto-tuners for PI/PID control of HVAC systems are designed based on a combination of relay and step tests. The auto-tuners show better performance than manual tuning and standard relay auto-tuning.

The response from valve OD to superheat is in general very nonlinear, making controller tuning difficult. The need for gain scheduling in [5] is eliminated in [7], by transferring the superheat to a referred variable. In both papers a cascaded control setup is utilized, where a flow meter is used to control the refrigerant mass flow in an inner loop. However, most refrigeration systems does not have such a sensor and [8] instead proposes a cascaded control, where evaporator pressure measurements are used in an inner loop to reduce the nonlinearities. Backstepping can also be used to design a nonlinear controller, as done in [9]. This controller can be made almost independent of the cooling capacity and therefore does not require any gain scheduling. Another possibility is to control the superheat with the compressor and the cooling capacity with the valve. In [10], backstepping is again used to derive a nonlinear controller. However, extensive model knowledge is required in both cases and some model parameters are only partly known and vary with the operating conditions, thus requiring adaptive methods for finding these parameters. These have been pursued in [10].

All the controllers mentioned so far require at least a temperature sensor and a pressure and/or a flow meter to control the filling of the evaporator. In this paper, we will present a novel control method capable of controlling the filling with only one temperature sensor placed at the outlet of the evaporator. This will make it easier to install and buy superheat controllers based on electronic valves. The method utilizes the fact that the variance of the outlet temperature increases when the evaporator is close to overflowing and this gives a fix point, where the gain, in a simple linear model relating the valve OD to the pressure, can be identified. The estimated pressure can then be converted into evaporation temperature and thus a reference for a simple PI controller for the outlet temperature. Furthermore, the reference is slowly decreased until the fix point is reached and then stepped back. This makes it possible to adaptively correct the gain in the linear model each time the fix point is reached and ensures that the system is continuously operated close to where the evaporator is fully filled (low superheat). In other words, qualitative system knowledge is used to identify when the filling of the evaporator is suitable and it has been shown in tests that the method works on two completely different refrigeration systems. Additionally, only two open-loop tests are required to set the control parameters and these tests can be performed in an automated fashion. Another benefit of the proposed controller is that no a priori model knowledge is required, which is often the case when e.g. gain scheduling and nonlinear control design methods are used.

The structure of this paper is as follows. The two test refrigeration systems are first presented in Section 2. Then, calculation of variance of the outlut temperature is shown in Section 3, followed by a presentation of the control strategy in Section 4. Then, an adaptive pressure estimator is derived in 5 and the startup procedure is shown in Section 6. Finally, test results are presented in Section 7 and conclusions are drawn in Section 8.

2 System Description

The proposed superheat control method in this paper is designed for unknown vapor compression type refrigeration systems, where no a priori model knowledge is assumed. The method should work on a wide variety of setups and two different types of refrigeration systems have therefore been used for test. The first system is an air conditioning system and the second is a refrigeration system with a water tank and heater as load on the evaporator. Simplified drawings of these systems are shown in Fig. 4.1.

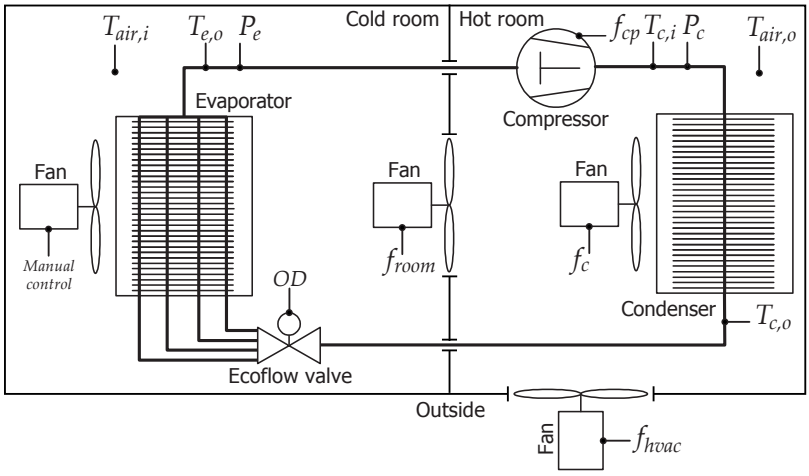

(a)

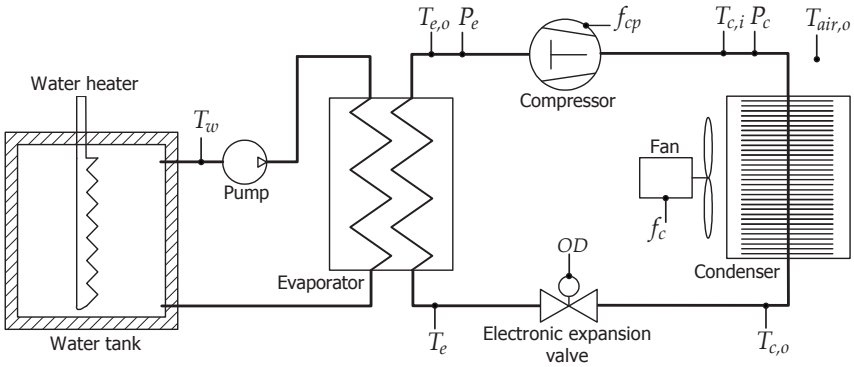

(b)

Figure 4.1: Simplified drawings of the two available test systems. T, P and f are indicators for temperature sensors, pressure sensors and frequency control, respectively. Only $T_{e,o}$ and OD are used for the superheat control and the other sensors are used for verification purposes. System (a) is an air conditioning system and system (b) is a refrigeration system with water on the secondary side of the evaporator.

The air conditioning system in Fig. 4.1a has a four channel finned-tube evaporator and a Danfoss Ecoflow^{TM}valve. It is possible to control the OD of the valve and the

distribution of flow into the individual pipes, however, the distribution is kept constant in this setup. Furthermore, it is possible to control the frequency of both the evaporator and condenser fans, and also the frequency of the fans between the cold room, the hot room and the outside. The compressor frequency is also controllable and sensors measure temperature and pressure at the indicated places.

The refrigeration system in Fig. 4.1b has an evaporator with water on the secondary side, which is connected to a water tank with controllable heater and pump. It is possible to control the OD of the electronic expansion valve and the frequency of the condenser fan. The compressor frequency is again controllable and sensors measure temperature and pressure at the indicated places. Both systems are monitored and controlled using the XPC toolbox for Simulink.

Evaporator superheat T_{sh} is defined as the outlet temperature $T_{e,o}$ minus the evaporation temperature T_e (evaporator saturation temperature). The evaporation temperature is normally measured indirectly by measuring the evaporation pressure P_e. We propose a control method, which does not require an direct or indirect measurement of T_e, but only the $T_{e,o}$ measurement. Instead, qualitative system knowledge is used to calculate the variance on $T_{e,o}$ to estimate P_e, which is further discussed in Section 3. This makes this controller easier to install and buy, compared to other superheat controllers using electronic expansion valves, since we save a pressure sensor.

In the following it is assumed that the condenser pressure is controlled separately and that the compressor is running at constant frequency, which means that any change is considered as a disturbance.

3 Variance Calculation

An open-loop test has been performed on each of the test systems, where the OD signal was increased slowly while outlet temperature $T_{e,o}$ measurements were saved. By calculating the sample variance as

$$\sigma^2 = \frac{1}{n}\sum_{i=1}^{n}(x_i - \bar{x})^2, \bar{x} = \frac{1}{n}\sum_{i=1}^{n} x_i, \tag{4.1}$$

where σ^2 is the sample variance using n samples, x_i is the i'th sample and $\bar{x}$ is the sample mean, then it is possible to get an estimate of the variance in the outlet temperature. Fig. 4.2 and 4.3 shows the test results using a five minute sample window on the air conditioning system and the refrigeration system, respectively. The system response is clearly different between the two systems, however, the tests indicate, in both cases, that the variance increases considerably at low superheat and then decreases again when the evaporator is flooded. This increase in variance can be used to identify when the evaporator is nearly flooded and provides an alternative way of controlling the filling of the evaporator compared to conventional control.

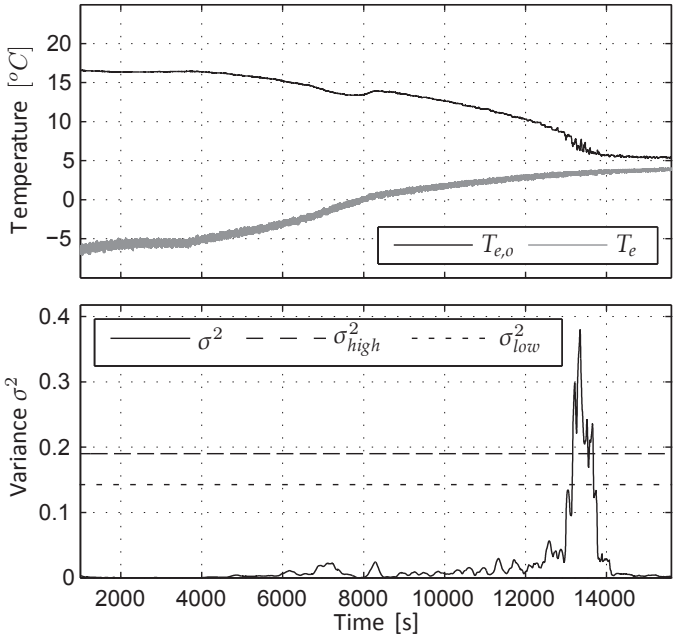

Figure 4.2: Evaporator outlet temperature and variance during an OD sweep on the air conditioning system. Variance thresholds are also indicated.

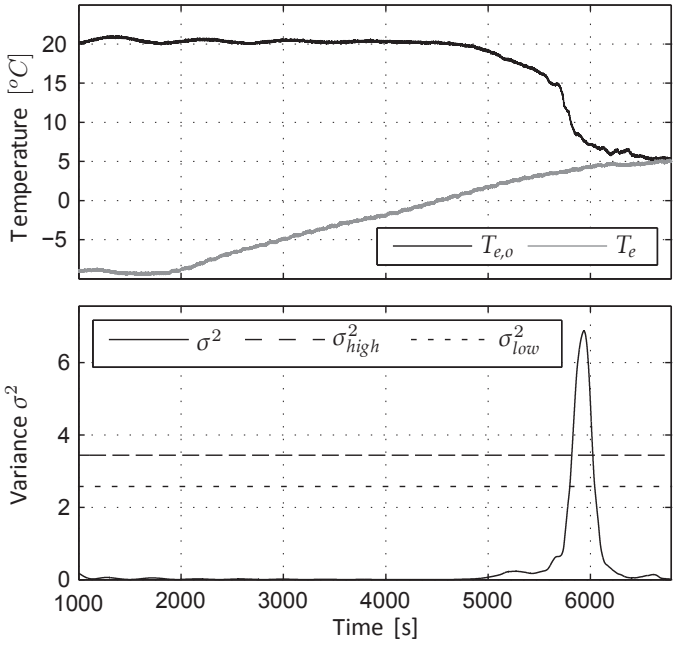

Figure 4.3: Evaporator outlet temperature and variance during an OD sweep on the refrigeration system. Variance thresholds are also indicated.

4 Control Strategy

The control strategy is illustrated in Fig. 4.4. A simple PI feedback control is used in an inner loop to control the evaporator outlet temperature $T_{e,o}$ and an outer loop provides the temperature controller with a suitable reference setpoint.

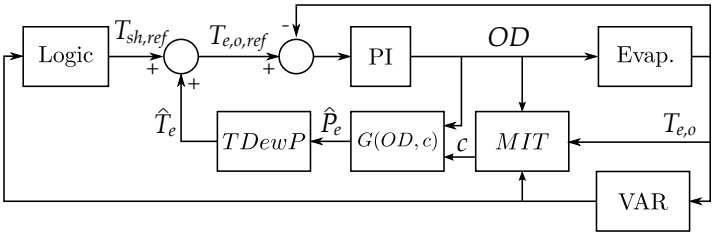

Figure 4.4: Control structure for control of the evaporator outlet temperature. A suitable reference is found based on adaptive estimation of the evaporation temperature and superheat reference logic.

The Logic block in Fig. 4.4 controls the superheat reference, which is implemented so that it continuously decreases in temperature until the variance has increased to a predetermined variance level σ^2_{high}. Then it is stepped back and the cycle is repeated, so that the superheat is constantly kept at a low level despite a change in system load. A waiting period is introduced during startup, which prevents the reference from decreasing until the system has calmed down and the variance is below the hysteresis bound σ^2_{low}, see Fig. 4.2 for a definition of the variance levels. Furthermore, a step back in reference can only be made if the system has calmed down since last step, since a step will cause a temporary increase in variance. A larger step back in reference is taken if the system has not calmed down since the last step and the reference has decreased to its level from before the previous step. For further safety, the reference is also stepped back if the superheat reference goes below 1 degree.

The reference to the inner loop $T_{e,o,ref}$ is made by adding the superheat reference $T_{sh,ref}$ with an estimated evaporation temperature $\hat{T}_e$. The estimated evaporation temperature is based on an estimate of the evaporator pressure, which in steady state can be approximated as being proportional to the OD signal. The gain c from OD to $\hat{P}_e$ is adapted using the MIT rule (see e.g. [4]) and updated each time the reference logic brings the evaporator to a state where it is nearly flooded, which can be identified by an increase in variance. It is important to note that no pressure sensor is used in this setup.

The startup procedure should be made so that the control can start automatically and work on a wide variety of refrigeration systems. In Section 6 it is explained how the controller can be tuned based on two open-loop tests.

5 Pressure Estimator Design and Adaptation

The fundamental concept of conservation of mass in physics (refrigerant is neither added nor removed from the system), implies that the mass flow rate $\dot{m}_v$ through a tube is constant (assuming incompressibility) and equal to the product of the density ρ, velocity

v and cross-sectional area A,

$$\dot{m}_v = \rho v A. \tag{4.2}$$

If assuming laminar, inviscid and incompressible refrigerant mass flow rate through the expansion valve, then Bernoulli's equation furthermore states that

$$\frac{1}{2}v^2 + gz + \frac{P}{\rho} = k, \tag{4.3}$$

where g is the gravitational constant, z is the elevation, P is the pressure and k is a constant, which does not change across the valve. Combining (4.2) and (4.3), while isolating for the valve mass flow $\dot{m}_v$, gives

$$\begin{aligned} \frac{1}{2}\left(\frac{\dot{m}_v}{A_c\rho_l}\right)^2 + gz + \frac{P_c}{\rho_l} &= \frac{1}{2}\left(\frac{\dot{m}_v}{A_e\rho_l}\right)^2 + gz + \frac{P_e}{\rho_l} \\ \dot{m}_v &= \sqrt{P_c - P_e}\sqrt{\rho_l}C_v, \end{aligned} \tag{4.4}$$

where P_c and P_e are the pressures in the condenser and the evaporator, ρ_l is the density of the liquid refrigerant, A_c and A_e are the cross-sectional area before and after the valve, and C_v is a collection of constants. Equation (4.4) is consistent with the result in e.g. [11] for a fully open expansion valve and C_v is also called the orifice coefficient. A valve with variable opening degree OD is added to (4.4). The valve OD is in most refrigeration systems linear going from zero (closed) to one (fully open),

$$\dot{m}_v = OD\sqrt{P_c - P_e}\sqrt{\rho_l}C_v. \tag{4.5}$$

In steady state, the mass flow through the valve $\dot{m}_v$ must be equal to the mass flow through the compressor $\dot{m}_c$, which can be calculated as the product between the compressor frequency f_{cp}, the compressor inlet volume V_{cp} and the density of the gaseous refrigerant ρ_g,

$$\dot{m}_v = \dot{m}_c = f_{cp}V_{cp}\rho_g. \tag{4.6}$$

The mass flow $\dot{m}_c$ is essentially the product between a constant and the evaporator pressure P_e, when the system is in steady state (P_e is proportional to ρ_g). However, this is only true if the compressor speed is held constant. Equation (4.5) can also be simplified if assuming that the fluctuations in the square root of the pressure difference is negligible small and that the density of the refrigerant is constant. Combining (4.5) and (4.6) with simplifications, gives a steady state equation for the evaporator pressure P_e with variable input control signal OD,

$$P_e = cOD, \tag{4.7}$$

where c is a further collection of constants. A first order filter is now introduced, since the outer loop has to be slower than the inner loop for stability. This can be handled by choosing the time constant τ appropriately,

$$G(s) = \frac{P_e(s)}{OD(s)} = \frac{c}{\tau s + 1}. \tag{4.8}$$

The gain c in the simplified expression is very dependent on the operating point and on the characteristics of the given refrigeration system. Therefore, an adaptive update of the constant c is introduced, in order to better estimate the pressure. By continuously calculating the variance of the outlet temperature, while slowly increasing the OD signal, it is possible to detect the point when the evaporator is close to being fully flooded. This was also discussed in Section 3 and the point is used as a fix point to find a good estimate of the gain c^* in the fix point, by using (4.7), since OD is known along with the pressure at the fix point P_e^*. The pressure is not measured directly but can be calculated based on the measured evaporator outlet temperature $T_{e,o}^*$ and a predetermined offset temperature T_{off} as

$$P_e^* = PDewT(T_{e,o}^* - T_{off}), \tag{4.9}$$

where the refrigeration equation software package RefEqns by Morten Juel Skovrup has been used, however, there are many other software packages that can do the conversion. Fig. 4.5 shows a plot of the evaporator pressure P_e, while OD is gradually increased from 0.28 to 0.80 in open-loop on the air conditioning system shown in Fig. 4.1a. The dot marks the identified fix point, where the evaporator is nearly flooded. The estimated linear pressure $\hat{P}_e$ based on the estimated gain c is also shown in the figure. Note that OD has been replaced by $OD^{0.5}$ on the air conditioning system, to better account for valve nonlinearities. However, this is not necessary when the gain c is continuously adapted.

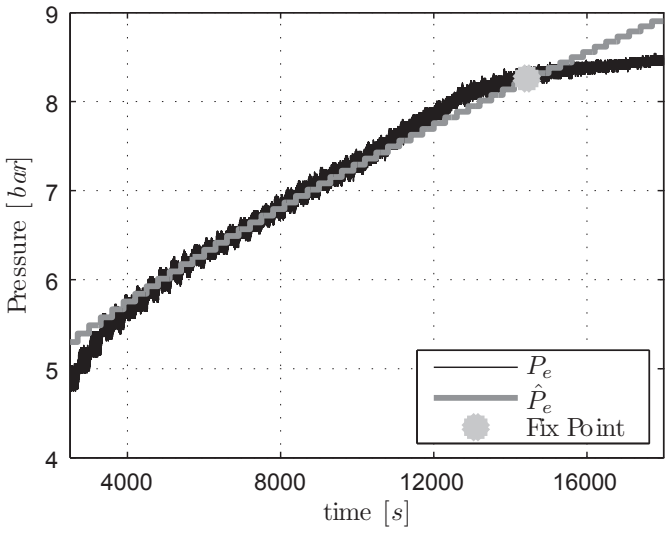

Figure 4.5: Measured evaporator pressure during an OD sweep and resulting linear estimated pressure based on the gain c, found in the marked fix point.

It is undesirable to change the value of the gain c instantly in closed-loop, since this could result in unstable behavior. The MIT rule is therefore used to adapt the gain c

slowly and it is defined as (see e.g. [4]):

$$J = \frac{1}{2}e^2 \tag{4.10}$$

$$\frac{d\theta}{dt} = -\gamma\frac{\partial J}{\partial \theta} = -\gamma e\frac{\partial e}{\partial \theta}, \tag{4.11}$$

where J is an objective function to be minimized, e is the error, θ is the adjustable parameter to be adapted and γ is the adaptation gain. The MIT rule can be interpreted as a gradient method for minimizing the error and in the case of adapting the gain c we have

$$\theta = c \tag{4.12}$$

$$e_c = c - c^* \tag{4.13}$$

$$\frac{dc}{dt} = -\gamma e_c, \tag{4.14}$$

since the partial derivative of e_c is equal to 1. The gain c^* is the gain obtained at the last fix point and the gain c is the current gain. Only the adaptation gain γ has to be chosen. In general a small γ means slow convergence and a large γ means fast convergence and possibly instability. However, it is hard to say in general how γ influences time-variant systems. In the tests on the refrigeration systems γ has been chosen small and thus conservatively. Another possibility would be to use the normalized MIT rule, which would lead to less sensitivity towards signal levels or one could use Lyapunov stability theory to adapt the gain c, and most likely obtain faster adaptation and stability guarantees.

6 Startup Procedure

All parameters in the controller can be determined based on two open-loop tests. The OD signal is increased slowly in the first test, while the temperature $T_{e,o}$ is measured and its variance is calculated. The test is stopped when the variance plot shows a clear peak and has decreased to a low level again. The result on each of the systems is presented in Fig. 4.2 and 4.3. The variance levels σ^2_{low} and σ^2_{high} are set to

$$\sigma^2_{high} = \frac{1}{2}max(\sigma^2) \tag{4.15}$$

$$\sigma^2_{low} = \frac{3}{4}\sigma^2_{high}, \tag{4.16}$$

where $max(\sigma^2)$ is the highest variance during the test. These have shown to be reasonable values based on multiple tests on the two different systems introduced in Section 2.

A temperature offset T_{off} is required in (4.9) to determine the gain c and thus the evaporator pressure. This temperature offset accounts for the temperature difference between the outlet temperature $T^*_{e,o}$, when the high variance threshold σ^2_{high} is reached and an estimate of the evaporation temperature. This estimate is set to be the lowest outlet temperature measured during the OD sweep test and gives $T_{off} = T^*_{e,o} - min(T_{e,o})$. A start guess of the gain c is then obtainable from (4.7) and (4.9).

The second open-loop test is a small upward step in OD at low superheat, while $T_{air,i}$ or T_w is close to T_e, which is considered as a worst case operating point. This test is used

to tune the PI controller based on Ziegler-Nichols tuning with quarter decay ratio, see e.g. [12]. The transfer function of the PI controller is defined as

$$D(s) = k_p \left(1 + \frac{1}{T_I s}\right) \tag{4.17}$$

$$k_p = \frac{0.9}{RL} \tag{4.18}$$

$$T_I = \frac{L}{0.3}, \tag{4.19}$$

where R is the slope of the reaction curve and L is the lag obtained from the step test. The PI controller is tuned at an operating point, where the temperature and refrigerant flow is low, which gives the highest system gain. This gives a conservative controller and ensures that the system is stable at all other operating points. The selected worst case operating point is supported by e.g. [13]. The slope R was measured to be -8.08 and -0.95, for the air conditioning system and refrigeration system, respectively, and the lag L was 23.6 and 27.6. These parameters can also be used to determine a suitable value for the reference decrease rate and the time constant τ, since these measures gives an indication of how fast/slow the system is. During the tests, the reference decrease rate and reference step size was set to 3/1000 and 3, respectively, and τ was set to 30 seconds.

7 Test Results

Fig. 4.6 shows the result from a test of the controller on the air conditioning system. The estimated superheat $\hat{T}_{sh}$ follows the reference well and the reference is slowly decreased and then stepped back each time the variance gets too high, which indicates low superheat. The measured superheat T_{sh}, using a pressure sensor, is shown for comparison and the difference between the estimated and measured superheat gets smaller as the estimate of the gain c is adjusted (γ was set to 0.0005).

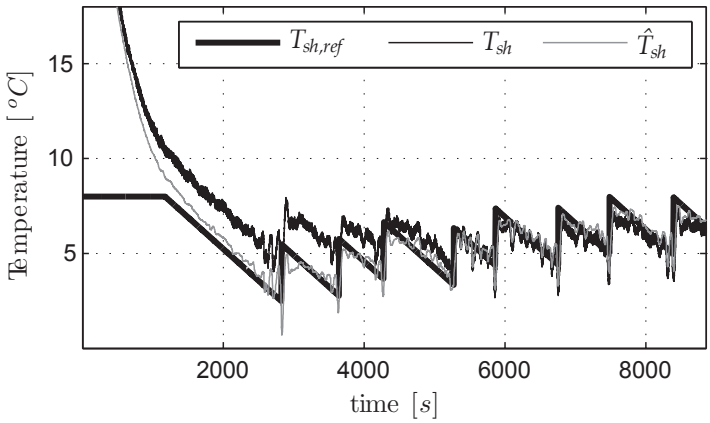

Figure 4.6: Closed-loop test results on the air conditioning system.

A similar test was conducted on the air conditioning system, where the load was changed by blowing air from the hot room to the cold room. This caused a sudden rise in

ambient temperature and thus a change in the load. Fig. 4.7 shows that this disturbance is handled by the controller.

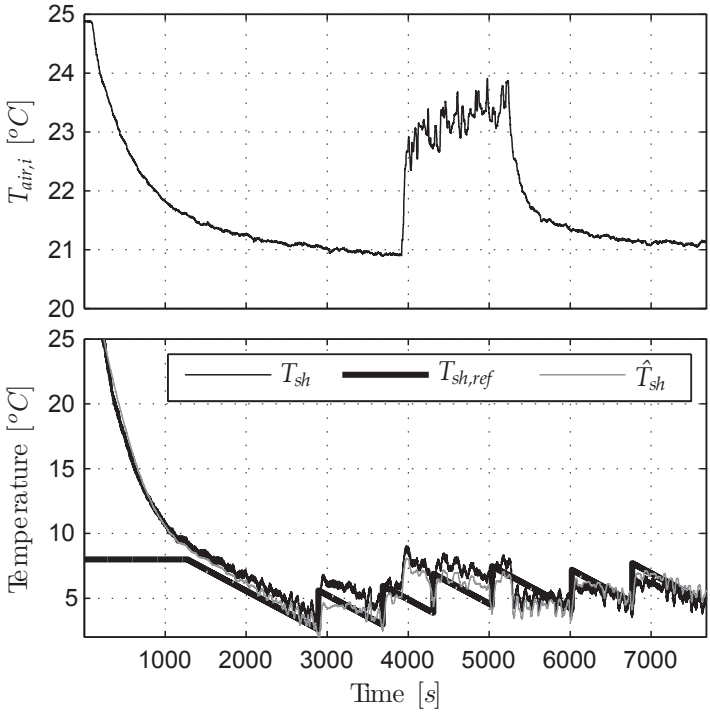

Figure 4.7: Closed-loop test results on the air conditioning system with a sudden change the in ambient air temperature T_{air}.

Fig. 4.8 finally shows the result from a test of the controller on the refrigeration system. A change in load was also made in this test, by changing the temperature setpoint in the water tank with the water heater shown in Fig. 4.1b.

The estimated superheat follows the reference superheat and is stepped back each time the variance gets too high, as anticipated. However, there is approximately a 5 degree temperature offset between the estimated and measured superheat. This is because the variance starts to increase a little earlier in closed-loop, and the temperature offset T_{off} was estimated in open-loop. The T_{off} estimate could be improved by allowing a small overflow in closed-loop. However, if comparing the actual superheat of about 15 degree with Fig. 4.3, then this superheat corresponds to a working point just before the steep slope, which happens over 2-3 quantizations in OD. Controlling the superheat to a point on the middle of the slope is quite difficult and the result is close to optimal.

The PI controller parameters are chosen conservatively in a situation with low flow and temperature. The controller response time could possibly be improved by limiting the operating range of the system or by adding some kind of gain scheduling. However, the gain scheduling should only be based on the information given by the evaporator outlet temperature measurement. Feedforward, when a step in the reference is made, could also improve the controller.

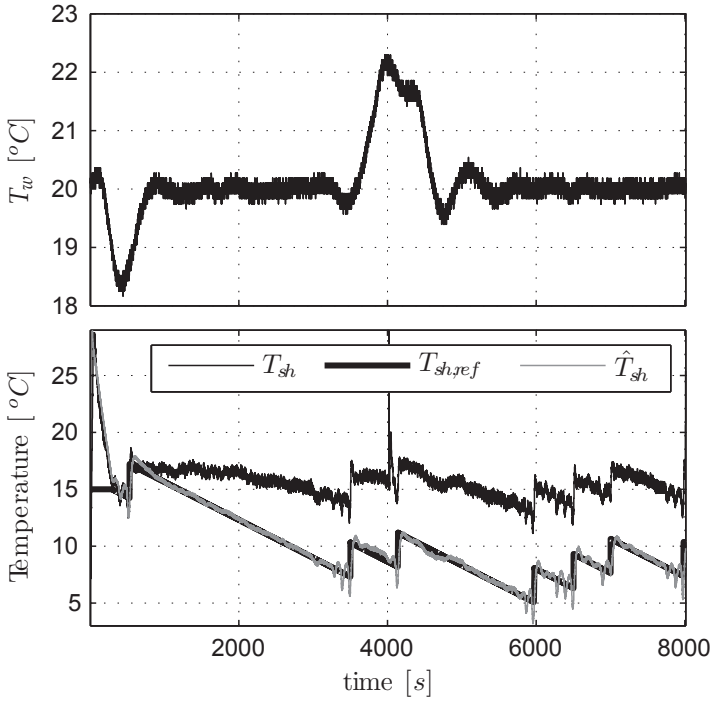

Figure 4.8: Closed-loop test results on the refrigeration system with a sudden change in the water temperature T_w.

8 Conclusion

Evaporator superheat control is important in order to optimize the heat transfer in refrigeration systems and to prevent compressor wear. The superheat is conventionally obtained by subtracting the evaporation temperature, given by a pressure sensor, from the temperature at the evaporator outlet. In this paper we have shown that the pressure sensor can be saved by looking at the variance in the outlet temperature, which have shown to increase at low superheat. Results from tests on two different refrigeration systems indicate that the proposed controller, using qualitative system knowledge, can control the evaporator superheat to a low level giving close to optimal filling of the evaporator, with only one temperature sensor. No a priori model knowledge was used and it is anticipated that the method is applicable on a wide variety of refrigeration systems.

Acknowledgments

The authors gratefully acknowledge Danfoss A/S for disclosing initial ideas on possible approaches.

References

[1] I. Dincer and M. Kanoglu, *Refrigeration Systems and Applications*, 2nd ed. Wiley, 2010.

[2] J. E. Seem, "A New Pattern Recognition Adaptive Controller with Application to HVAC Systems," *Automatica*, vol. 34, no. 8, pp. 969–982, August 1998.

[3] K. J. Åström and T. Hägglund, *Automatic Tuning of PID Controllers*. Instrument Society of America, 1988.

[4] K. J. Åström and B. Wittenmark, *Adaptive Control*, 2nd ed. Addison-Wesley Publishing, 1995.

[5] H. Rasmussen, C. Thybo, and L. F. S. Larsen, "Automatic Tuning of the Superheat Controller in a Refrigeration Plant," in *Portuguese Conference on Automatic Control*, Lisboa, Portugal, September 2006.

[6] Q. Bi, W. Cai, Q. Wang, C. Hang, E. Lee, Y. Sun, K. Liu, Y. Zhang, and B. Zou, "Advanced controller auto-tuning and its application in HVAC systems," *Control Engineering Practice*, vol. 8, no. 6, pp. 633–644, June 2000.

[7] H. Rasmussen, C. Thybo, and L. F. S. Larsen, "Nonlinear Superheat and Evaporation Temperature control of a Refrigeration Plant," in *IFAC ESC'06: Energy Saving Control in Plants and Buildings*, Bansko, Bulgaria, October 2006, pp. 252–254.

[8] M. S. Elliott and B. P. Rasmussen, "On reducing evaporator superheat nonlinearity with control architecture," *International Journal of Refrigeration*, vol. 33, no. 3, pp. 607–614, May 2010.

[9] H. Rasmussen and L. F. S. Larsen, "Nonlinear superheat and capacity control of a refrigeration plant," in *Mediterranean Conference on Control & Automation*, Thessaloniki, Greece, June 2009, pp. 1072–1077.

[10] H. Rasmussen, "Adaptive Superheat Control of a Refrigeration Plant using Backstepping," in *International Conference on Control, Automation and Systems*, Seoul, Korea, October 2008, pp. 653–658.

[11] X.-D. He, S. Liu, H. H. Asada, and H. Itoh, "Multivariable Control of Vapor Compression Systems," *HVAC&R Research*, vol. 4, no. 3, pp. 205–230, February 1998.

[12] G. F. Franklin, J. D. Powell, and A. Emami-Naeini, *Feedback Control of Dynamic Systems*, 5th ed. Pearson Prentice Hall, 2006.

[13] D. Lim, B. P. Rasmussen, and D. Swaroop, "Selecting PID Control Gains for Nonlinear HVAC&R Systems," *HVAC&R Research*, vol. 15, no. 6, pp. 991–1019, 2009.

Paper B

Utilization of Excitation Signal Harmonics for Control of Nonlinear Systems

Kasper Vinther, Henrik Rasmussen, Roozbeh Izadi-Zamanabadi, and Jakob Stoustrup

This appendix is based on a paper published in:
The proceedings of the IEEE Multi-conference on Systems and Control (MSC), October 2012

Abstract

Many model-based control methods exist in the literature. Producing a sufficient system model can be cumbersome and a new non model-based method for control of nonlinear systems with input/output maps exhibiting sigmoid function properties is therefore proposed. The method utilizes an excitation signal together with Fourier analysis to generate a feedback signal and simulations have shown that different system gains and time constants does not change the global equilibrium/operating point. An evaporator in a refrigeration system was used as example in the simulations, however, it is anticipated that the method is applicable in a wide variety of systems satisfying the sigmoid function properties.

1 Introduction

Most physical systems or processes are inherently nonlinear in nature, which makes design and tuning of controllers difficult, especially if the controller is expected to work in a large operation area, thus experiencing the full effect of the nonlinearity. Additionally, most systems are also time-varying to some degree and change with unpredictable operating conditions and disturbances. This makes controller design even more difficult and often result in poorly tuned controllers. Possible ways to control these systems are with gain scheduling for time-varying systems, see e.g. [1, 2], or adaptive backstepping control, see e.g. [3, 4].

Producing a sufficient nonlinear model for control purposes can be cumbersome, especially for time-varying systems. Furthermore, a suitable reference operating point is often not known beforehand. A good alternative is therefore to look at non model-based methods such as extremum-seeking control, if it is desirable to drive the process output towards an extremum. If the input/output map does not have an extremum, but is instead "S" shaped exhibiting sigmoid function properties, then it is possible to use slope-seeking control. This is just a generalization of extremum-seeking control, where the reference slope is not zero. There are many examples of extremum- and slope-seeking control applied to practical control problems, see e.g. [5–7].

In this paper we look at a non model-based approach for control of time-varying nonlinear systems, where the input/output map exhibits sigmoid function properties. A problem with slope-seeking control is that it can be hard to identify a reference slope, since the slope is often dependent on systems parameters that change with operating conditions. Another problem is that a badly chosen reference slope can make the system unstable, since a reference slope will be mirrored around the middle of the "S" shaped curve. If for example one chooses the slope at the middle of the curve as reference, then the slope will decrease in both directions leading to instability. An example of a system where the middle of the curve could be a desirable operating point is given in Section 2.

We instead propose a novel control method called harmonic control for such types of systems. A Fourier analysis is conducted in this method to identify the distortion of an excitation signal as it passes the system nonlinearity. Taking the cross product between the first and second harmonic of the excitation signal gives an error signal which is negative and positive depending on which side of the middle of the "S" shaped curve the current operating point is located. In other words, qualitative knowledge about the system nonlinearity is used together with Fourier analysis of an excitation signal to generate an

error signal for feedback purposes. The amplitude of the excitation signal can furthermore be adapted to better suite the current gain in the system, giving a controllable amount of excitation in the output. The proposed method has potential in any system having a nonlinear "S" shaped input/output map and it does not require any reference setpoint nor does it have the instability problem experienced with slope-seeking control. Replacing sensors with qualitative knowledge in the control loop also has the potential of reducing the commissioning costs and in some systems it might also be difficult or even impossible to measure certain states.

The structure of this paper is as follows. An example of a nonlinear system is first given in Section 2, which will be used for simulation purposes. Then, the concept of harmonic control is given in Section 3, which entails a presentation of the control strategy, how the error and control signal is generated, and adaptation of the excitation signal amplitude. The harmonic control is then applied to the nonlinear system in simulation and compared with slope-seeking control and the results are presented in Section 4. Finally, conclusions are drawn in Section 5.

2 System Nonlinearity

The nonlinear system given as example in this paper is an evaporator in a refrigeration system. Refrigeration systems normally operate by continuous vaporization and compression of refrigerant. This process is maintained by a valve, an evaporator, a compressor and a condenser, and this setup remains to a considerable extent the same. The details of the vapor compression type refrigeration process are not given here, but can be found in e.g. [8].

Refrigeration systems are typically controlled by decentralized control loops and evaporator superheat is controlled in one of these loops by regulating the opening degree OD of a valve, see e.g. [9–11]. Superheating the refrigerant beyond the evaporation temperature is important, since no superheat means that two-phase refrigerant will enter the compressor and increase the power consumption and wear. Therefore, the valve flow must be kept at a level, where all refrigerant is evaporated before it reaches the compressor. However, there should be as much two-phase refrigerant in the evaporator as possible, to increase the heat transfer and thus optimize the refrigeration process.

The level of superheat in the evaporator is traditionally determined using at least a temperature sensor at the evaporator outlet and a pressure sensor, which can be used to calculate an evaporation temperature. The response from input to output in the evaporator is in general very nonlinear, making controller tuning difficult. However, it has been observed that the nonlinear response from valve OD to evaporator outlet temperature in some refrigeration systems follow an "S" shaped curve, and it is believed that exploiting this qualitative system knowledge not only has the potential of saving a pressure sensor, since this behavior is observable in the outlet temperature alone, but can also simplify the controller design significantly.

A test was conducted on a refrigeration system with a water tank and heater as load on the evaporator. The system has an Electronic Expansion Valve (EEV) with controllable OD and controllable compressor and condenser fans. Sensors furthermore measure temperatures, pressures and flow and the system is monitored and controlled using the XPC toolbox for Simulink. In the test the OD of the EEV was slowly increased while the

evaporator outlet temperature was measured (the compressor speed and condenser pressure was kept constant during this test). The result of this test is presented in Fig. 5.1. The evaporator outlet temperature $T_{e,o}$ for this refrigeration system follows an "S" shaped curve, and this system nonlinearity is then approximated using the inverse trigonometric function $atan$ shown in the bottom graph in Fig. 5.1. The mathematical expression is

$$y = \left(-atan\left(\frac{4\pi\left(u - 50\right)}{50} \right) + \frac{\pi}{2} \right) 10, \tag{5.1}$$

where y is the output (evaporator outlet temperature $T_{e,o}$) and u is the input (OD). The OD is limited to a value between 0-100% open, where $OD = 50\%$ is located in the middle of the "S" shaped curve. This point in the "S" shaped curve also represents a close to optimal setpoint for the outlet temperature, as the evaporator is nearly filled (low superheat). A lower superheat is hard to maintain and does not provide that much safety margin.

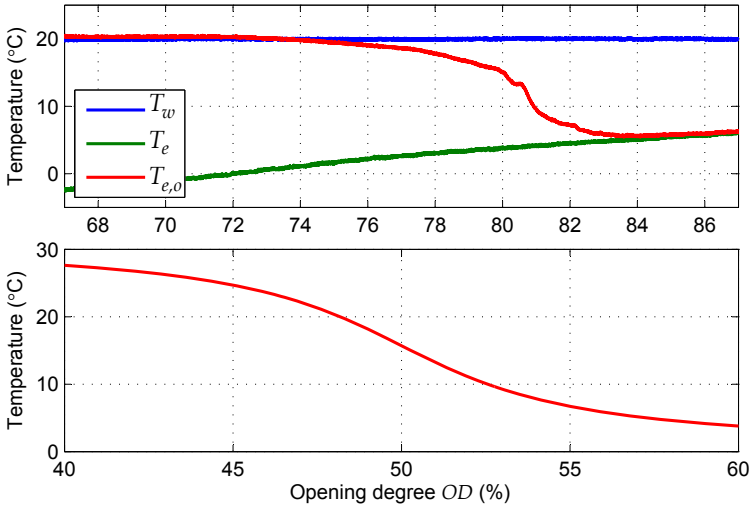

Figure 5.1: The top graph shows the evaporation temperature T_e, outlet temperature $T_{e,o}$ and ambient water temperature T_w for an evaporator during a sweep in the OD of the EEV. The bottom graph is an approximation of the nonlinearity seen in the outlet temperature.

The approximation in Fig. 5.1 is shown again in Fig. 5.2 where the system input has been overlayed with a sine excitation signal in three different operating points. It is clear from the output of the system that the sine excitation has been distorted. This is due to the nonlinearity in the system. In point (1) and (3) the sine is distorted more to one side than the other and in point (2) the distortion is equally large in both directions. Looking at the power spectrum density made over 80 periods of the excitation signal, it is observable that the output consist mainly of an offset and the first and second harmonic of the excitation signal.

A system time constant T_{sys} and delay T_d is furthermore added to the approximation

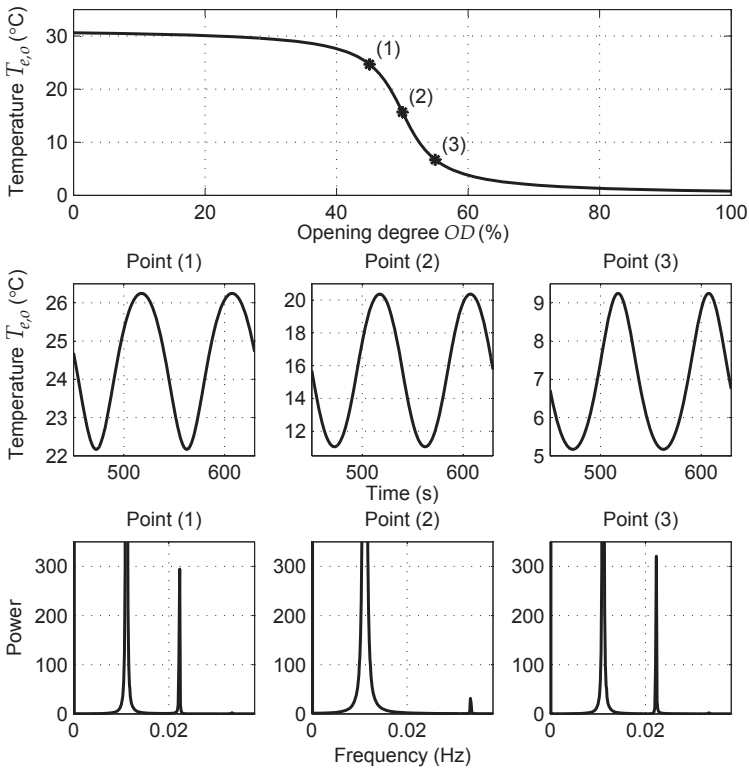

Figure 5.2: The top graph shows the nonlinear input/output map with three operating points marked as (1), (2) and (3). The system is excited with a sine wave in each of these points and the steady state output is shown in the middle graphs along with a power spectrum density analysis in each operating point (bottom graphs).

of the output described in (5.1), given in the Laplace domain as

$$G(s) = \frac{1}{1 + sT_{sys}} e^{-sT_d}. \tag{5.2}$$

The value of T_{sys} and T_d can be chosen almost arbitrarily and in this simulation example they are set to 25 and 10 seconds, respectively. Note that (5.1) and (5.2) combined gives a Hammerstein model structure.

The system nonlinearity used in this paper is taken from a test refrigeration system, with valve OD as input and evaporator outlet temperature $T_{e,o}$ as output. However, it is important to remember that the method applies in general for systems, with nonlinearities that can be approximated with sigmoid functions.

3 Harmonic Control

This section introduces the concept of harmonic control. Various situations are analyzed through simulation and indicative conclusions are drawn based on the observed behavior

of the excited system.

Control Strategy

The distortion seen in Fig. 5.2 can be used to generate an error signal. This distortion is measurable through Fourier analysis and requires a continuous excitation of the system, e.g. using a sine wave. The error signal ξ_n can then be used to drive the nonlinear system to the state with the highest gain (the middle of the "S" shaped nonlinearity), e.g. using Proportional-Integral (PI) control. Additionally, the Fourier analysis can give an estimate of the amplitude of the excitation in the output, which provides a way to adapt the amplitude of the excitation signal A_{ex} at the input, in order not to disturb the system more than what is necessary. The proposed control strategy called harmonic control is depicted in Fig. 5.3. In case there is saturation on the input it can help to add anti-windup to the integral part of the PI control. Furthermore, using the harmonics to generate the error signal acts as a powerful way of filtering the measurement. However, an adequate time scale separation between the system dynamics, the excitation frequency (Fourier analysis), and the PI controller is required, which is also the case with extremum- and slope-seeking control, see [5]. The next two subsections will address error signal generation and adaptation of the excitation signal amplitude.

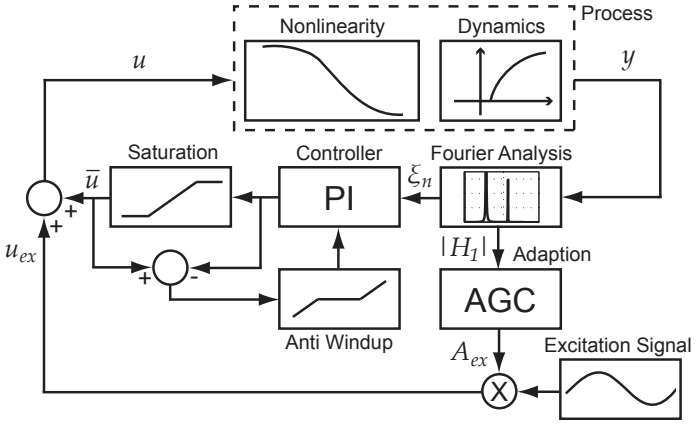

Figure 5.3: Block diagram of proposed closed-loop harmonic control.

Error Signal Generation

The discrete Fourier series $F(t)$ of a periodic function $f(t)$, sampled at time t_n with sampling time T_{ex}/N (N is the number of samples in one period T_{ex}), is given as

$$F(t) = a_0 + \sum_{p=1}^{M} \left[a_p cos(p\frac{2\pi}{T_{ex}}t) + b_p sin(p\frac{2\pi}{T_{ex}}t) \right] \tag{5.3}$$

$$
\begin{aligned}
a_0 =& \frac{1}{N}\sum_{n=1}^{N} f(t_n) \\
a_p =& \frac{2}{N}\sum_{n=1}^{N} f(t_n) cos\left(p\frac{2\pi}{N}n\right),\ p = 1, ..., \frac{N}{2} - 1 \\
b_p =& \frac{2}{N}\sum_{n=1}^{N} f(t_n) sin\left(p\frac{2\pi}{N}n\right),\ p = 1, ..., \frac{N}{2} - 1,
\end{aligned}
$$

where a_p and b_p are the Fourier coefficients for each of the M harmonics denoted by p. If taking N samples it is possible to determine $M = N/2$ harmonics. Mathematical study of the overlapping waves is called harmonic analysis and the Fourier coefficients of the first and second harmonic can be used to generate a scalar error signal ξ using the cross product of vectors in $\mathbb{R}^2$ given as

$$
\xi = \begin{bmatrix} a_1 \\ b_1 \end{bmatrix} \times \begin{bmatrix} a_2 \\ b_2 \end{bmatrix} = a_1 b_2 - a_2 b_1. \tag{5.4}
$$

The cross product between the first and second harmonic is also defined as

$$
\begin{aligned}
\begin{bmatrix} a_1 \\ b_1 \end{bmatrix} \times \begin{bmatrix} a_2 \\ b_2 \end{bmatrix} =& |H_1||H_2| sin(\theta_{12}) \\
|H_1| = \sqrt{a_1^2 + b_1^2}, |H_2| =& \sqrt{a_2^2 + b_2^2},
\end{aligned} \tag{5.5}
$$

where $|H_1|$ and $|H_2|$ are the amplitudes of the first and second harmonic respectively and θ_{12} is the angle from the first harmonic to the second harmonic. The cross product is a normal vector and it is positive if the operating point is located to the right of the middle of the "S" shaped nonlinearity and negative to the other side. If there is enough time separation between system dynamics and excitation, then the two vectors in the cross product will be almost perpendicular. Equation (5.4) therefore provides a usable error signal for feedback. However, the error signal is still nonlinear, which can be corrected by making a normalization with respect to the cubed amplitude of the first harmonic.

$$
\xi_n = \frac{a_1 b_2 - a_2 b_1}{\sqrt{a_1^2 + b_1^2}^3} = \frac{a_1 b_2 - a_2 b_1}{\left(a_1^2 + b_1^2\right)^{1.5}}. \tag{5.6}
$$

The normalized error signal ξ_n is calculated at different OD values in Fig. 5.4, 5.5, 5.6 and 5.7 under different situations to visualize the effects on the error signal. Note that the Fourier coefficients a_1, b_1, a_2, and b_2 are determined online in the implementation using time-invariant linear FIR filters with the same sample time as the rest of the system and a ring buffer of size N in accordance with (5.3).

Fig. 5.4 shows the error signal using three different system time constants. The normalized error remains linear in all cases. A change in the system delay T_d has the same effect, however, an increase gives a decrease in the slope of the normalized error. Fig. 5.4 also indicates that the generated error can give a globally stable controller with only one equilibrium at the point of zero mean curvature. This is under the assumption that the nonlinearity fulfill the properties of a sigmoid function and that the succeeding controller is sufficiently slow compared to the excitation of the system.

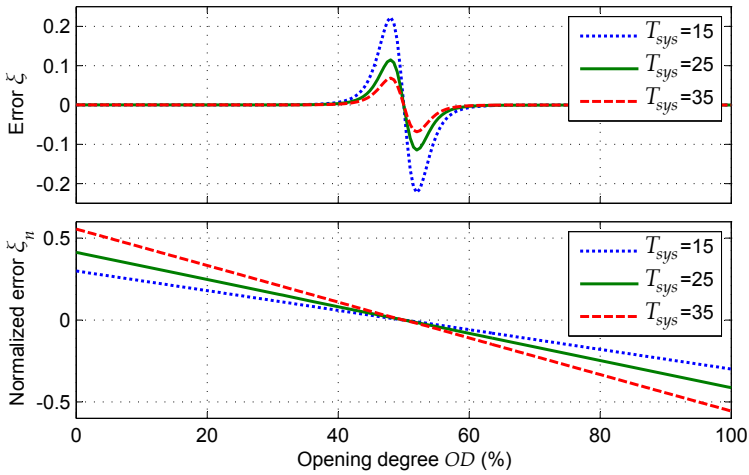

Figure 5.4: Error signal and normalized error signal at different OD values. Same system nonlinearity as in Fig. 5.2 with dynamics and different system time constants.

Fig. 5.5 shows the error signal with three different system gains (the total gain in the system is changed $\pm 25\%$). Again the normalized error signal remains linear in all cases and the closed-loop system will converge to the same point. This is not achievable with slope-seeking control, since the reference slope will have to be changed.

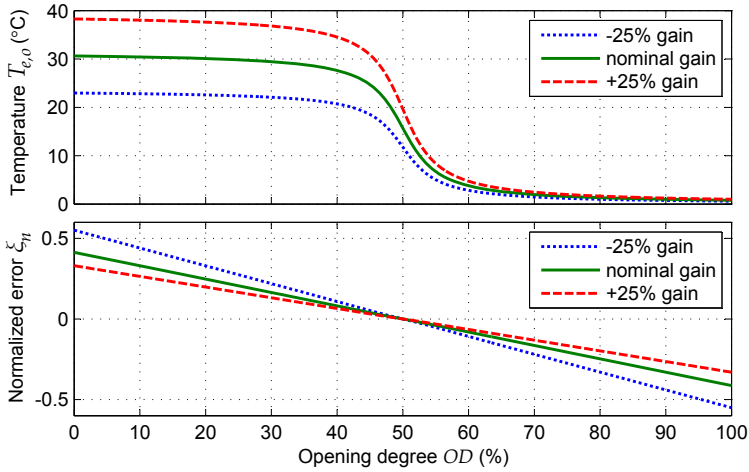

Figure 5.5: Top graph shows the system with three different gains and the bottom graph shows the corresponding normalized error signal at different OD values.

Fig. 5.4 and 5.5 also indicates that the slope of the normalized error signal increases when the time constants increases and decreases when the delay and gain in the system increases. Therefore, the controller gain should be chosen based on the worst case values of the system time constant, delay and gain, assuming that the system can be approximated

with the dynamics described in (5.2) including a parameter varying nonlinear gain.

The system time constant and delay also determines the period of the excitation signal as this period should be slow enough to make the excitation visible in the output and at the same time as fast as possible to speed up the controller. Fig. 5.6 shows the error signal using three different excitation signal periods T_{ex}. Using $T_{ex} = 45$ makes the closed-loop system loose global stability at low OD values. Simulations have shown that the excitation signal period should at least be twice the combined system time constant and delay. Any higher period time gives approximately the same normalized error, which means that it does not affect the controller gain.

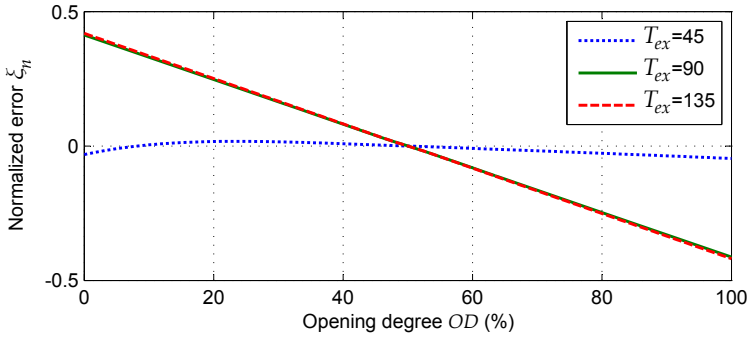

Figure 5.6: Normalized error signal at different OD values. Same system nonlinearity as in Fig. 5.2 with dynamics and different excitation periods.

Fig. 5.7 finally shows the error signal using three different excitation signal amplitudes A_{ex}. Changing the amplitude between 2% to 4% in OD does not change the normalized error signal and the amplitude can therefore be adapted without compromising the controller. However, the amplitude should still be within reasonable bounds and large enough to overcome any noise and quantizations in the measurement.

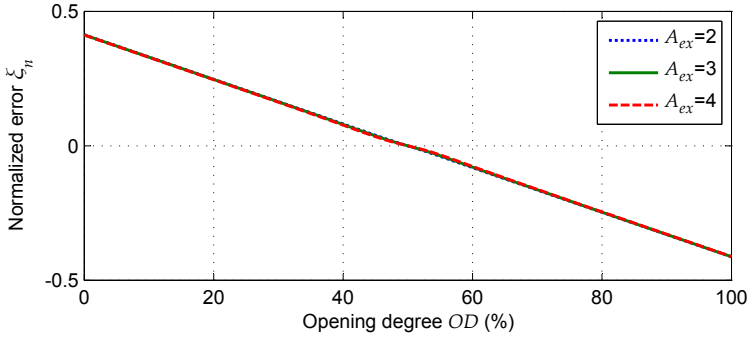

Figure 5.7: Normalized error signal at different OD values. Same system nonlinearity as in Fig. 5.2 with dynamics and different excitation amplitudes.

One problem with Fourier analysis is that the Fourier series defined in (5.3) only converge to the output if the system is periodic. This is not the case when the system

is operated in closed-loop, especially during startup, unless the controller is tuned so slow that the output looks periodic. Fig. 5.8 shows an open-loop simulation, where the OD is kept constant and then slowly increased giving a periodic and an aperiodic part. The power spectrum density is calculated for each part and the aperiodic part has more low frequency content. However, reconstructing the signal using a Fourier series is not required, since we only use the two first harmonics to calculate an error signal and these harmonics are still present.

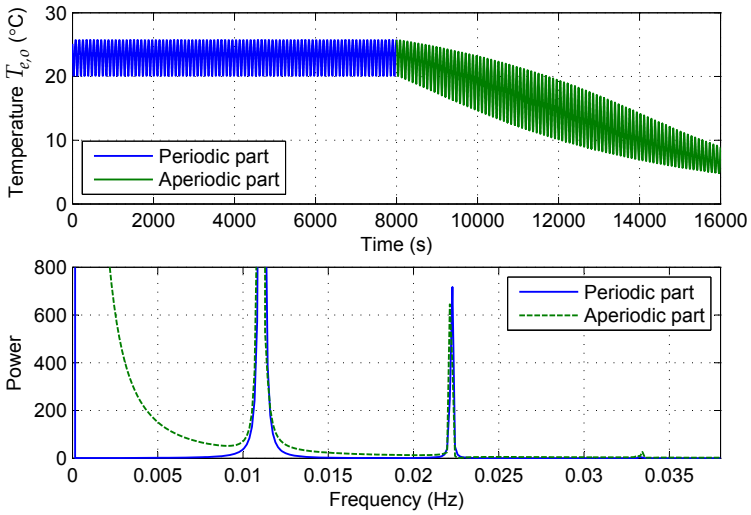

Figure 5.8: Power spectrum density analysis of periodic steady state operation and aperiodic operation. The OD was slowly increased in the simulation between 8000 to 16000 seconds, giving the aperiodic output.

Adaptation of Excitation Signal Amplitude

The gain in the nonlinear system is largest at the equilibrium point. In order to be able to generate enough excitation of the output at low gains, while still maintaining an acceptable level of excitation when the gain is highest, it is often necessary to adapt the excitation amplitude. The harmonic analysis used to calculate the error signal can also be used for adaptation. The amplitude of the first harmonic $|H_1|$, calculated as in (5.5), is a good approximation of the amplitude of the excitation at the output. Keeping this amplitude close to a reference can be achieved by changing the input excitation signal amplitude. However, it is undesirable to change the amplitude instantly in closed-loop, since this will result in unstable behavior. The MIT rule is therefore used to adapt the amplitude slowly and it is defined as (see e.g. [12]);

$$J = \frac{1}{2}e^2 \tag{5.7}$$

$$\frac{d\theta}{dt} = -\gamma\frac{\partial J}{\partial \theta} = -\gamma e\frac{\partial e}{\partial \theta}, \tag{5.8}$$

where J is an objective function to be minimized, e is the error, θ is the adjustable parameter to be adapted and γ is the adaptation gain. The MIT rule can be interpreted as a gradient method for minimizing the error and in the case of adapting the amplitude $|H_1|$ we have

$$\theta = |H_1| \tag{5.9}$$

$$e_{|H_1|} = |H_1|_{ref} - |H_1| \tag{5.10}$$

$$\frac{dc}{dt} = \gamma e_{|H_1|}, \tag{5.11}$$

since the partial derivative of $e_{|H_1|}$ is equal to -1. The amplitude $|H_1|_{ref}$ is the desired reference amplitude of the first harmonic. Only the adaptation gain γ has to be chosen. In general a small γ means slow convergence and a large γ means fast convergence and possibly instability. However, it is hard to say in general how γ influences time-variant systems, but a general rule is that the adaptation must be slower than the control loop. Another possibility would be to use the normalized MIT rule, which would lead to less sensitivity towards signal levels or one could use Lyapunov stability theory to adapt the amplitude $|H_1|$, and most likely obtain faster adaptation and stability guarantees.

4 Simulation Results

The performance of harmonic and slope-seeking control is compared in this section. The reference slope in slope-seeking was set manually to a value giving a reference operating point just above point (2) and below (1), see Fig. 5.2. Note that (2) is an unstable point in slope-seeking control.

The proportional gain $K_{p,h}$, the integral time T_i and integral reset time T_t were tuned manually for the harmonic controller and set to 0.2, 2 and 2 respectively. This gives a good compromise between convergence speed and robustness. The system can maintain a stable limit cycle at a critical controller gain, which can be found approximatively using the describing function method. Due to space limitations this analysis will not be part of this paper, but will be considered in future publications. The slope-seeking control gain $K_{p,s}$ was also tuned manually and set to 0.04, which is small enough to give acceptable oscillations in the control signal. The oscillations appear after the demodulator and a low pass filter can help filter this out [5].

The OD signal has a saturation limit of 0 to 100%, and this was lowered in the controller to between 5 to 95% to allow the excitation signal to get through uncut. The adaptation gain γ in the harmonic controller should be slower than the PI control and was set to 0.00003, with a reference amplitude $|H_1|_{ref}$ of 2. Furthermore, the excitation signal amplitude was set to 2 in the slope-seeking controller. Fig. 5.9 shows the performance of the two controllers in a simulation without measurement noise and disturbances. The slope-seeking controller reaches a settling boundary of 5% of the step size about twice as fast as the harmonic controller, however, the harmonic controller can go to 50 in control signal without becoming unstable. If the reference slope was changes just slightly up or if the gain in the slope-seeking controller was raised giving more pronounced oscillations, it would make the controller go to the saturation limit of 95. The excitation signal amplitude was adapted during the simulation shown in Fig. 5.9 and the results are presented in Fig. 5.10. The excitation signal amplitude is slowly adapted from 5 to approximately 1.7,

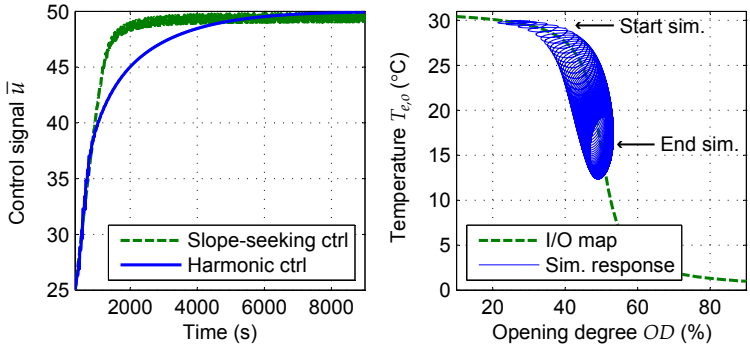

Figure 5.9: Harmonic and slope-seeking control performance. Both controllers are started at a control signal value of 25 and the desired value is 50. Right plot shows the simulation response of the harmonic control in an I/O map.

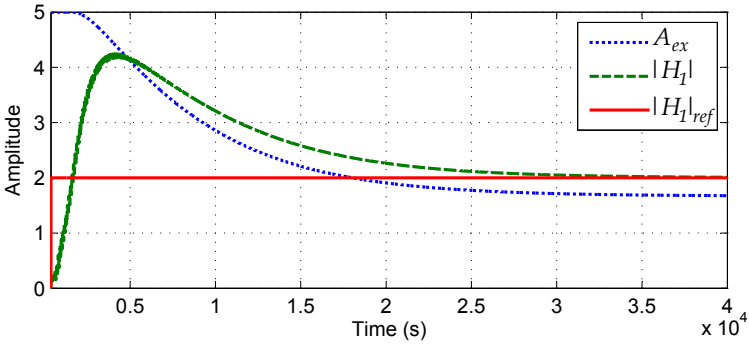

Figure 5.10: Adaptation of the excitation signal amplitude A_{ex} during the simulation shown in Fig. 5.9. The amplitude of the first harmonic $|H_1|$ is used as feedback signal.

which makes the amplitude of the first harmonic $|H_1|$ converge to the reference of 2. The upper limit is 5 due to the saturation limits.

Fig. 5.11 shows the performance of the two controllers in a simulation with measurement noise ($2\sigma = 0.14°C$) and a disturbance in the system nonlinearity. The performance is similar to the performance without noise, however, the harmonic controller experiences small oscillations in the control signal when the gain in the system is low ($\bar{u}$ between 25 to 37), but it does converge to the correct operating point. Quantization on the measurement of $0.1°C$ and on the valve of 0.2% was also added in the simulation shown in Fig. 5.11 to simulate realistic conditions. This quantization does not disturb the controllers noticeably.

The disturbance was made as an increase in the total gain in the system of 25%, see Fig. 5.5, introduced with a time constant of 10 seconds, 15000 seconds into the simulation. This corresponds to a decrease in the flow in the refrigeration system and causes the control signal in the slope-seeking controller to decrease as the reference slope now corresponds to a different operating point. If the disturbance was made as a decrease

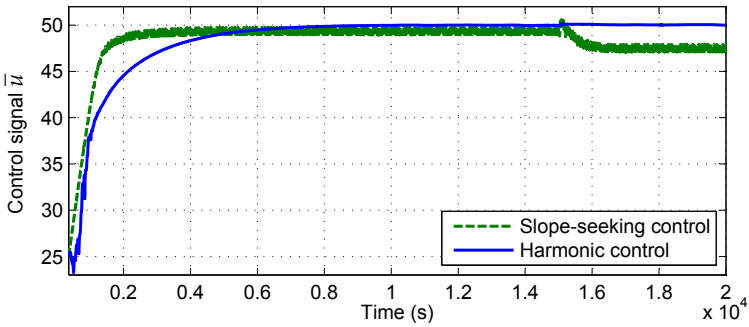

Figure 5.11: Same simulation as in Fig. 5.9, but with added measurement noise, measurement quantization and actuator quantization. The system nonlinearity is changed slightly at 15000 seconds.

in the gain, then the slope-seeking controller would have become unstable. In comparison the harmonic controller does not deviate from the operating point.

The promising simulation results have lead to the implementation of the control method on two different test refrigeration system in our laboratory and the results are presented in [13].

5 Conclusion

A new non model-based method for control of nonlinear systems with input/output map exhibiting sigmoid function properties have been proposed. The method is called harmonic control and utilize an excitation signal together with Fourier analysis to obtain qualitative knowledge about where on the nonlinearity the closed-loop system is located.

It was discovered that the excitation signal amplitude and period has little to no effect on the linear error signal as long as the period is about twice as large as the system time constant and delay. The amplitude of the signal can therefore be adapted to limit the unavoidable oscillations in the output due to the excitation. The control method was also simulated using different system gains and time constants, which did not change the global equilibrium/operating point. This was not the case with slope-seeking control. Furthermore, slope-seeking has stability problems if the reference slope is not chosen carefully and in general it can be difficult to obtain a suitable reference slope.

An evaporator in a refrigeration system was used as example in the simulations. However, it is anticipated that the method in general is applicable when the point of zero mean curvature of the system nonlinearity is close to the desired operating point and when the system input/output map satisfies the sigmoid function properties.

References

[1] D. J. Leith and W. E. Leithead, "Survey of gain-scheduling analysis and design," *International Journal of Control*, vol. 73, no. 11, pp. 1001–1025, 2000.

[2] J. Jang, A. M. Annaswamy, and E. Lavretsky, "Adaptive control of time-varying systems with gain-scheduling," in *American Control Conference*, Seattle, Washington, USA, June 2008, pp. 3416–3421.

[3] J. Zhou and C. Wen, "Adaptive backstepping control of uncertain systems," in *Control and Information Science*, M. Thoma and M. Morari, Eds. Springer, 2008.

[4] H. Rasmussen, "Adaptive Superheat Control of a Refrigeration Plant using Backstepping," in *International Conference on Control, Automation and Systems*, Seoul, Korea, October 2008, pp. 653–658.

[5] K. B. Ariyur and M. Krstić, *Real-Time Optimization by Extremum-Seeking Control*. Wiley-Interscience, 2003.

[6] M. Guay, D. Dochain, and M. Perrier, "Adaptive extremum-seeking control of non-isothermal continuous stirred tank reactors," *Chemical Engineering Science*, vol. 60, no. 13, pp. 3671–3681, 2005.

[7] L. Henning, R. Becker, G. Feuerbach, R. Muminovic, R. King, A. Brunn, and W. Nitsche, "Extensions of adaptive slope-seeking for active flow control," *Proceedings of the Institution of Mechanical Engineers, Part I: Journal of Systems and Control Engineering*, vol. 222, no. 5, pp. 309–322, May 2008.

[8] I. Dincer and M. Kanoglu, *Refrigeration Systems and Applications*, 2nd ed. Wiley, 2010.

[9] H. Rasmussen and L. F. S. Larsen, "Nonlinear superheat and capacity control of a refrigeration plant," in *Mediterranean Conference on Control & Automation*, Thessaloniki, Greece, June 2009, pp. 1072–1077.

[10] L. F. S. Larsen, C. Thybo, J. Stoustrup, and H. Rasmussen, "A Method for Online Steady State Energy Minimization, with Application to Refrigeration Systems," in *IEEE Conference on Decision and Control*, Paradise Island, Bahamas, December 2004, pp. 4708–4713 Vol. 5.

[11] M. S. Elliott and B. P. Rasmussen, "On reducing evaporator superheat nonlinearity with control architecture," *International Journal of Refrigeration*, vol. 33, no. 3, pp. 607–614, May 2010.

[12] K. J. Åström and B. Wittenmark, *Adaptive Control*, 2nd ed. Addison-Wesley Publishing, 1995.

[13] K. Vinther, H. Rasmussen, R. Izadi-Zamanabadi, and J. Stoustrup, "Single Temperature Sensor based Evaporator Filling Control using Excitation Signal Harmonics," in *IEEE Multi-Conference on Systems and Control*, Dubrovnik, Croatia, October 2012, pp. 757–763.

Paper C

Single Temperature Sensor Based Evaporator Filling Control Using Excitation Signal Harmonics

Kasper Vinther, Henrik Rasmussen, Roozbeh Izadi-Zamanabadi, and Jakob Stoustrup

This appendix is based on a paper published in:
The proceedings of the IEEE Multi-conference on Systems and Control (MSC), October 2012

Abstract

An important aspect of efficient and safe operation of refrigeration and air conditioning systems is superheat control for evaporators. This is conventionally controlled with a pressure sensor, a temperature sensor, an expansion valve and Proportional-Integral (PI) controllers or more advanced model-based control. In this paper we show that superheat can be controlled without a pressure sensor and without a model of the system. This is achieved by continuous excitation of the system and by applying Fourier analysis, which gives an error signal that can be used together with standard PI control. The proposed method works for systems with "S" shaped input/output maps that satisfy sigmoid function properties and such behavior has been identified in both an air conditioning and a refrigeration system. Tests on these systems show that the superheat can be controlled to a low level over a large operating range with only one sensor. It is believed that the method in general is applicable to a wide variety of nonlinear systems for which the desired operating points are close to points of zero mean curvature of system nonlinearities.

1 Introduction

Maximization of two-phase refrigerant flow in evaporators is an important aspect of efficient operation of refrigeration and air conditioning systems, because liquid refrigerant accounts for the majority of cooling. At the same time it is important that all refrigerant is vaporized before it enters the compressor to avoid the risk of compressor damage. Control of the evaporator filling level is also known as superheat control, where superheat is the difference between the evaporation temperature and the temperature of the vapor leaving the evaporator. Superheat control is generally achieved using an expansion valve and the most commonly used devices are the Thermostatic Expansion Valve (TXV) and the Electronic Expansion Valve (EEV).

The significant nonlinear response from the opening degree (OD) of the expansion valve to the evaporator superheat poses as a control challenge. TXV's operate well within a certain operating range, but are limited by a constant control gain, which is problematic, since changes in operating conditions for the nonlinear system can cause unstable behavior and actuator hunting [1, 2]. The EEV allows for much greater freedom in expansion valve control and introduces the possibility of using PID control, which is used in the majority of EEV superheat control setups seen today [2]. However, there is still a need for adaptation of the controller to changes in operating conditions, which is often solved using some variant of gain scheduling, see e.g. [3].

There are also alternatives to gain scheduling. In [4] nonlinearity compensation in the valve to superheat response is achieved using a cascaded feedback loop, [5] uses feedback linearization to compensate for nonlinearities and the backstepping design method is used in [6] to find a nonlinear superheat controller that works for a wide range of operating points. Another alternative is to use the compressor, instead of the valve, to control the superheat as done in [7]. There are many possibilities, however, a problem with advanced methods is that they often require a good model of the system, which can be difficult to produce and furthermore each system is often composed of components from many different manufactures making most systems unique. The desire for cheap systems in the industry also means less sensors and thus a need for even more accurate models.

We will in this paper show that the evaporator superheat can actually be controlled over a wide range of operating conditions using only a single temperature measurement at the outlet of the evaporator, thus saving a pressure sensor. Furthermore, this is achieved without using a model of the system and very little a priori system knowledge. Qualitative knowledge about the evaporator nonlinearity from valve input to evaporator outlet temperature is used instead of quantitative knowledge to control the filling of the evaporator. This is possible for Input/Output (I/O) relationships that have sigmoid function properties ("S" shaped I/O-map).

The proposed method has taken inspiration from excitation signal based extremum- and slope-seeking control, which are gradient descent non model-based methods (this subject is well covered in e.g. [8]). Extremum-seeking control has e.g. been used in [9] for optimization of condenser water temperature in chilled water cooling plants resulting in a minimization of the total sum of chiller and cooling tower power consumption and in [10] for optimization of air-side economizers in HVAC systems. However, the more general slope-seeking control is better suited for superheat control, since the nonlinear I/O-map is "S" shaped and the optimal superheat will be at a certain slope rather than where the slope is zero. A reasonable sub-optimal choice in general is where the slope is largest, since this gives an evaporator outlet temperature that lies between the surrounding temperature and evaporation temperature. However, finding an appropriate reference slope can be very difficult, since this changes with operating conditions and load.

While still using an excitation signal, as in slope-seeking control, we instead propose to use Fourier analysis to calculate an error signal for feedback. We have called this method harmonic control and it is presented in [11]. This is another approach for single-sensor superheat control than the variance-based method we presented in [12] and the benefit of harmonic control is that it does not require a system model, it works for a wide operating range, and it does not require any reference setpoints, which together means that it has a high degree of Plug and Play.

The structure of this paper is as follows. Two different test systems are first introduced in Section 2 followed by a description of the harmonic control method and simulation results in Section 3. Then safety logic is added to the control concept in Section 4 and the controller is tested on the two systems with results presented in Section 5. Finally, conclusions are drawn in Section 6.

2 System Descriptions

The proposed harmonic controller is designed for systems with steady state I/O-maps that exhibit sigmoid function properties and such qualitative behavior has been identified in the relation between the OD of an EEV and the outlet temperature $T_{e,o}$ of evaporators in two different refrigeration systems located at Aalborg University (`www.es.aau.dk/projects/refrigeration/`). This behavior is utilized for evaporator filling (superheat) control and the physical layout of the two systems are therefore described in the two following subsections, along with presentation of the qualitative behavior of the evaporator outlet temperature.

Air Conditioning System

A simplified schematic of the air conditioning system is presented in Fig. 6.1. This

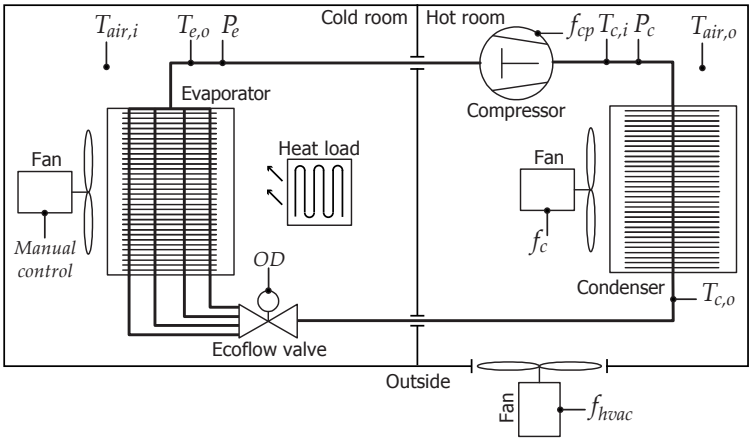

Figure 6.1: Simplified schematic of the air conditioning system. T, P and f are indicators for temperature sensors, pressure sensors and frequency control.

air conditioning system uses refrigerant type R410a and has a finned-tube evaporator with four channels and a cooling capacity of 11 kW. The refrigerant flow is controllable with a Danfoss Ecoflow™valve. It is possible to control the OD of the valve and the distribution of flow into the individual pipes, however, the distribution is kept constant in this setup. Furthermore, it is possible to control the frequency of both the evaporator and condenser fans, and also the frequency of the fans between the cold room, the hot room and the outside. The scroll compressor frequency is also controllable and sensors measure temperature and pressure at the indicated locations with a sampling interval of 1 second.

A test was conducted on the air conditioning system, where the OD of the valve was gradually increased with 0.01 $\%/s$ from low opening until the refrigerant overflows the evaporator (low superheat). The cold room temperature $T_{air,i}$, the evaporator fan speed, the compressor frequency f_{cp} and the condenser pressure P_c were kept constant during the OD sweep and the test result is shown in Fig. 6.2. The I/O-map is almost flat when

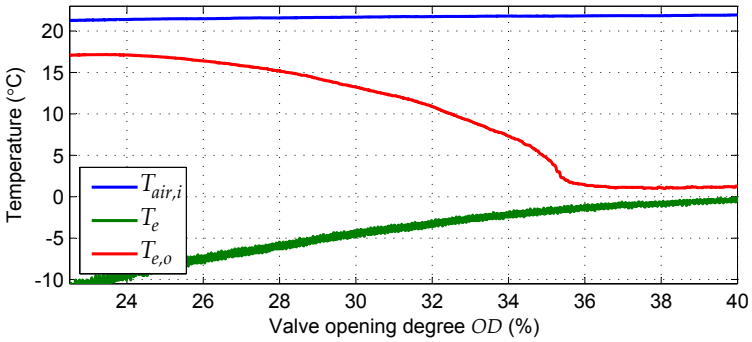

Figure 6.2: Evaporator outlet temperature $T_{e,o}$, room air temperature $T_{air,i}$ and evaporation temperature T_e during a sweep in OD.

the valve OD is below 25% and above 37%. Furthermore, it is approximately "S" shaped inbetween, with steepest decline at about 35% OD for the given operating conditions.

Refrigeration System

A simplified schematic of the refrigeration system is presented in Fig. 6.3. This refrigeration system has an evaporator with water on the secondary side, which is connected to a water tank with controllable heater and pump. The cooling capacity of the evaporator is 4 kW and the refrigerant type is R134a. It is possible to control the OD of the EEV and the condenser fan frequency. The compressor frequency is again controllable and sensors measure temperature and pressure at the indicated locations with a sampling interval of 1 second.

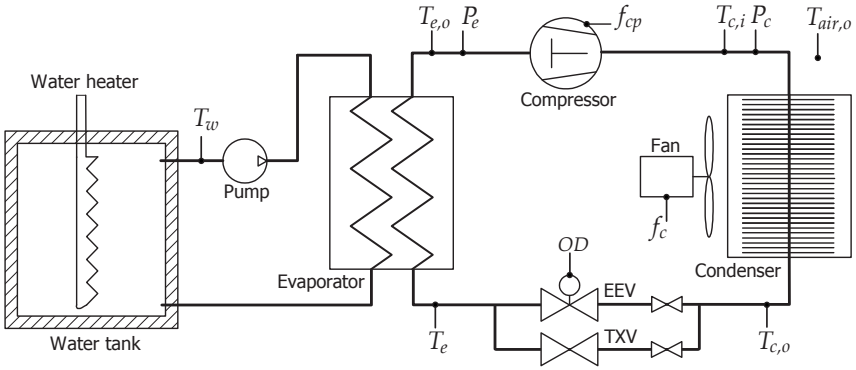

Figure 6.3: Simplified schematic of the refrigeration system. T, P and f are indicators for temperature sensors, pressure sensors and frequency control.

An OD sweep test was also conducted on the refrigeration system. The water temperature T_w, the pump speed, the compressor frequency f_{cp} and the condenser pressure P_c were again kept constant and the result is shown in Fig. 6.4. The I/O-map is similar to

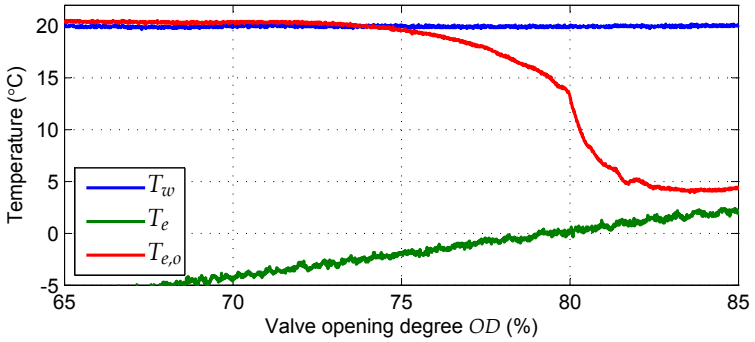

Figure 6.4: Evaporator outlet temperature $T_{e,o}$, water temperature T_w and evaporation temperature T_e during a sweep in OD.

the one shown in Fig. 6.2, however, with steepest decline at about 80% OD and more "S" shaped. In the following, we will utilize the observed qualitative behavior of the nonlinear I/O-map of the two systems, which exhibit sigmoid function properties.

3 Harmonic Control

We have in [11] presented the harmonic control concept. This control concept is intended for systems with a steady state nonlinear "S" shaped I/O-map that exhibits sigmoid function properties. A short description of harmonic control is given in the rest of this section and simulations, using the example system defined in (6.1) and (6.2), will be given, to show how the method works.

In the following the inverse trigonometric function $atan$ will be used as system nonlinearity. Note, however, that any function with sigmoid function properties could be used. The mathematical expression is

$$y = \left(-atan\left(k_1 \frac{(u - k_2)}{k_2} \right) + k_3 \right) k_4, \tag{6.1}$$

where y is the output, u is the input, and the rest ($k_1 = 10\pi$, $k_2 = 50$, $k_3 = \pi/2$, $k_4 = 7$) is arbitrary scaling. This gives the I/O-map shown in Fig. 6.5, where u is limited to values between 0-100 simulating an input saturation, which is seen in most systems. The input $u = 50$ is located in the middle of the "S" shaped curve and this also represents the desired operating point. In addition, first order dynamics with time constant T_{sys} and delay T_d is added;

$$G(s) = \frac{1}{1 + sT_{sys}} e^{-sT_d}. \tag{6.2}$$

The value of T_{sys} and T_d can be chosen almost arbitrarily and are set to 30 and 10 seconds respectively, in the simulation results presented in this paper. The nonlinear gain, input saturation, system time constant and delay are chosen to resemble the characteristics of the evaporator in the refrigeration system shown in Fig. 6.3.

The basic idea of harmonic control is to exploit the curvature of the nonlinear "S" shaped I/O-map. If a ramp signal is used as the input to such an I/O-map, then the first derivative is "bell" shaped and the second derivative (indicator of the curvature) is negative and positive respectively to each side of the middle of the "S" shaped I/O-map, as shown in Fig. 6.5. This makes the second derivative usable for feedback, if the middle of the "S" shape is a suitable operating point.

Finding the second derivative of a signal can be problematic due to e.g. measurement noise. The second derivative in the example simulation given above was about 4×10^4 times as small as the measured output. Furthermore, it is also necessary to somehow excite the system to "see" a derivative.

We propose, with the harmonic control method, to continuously excite the system using a sine wave. This makes it possible to indirectly measure the curvature of the I/O-map, locally at an operating point, by looking at the distortion of the excitation signal. This distortion is detectable through Fourier analysis, since distortion of a sine wave gives higher order harmonics.

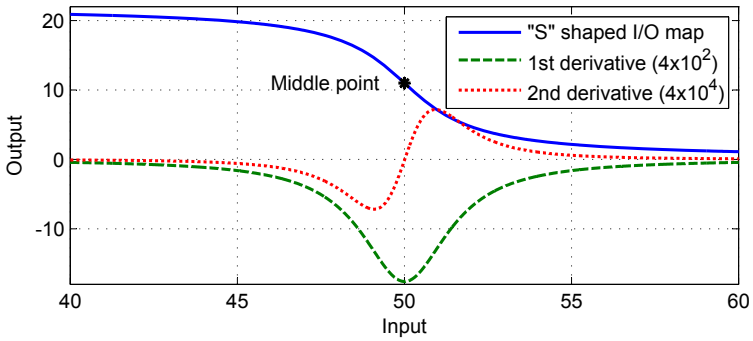

Figure 6.5: "S" shaped I/O-map (defined in (6.1)) and corresponding scaled first and second derivative when a ramp is used as input (rate 0.01 per second).

The discrete Fourier series $F(t)$ of a periodic function $f(t)$, sampled at time t_n with sampling time T_{ex}/N, where N is the number of samples in one period T_{ex}, is given as

$$
\begin{aligned}
F(t) =& a_0 + \sum_{p=1}^{M} \left[a_p cos(p\frac{2\pi}{T_{ex}}t) + b_p sin(p\frac{2\pi}{T_{ex}}t) \right] \qquad (6.3)\\
a_0 =& \frac{1}{N}\sum_{n=1}^{N} f(t_n)\\
a_p =& \frac{2}{N}\sum_{n=1}^{N} f(t_n) cos\left(p\frac{2\pi}{N}n\right),\ p = 1, ..., \frac{N}{2} - 1\\
b_p =& \frac{2}{N}\sum_{n=1}^{N} f(t_n) sin\left(p\frac{2\pi}{N}n\right),\ p = 1, ..., \frac{N}{2} - 1,
\end{aligned}
$$

where a_p and b_p are the Fourier coefficients for each of the M harmonics denoted by p. These coefficients can be used to calculate a scalar error signal ξ for feedback purposes and a power spectrum density analysis, presented in [11], showed that most of the energy is contained in the first two harmonics. The calculation of a_1, b_1, a_2, and b_2 is performed online in the implementation with time-invariant linear FIR filters defined as

$$
\begin{aligned}
a_p(k) =& \frac{2}{N}\sum_{n=1}^{N} y(k-N+n) cos\left(p\frac{2\pi}{N}n\right),\ p = 1, 2 \qquad (6.4)\\
b_p(k) =& \frac{2}{N}\sum_{n=1}^{N} y(k-N+n) sin\left(p\frac{2\pi}{N}n\right),\ p = 1, 2, \qquad (6.5)
\end{aligned}
$$

where $y(k)$ is the measured output from the system at time k. Taking the cross product of

vectors in $\mathbb{R}^2$ of these coefficients gives an error signal defined as

$$\begin{aligned}\xi = \begin{bmatrix} a_1 \\ b_1 \end{bmatrix} \times \begin{bmatrix} a_2 \\ b_2 \end{bmatrix} &= a_1 b_2 - a_2 b_1 = |H_1||H_2| sin(\phi) \\ |H_1| &= \sqrt{a_1^2 + b_1^2} \\ |H_2| &= \sqrt{a_2^2 + b_2^2},\end{aligned} \tag{6.6}$$

where $|H_1|$ and $|H_2|$ are the amplitudes of the two first harmonics and ϕ is the angle from the first harmonic to the second harmonic. The cross product is a normal vector and it is positive if the operating point is located to the right of the middle point of the "S" shaped nonlinearity and negative to the other side.

It can be a good idea to normalize the error signal ξ, since the amplitude of the excitation signal at the output is dependent on the operating point dependent gain in the system. In (6.7), the error signal is normalized with the cubed amplitude of the first harmonic, which gives an almost linear feedback signal.

$$\xi_n = \frac{a_1 b_2 - a_2 b_1}{\sqrt{a_1^2 + b_1^2}^3} = \frac{a_1 b_2 - a_2 b_1}{(a_1^2 + b_1^2)^{1.5}}. \tag{6.7}$$

Other normalizations can be used as well and some of them are shown in Fig. 6.6. The first three normalized error signals looks similar to the second derivative in Fig. 6.5 except for a much larger amplitude (the signal is also flipped, but this depends on the order in the cross product). Another benefit of Fourier analysis is that it is a very powerful way of filtering out unwanted noise, since only the content at the frequencies of the first and second harmonic are considered. The choice of normalization is not important, but can

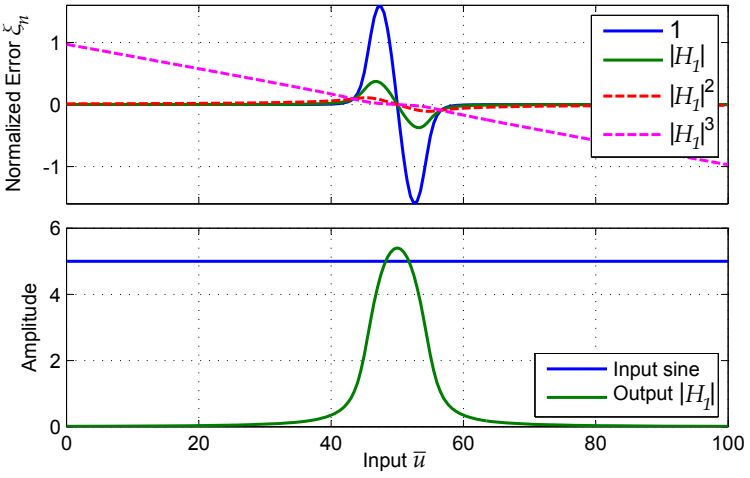

Figure 6.6: Four normalizations of the error signal. The error signal is calculated at different offsets in input $\bar{u}$ in steady state and the corresponding amplitude of the first harmonic in the output, together with the amplitude of the input sine.

improve the response of the controller. In this simulation example the nonlinearity is quite severe, which is indicated by the amplitude of the excitation signal at the output. This amplitude is very small when the input $\bar{u}$ is below 35 and above 65. In theory this should not matter when using the normalization in (6.7), however, noise and modeling errors could make the method unstable when the excitation vanishes at the output. Therefore, in some cases it might be better to use e.g. $|H_1|$ or $|H_1|^2$ as normalization, since it better resembles how well the Fourier analysis can be trusted.

After the Fourier analysis and calculation of a normalized error signal, it is now possible to close the loop using e.g. a PI controller. Anti-windup can optionally be added if there is input saturation. Furthermore, it is possible to adapt the amplitude of the input excitation signal using the amplitude of the first harmonic, since a large magnitude improves the Fourier analysis but also disturbs the system more. A healthy balance should be maintained, however, adaptation of the excitation signal will not be treated further in this paper (we briefly addressed this issue in [11]). Fig. 6.7 depicts the proposed harmonic control strategy. The input to the system u is the sum of the input from the control part $\bar{u}$ and the excitation signal u_{ex} and A_{ex} is the amplitude of the excitation signal, which in this paper is considered constant.

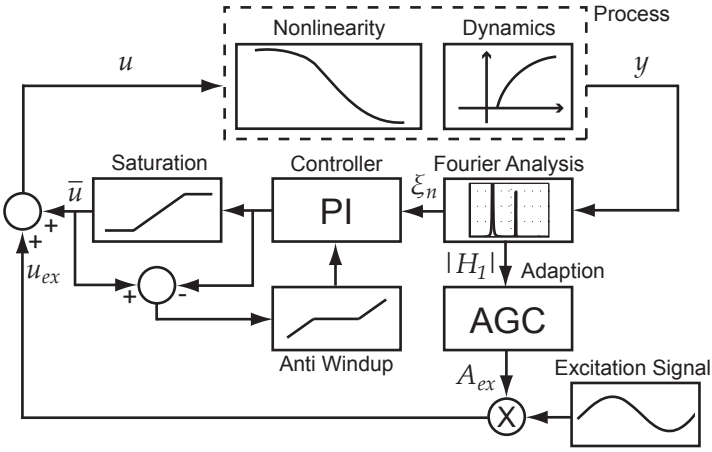

Figure 6.7: Harmonic Control Structure. Anti-windup is optional.

The controller has been tested in simulation using the setup shown in Fig. 6.7 and the system equations defined in (6.1) and (6.2). The period of the excitation signal was set to 135 s and the amplitude A_{ex} to 5. Furthermore, the normalization $|H_1|^2$ was used together with PI proportional gain $K_p = 1$, integral time $T_i = 15$ and anti-windup reset time $T_t = T_i/3$. Different starting values of OD ($\bar{u}$) were used and the result is presented in Fig. 6.8. The operating point converges to the desired value of $\bar{u} = 50$ in all the simulations, however, the response is more uncertain when noise and quantization is added. This is not surprising, since the amplitude of the harmonics are very small compared to the noise, when the valve OD is below 35% and above 65%, see Fig. 6.6.

Note that slope-seeking control could not have stabilized the system to the same operating point, because the slope decreases on both sides of the operating point. If slope-seeking control is used, one would have to choose a reference slope that deviates from

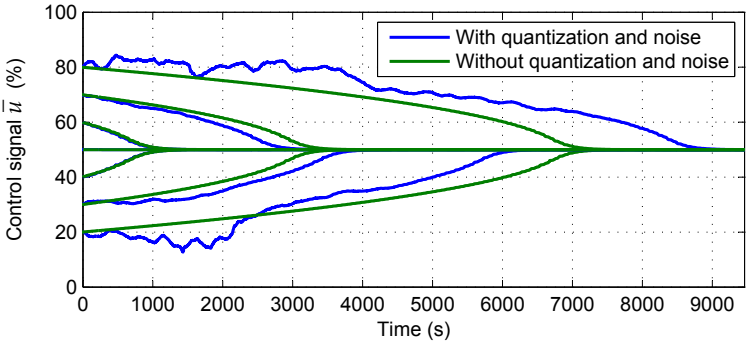

Figure 6.8: Simulation results showing closed-loop harmonic control applied to the example system given in (6.1) and (6.2) for different initial conditions. Input and output quantization (0.2 and 0.1 respectively) and measurement noise ($2\sigma = 0.1$) is added to some of the simulations and the desired operating point is $\bar{u} = 50$.

the middle of the "S" shaped curve, well aware that this slope will be mirrored around the middle of the curve, giving only local stability. Furthermore, choosing a suitable reference can be difficult in itself, since the slope changes when the operating conditions and hence the system nonlinearity changes in the time-varying system, giving an unpredictable operating point.

The PI control part of the harmonic controller has been tuned manually in the simulations and tests presented in this paper. However, automatic tuning of the controller will be pursued in future research. When tuning it is important to remember that the Fourier analysis is meant for periodic signals, which means that the controller should not be tuned too aggressively. However, slow variations will only give frequency content in the lower spectrum, which also indicates that the frequency of the excitation should be high. Simulations have also shown that the period of the excitation T_{ex} should approximately be at least twice as large as the combined system time constant T_{sys} and delay T_d.

4 Safety Logic

Before applying harmonic control to the test systems presented in Section 2, some safety logic is added. This logic handles situations when the amplitude of the first harmonic is low, which can give uncertain response as indicated by the simulations shown in Fig. 6.8. The safety logic is designed to step the valve OD down to a known situation that gives low flow ($\bar{u}_{min}$), when the amplitude of the first harmonic $|H_1|$ gets below a predefined threshold $|H_1|_{t,verylow}$. The control signal $\bar{u}$ is then ramped up, until the amplitude of the first harmonic is larger than a threshold $|H_1|_{t,high}$. However, to speed things up, the information given by the step down in OD can be used to detect if the low amplitude was caused by low flow or overflow in the evaporator. If it was low flow, then the step will not give a noticeable change (more than defined by a threshold $T_{e,o,t}$) between the temperature before the step $T_{e,o,old}$ and the new evaporator outlet temperature $T_{e,o}$ and the ramp can therefore start at the OD value before the step was made. For added safety, a timer is also implemented, with the purpose of checking if the amplitude $|H_1|$ is consis-

tently lower than a less restrictive threshold $|H_1|_{t,low}$. This will give the controller time to recover by itself, but if it does not do so within a time frame, then recovery is activated automatically. A flowchart giving an overview of the safety logic is presented in Fig. 6.9.

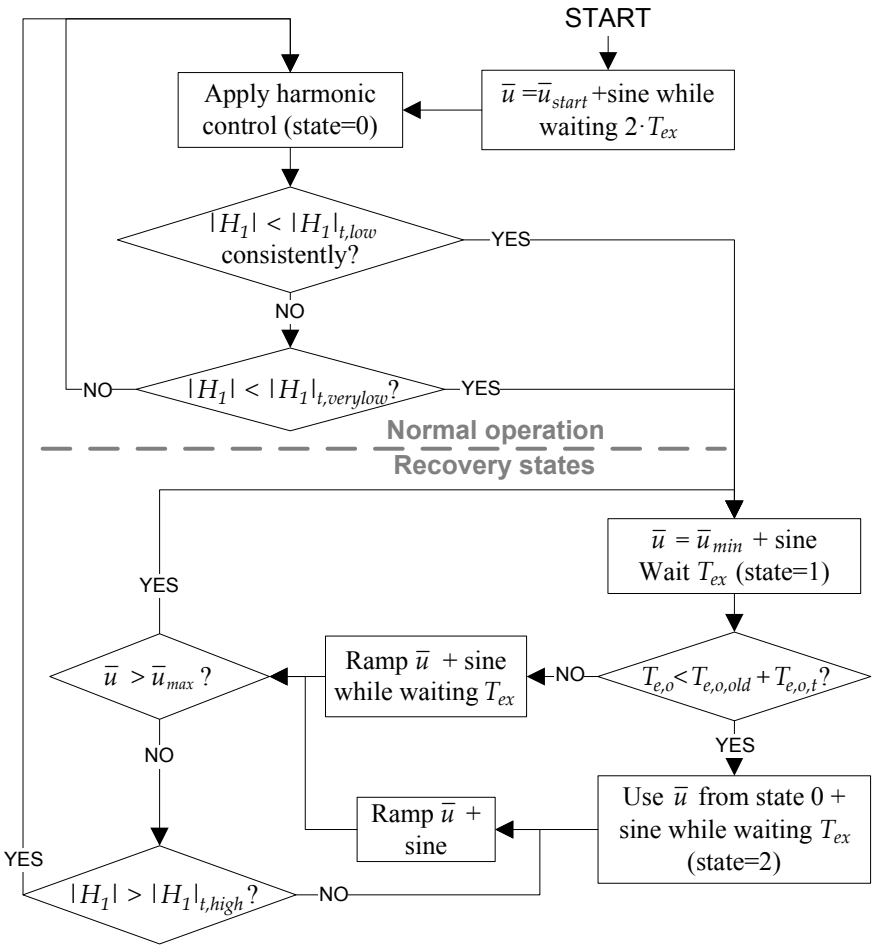

Figure 6.9: Flowchart describing the safety logic. State 0 is normal operation (top part of the flowchart), state 1 indicates recovery from overflow situation and state 2 indicates recovery from low flow situation. $\bar{u}$+sine means that the EEV is applied a control signal $\bar{u}$ superimposed with sine excitation.

5 Test Results

The two systems described in Section 2 have multiple temperature and pressure sensors, however, the proposed evaporator superheat control only uses the evaporator outlet tem-

perature $T_{e,o}$ to control the valve OD. This eliminates the need for a pressure sensor when comparing with conventional control or gives fault tolerant control possibilities.

An 8.33 hour test has been conducted on both systems, where the compressor frequency and heat load was changed in steps according to the test sequence described in [13]. The sequence is also shown in the bottom plot in Fig. 6.10 and 6.11. The compressor frequency limits are 35-60 Hz for the refrigeration system and 25-60 Hz for the air conditioning system. In the following it is assumed that the condenser pressure is controlled separately to 9 and 22 bar for the refrigeration system and the air conditioning system, respectively, and that the condenser room temperature is maintained at approximately $22.5°C$.

Fig. 6.10 shows the test result for the refrigeration system, where the controller parameters were set to $T_{ex} = 135$, $A_{ex} = 10$, $K_p = 4$, $T_i = 15$ and $T_t = T_i/3$. These signal parameters gives adequate excitation of the system and the controller is tuned to give a good compromise between convergence speed and robustness towards disturbances. Furthermore, the safety logic parameters where set to $|H_1|_{t,verylow} = 0.5$, $|H_1|_{t,low} = 1.5$, $|H_1|_{t,high} = 2.5$, $T_{e,o,t} = 4$, $\bar{u}_{min} = 10$, $\bar{u}_{max} = 90$ and ramp rate $= 10/T_{ex}$. Fig. 6.11

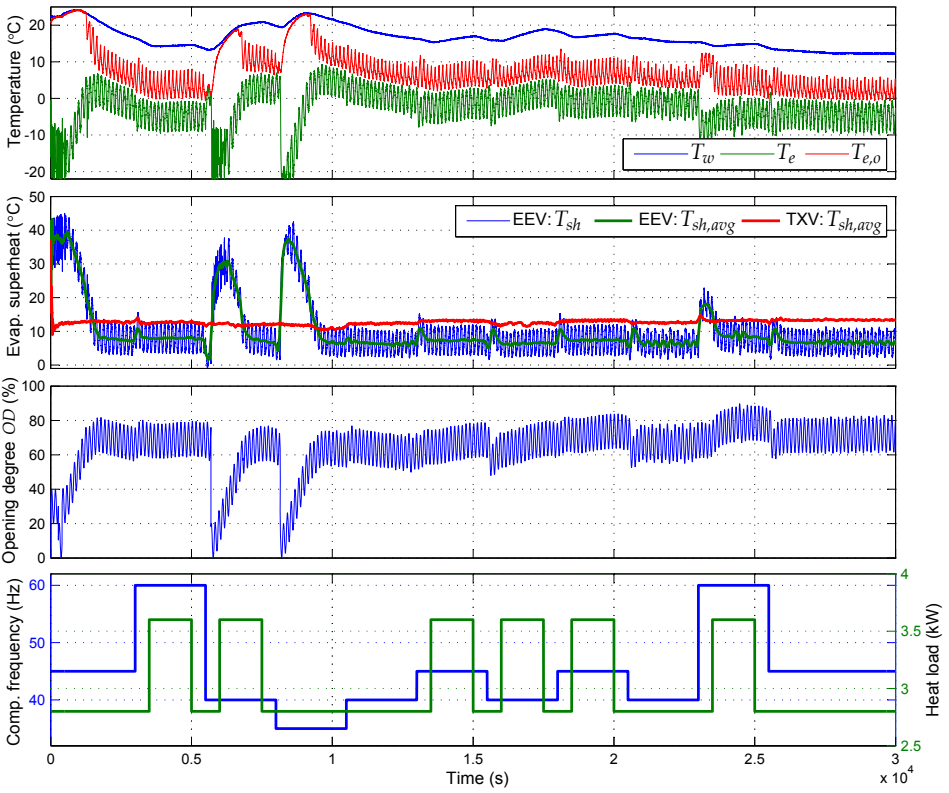

Figure 6.10: Test of the harmonic controller on the refrigeration system. The load in the bottom plot is approximately the heat applied to the water tank. The same time scale is used for all four plots. The average superheat achieved with a TXV in a similar test without harmonic control is shown for comparison.

shows the test result for the air conditioning system. The PI parameters were changed to $K_p = 2$ and $T_i = 20$ giving a less aggressive controller and the excitation signal period T_{ex} and amplitude A_{ex} were set to 180 and 8 respectively, corresponding to the slightly larger and slower system.

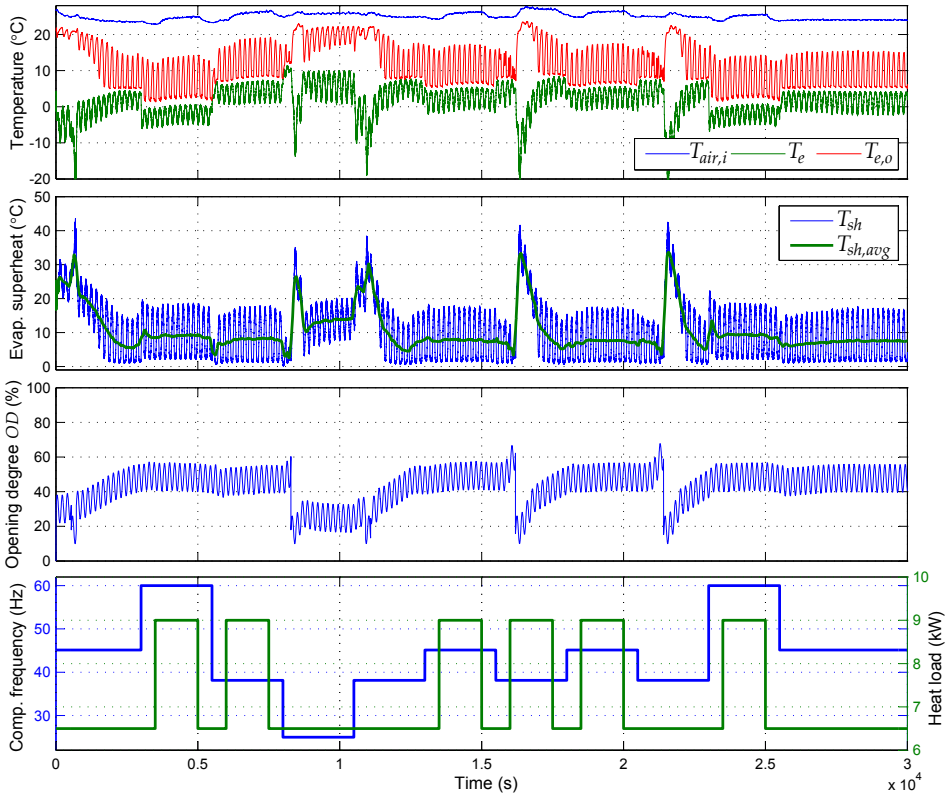

Figure 6.11: Test of the harmonic controller on the air conditioning system. The load in the bottom plot is approximately the heat applied to the air conditioned room using an electric heater. The same time scale is used for all four plots.

The average superheat was controlled to a low level in both tests using only the evaporator outlet temperature $T_{e,o}$. There are a couple of places where the safety logic is activated. It is also activated in the beginning where the OD is low. This gives faster convergence and means that the controller can be started with a very low OD. All except one activation (going up from lowest compressor frequency in air conditioning system) is caused by evaporator overflow, which gives a very low first harmonic amplitude. The step back in OD causes the superheat to increase and thus gives a performance degradation. However, this mostly happens when there are steps down in compressor frequency and not every time (the timing of the step during the excitation has an effect) and the controller does slowly optimize itself again. The average superheat in the test on the refrigeration system was $10.18°C$ and only $7.39°C$ if looking at the time from 10000 to 30000 seconds. This is lower that the average obtained with the TXV, which was $12.68°C$. Manual

fine tuning of the mechanical TXV could potentially have made the superheat lower, however, it could also have been higher depending on the skill of the operator. There are also oscillations in the superheat due to valve hunting when using a TXV, which is comparable to those seen while using continuous excitation and an EEV. However, the superheat oscillations seen in all three tests do not affect the water or room temperature on the secondary side of the evaporator. The average superheat in the test on the air conditioning system was $10.31°C$.

6 Conclusion

The proposed non model-based harmonic controller, for nonlinear systems with I/O-maps exhibiting sigmoid function properties, have shown, in tests on two different refrigeration systems, that it is possible to control the superheat without a pressure sensor. Furthermore, the method does not require a reference setpoint and works in a large operating range. The method has shown real Plug and Play potential and convergence can be improved by proper tuning of the PI control parameters, and the amplitude and period of the excitation signal. The speed of the feedback loop is limited by the excitation signal frequency and the method is therefore mostly useful for relatively calm systems. However, there is a big potential in connection with fault tolerant control in case of pressure sensor dropout.

References

[1] W. D. Gruhle and R. Isermann, "Modeling and Control of a Refrigerant Evaporator," in *American Control Conference*, Boston, MA, USA, March 1985, pp. 287–292.

[2] D. Lim, B. P. Rasmussen, and D. Swaroop, "Selecting PID Control Gains for Nonlinear HVAC&R Systems," *HVAC&R Research*, vol. 15, no. 6, pp. 991–1019, 2009.

[3] X.-D. He, S. Liu, H. H. Asada, and H. Itoh, "Multivariable Control of Vapor Compression Systems," *HVAC&R Research*, vol. 4, no. 3, pp. 205–230, February 1998.

[4] M. S. Elliott and B. P. Rasmussen, "On reducing evaporator superheat nonlinearity with control architecture," *International Journal of Refrigeration*, vol. 33, no. 3, pp. 607–614, May 2010.

[5] X.-D. He and H. Asada, "A New Feedback Linearization Approach to Advanced Control of Multi-Unit HVAC Systems," in *American Control Conference*, Denver, CO, USA, June 2003, pp. 2311–2316.

[6] H. Rasmussen and L. F. S. Larsen, "Nonlinear superheat and capacity control of a refrigeration plant," in *Mediterranean Conference on Control & Automation*, Thessaloniki, Greece, June 2009, pp. 1072–1077.

[7] H. Rasmussen, "Nonlinear Superheat and Capacity Control of a Refrigeration Plant," in *IEEE International Conference on Control Applications*, San Antonio, Texas, USA, September 2008, pp. 97–101.

[8] K. B. Ariyur and M. Krstić, *Real-Time Optimization by Extremum-Seeking Control*. Wiley-Interscience, 2003.

[9] H. S. Sane, C. Haugstetter, and S. A. Bortoff, "Building HVAC Control Systems - Role of Controls and Optimization," in *American Control Conference*, Minneapolis, Minn., USA, June 2006, pp. 1121–1126.

[10] P. Li, Y. Li, and J. E. Seem, "Efficient Operation of Air-Side Economizer Using Extremum Seeking Control," *Journal of Dynamic Systems, Measurement, and Control*, vol. 132, no. 3, p. 031009 (10 pages), April 2010.

[11] K. Vinther, H. Rasmussen, R. Izadi-Zamanabadi, and J. Stoustrup, "Utilization of Excitation Signal Harmonics for Control of Nonlinear Systems," in *IEEE Multi-Conference on Systems and Control*, Dubrovnik, Croatia, October 2012, pp. 1627–1632.

[12] K. Vinther, C. H. Lyhne, E. B. Sørensen, and H. Rasmussen, "Evaporator Superheat Control with One Temperature Sensor using Qualitative System Knowledge," in *American Control Conference*, Montreal, Canada, June 2012, pp. 374–379.

[13] R. Izadi-Zamanabadi, K. Vinther, H. Mojallali, H. Rasmussen, and J. Stoustrup, "Evaporator unit as a benchmark for Plug and Play and fault tolerant control," in *8th IFAC Symposium on Fault Detection, Supervision and Safety of Technical Processes*, Mexico City, Mexico, August 2012, pp. 701–706.

Paper D

Single Temperature Sensor Superheat Control Using a Novel Maximum Slope-seeking Method

Kasper Vinther, Henrik Rasmussen, Roozbeh Izadi-Zamanabadi, and Jakob Stoustrup

This appendix is based on a paper published in:
International Journal of Refrigeration, 36(3), pp. 1118Ű-1129, May 2013

Abstract

Superheating of refrigerant in the evaporator is an important aspect of safe operation of refrigeration systems. The level of superheat is typically controlled by adjusting the flow of refrigerant using an electronic expansion valve, where the superheat is calculated using measurements from a pressure and a temperature sensor. In this paper we show, through extensive testing, that the superheat or filling of the evaporator can actually be controlled using only a single temperature sensor. This can either reduce commissioning costs by lowering the necessary amount of sensors or add fault tolerance in existing systems if a sensor fails (e.g. pressure sensor). The solution is based on a novel maximum slope-seeking control method, where a perturbation signal is added to the valve opening degree, which gives additional information about the system for control purposes. Furthermore, the method does not require a model of the system and can be tuned automatically.

1 Introduction

Refrigeration systems are a big part of our society. Typical examples range from small fridges and freezers in our homes to residential air conditioning systems and supermarket systems with multiple display cases. All these systems typically rely on a vapor compression cycle where refrigerant is evaporated in an evaporator, while extracting heat from the surroundings. Details of the refrigeration cycle is not given here (the reader is referred to references such as [1, 2]), but the cooling capacity of the system is in general increased in two ways: either by lowering the evaporation temperature or by having as much liquid refrigerant in the evaporator as possible [3]. However, lowering of the evaporation temperature requires more compressor work and care must be taken not to let liquid refrigerant enter the compressor, as this can increase the wear and possibly damage it. After all refrigerant is evaporated into gas it will start to superheat and the level of superheat, T_{sh}, is an indirect measure of the filling of the evaporator. The superheat is calculated using a temperature sensor located at the outlet of the evaporator, $T_{e,o}$, and a pressure measurement that can be converted to the evaporation temperature, T_e, and it is typically controlled using an electronic expansion valve (EEV), where the opening degree (OD) of this valve determines the refrigerant flow (see e.g. [3, 4]). This is shown in Fig. 7.1, where the input/output (I/O) map shows the qualitative connection between OD and temperature. Alternatively, the superheat can also be controlled with the compressor speed as in [5] or a combination as in [1, 6]. However, using the compressor to control the superheat is not done in multi evaporator systems (they each have different flow requirements).

Pressure sensors are expensive to buy and install compared to temperature sensors; especially in multi evaporator systems with different evaporation pressures as multiple sensors are needed. An alternative is to use two temperature sensors instead ($T_{e,i}$ and $T_{e,o}$), since temperature transducers are cheaper. However, this also requires installation of at least two sensors and they could be placed incorrectly. Additionally, control relying on multiple sensors introduces multiple possible points of failure (sensor malfunction). We have therefore investigated the possibility of controlling the filling using only a single temperature sensor and an EEV. This could provide fault tolerant control possibilities in existing systems and potentially reduce commissioning costs by requiring fewer sensors.

The challenge is to extract enough information out of the single temperature measurement to be able to control the valve and the refrigerant flow. One possibility would be simply to use a fixed temperature reference. However, a suitable reference will depend on operating conditions, the type of refrigeration system in question, and disturbances, which is why a fixed reference is not a suitable solution (finding a suitable reference superheat in conventional two-sensor control is also a challenge). An alternative is to use qualitative knowledge about the system and the behavior of the evaporator outlet temperature. A variance-based control method was investigated in [7], where it was discovered that the variance of the outlet temperature increased at low superheat, which can be used for feedback purposes. This is also closely related to the automatic variance control method [8], which in some cases has been used in the conventional two-sensor superheat control to adjust the reference. A problem with the variance-based method is its sensitivity to operating conditions and to large disturbances, as this can change the variance level.

One can also use continuous excitation to gain the required knowledge to control the system. Extremum- and slope-seeking control are examples of this, where the objective is to drive the output to an extremum or certain slope in the system I/O-map. These methods are well covered in [9] and [10]. Furthermore, [11] and [12] provides examples of faster observer-based extremum-seeking and there exist multiple examples of the applicability of extremum- and slope-seeking control. A refrigeration system example is given in [13], where the total sum of cooling tower and chiller power consumption is minimized in a chilled water cooling plant, by optimization of the condenser water temperature with extremum-seeking (the I/O-relation between power consumption and condenser water temperature is concave). A similar example is given in [14].

As we will show in this paper, the I/O-map between evaporator valve OD and outlet temperature can be approximated by a smooth function, with sigmoid function properties, which is differentiable, and has a bell shaped non-positive first derivative (see Fig. 7.1). Additionally, a suitable operating point is located at the point of maximum negative slope in the I/O-map, as this corresponds to a good filling level of the evaporator. Slope-seeking and not extremum-seeking control should therefore be used, but the maximum slope is time-varying and unknown, and providing the slope-seeking control with the maximum slope as reference makes it unstable, as the slope reduces in both directions of the I/O-map.

We previously introduced the idea of searching for a maximum in the derivative or slope of an I/O-map in [15] and [16]. The novel solution named Maximum Slope-Seeking (MSS) control is closely related to extremum- and slope-seeking control, since they all rely on continuous excitation of the system. This excitation provides a means of getting gradient information about the I/O-map in the extremum- and slope-seeking case and curvature information in the MSS case. At the place of maximum slope, the mean curvature will be zero producing no second harmonic and the second harmonic flips 180 degrees around this point also reflecting the sign of the curvature. This information can be used to drive the system toward the maximum slope of the I/O-map. The proposed method is highly non-standard and perhaps non-intuitive and we will need to accept that the superheat will oscillate due to the constant perturbation, which is required to gain the missing information for control purposes in the single sensor setup. However, we are applying a controlled oscillation.

This paper presents the MSS control and provides new single sensor evaporator control results for three widely different refrigeration systems. This includes tests on a super-

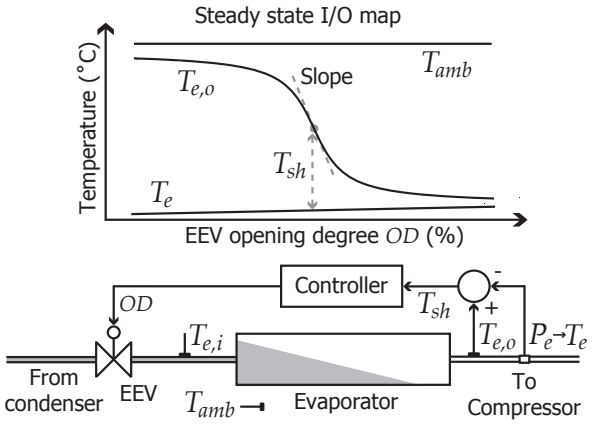

Figure 7.1: Evaporator steady state I/O-map and typical superheat control using a pressure transducer, a temperature transducer, and an EEV.

market system, and evaluation of the performance compared to a conventional two-sensor superheat control. Procedures for system identification and controller tuning is also proposed.

The paper is organized in the following way. Section 2 presents the MSS control method with a simple example simulation and Section 3 describes three different refrigeration system test facilities, which have been used to verify the method. Tuning of the MSS control for refrigeration systems is then treated in Section 5 and the final control setup including necessary safety logic is presented in Section 6. Finally, test results and discussions are presented for each of the test facilities in Section 7 and conclusions are drawn in Section 8.

2 Maximum Slope-seeking Control

Fig. 7.2 illustrates the MSS control concept applied to a continuous time process or system with input dynamics $F_i(s)$, an I/O-map with sigmoid function properties, and output dynamics $F_o(s)$, constituting a Wiener-Hammerstein model structure ($\mathbb{R} \rightarrow \mathbb{R}$). The goal of the MSS control is to find the desired control signal u^* that brings the system output $f(u^*)$ to the place of maximum slope in the unknown I/O-map.

This is achieved by first of all applying sample $\mathcal{S}$ and hold $\mathcal{H}$ on the system and then filtering the sampled system output y with two separate time-invariant linear FIR filters $F_1(z)$ and $F_2(z)$, which extracts the coefficients of the first and second harmonics H_1 and H_2 generated by the perturbation sine signal $A_{ex}sin(\omega_{ex}n)$ at the input with amplitude A_{ex} and angular frequency ω_{ex}. The cross product of vectors in $\mathbb{R}^2$, formed by the coefficients of the harmonics, are then taken and the result is normalized with respect to the first harmonic in M, which gives a normalized error signal ξ_n. This error signal will be zero at the desired operating point $f(u^*)$, where the mean curvature is zero, since this gives no second harmonic in the output. The signal will also be positive and negative, respectively, on each side of this point due to the curvature of the I/O-map, which is illustrated in [16]. An integral controller $C(z)$ is then used to drive the control signal $\bar{u}$

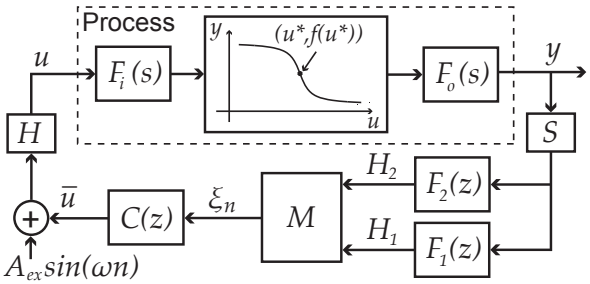

Figure 7.2: MSS control structure applied on a process with a Wiener-Hammerstein model structure.

toward u^*. The equations involved in the MSS controller are given in Eq. (7.1), (7.2), (7.3), and (7.4).

$$F_1(z) = \frac{2}{N}\sum_{n=1}^{N} z^{n-N}\left(cos\left(\omega_{ex}\left(n-N_d\right)\right) - jsin\left(\omega_{ex}\left(n-N_d\right)\right)\right), \tag{7.1}$$

$$F_2(z) = \frac{2}{N}\sum_{n=1}^{N} z^{n-N}\left(cos\left(2\omega_{ex}\left(n-N_d\right)\right) - jsin\left(2\omega_{ex}\left(n-N_d\right)\right)\right), \tag{7.2}$$

$$M = \frac{|H_1|\,|H_2|\,sin\left(\theta_{12}\right)}{|H_1|^2} = \frac{|H_2|\,sin\left(\theta_{12}\right)}{|H_1|}, \tag{7.3}$$

$$C(z) = \frac{Kt_s}{z-1}, \tag{7.4}$$

where $N = T_{ex}/t_s$ is the number of samples in one perturbation period T_{ex} of ω_{ex}, t_s is the sample time, N_d is estimated amount of samples equivalent to the delay in the system, θ_{12} is the angle from the first to the second harmonic, and K is the integral gain. The sample time is assumed to be small relative to the perturbation period.

If the dynamics in the system are negligible, compared to the perturbation period T_{ex}, then it is enough to only consider the real part of the second harmonic and use that alone as error signal. In other words, if the phase shift on the second harmonic exceeds 90 degrees, then we would have to change the sign of the feedback. However, avoiding this either requires that the system has fast dynamics or that T_{ex} is very large resulting in a slow feedback loop. Taking the cross product between the harmonic coefficients relates the second harmonic to the first, which means that it is enough to guarantee that only the difference in phase shift, between the first and second harmonic $\Delta\theta_{12}$, is less than 90 degrees (there is already 90 degrees phase shift due to the properties of the harmonics). This means that the time separation between the dynamics and T_{ex} can be lowered. Furthermore, it is possible to compensate for the phase shift introduced by system delay by aligning the cosine and sine terms in Eq. (7.1) and (7.2) with the output by shifting them with the estimated delay samples N_d. This is particularly useful in systems with large delays. For a more detailed description of maximum slope-seeking see [15] and [16].

Simulating an academic example system gives the response shown in Fig. 7.3. Here

we have used Eq. (7.5) to describe the steady state I/O-map

$$y = -k_1 atan\left(k_2 u\right), \tag{7.5}$$

where y is the dimensionless output, $k_1 = 6$ determines the gain in the system, $k_2 = 0.5$ determines the nonlinearity of the system, and u is the dimensionless input. Furthermore, fast first order dynamics are used in $F_i(s)$ with a time constant of 2 seconds and first order plus dead time (FOPDT) dynamics are used in $F_o(s)$ with a time constant of 30 seconds and a relatively large delay of 15 seconds. The perturbation signal amplitude A_{ex} was set to 4 and the period T_{ex} was set to 3 times the dominant time constant in the system (90 seconds). Finally, the integral gain was manually tuned and set to $K = 0.05$, with sample time chosen to be $t_s = 1$. Fig. 7.3 illustrates how the response starts to circle around $\bar{u} = -10$ in the I/O-map and converges to zero at the maximum slope.

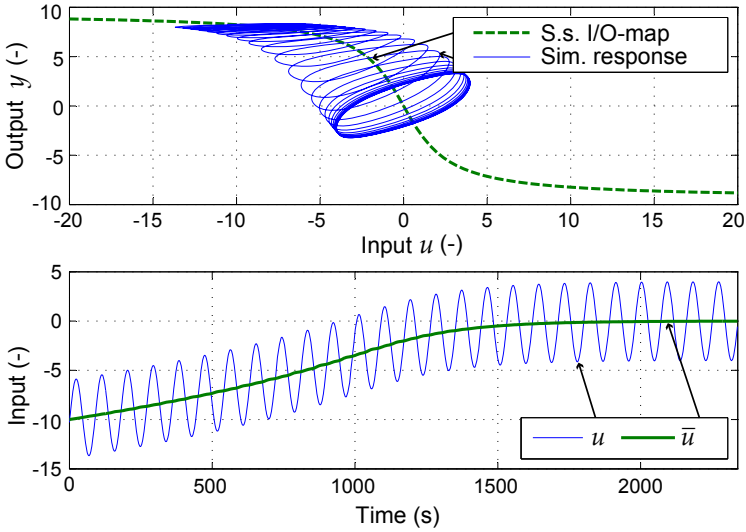

Figure 7.3: MSS control applied to a steady state I/O-map with sigmoid function properties. The simulation is started at $\bar{u} = -10$ and converges to the desired operating point $u^* = 0$.

Normalizing the error signal ξ is not a requirement, but using the amplitude of the first harmonic to normalize the error signal gives a way of compensating for changes in system gain. In Eq. (7.3) we have normalized with the squared amplitude, however, other normalizations such as $|H_1|^{-1}$ or $|H_1|^{-3}$ could have been used as well. Fig. 7.4 shows the error signal using different normalization at different input offsets or control signals $\bar{u}$, with the example system presented in Fig. 7.3. The error signal is all positive to the left and all negative to the right of the middle point where the gain in the system is highest. At $\bar{u} = 0$ the amplitude of the second harmonic is also zero and the amplitudes are very small when $\bar{u}$ gets far from the middle point. The drop in amplitude or system gain could make the control method unstable due to noise and modeling errors, which is also why $|H_1|^{-2}$ in some case is a better normalization than $|H_1|^{-3}$, since the error signal decreases again when the amplitude decreases and thus better resembles how well the Fourier analysis can

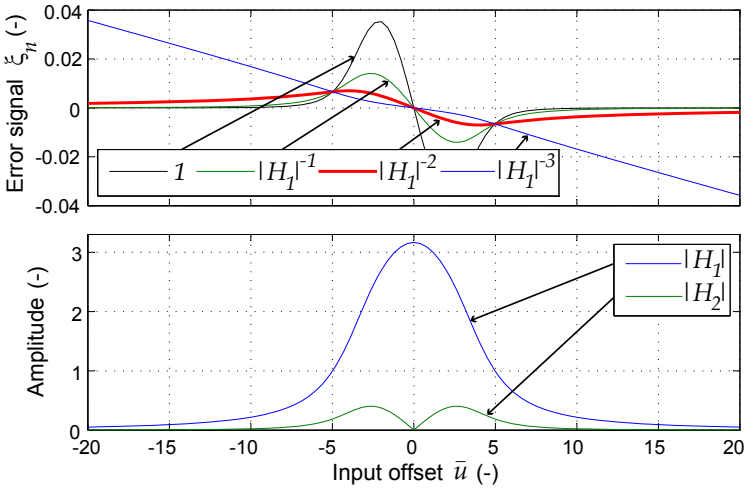

Figure 7.4: Error signal normalized with 1, $|H_1|^{-1}$, $|H_1|^{-2}$, and $|H_1|^{-3}$ at different input offsets, together with the corresponding amplitude of the first and second harmonic.

be trusted. However, remark that Eq. (7.1) and (7.2) acts as a powerful way of filtering out unwanted noise.

3 Test Facilities

Three refrigeration system test facilities have been used. The first is a residential air conditioning system, with a max capacity of approximately 11 kW, shown in Fig. 7.5(a). This system uses refrigerant R410a and has a finned tube evaporator with a pulse-width modulation (PWM) controlled Danfoss Ecoflow^{TM} valve (10 s period). The second system, shown in Fig. 7.5(b), is a water chiller system with an approximate capacity of 4 kW. This system uses refrigerant R134a and has water on the secondary side of the evaporator and interchangeable valves (either stepper motor EEV or Thermostatic Expansion Valve (TXV)). The last system, shown in Fig. 7.5(c), is a supermarket refrigeration system with the possibility of connecting a water chiller as additional load. This system uses refrigerant R404a, has PWM controlled valves (6 s period), and has up to two Type 1 and two Type 2 display cases connected. Each display case has a night cover and defrost heater. The compressor rack consists of three compressors, which are controlled separately to keep a setpoint evaporation temperature T_e and the condenser unit is also set to keep a setpoint condensation temperature T_c.

These test facilities constitutes a wide variety of refrigeration systems and thus gives a good basis for test of the MSS-based single sensor evaporator control. The air conditioning system and the water chiller system is monitored and controlled using the Matlab XPC toolbox for Simulink and the supermarket system uses MiniLog software. They are all sampled at 1 Hz and further information can be found at `http://www.es.aau.dk/projects/refrigeration/`.

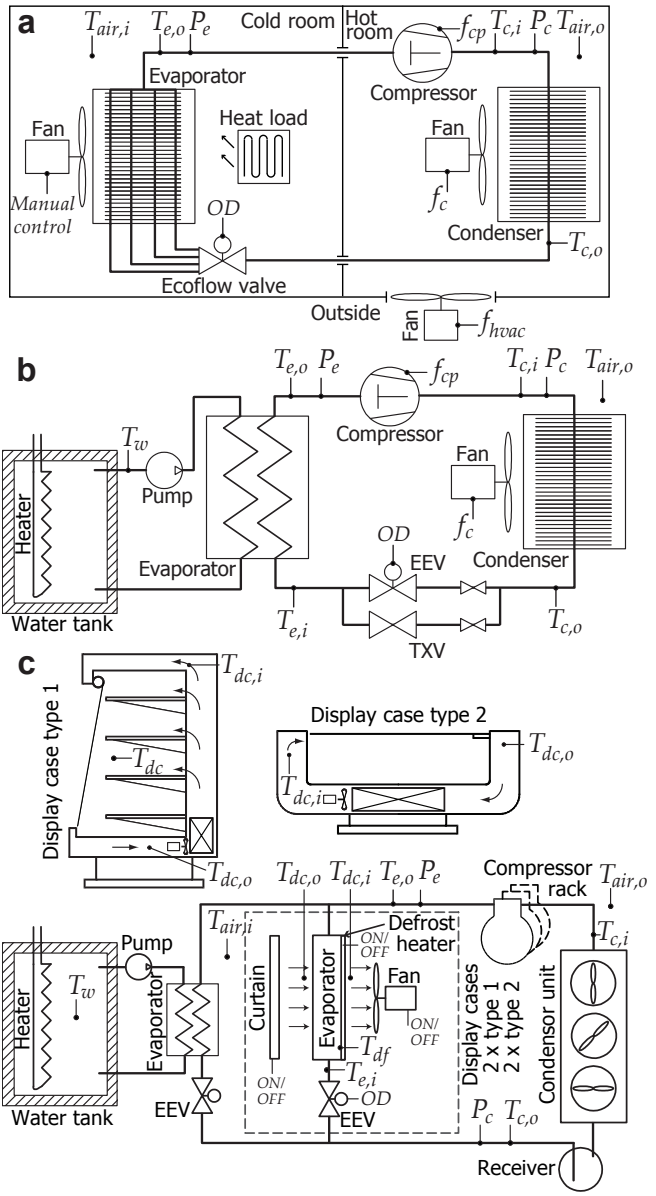

Figure 7.5: Simplified schematics of the air conditioning system (a), the water chiller refrigeration system (b), and the supermarket refrigeration system (c) test facilities with indication of sensors and control signals.

4 Qualitative Behavior of Evaporator Outlet Temperature

We are interested in control of the evaporator filling using only the valve OD and the evaporator outlet temperature measurement $T_{e,o}$. Therefore, the steady state I/O-map is

found using a slow sweep in the input OD from low to high value. This sweep should be stopped when $T_{e,o}$ flattens out again at high OD, when the superheat is low, in order not to let unevaporated refrigerant enter the compressor. However, a small amount of refrigerant spray is tolerable and extra evaporation in the suction line and/or manifold also allows us to have a short period with superheat close to $0°C$. The result for each refrigeration system is shown in Fig. 7.6.

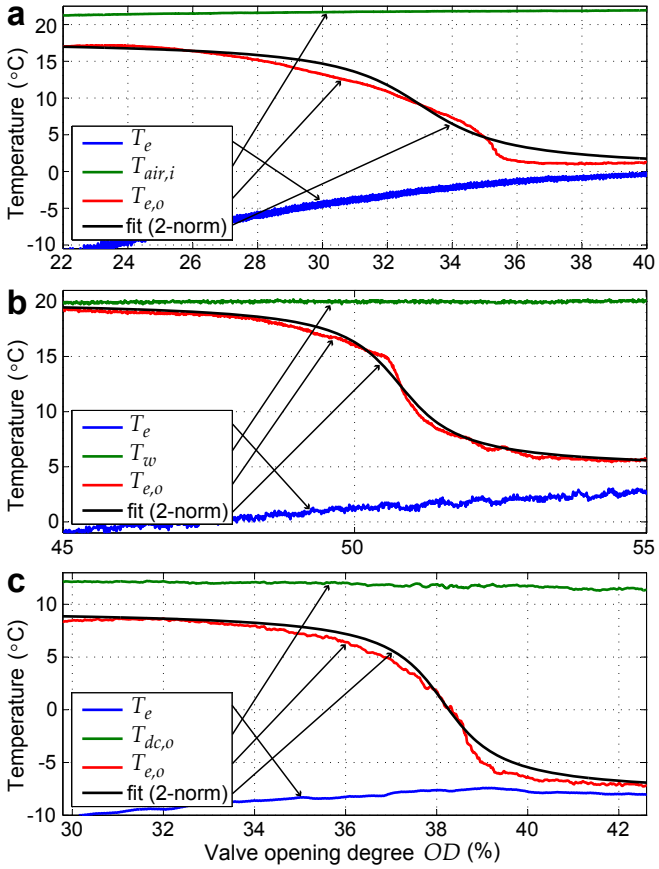

Figure 7.6: Evaporator I/O-map revealed by a slow sweep in the input for the air conditioning system (a), the water chiller refrigeration system (b), and the supermarket display case (c). The input is the valve OD and the output is the evaporator outlet temperature $T_{e,o}$. Ambient temperatures are also shown.

All three evaporators show the same qualitative behavior of the outlet temperature $T_{e,o}$; it has two horizontal asymptotes determined by the temperature of the surrounding medium ($T_{air,i}$, T_w, $T_{dc,o}$) and the evaporation temperature T_e, and a middle temperature where the slope in the system is lowest (negative gain). This point also corresponds to a good superheat or filling level of the evaporator and shows that it is reasonable to search for the point of maximum slope in the I/O-map. Note here that if the surrounding temperature or the evaporation temperature changes then it will result in a change in the

suitable outlet temperature, which is the main reason for not using a fixed reference. Note also that the typical lumped parameter model used in the literature (see e.g. [1]) does not have a smooth S-shape, but rather a sharp corner when $T_{e,o}$ reaches T_e. However, actual evaporator behavior does not exhibit sharp corners because of refrigerant spray and sensor dynamics, because of superposition of separate evaporator sections (investigated in [17]), and because it is a distributed parameter system.

For simulation and controller tuning purposes, models for the steady state I/O-map of each refrigeration system is identified. An $atan$ function similar to Eq. (7.5) is used with the expression

$$T_{e,o} = -k_1 atan\left(k_2\left(OD + OD^*\right)\right) + T^*_{e,o}, \tag{7.6}$$

since this equation satisfies the sigmoid function properties and because it is relatively easy to fit. The input and output offsets OD^* and $T^*_{e,o}$ also represent the desired operating point and the temperature $T^*_{e,o}$ is determined as

$$T^*_{e,o} = \frac{\left(T_{e,o,max} + T_{e,o,min}\right)}{2}, \tag{7.7}$$

where $T_{e,o,max}$ and $T_{e,o,min}$ are the maximum and minimum temperatures during the OD sweep shown in Fig. 7.6. The valve opening degree OD^* corresponding to $T^*_{e,o}$ is then found and the gain k_1 is given as

$$k_1 = \frac{\left(T_{e,o,max} - T_{e,o,min}\right)}{\pi} k_3, \tag{7.8}$$

where k_3 is an optional scaling factor set to 1.1, to add 10% to the gain k_1 in order to account for the fact that $T_{e,o}$ has not reached the horizontal asymptotes yet during the OD sweep. However, conservativeness in controller gain can also account for this model uncertainty, which is why k_3 is optional. The last parameter k_2 is used to fit Eq. (7.6) to the test data. This is done by using the bisection algorithm on k_2 with an Euclidian error measure. The resulting parameters are listed in Table 7.1 and the fit is shown in Fig. 7.6. If the I/O-map is not well approximated by a sigmoid function (does not have a unique point of maximum slope), then there is a possibility of having multiple equilibria. However, this has not been experienced with any of the three test setups.

System	$T^*_{e,o}$	OD^*	k_1	k_2
Air con.	9.08	33.02	5.68	0.50
Chiller	12.41	50.78	4.89	1.31
Supermarket	0.71	38.15	5.59	1.07

Table 7.1: Evaporator model parameters for the air conditioning, water chiller, and supermarket refrigeration systems.

5 Controller Tuning

As an overall guideline, the time scales in the controlled system should be:

- Fastest - system dynamics.
- Medium - periodic perturbation.
- Slow - integral control.

The perturbation signal period T_{ex} should be large enough to ensure that any possible change in system dynamics will not result in a difference in phase shift between the two harmonics of more than 90 degrees and large enough to ensure that the perturbation is detectable in the output. The double frequency should also not be a persistent frequency in the noise, since this will directly add to the second harmonic. A suitable large amplitude of the perturbation signal can, however, compensate for the noise. Furthermore, the Fourier analysis implemented with the two filters in Eq. (7.1) and (7.2) are intended for periodic signals, which means that the integral control closing the feedback loop should not be tuned too aggressively. Additionally, if the I/O-map has a non-positive first derivative (as in the cases shown in Section 4) then the integral gain K should be positive and negative in the other case. Previously, in [15] and [16], we used PI control instead of just integral control, which made it more difficult to tune the control and the P term can also make the output look less periodic due to jumps in the input signal, which results in a poorer estimation of the first and second harmonic.

A method to tune the MSS controller for control of the evaporator filling in a refrigeration system will be given in the following, since the above guidelines are general in their statements. For this purpose a Wiener-Hammerstein model structure, as shown in Fig. 7.2, is used. It is assumed that the input dynamics F_i can be approximated as being fast and thus negligible compared to the output dynamics (time constant set to 2 seconds in this paper). Since we already identified the nonlinear I/O-map, in Section 4, using an OD sweep on the system, we are left with identifying the output dynamics F_o. A simple way to do this is to perform a relay feedback test around the desired point of operation and approximate the dynamics with a FOPDT model (this approximation is derived in [18]). However, note that the parameters can vary up to 50% and possibly more [18], depending on the characteristics of the used components in the system and the changes in operating conditions. Furthermore, as it can be difficult to separate system nonlinearity from dynamics, we are left with a very rough estimate of the system parameters. Better models could be obtained and more sensor data could be used, but importance have been put in deriving a model with little effort based only on valve input OD and the measured evaporator outlet temperature $T_{e,o}$. Additionally, importance have been put in only using tests that can be automated to ensure that the control setup has a high degree of plug and play (easy to move from system to system).

A biased relay feedback test was performed on each of the three refrigeration systems. The test starts with a low OD to ensure that $T_{e,o}$ is high. However, the starting OD should be high enough to ensure that the compressor does not turn on and off all the time in one-to-one systems (one compressor, one evaporator). A large step up in OD was then made to make the evaporator outlet temperature $T_{e,o}$ drop and OD was stepped back afterward. In order to know when to step back in OD, the rate of change of the temperature $T_{e,o}$ was calculated and filtered and the step was made when a clear peak in the rate of change was detected. A suitable middle temperature was then determined and used as reference for the biased relay feedback test. This test first had three large steps in OD, with the purpose of estimating an OD offset to center three additional relays with

smaller amplitude around, providing a better parameter estimate. The last three relays had an amplitude ± 10 in OD and a hysteresis on the temperature of 0.5 degree. Note that only the last relay in the series was used for system identification and one could have taken an average and/or performed more steps.

The ultimate gain K_u is given as (see e.g. [19])

$$K_u = \frac{4A_i}{\pi A_o}, \tag{7.9}$$

where A_i is the input step amplitude and A_o is the amplitude of the oscillation in the output. Furthermore, the ultimate period T_u is the time of one relay period. This together with the input and output measurements can be used to calculate the system gain K_{sys} and the system time constant T_{sys} using Eq. (7.10) and (7.11) (see e.g. [19]).

$$K_{sys} = \frac{\int^{T_u}(T_{e,o}(t) - T_{e,o,ref}(t))dt}{\int^{T_u}(OD(t) - OD_{offset}(t))dt}, \tag{7.10}$$

$$T_{sys} = \frac{2\pi\sqrt{(K_u K_{sys})^2 - 1}}{T_u}, \tag{7.11}$$

Finally, there are multiple ways of determining the delay T_d in the system. In this paper we have taken the average time from a step in the input to a change is visible in the output. A detailed review of the biased relay feedback method will not be given in this paper, however, the reader is referred to e.g. [19] or [20] for more details.

Fig. 7.7 shows the relay feedback tests performed on the test facilities. The air conditioning system parameters are $T_{sys} = 23.07$ and $T_d = 15$, the water chiller parameters are $T_{sys} = 31.51$ and $T_d = 26$, and finally the supermarket display case parameters are $T_{sys} = 59.52$ and $T_d = 29$.

The estimated delay can be used for delay compensation ($N_d = round(T_d)$) and the estimated dominant system time constant T_{sys} can help determine a suitable perturbation time constant T_{ex}. A reasonable value for T_{ex} depends on the confidence in the estimated T_{sys}. With our relatively simple system identification and the large operating point dependence, we will use values between 3 and 5 times the estimated system time constant T_{sys}. The perturbation amplitude A_{ex} should be as large as possible for robustness, while not exceeding the acceptable level of output excitation. The identified system model can be used to find a suitable A_{ex} and we have used the FOPDT model and iterated A_{ex} until the amplitude of the first harmonic $|H_1|$ is approximately 3, which is acceptable for the three considered refrigeration systems. Finally, we are left with the last MSS control parameter, which is the integral gain K. A possible way to tune K is to use the identified Wiener-Hammerstein model and iterate K until the desired response is achieved. In this paper a convergence test is used and K is iterated until the response have an overshoot of 10%. If the starting value of $\bar{u}$ is 10 larger than the value at the desired operating point u^*, then it corresponds to allowing 1% OD overshoot. Both a negative and a positive convergence test is made and half of the smallest K value is used to account for model uncertainty. Additionally, the stability limit on the gain K is checked when the system is started at the desired operating point u^*, where the system gain is highest.

The chosen control parameters and identified control gains for the three refrigeration systems are listed in Table 7.2. The perturbation signal period T_{ex} is approximately five

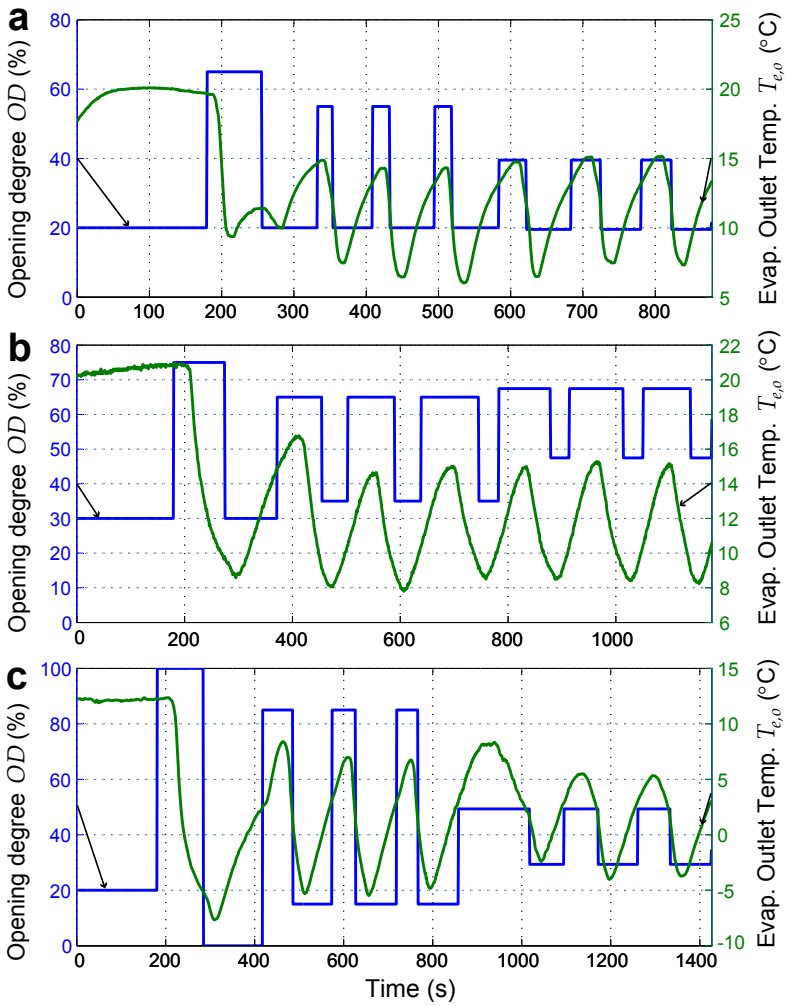

Figure 7.7: Relay feedback test on the air conditioning system (a), the water chiller refrigeration system (b), and the supermarket display case (c).

times, four times, and three times the system time constant for the air conditioning system, water chiller system, and the supermarket display case system, respectively. This gives in all cases a difference in phase shift much lower than the limit of 90 degree. Furthermore, the stability limit on K is much higher than the value obtained in the convergence tests and correspondingly the value used in the tests presented in Section 7.

Par.	Air con.	Chiller	Display
T_{ex}	120	130	180
A_{ex}	8.5	10.8	8.0
$\Delta\theta_{12}$	17.13	15.12	12.17
K (neg. start)	0.160	0.136	0.084
K (pos. start)	0.158	0.135	0.085
K (limit)	0.960	0.645	0.468
K (used)	0.079	0.067	0.042

Table 7.2: Chosen perturbation signal values, difference in phase shift between first and second harmonic $\Delta\theta_{12}$, and integral control gain values.

6 Control Setup and Safety Logic

The MSS setup applied to a refrigeration system for single sensor evaporator control is illustrated in Fig. 7.8. The valve OD input is limited between 0 and 100 %, which means that the control signal must be within the limits $A_{ex} \leq \bar{u} \leq 100 - A_{ex}$, to leave space for the perturbation. Anti-windup is therefore added to the integral control.

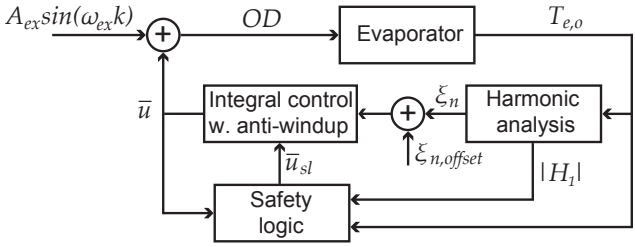

Figure 7.8: MSS control setup with safety logic applied to a refrigeration system evaporator. The harmonic analysis block includes the filters F_1 and F_2 and the normalized crossproduct operation (see e.g. Figure 7.2). When the safety logic is activated $\bar{u}$ is replaced by $\bar{u}_{sl}$.

The normalized error signal ξ_n is calculated based on measurement of the excited evaporator outlet temperature $T_{e,o}$. An offset $\xi_{n,offset}$ can be added to lift or lower the outlet temperature if the point of maximum slope lies too close or too far away from a suitable filling of the evaporator. In the air conditioning system and the supermarket system a small offset has been added to lift $T_{e,o}$ one to two degrees. $\xi_{n,offset}$ was set to -0.1 and -0.05 for the air conditioning system and the supermarket display case, respectively. The value can e.g. be determined based on the same simulation that was used to find the integral gain K.

An important note to make is that the cost of adding an offset is that the system will not stabilize at the desired operating point if the input gets far from the desired operating point, which can be deduced from Fig. 7.4. Lowering the error signal means that low values of $\bar{u}$ will not result in a positive error signal as required. Safety logic is therefore added in order to solve this problem, which occurs when the amplitude of the first harmonic is low. The role of the safety logic is to monitor the amplitude of the first harmonic.

If this amplitude is consistently below a threshold, a step back in $\bar{u}$ is made to ensure that we are in the low flow situation and $\bar{u}$ is then ramped up until the amplitude gets above an upper threshold again. A flow diagram is shown in Fig. 7.9 which illustrates the safety logic. Another benefit of having the safety logic is that low refrigerant flow or evaporator overflow is quickly detected and taken care of, even if the feedback loop is tuned conservatively. The outlet temperature is monitored when a step back in $\bar{u}$ is made to determine if the low amplitude was caused by a low flow or an overflow situation. In the low flow situation $\bar{u}$ can be stepped back up and ramped from there instead.

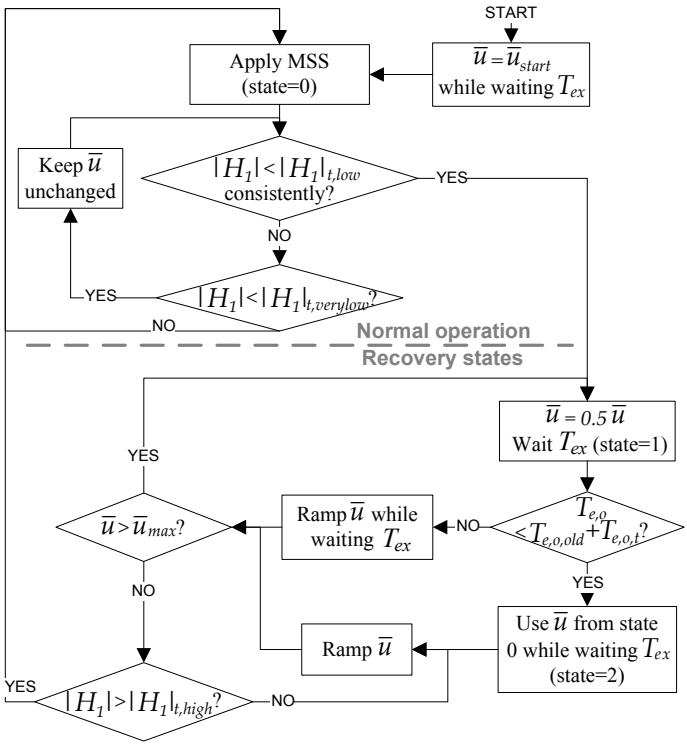

Figure 7.9: Safety logic illustrated with a flowchart. State 0 indicates normal operation, state 1 is recovery from evaporator overflow and state 2 is recovery from low refrigerant flow situation. A sine signal is always superimposed on the control signal $\bar{u}$ giving the applied valve OD.

The wait periods that allows the system to settle after steps in $\bar{u}$ are dependent on the particular perturbation period T_{ex}. The thresholds $|H_1|_{t,verylow}$, $|H_1|_{t,low}$, and $|H_1|_{t,high}$ depends on the amplitude A_{ex}, which was adapted to give the same excitation in the three systems. The thresholds were set to 0.33, 1.5, and 2, respectively, for the air conditioning and the water chiller systems, which are one compressor one evaporator systems. The values for the supermarket system was set a little lower at 0.33, 1 and 1.5. Furthermore, the amplitude $|H_1|$ was considered consistently low after $0.67T_{ex}$ and the ramp rate was set to $0.5A_{ex}/T_{ex}$. Finally, the temperature threshold $T_{e,o,t}$ used to detect low flow situations was set to $4^{\circ}C$. The safety logic parameters can be adjusted to give the desired

sensitivity toward low flow or overflow situations, but they are not that important if the error signal offset is zero and the control can be tuned non-conservatively.

7 Results and Discussions

The single sensor MSS control with safety logic has been tested on each of the three refrigeration systems.

Water Chiller Refrigeration System Test

Fig. 7.10 shows the test result from an 8 hours and 20 minutes test conducted on the water chiller refrigeration system. The condensation pressure was controlled separately with a PI controller on the condenser fan, with the reference $P_{c,ref} = 9$ bar. The compressor frequency was changed in steps between the four levels 60, 45, 40, and 35 Hz. This gives large disturbances in the evaporation temperature and the heat load was additionally changed between approximately 2.8 kW and 3.6 kW with a constant water mass flow of 0.31 ls^{-1}. The chosen disturbance pattern is based on the test description in [18] and equal to the test conducted in [15]. This makes it possible to compare the proposed MSS control setup and safety logic with previous results and the TXV result obtained in [15], which is also shown in Fig. 7.10.

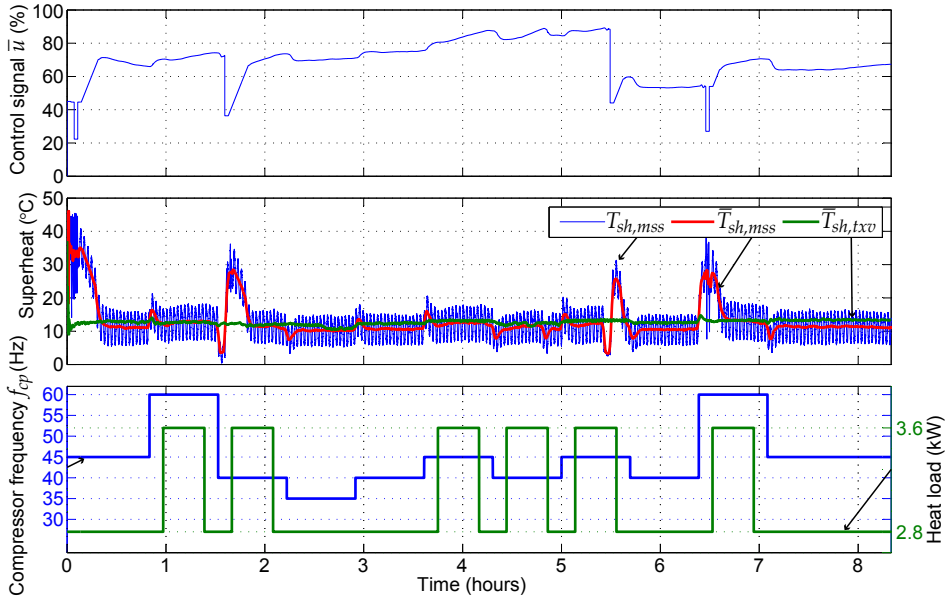

Figure 7.10: Test result with MSS applied on the water chiller refrigeration system for single temperature sensor evaporator filling control. Average superheat obtained with the TXV instead of MSS is shown for comparison.

The top graph in Fig. 7.10 shows the control signal $\bar{u}$, which was stepped back four times during the test by the safety logic. The first time was in the start because the

starting OD was too low giving a low flow situation. Then two overflow situations were detected after the largest step down in compressor frequency and approximately 5.5 hours into the test. Finally, the largest step up in compressor frequency caused a low flow situation. A safety logic activation causes a period of approximately 15 minutes with higher superheat before the control converges again, however, the average superheat for the whole test was $\overline{T}_{sh,mss} = 12.90°C$, which is very close to the superheat obtained with the TXV valve $\overline{T}_{sh,txv} = 12.68°C$. If comparing the superheat when the safety logic is not activated with the TXV result, then lower superheat is obtained with the single sensor MSS controller.

An important thing to remember is that the single sensor MSS control maintains a low average superheat during the entire test without actually measuring the superheat. A requirement though is that the system is continuously perturbed, which results in higher fluctuations in the superheat. However, this fluctuation is not visible in the water temperature T_w (or in the air temperature in the following tests on the other two systems). Using a fixed outlet temperature reference would not be possible as the average outlet temperature varies between $6°C$ and $12.4°C$ in the test. This is mainly because of changes in water temperature, which were $T_w = 14.65$ and $T_w = 20.8°C$ in the two cases.

A small part of the 8 hours and 20 minutes test is shown in Fig. 7.11. The top graphs shows the excited evaporator outlet temperature $T_{e,o}$ in between the water temperature T_w and the evaporation temperature T_e. The bottom graph shows how the step down in compressor frequency results in a change in the normalized error signal that decreases $\bar{u}$, which is the correct response, since the refrigerant mass flow is lowered.

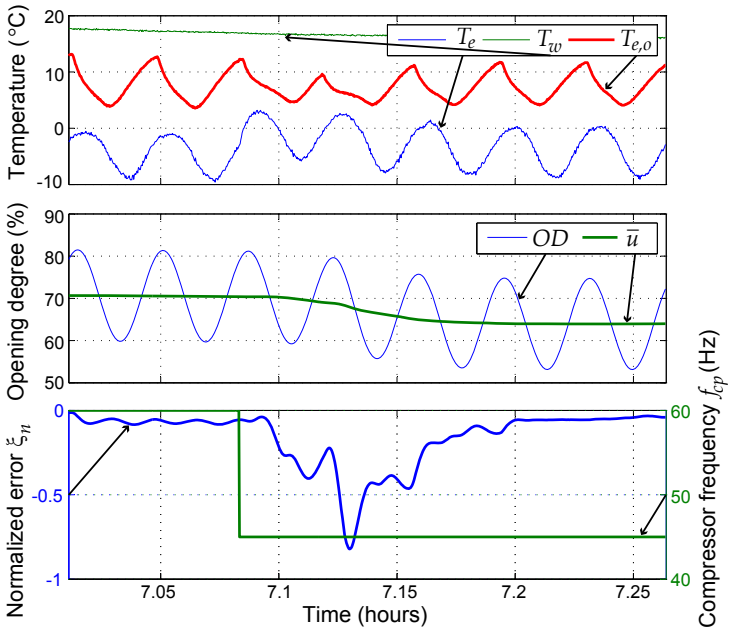

Figure 7.11: Small part of the test result shown in Fig. 6.10. Two periods before and five periods after a step down in compressor speed.

Air conditioning System Test

Fig. 7.12 shows a similar test conducted on the air conditioning system. The condensation pressure was again controlled separately to the reference $P_{c,ref} = 24$ bar. In this test the compressor frequency was stepped up and down between the levels 50, 42.5, 35, and 25 Hz and the heat load was changed between 4.5 and 9 kW with the air flow across the evaporator set to approximately 66% of max.

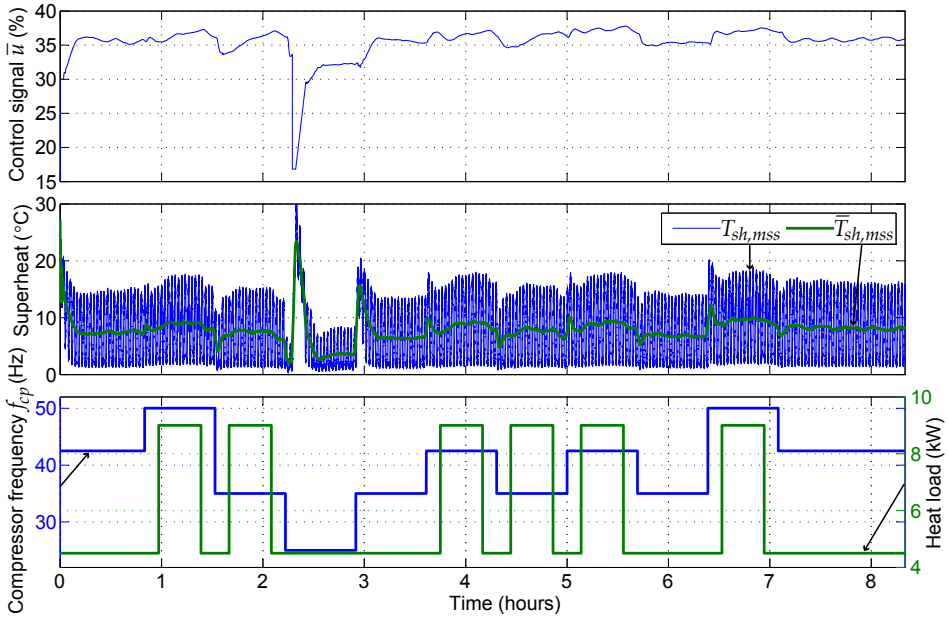

Figure 7.12: Test result with MSS applied on the air conditioning system for single temperature sensor evaporator filling control.

The average superheat for the whole test was $\overline{T}_{sh,mss} = 7.90°C$ and the safety logic was only activated once when the compressor frequency was stepped down to the lowest level. This is an improvement compared with the result obtained in [15], where the safety logic was activated 5 times and the average superheat was $10.31°C$. This is mainly achieved by lowering the perturbation period from 180 to 120 s made possible with the delay compensation and the small offset in the normalized error signal.

Supermarket Refrigeration system Tests

The condensation pressure was controlled separately in all the tests on the supermarket refrigeration system giving an almost constant condensation temperature $T_c = 35°C$. Additionally, a controller on the compressor rack ran with an evaporation temperature reference $T_{e,ref} = -15°C$. The compressor rack consists of three compressors with max power consumption of 4, 6, and 13 kW (delivered power to compressor). The controller switches the total power consumption of the rack in steps of approximately 1.1 kW. This gives large variations in evaporation temperature T_e.

Fig. 7.13 shows the test result of a test conducted on the supermarket refrigeration system. Single temperature sensor MSS control was applied on one Type 1 display case (see Fig. 7.5(c)) and another Type 1 display case had a conventional two-sensor superheat controller with temperature control. The valve on/off behavior of the second display case gives large disturbances in the evaporation temperature, which is shown in the bottom graph. This causes the compressor rack to shift between five levels (approx. 1.1-5.5 kW). However, in spite of the disturbances an average superheat of $\overline{T}_{sh,mss} = 8.81°C$ is still maintained.

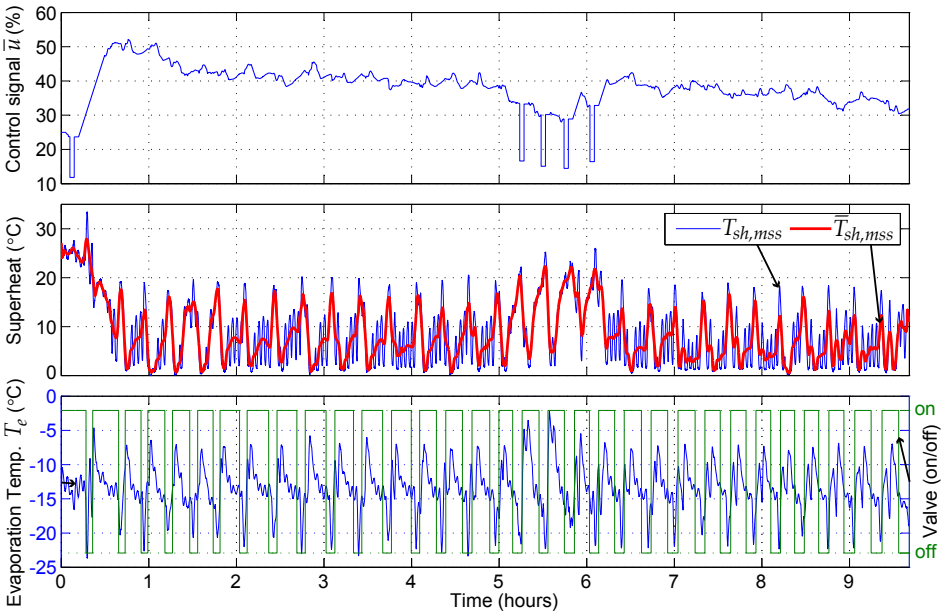

Figure 7.13: Test result with MSS applied on the supermarket refrigeration system display case for single temperature sensor evaporator filling control. Valve (on/off) refers to a secondary display case running conventional two-sensor superheat control with temperature control, which gives large evaporation temperature disturbances.

Four low flow situations are encountered in the middle of the test between 5 and 6 hours, but they are handled by the safety logic. A gradual frost build up in the evaporator causes the control signal $\bar{u}$ to slowly decrease, since the defrost algorithm is deactivated, which causes a decrease in heat transfer.

Two tests have been conducted in order to compare the performance of the single sensor MSS control against the conventional two-sensor superheat control (both controllers use an EEV). Only one display case was connected to the supermarket refrigeration system during the test and each test included two different operating conditions (with and without night cover). The superheat during the tests is presented in Fig. 7.14. The average superheat during the period without cover is $\overline{T}_{sh,mss} = 6.83$ for the single sensor control and $\overline{T}_{sh,conv} = 11.56$ for the two-sensor control and with cover it is $\overline{T}_{sh,mss} = 7.54$ and $\overline{T}_{sh,conv} = 12.19$. The superheat is considerably lower in the MSS case, which means a better utilization of the evaporator and potentially higher cooling capacity. This does

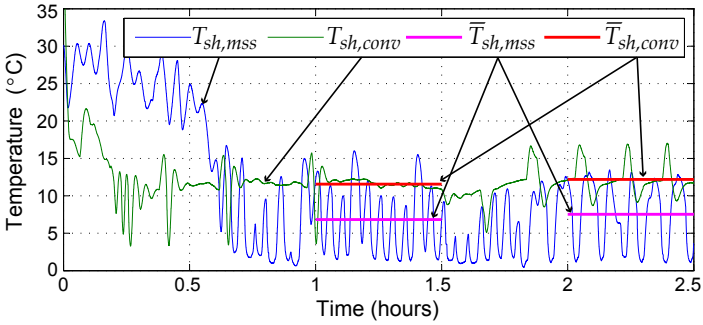

Figure 7.14: Superheat and average superheat during two separate but equivalent tests on the supermarket refrigeration system with MSS and conventional control, respectively. The average values are calculated between 1 and 1.5 hours (no cover) and 2-2.5 hours (cover).

not necessarily give a better COP and longer tests in a climate controlled chamber with power measurements would be required, before a conclusion can be made about any long term economic difference in the two methods. However, preliminary tests have indicated that the methods are comparable in terms of efficiency.

Finally, the single sensor MSS is tested together with valve on/off temperature control. The on/off control is implemented so that it opens the valve fully for a short period after an off period in order to quickly refill the evaporator. The full opening is stopped and MSS control is started when a clear peak in the rate of change of $T_{e,o}$ is detected (same procedure as in the start of the relay test, see Section 5). Fig. 7.15 shows the control signal $\bar{u}$, the valve OD, the achieved superheat T_{sh}, and the display case temperature T_{dc} (hysteresis 0-5$°C$). The on versus off period is approximately equal and the on period is

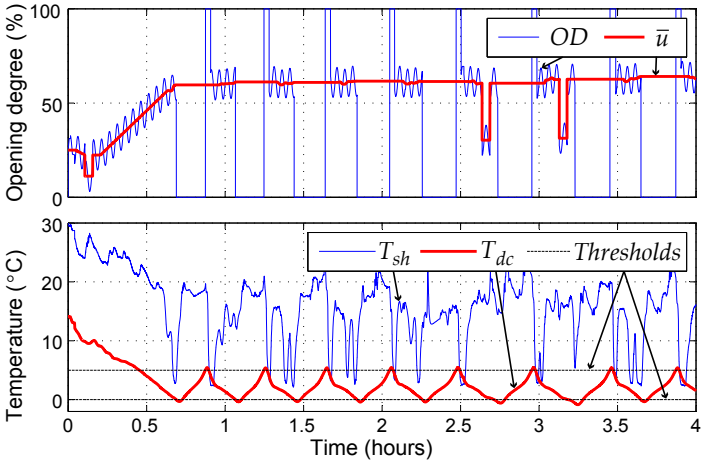

Figure 7.15: MSS with valve on/off control on the display case temperature in the supermarket refrigeration system.

barely long enough for the single sensor MSS control to take effect, but it does optimize and maintain a reasonable superheat when the valve is on. Better performance can be obtained if the on period is made longer.

8 Conclusion

Tests on three widely different refrigeration systems have shown, that it is possible to control the superheat or filling of the evaporator to a suitable level, using only a single temperature measurement combined with an EEV. A novel MSS method has ensured that this level could be obtained and the method relies on continuous perturbation of the system. This perturbation generates higher harmonics in the output due to the curvature of the I/O-map and these harmonics can then be used to drive the system toward the point of maximum slope, where the mean curvature is zero. Additional safety logic was added to ensure faster recovery from low flow or overflow situations.

Long tests with disturbances have shown the robustness of the method. The single sensor solution had a considerably lower average superheat, which can give a higher cooling capacity. A final test showed that the display case temperature in a supermarket refrigeration system can be controlled simultaneously.

A tuning approach for the MSS controller has also been provided. The tuning relies on an slow OD sweep together with a relay feedback test. These tests only have to be run the first time the control is used and can be implemented to run automatically. Furthermore, the control method does not rely on a system model and is believed to have a high degree of plug and play potential. The only requirement is that the system under consideration can be approximated by a sigmoid function, and that the desired operating point is located at the point of maximum slope.

Acknowledgments

The authors gratefully acknowledge financial support from the Faculty of Engineering and Science at Aalborg University, the Danish Council for Independent Research - Technology and Production Sciences, and Danfoss A/S.

References

[1] X.-D. He, S. Liu, H. H. Asada, and H. Itoh, "Multivariable Control of Vapor Compression Systems," *HVAC&R Research*, vol. 4, no. 3, pp. 205–230, February 1998.

[2] I. Dincer and M. Kanoglu, *Refrigeration Systems and Applications*, 2nd ed. Wiley, 2010.

[3] M. S. Elliott and B. P. Rasmussen, "On reducing evaporator superheat nonlinearity with control architecture," *International Journal of Refrigeration*, vol. 33, no. 3, pp. 607–614, May 2010.

[4] D. P. Finn and C. J. Doyle, "Control and optimization issues associated with algorithm-controlled refrigerant throttling devices," *ASHRAE Transactions*, vol. 106, no. 1, pp. 524–533, 2000.

[5] H. Rasmussen, "Nonlinear Superheat and Capacity Control of a Refrigeration Plant," in *IEEE International Conference on Control Applications*, San Antonio, Texas, USA, September 2008, pp. 97–101.

[6] L. C. Schurt, C. J. Hermes, and A. T. Neto, "A model-driven multivariable controller for vapor compression refrigeration systems," *International Journal of Refrigeration*, vol. 32, no. 7, pp. 1672–1682, 2009.

[7] K. Vinther, C. H. Lyhne, E. B. Sørensen, and H. Rasmussen, "Evaporator Superheat Control with One Temperature Sensor using Qualitative System Knowledge," in *American Control Conference*, Montreal, Canada, June 2012, pp. 374–379.

[8] T. J. Moir, "Automatic Variance Control and Variance Estimation Loops," *Circuits Syst. Signal Process*, vol. 20, no. 1, pp. 1–10, 2001.

[9] K. B. Ariyur and M. Krstić, *Real-Time Optimization by Extremum-Seeking Control*. Wiley-Interscience, 2003.

[10] C. Zhang and R. Ordóñez, *Extremum-Seeking Control and Applications: A Numerical Optimization-Based Approach*, ser. Advances in Industrial Control. Springer, 2012.

[11] W. H. Moase and C. Manzie, "Fast extremum-seeking on Hammerstein plants," in *18th IFAC World Congress*, Milan, Italy, August 2011, pp. 108–113.

[12] L. Henning, R. Becker, G. Feuerbach, R. Muminovic, R. King, A. Brunn, and W. Nitsche, "Extensions of adaptive slope-seeking for active flow control," *Proceedings of the Institution of Mechanical Engineers, Part I: Journal of Systems and Control Engineering*, vol. 222, no. 5, pp. 309–322, May 2008.

[13] H. S. Sane, C. Haugstetter, and S. A. Bortoff, "Building HVAC Control Systems - Role of Controls and Optimization," in *American Control Conference*, Minneapolis, Minn., USA, June 2006, pp. 1121–1126.

[14] X. Li, Y. Li, J. E. Seem, and P. Li, "Extremum Seeking Control of Cooling Tower for Self-Optimizing Efficient Operation of Chilled Water Systems," in *American Control Conference*, Montreal, Canada, June 2012, pp. 3396–3401.

[15] K. Vinther, H. Rasmussen, R. Izadi-Zamanabadi, and J. Stoustrup, "Single Temperature Sensor based Evaporator Filling Control using Excitation Signal Harmonics," in *IEEE Multi-Conference on Systems and Control*, Dubrovnik, Croatia, October 2012, pp. 757–763.

[16] ——, "Utilization of Excitation Signal Harmonics for Control of Nonlinear Systems," in *IEEE Multi-Conference on Systems and Control*, Dubrovnik, Croatia, October 2012, pp. 1627–1632.

[17] C. H. Lyhne and E. B. Sørensen, "Generic Superheat Control of Evaporators using One Sensor and One Actuator," 2011, aalborg University, Denmark. Master thesis.

[18] R. Izadi-Zamanabadi, K. Vinther, H. Mojallali, H. Rasmussen, and J. Stoustrup, "Evaporator unit as a benchmark for Plug and Play and fault tolerant control," in *8th IFAC Symposium on Fault Detection, Supervision and Safety of Technical Processes*, Mexico City, Mexico, August 2012, pp. 701–706.

[19] S.-H. Shen, J.-S. Wu, and C.-C. Yu, "Use of Biased-Relay Feedback for System Identification," *AIChE Journal*, vol. 42, no. 4, pp. 1174–1180, April 1996.

[20] Q.-G. Wang, C.-C. Hang, and B. Zou, "Low-Order Modeling from Relay Feedback," *Ind. Eng. Chem. Res.*, vol. 36, no. 2, pp. 375–381, 1997.

Paper E

A Fault Tolerant Superheat Control Strategy for Supermarket Refrigeration Systems

Kasper Vinther, Roozbeh Izadi-Zamanabadi, Henrik Rasmussen, and Jakob Stoustrup

This appendix is based on a paper published in:
The proceedings of the International Conference on Control and Fault-Tolerant Systems (SysTol), October 2013

Abstract

In this paper, a fault tolerant control (FTC) strategy is proposed for evaporator superheat control in supermarket refrigeration systems. Conventional control uses a pressure and temperature sensor for this purpose, however, the pressure sensor can fail to function. A contingency control strategy, based on a maximum slope-seeking control method and only a single temperature sensor, is developed to drive the evaporator outlet temperature to a level that gives a suitable superheat of the refrigerant. The FTC strategy requires no a priori system knowledge or additional hardware and functions in a plug and play fashion. The strategy is outlined by means of procedural steps as well as a flow chart that also illustrates the process of automatic tuning of the maximum slope-seeking controller. Test results are furthermore presented for a display case in a full scale CO_2 supermarket refrigeration system.

1 Introduction

Maintaining temperature of the foods within predefined intervals has the highest priority in the refrigeration systems of supermarkets/stores as it has direct impact on quality and safety requirements. In addition, enrolling maintenance people, when a fault occurs in the system, will increase the operation costs substantially. These are some of the natural incentives for the attempts to develop fault-tolerant control (FTC) strategies. In supermarkets, goods are stored in display cases/freezers until they have been purchased by the customers. Fig. 8.1 conceptually illustrates the basic functionality of such units: The inlet air traverse over the evaporator, by means of fans, and exchanges heat with the refrigerant that flows inside the evaporator. The resulting cold air maintains the cold air curtain and hence the goods temperature at a desired level. The cooling process in each of these refrigeration units is regulated by means of controlling the mass flow of the refrigerant in the corresponding evaporator unit using an electronic expansion valve (EEV). The objective of controlling the mass flow into the evaporator is to fill the evaporator and thereby maximize the heat transfer between the air and the refrigerant inside the evaporator. At the same time, flooding the evaporator, such that there exists refrigerant in liquid state at

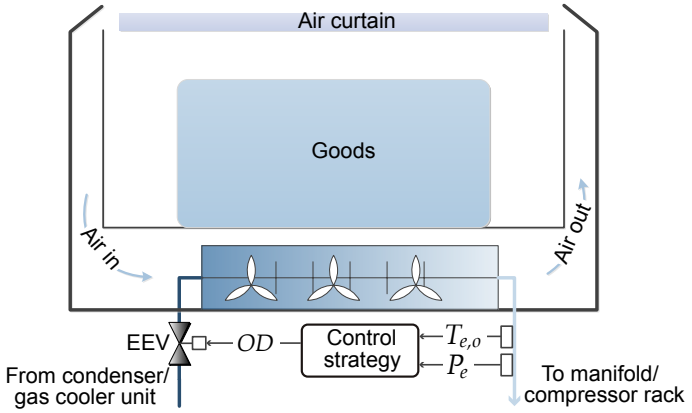

Figure 8.1: Conceptual illustration of a refrigeration unit (display case / freezer).

the outlet of the evaporator, should be avoided as it could harm the compressors. To be able to measure the distance of the liquid/gas boundary from the outlet of the evaporator, two sensors are predominantly used: a temperature sensor which measures the refrigerant temperature at gas state at the outlet of evaporator and a pressure sensor that provides the evaporation pressure (and hence evaporation temperature). The difference between these two temperatures is called superheat and can be used as an indication for how far the liquid/gas boundary is from the outlet. Ideally, the superheat (SH) should be small (positive). A $SH = 0$ indicates that the evaporator is flooded.

Loosing the ability of appropriately controlling the mass flow will have: a) dire consequences on the quality of goods in the corresponding refrigeration unit, and b) possibility for degrading the compressor unit's performance. Therefore, there is a need for a control strategy that can be activated as a contingency control option when a sensor fault occurs. The areas of fault diagnosis and fault-tolerant control has been subject to intense research in the past three decades resulting in a large amount of well-developed and well-documented theoretical methods and approaches ([1–4]). In [5] we initially proposed an evaporator unit of a residential air condition (RAC) as a benchmark for FTC. This paper provides an innovative FTC solution that will be utilized as contingency control for refrigeration units in supermarkets/stores so that the control functionality is preserved even in the case of a (pressure) sensor failure. Our approach is based on maximum slope-seeking (MSS) control, where the basic idea is to utilize the inherent nonlinear characteristics of the outlet temperature behavior at the vicinity of the evaporation temperature, which can be detected by actively perturbing the system dynamics. This is done instead of trying to estimate the evaporation temperature in a reliable and robust manner, which is a difficult task and requires full system knowledge. Estimating the temperature is also challenging since each system is different, subject to changing operating conditions, and nonlinear.

MSS was first presented by the authors in [6] and applied with success to different refrigeration systems in [7] and [8]. Stability was later studied in [9]. In this paper we will investigate automatic tuning of the controller due to the fact that evaporators and refrigeration systems in supermarkets are of different shape and sizes and hence differ in their dynamics. Therefore, the developed controller has to function in a plug and play [10] fashion by identifying the underlying system dynamics and determining its own parameters. Further requirements that must be fulfilled are: flooding avoidance, maintaining low superheat, and being robust against changes in operating conditions (such as suction pressure, load, and ambient temperature).

The paper is organized as follows: A short description of supermarket refrigeration systems is provided in Section 2 and the problem associated with sensor fault is explained. Section 3 provide a short introduction to the MSS control method. Section 4 provides strategies for immediate reaction to a flooding situation. In Section 5 we describe the procedure that is used to automatically tune the controller. Test results of the developed method on a display case in a full-scale supermarket system is finally presented.

2 CO2 Supermarket Refrigeration System

Supermarket refrigeration systems typically have a physical configuration as shown in Fig. 8.2. The refrigerating units are divided in two zones - a low temperature zone and a medium temperature zone. Low temperature zones typically include the freezers and

the medium temperature zones include refrigerators. Furthermore, dedicated compressor racks are employed to maintain an appropriate suction pressure in each zone. The display cases/freezers in each zone operate either individually or in an "island" configuration, i.e. a group of refrigeration units that share some sensors like a pressure sensor.

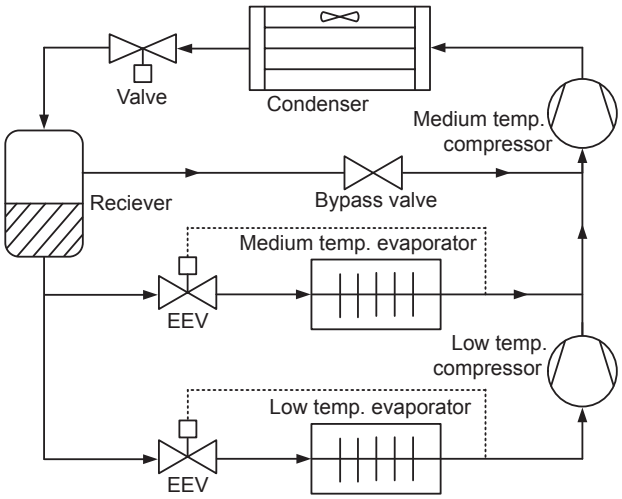

Figure 8.2: Typical configuration of a medium-sized supermarket refrigeration system. Only one medium and one low temperature evaporator is shown out of many in parallel (each having its own valve and superheat control).

The Control Challenges

Measurements from pressure sensors are instrumental for calculating the superheat defined as:

$$T_{sh} = T_{e,o} - T_e \tag{8.1}$$

where $T_{e,o}$ is the temperature of the refrigerant in gas form measured at the outlet of the evaporator and $T_e = f_e(P_e)$ is the evaporation temperature obtained with the measured evaporation pressure P_e. f_e is an injective function and is commonly realized by means of dedicated thermodynamic tables. The common approach to superheat control is to compare the calculated T_{sh} (based on the $T_{e,o}$ and P_e measurements) with a predefined $T_{sh,ref}$ and manipulate the opening degree (OD) of the related EEV by means of a dedicated control strategy (PI(D) controllers are commonly used). When the pressure sensor measurements become faulty then the calculated T_{sh} will become erroneous and, hence, the control algorithm will fail to function.

Pressure Sensor Failure

The evaporation pressure sensor may fail to operate due to a combination of oil and impurities/dirt blocking a passage in the device. When the fault occurs the measurement

signal "freezes". This phenomenon can be described as:

$$P_{e,m}(t) \equiv P_{e,0} \qquad \text{for } t \geq t_0$$

where $P_{e,0}$ is the last healthy measurement signal at time t_0.

Detection Procedure

As mentioned the faulty sensor will deliver a constant signal. The only variations in the measurements will be due to the digitizing accuracy in the A/D converters. In this case the following hypothesis can be established:

$$\begin{aligned} \mathcal{H}_0 &: \sigma^2(t) > \sigma_0^2 && \text{no fault,} \\ \mathcal{H}_1 &: \sigma^2(t) \leq \sigma_0^2 && \text{fault,} \end{aligned}$$

where $\sigma^2(t)$ is the variance of the test signal and σ_0^2 is defined based on the used A/D converters digitalization precision. The test signal is obtained by first high pass filtering the signal and then using a statistical detection method such as CUSUM to identify the relevant hypothesis.

3 Maximum Slope-seeking Control

The purpose of MSS control is to drive a nonlinear system towards a maximum in the slope of the system's steady state I/O-map. The method is therefore applicable if such an extremum is also a desired/optimal operating point. A requirement is that the maximum slope point is unique in the operating range, which is ensured if the static nonlinearity is smooth and has a bell shaped first derivative, which is either non-positive or non-negative. Functions having these properties are called sigmoid functions.

The MSS method relies on perturbation of the system and is closely related to the more general slope-seeking control presented in e.g. [11]. Fig. 8.3 illustrates the structure of MSS control. It is assumed that the system to be controlled can be adequately approximated by a Hammerstein model structure with a static nonlinearity $f(u)$ with sigmoid function properties and linear output dynamics F_o. The desired operating point is denoted $(u^*, f(u^*))$ and the objective is to drive the input offset $\bar{u}$ towards the unknown optimal input u^*. This is achieved by perturbing the system with a sine signal $A_{ex}\sin(\omega_{ex}k)$ and

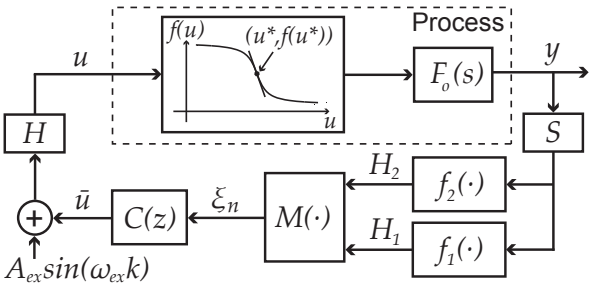

Figure 8.3: Structure of MSS control applied to a nonlinear system.

sampling the output y. The sampled signal is then filtered with periodic FIR filters $f_1(k)$ and $f_2(k)$, with k being the discrete time index. These filters are periodic with period $T_{ex} = \frac{2\pi t_s}{\omega_{ex}}$ and they extract the first and second harmonic (H_1 and H_2) of the perturbation signal in the output y. The second harmonic (and higher harmonics) is generated by the curvature of the I/O-map. If we assume that the I/O-map is symmetric around the maximum slope point, then the mean curvature experienced by the perturbation will be zero in this point and positive and negative to each side, respectively, which can then be used for feedback purposes. The convergence will be offset if the function is not symmetric around the maximum slope point, however, if the perturbation amplitude is chosen sufficiently small, then this potential offset will become negligible. The real part of the complex second harmonic could in principle be used as a feedback signal alone. However, if the phase shift caused by dynamics in the system is larger than 90 degrees, then the sign of the feedback signal should be changed. The cross product defined in $\mathbb{R}^2$ between the first and second harmonic is therefore taken so that we will only have to ensure that the difference in phase shift between these two frequencies is less than 90 degrees, which is easier to ensure, since they are only an octave apart. Furthermore, a normalization of the resulting error signal, with respect to the first harmonic, is performed giving ξ_n. This signal is then integrated in C and with proper choice of integral gain then $\bar{u} \to u^*$ as $k \to \infty$. The periodic FIR filters, the normalized cross product, and the integral control are defined as

$$f_p(k) = \frac{2}{N} \sum_{n=1}^{N} y(k - N + n)$$
$$\left(\cos\left(p\omega_{ex}\left(n + k - N_\phi\right)\right) - j\sin\left(p\omega_{ex}\left(n + k - N_\phi\right)\right)\right), \tag{8.2}$$

$$M(H_1, H_2) = \frac{|H_1|\,|H_2|\sin(\theta_{12})}{|H_1|^2} = \frac{|H_2|\sin(\theta_{12})}{|H_1|}, \tag{8.3}$$

$$C(z) = \frac{Kt_s}{z - 1}, \tag{8.4}$$

where $p = [1, 2]$ is the harmonic, N is the number of samples in one period T_{ex}, θ_{12} is the angle from the first harmonic to the second, K is the integral gain, and t_s is the sample time. N_ϕ is an optional phase shift compensation, which is useful if the delay in the system is large. Anti-windup in the integral control is necessary if the input u has saturation limits and the integral control should not be activated before a full period of N samples of y is available after startup.

As a general guideline, the control should be tuned so that the system dynamics is faster than the periodic perturbation, which at the same time should be faster than the integral control. More detail on the MSS control method and tuning of it can be found in our previous work [6–9]. In this paper we will tune the control by acquiring an approximate Hammerstein model of the system, which can be used to find appropriate control parameters through simulation. The procedure is explained in Section 5, however, before that a simulation example is given using parameters identified from the supermarket refrigeration system described in Section 2.

Fig. 8.4 shows the simulation result using (8.5) and (8.10) as system model, with the system and control parameters given in Table 8.1. The input u to the system is the valve opening degree OD in percentage, the output y is the evaporator outlet temperature $T_{e,o}$

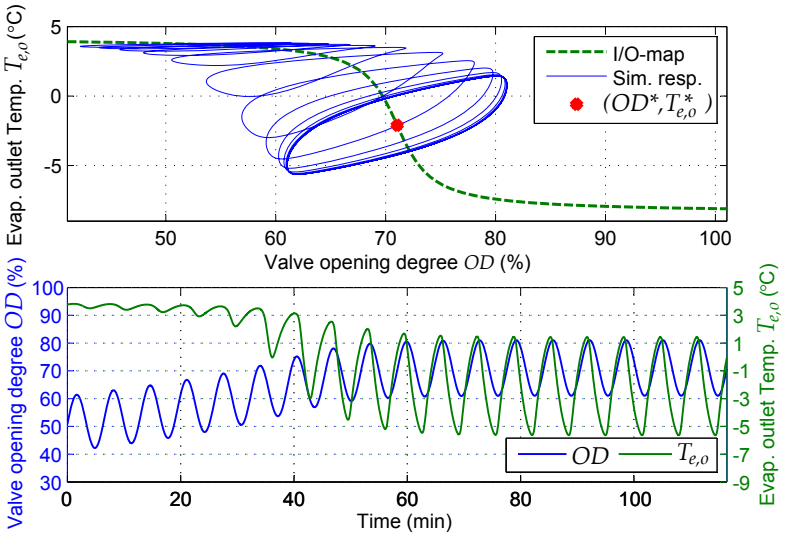

Figure 8.4: Simulation example showing convergence using maximum slope-seeking. The top graph shows the steady state I/O-map, the simulation response, and the maximum slope point $(OD^*, T^*_{e,o})$. The bottom graph shows the time evolution of the input and output in the same simulation.

and the input is perturbed with a sinusoidal signal. The offset OD (corresponding to $\bar{u}$ in Fig. 8.3) starts 20% away from OD^* and has converged after about 55 min. The top graph in Fig. 8.4 also shows how the output ends up circling around the desired operating point $(OD^*, T^*_{e,o})$ due to the continouos input perturbation and the system dynamics. Note that the MSS controller does not use the system model and does not know where the desired operating point (maximum slope point) lies, but does converge to this point, which gives a superheat that corresponds to a close to optimal filling of the evaporator. This means that the evaporator filling can be controlled by only measuring the outlet temperature $T_{e,o}$ in cases where the pressure sensor measurement is faulty.

4 Safety Logic

The proposed MSS is a relatively slow adaptive control method. Safety logic is therefore added in the evaporator filling control case, since it is important to react fast if large changes in compressor speed or load suddenly occurs. These changes can quickly flood the evaporator, which should be avoided. The compressor speed is assumed unknown. However, the amplitude of the first harmonic of the perturbation signal measured at the output gets small when the evaporator floods and if it has a very low filling, see e.g. Fig. 8.4.

The safety logic switches to a recovery mode if the amplitude of the first harmonic is consistently small. A step back in OD is made, when entering recovery mode, to ensure that the evaporator is not flooded. A check is then made to see if the low amplitude was caused by a low flow situation or a flooding situation. This is detectable by looking at $T_{e,o}$,

which will only have a large change after a step back in OD from the flooding situation. The input offset $\bar{u}$ (in this case $\bar{OD}$) is then slowly ramped up until the amplitude of the first harmonic is above an upper threshold. If it was a low flow situation, the ramping can start from the original OD before a step back was made. The safety logic is described in more detail in [8] and also shown in Fig. 8.5.

5 Autotuning Procedure

A procedure is proposed in the following for automatic tuning of the MSS control. The control parameters, which have to fit the particular system, are the perturbation period T_{ex}, which should be chosen relative to the system time constant, the phase shift compensation N_ϕ, which can be set to match the system delay, and finally the integral gain K, which has to match the nonlinearity of the system. The perturbation amplitude A_{ex} is not highly critical. Multiple tests have shown that a fixed value of $A_{ex} = 10$ gives an adequate perturbation on different refrigeration systems compared to the noise level and disturbances.

An model giving the relationship between the input OD and the output $T_{e,o}$ is derived to be able to choose a suitable integral gain K through simulation. A good approximation of the static nonlinear I/O-map is given as

$$T_{e,o} = -\, k_1 atan\left(k_2\left(OD + OD^*\right)\right) + T^*_{e,o}, \tag{8.5}$$

where k_1, k_2, $T^*_{e,o}$, and OD^* should be fitted so that the model matches the real system. This approximation have shown to fit well with measurements (see e.g. [8]) and (8.5) has sigmoid function properties with horizontal asymptotes determined by the evaporation temperature (lower bound) and the temperature of the air flowing across the evaporator (upper bound). A slow ramping of the input reveals the static I/O-map and the parameters are fitted in the following way:

$$k_1 = \frac{\left(T_{e,o,max} - T_{e,o,min}\right)}{\pi}, \tag{8.6}$$

where $T_{e,o,max}$ and $T_{e,o,min}$ are the maximum and minimum temperature, respectively, encountered during the slow ramp test going from a low OD to a high OD. The offset temperature $T^*_{e,o}$ is calculated as

$$T^*_{e,o} = \frac{\left(T_{e,o,max} + T_{e,o,min}\right)}{2}, \tag{8.7}$$

and the offset opening degree OD^* corresponding to $T^*_{e,o}$ is determined by going through the measured data during the ramp test. These two values are also a good estimate of the real maximum slope point in the system. Finally, a range of k_2 values is simulated and the one with best match to the test data is used. Using the 1-norm (instead of 2-norm) as error measure between model and data gives a good indication of fitness in cases with a lot of disturbances.

The ramp test needs to be stopped before the evaporator is fully flooded. This can be achieved by calculating the rate of change of a filtered version of the outlet temperature $T_{e,o}$ denoted RoC. The maximum slope point is passed when a clear negative peak in

RoC is detected, which means that the test can be stopped. The equations involved are;

$$T_{e,o,f}(k) = T_{e,o,f}(k-1)\frac{\tau - t_s}{\tau} + T_{e,o}(k)\frac{t_s}{\tau}, \tag{8.8}$$

$$RoC(k) = \frac{T_{e,o,f}(k) - T_{e,o,f}(k-1)}{t_s}, \tag{8.9}$$

where $T_{e,o,f}$ is the filtered $T_{e,o}$ with filter coefficient τ and sample time t_s. $T_{e,o}$ also needs to drop at least 4-5 K from the starting value at low OD, in order to remove false detections of a peak in RoC and a maximum time horizon from the last detected peak is used to know when to stop searching for the peak. Note that the RoC is also used as a quick evaporator refill algorithm during control of the display case air temperature T_{dc}, which is controlled using conventional valve on/off hysteresis temperature control. The evaporator is emptied for refrigerant due to the valve off period and when T_{dc} reaches the upper temperature threshold, where the valve switches on again, the refill algorithm will run first with high OD to quickly fill the evaporator and to maximize the heat transfer. When the RoC peak is detected the normal PI(D) or MSS control takes over and ensures a suitable superheat level in the valve on period.

The dynamics of the system are also approximated. As suggested in [5], a simple FOPDT model is used and identified using the biased relay feedback method, see e.g. [12, 13]. The FOPDT model is given as

$$F_o(s) = \frac{1}{(T_{sys}s + 1)}e^{-sT_d}, \tag{8.10}$$

where T_{sys} is the system time constant and T_d is the delay. The delay can be determined as the time from a step in the input is made to a change in the output is observed, and it is detectable in the transition from the ramp test to the relay feedback test, where we start by stepping OD down. Three relays are made before the ultimate gain K_u and period T_u is determined. These values can be used to determine the system time constant and K_u is given as

$$K_u = \frac{4A_i}{\pi A_o}, \tag{8.11}$$

where A_i is the input amplitude of the relay and A_o is the output amplitude. T_u is the total time of one relay (one low plus one high OD period). The time constant is then

$$T_{sys} = \frac{2\pi\sqrt{(K_u K_{sys})^2 - 1}}{T_u}, \tag{8.12}$$

$$K_{sys} = \frac{\int^{T_u}(T_{e,o}(t) - T_{e,o,ref}(t))dt}{\int^{T_u}(OD(t) - OD_{offset}(t))dt}, \tag{8.13}$$

where $T_{e,o,ref} = T^*_{e,o}$ and OD_{offset} is OD value where the relay is centered around. The gain K_{sys} accounts for the nonlinearity and K_{sys} is therefore set to 1 in (8.10) when both the static nonlinear model and dynamic model are used.

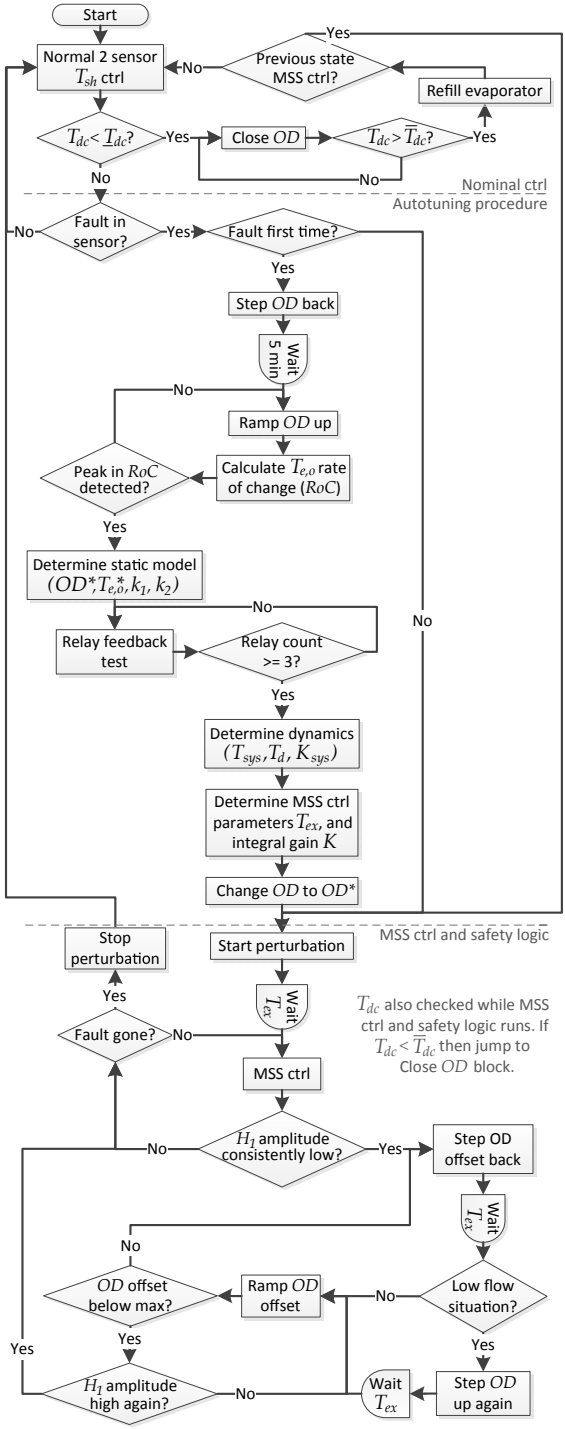

Figure 8.5: Flowchart overview of code implementation.

The system dynamics should be faster than the perturbation and the identified system specific T_{sys} can therefore be used to determine a suitable T_{ex}. The perturbation should at the same time not be too slow, however, to also account for parameter uncertainty T_{ex} is set to four times T_{sys}.

The final parameter K can now be determined based on the identified models given in (8.5) and (8.10). Here we make a convergence test, where the system is started away from the desired operating point and K is then iterated using the bisect algorithm to a value which gives exactly 5% overshoot. K is finally divided by two to account for model uncertainty. A flowchart of the code implementation is shown in Fig. 8.5.

6 Test Results

The automatic tuning procedure and MSS control is tested by inducing a pressure sensor fault in software. Nominal PI control of the superheat with on/off temperature control on the display case air temperature T_{dc} is first carried out and after 30 min the fault is induced. This starts the automatic tuning procedure and the test result is shown in Fig. 8.6.

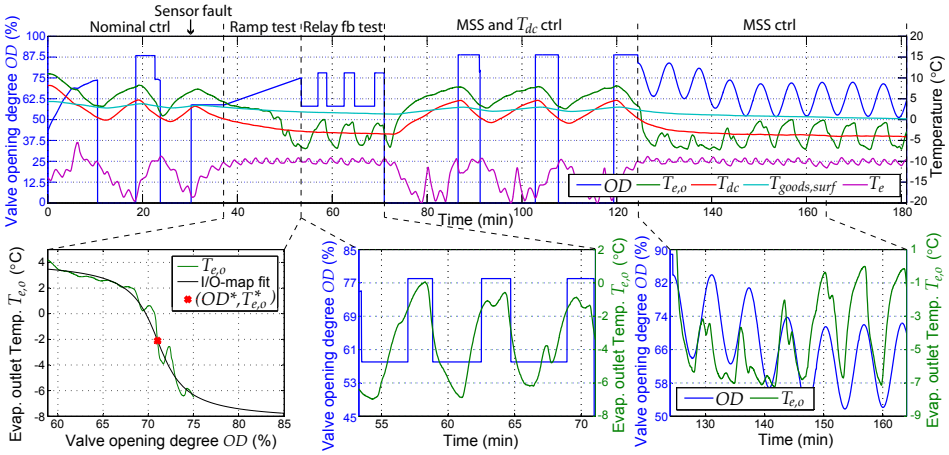

Figure 8.6: Result from 3 hour test. Only $T_{e,o}$ and T_{dc} are used in the code, however, T_e and $T_{goods,surf}$ are shown as well for comparison.

The ramp test is performed after the pressure sensor fault. A zoomed graph shows $T_{e,o}$ and the fitted static nonlinear model. The data does not show a smooth S-shaped curve due to disturbances in the evaporation pressure, but the model does show a good fit. The ramp test also stops before the evaporator gets fully flooded as expected and the relay feedback test takes over. The identified parameters are presented in Table 8.1. The MSS control then takes over approximately 71 min into the test (41 min after sensor fault). The display case air temperature T_{dc} is not controlled during the automatic tuning procedure and therefore reaches approximately -3 degree. However, the surface temperature of the goods in the display case $T_{goods,surf}$ stays between 0-5 degree. The valve on time is only 4-5 min before T_{dc} reaches the lower limit, due to a relatively aggressive evaporator

Table 8.1: Identified system model and autotuned control parameters.

	Parameter	Value
Static model	k_1 (-)	4.02
Static model	k_2 (-)	0.44
Static model	$T^*_{e,o}$ ($^\circ C$)	-2.10
Static model	OD^* (%)	71.04
FOPDT model	T_{sys} (s)	96.95
FOPDT model	K_{sys} (-)	-0.40
FOPDT model	T_d (s)	87
Ctrl. par.	N_ϕ (s)	87
Ctrl. par.	T_{ex} (s)	388
Ctrl. par.	A_{ex} (-)	10
Ctrl. par.	K (-)	0.0285

and refrigerant. This means that only the refill evaporator algorithm runs and the MSS control does not have time to run. The T_{dc} control is therefore deactivated 125 min into the test to see how the MSS controller performs. The last part of the test shows how the MSS controller adapts the average OD from 71% to roughly 50% giving a better $T_{e,o}$ and more appropriate filling of the evaporator. The superheat during the test is shown in Fig. 8.7. The nominal control first brings the superheat to the typical reference at 12 K and the T_{dc} temperature control then kicks in giving an average superheat of approximately 18 K during the first 30 min of the test. The same average superheat is also obtained with MSS with T_{dc} control (71 to 125 min into test). An average superheat of 6 K can be maintained with MSS without T_{dc} control, which gives a high efficiency of the evaporator.

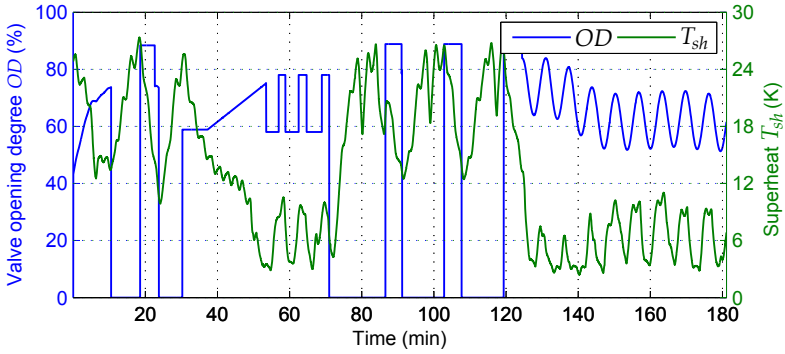

Figure 8.7: Valve OD and superheat T_{sh} during 3 hour test.

The superheat control challenge and performance benchmark outlined in [5] is mostly valid for a one compressor one evaporator systems. However, the proposed contingency control have shown to fulfill the outlined objectives. Potential improvements could involve having more relays and thus taking an average of the identified parameters if there are a lot of disturbances in the system. However, only an approximate model is needed for tuning purposes.

7 Conclusion

Pressure sensors are expensive and in refrigeration systems they sometimes experience freezing or could break. This can give problems because the evaporator filling or superheat level is conventionally controlled with this sensor and a temperature sensor placed at the outlet of the evaporator. We have shown how a novel MSS controller can be used as an FTC method, when a pressure sensor fault occurs, which can prevent deterioration of the foodstuff in the display cases. An automatic tuning procedure is proposed and tests have shown the effectiveness of the MSS method in keeping a low superheat and thus a high efficiency. The method does not require additional hardware or a priori system knowledge and also has potential as a cheap one sensor alternative to the conventional two-sensor solution. Future work include tests on other refrigeration systems for longer periods of time.

References

[1] J. Chen and R. J. Patton, *Robust Model-Based Fault Diagnosis for Dynamic Systems*. Springer, 1998.

[2] J. J. Gertler, *Fault Detection and Diagnosis in Engineering Systems*, 1st ed. Marcel Dekker Inc., 1998.

[3] M. Blanke, M. Kinnaert, J. Lunze, and M. Staroswiecki, *Diagnosis and Fault-Tolerant Control*. Springer, November 2010.

[4] R. Isermann, *Fault-Diagnosis Systems, An introduction from fault detection and fault tolerance*. Springer, 2006.

[5] R. Izadi-Zamanabadi, K. Vinther, H. Mojallali, H. Rasmussen, and J. Stoustrup, "Evaporator unit as a benchmark for Plug and Play and fault tolerant control," in *8th IFAC Symposium on Fault Detection, Supervision and Safety of Technical Processes*, Mexico City, Mexico, August 2012, pp. 701–706.

[6] K. Vinther, H. Rasmussen, R. Izadi-Zamanabadi, and J. Stoustrup, "Utilization of Excitation Signal Harmonics for Control of Nonlinear Systems," in *IEEE Multi-Conference on Systems and Control*, Dubrovnik, Croatia, October 2012, pp. 1627–1632.

[7] ——, "Single Temperature Sensor based Evaporator Filling Control using Excitation Signal Harmonics," in *IEEE Multi-Conference on Systems and Control*, Dubrovnik, Croatia, October 2012, pp. 757–763.

[8] ——, "Single temperature sensor superheat control using a novel maximum slope-seeking method," *International Journal of Refrigeration*, vol. 36, no. 3, pp. 1118–1129, May 2013.

[9] ——, "Control of a Class of Nonlinear Systems using a Maximum Slope-seeking Method," 2013, . Submitted for publication.

[10] J. Stoustrup, “Plug & play control: Control technology towards new challenges,” *European Journal of Control*, vol. 15, no. 3-4, pp. 311–330, May-August 2009.

[11] K. B. Ariyur and M. Krstić, *Real-Time Optimization by Extremum-Seeking Control*. Wiley-Interscience, 2003.

[12] S.-H. Shen, J.-S. Wu, and C.-C. Yu, “Use of Biased-Relay Feedback for System Identification,” *AIChE Journal*, vol. 42, no. 4, pp. 1174–1180, April 1996.

[13] Q.-G. Wang, C.-C. Hang, and B. Zou, “Low-Order Modeling from Relay Feedback,” *Ind. Eng. Chem. Res.*, vol. 36, no. 2, pp. 375–381, 1997.

Paper F

Control of a Class of Nonlinear Systems using a Maximum Slope-seeking Method

Kasper Vinther, Henrik Rasmussen, Roozbeh Izadi-Zamanabadi, and Jakob Stoustrup

This appendix is based on a paper (second revision) submitted for journal publication

Abstract

A non model-based maximum slope-seeking control method is proposed and the potential use of this method is investigated for a general class of nonlinear systems, where a suitable reference setpoint is unknown but qualitatively located at the point of maximum slope in the input/output-map. The control method ensures convergence to the maximum slope point by extraction of curvature information obtained through continuous perturbation of the system and harmonic filters. Stability and convergence conditions for the feedback control are provided together with tuning guidelines. These results are further strengthened through simulation on representative models of three different refrigeration system evaporators used as case studies. Test results from these systems finally show the applicability of the control method.

1 Introduction

Reference tracking is an important aspect of control, such as for optimizing the performance of a system or process. The identification of a suitable reference setpoint is not always trivial and optimality can be hard to quantify. Advanced model-based and supervisory control can help to operate processes optimally. However, the process of obtaining models and verifying them is usually costly and time consuming. Additionally, identification of a model and an optimal reference setpoint might still be required for systems which are similar in construction, since they do not necessarily have the same parameters. Time-varying and nonlinear systems can result in further difficulties, as the model might only be valid for certain operating ranges.

An alternative to model-based approaches and identification of a suitable reference value is the use of qualitative properties of systems for control purposes. This could be the case if there is a concave or convex input/output (I/O) relationship and the extremum of this relationship is a favorable operating point. Continuous perturbation revealing the nonlinear relationship could then provide the needed information for optimal control of the system rather than the use of model-based control. Extremum-seeking (ES) control is such a perturbation-based adaptive real-time optimization method, which does not require a model of the system. [1] is believed to be the first appearance of ES control, while a resurgence of interest was sparked with more rigorous assessment of stability in [2]. The method could be seen as gradient estimation where appropriate feedback control ensures convergence toward the zero slope point in the I/O-map (extremum). The generalized slope-seeking (SS) control method can then be used if a certain slope (other than zero) corresponds to a suitable operating point. Thorough books on the subject of ES and SS include [3, 4] and a survey of the literature is given in [5].

The use of ES control is beginning to emerge in optimization of refrigeration processes. In [6] a tunable thermoacoustic cooler is optimized using ES. The chilled water setpoint temperature in a cooling tower is optimized in [7] to a value giving the lowest total power consumption of the chiller compressors and cooling tower fans, which are the main power consumers in these heating, ventilation, and air conditioning (HVAC) systems. The same strategy as in [7] is pursued in [8] except that the fan speed is perturbed instead. Possible energy savings using ES control in HVAC systems is also investigated in [9], where outdoor air damper opening is optimized in air-side economizers. The use of ES for optimization of vapor compression cycles is also demonstrated in [10]. Here

the evaporator fan speed is perturbed, resulting in convergence to a setpoint which optimizes the total power consumption of the fan and the compressor. Furthermore, in [11] an alternative periodic FIR filter extracting first harmonic information is used as gradient estimator showing better performance than the traditional IIR filters used in ES and SS. The ES/SS control setup is shown in Fig. 9.1 for an example system. Here u^* denotes the system input at the desired reference slope f'_{ref} and the objective is to drive the input offset $\bar{u}(k)$ towards u^*, where the integer k is the discrete-time index. $\bar{u}(k)$ is superimposed with a perturbation signal $A_{ex}\sin(\omega_{ex}k)$, with amplitude A_{ex} and period defined by ω_{ex}. By applying sample and hold (S/H) it is possible to extract gain/gradient information about the system in the current operating point using the gradient estimator filter. Potential phase shift in the dynamics $f_o(t)$ can be compensated for with the variable N_ϕ in the demodulation. If the perturbation is applied in the extremum point of the convex (or concave) I/O-map, where the slope is zero, then the first harmonic disappears, the error signal $\xi(k)$ becomes zero, and it will be positive and negative, respectively, to each side of the extremum. An integral controller can then ensure that $\bar{u}(k)$ converges to u^*. Finally, a function $r(f'_{ref})$ can be used to offset the error signal $\xi(k)$ according to the desired reference slope f'_{ref}. If $r(f'_{ref}) = 0$ (corresponding to tracking a slope equal to zero) then the result will be ES control, since $f'_{ref} = 0$ occurs at the extremum of the I/O-map. Further detail and stability analysis can be found in e.g. [3, 11].

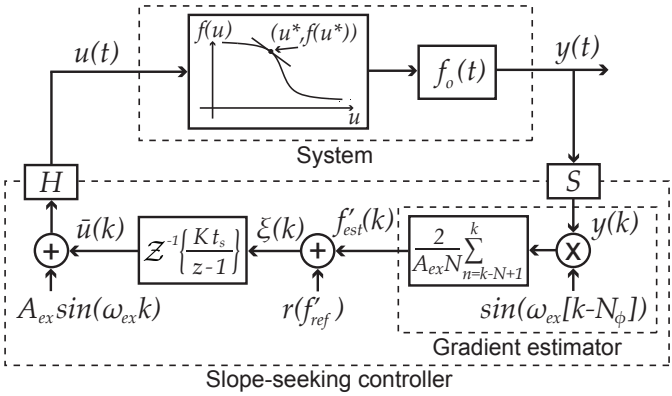

Figure 9.1: ES/SS control scheme.

The recent research in control and optimization of refrigeration systems using non model-based methods have led to the development of a maximum slope-seeking (MSS) control method. The idea is to use curvature information in the feedback loop, rather than gradient information as in ES and SS, and adapt the reference setpoint toward a maximum in the slope of the I/O-map. MSS control is intended for systems having an s-shaped nonlinear relationship between the input and the output (see Fig. 9.1) and when the maximum slope point is also a suitable operating point. The s-shaped I/O-map can also be described with sigmoid function properties, i.e. two horizontal asymptotes and a non-positive bell shaped first derivative. This ensures that there is a unique maximum slope point and that the curvature changes sign around this point. By use of a continuous perturbation signal and harmonic analysis of the resulting output signal, it is possible to extract the curvature information and converge toward the maximum slope point. Note

that SS control would not be able to use the maximum slope point as operating point, since the gradient decreases in both directions leading to instability. Additionally, one would have to estimate what the maximum slope is, which is especially problematic in time-varying systems. However, a reference slope is not required in MSS control, making it easier to implement, in cases where the maximum slope is a good operating point.

The MSS method has previously been introduced in [12] with simulations comparing MSS with SS and suggestions for automatic adaptation of the perturbation amplitude were given. The applicability of MSS was then shown in [13] in two refrigeration systems, where evaporator superheat was controlled to an unknown near optimal level using only a single sensor as opposed to the typical setup with two sensors. This was extended to include tests on a supermarket refrigeration system and tuning guidelines in [14]. Finally, in [15], an automatic tuning procedure was proposed, and tests on a fourth system showed the fault tolerant control possibilities of the method in case of pressure sensor failure.

This paper gives a more thorough presentation of MSS with clearly stated system assumptions, with motivation of the chosen filter through derivation. More importantly, conditions for closed-loop stability and convergence are provided. Furthermore, a method of estimating an upper limit on the feedback gain K is given and Monte Carlo simulations show the robustness of the method towards system parameter variations. Finally, the applicability of the method is shown on three evaporator systems. As with ES and SS control, the amplitude and frequency of the perturbation signal and the gain in the integral controller still need to be derived despite MSS being a non model-based method. Tuning guidelines are therefore provided for MSS. The intent of this paper is to promote the use of non model-based MSS control to engineering problems, where the reference setpoint is unknown but qualitatively located at the point of maximum slope in the I/O-map.

The paper is organized in the following way: The MSS scheme is explained in Section 2. This includes an outline of the control problem assumptions, conditions for convergence, and an upper bound estimate on the feedback gain. Section 3 then introduces the control of evaporator superheat in refrigeration systems as a motivating example for development of the MSS control method and models of such systems are used throughout the rest of the paper as simulation examples. Simulation results in Section 4 then illustrate convergence and instability based on the results from Section 2. This is then followed by a modified MSS scheme, which is more robust toward system dynamics, in Section 5, and Monte Carlo simulations in Section 6 shows the robustness of the MSS controller toward parameter uncertainty using the different example system models. Finally, test results from refrigeration systems are discussed in Section 7 followed by concluding remarks in Section 8.

2 Maximum Slope-seeking Control

Preliminary System Assumptions

In the following only SISO systems are considered, which can be represented with a Hammerstein model structure;

$$y(t) = (f_o \star f(u(\cdot)))(t), \tag{9.1}$$

where u is the input, y is the output, $f(\cdot)$ is a static nonlinear function, $f_o(\cdot)$ is the output dynamics function (with Laplace domain transfer function $F_o(s) = \mathcal{L}\{f_o(t)\}$), and $\star$ is

the convolution operator. The assumptions are further elaborated in the following.

Assumption 1*: The system under consideration either have a monotonic decreasing or monotonic increasing smooth bounded static time-invariant nonlinear I/O-map* $f(\cdot) \in \mathbb{R}$ *defined on an input set* $u \in U \subset \mathbb{R}$*. Furthermore, the first three derivatives with respect to* u *are also bounded and continuous, where* f' *is either non-positive or non-negative bell shaped with a unique extremum defined within the set* U*.*

The assumption states that there is exactly one time-invariant maximum slope point $(u^*, f(u^*))$ and that the second derivative f'' with respect to u has a unique zero crossing, see Fig. 9.2 for an example with a monotonic decreasing I/O-map. Practical experience shows that $f(\cdot)$ does not need to be smooth, in fact not even differentiable, as the approach has been shown also to work for a piecewise affine function. However, the analysis provided here would not apply for that situation as the required derivatives are not well-defined.

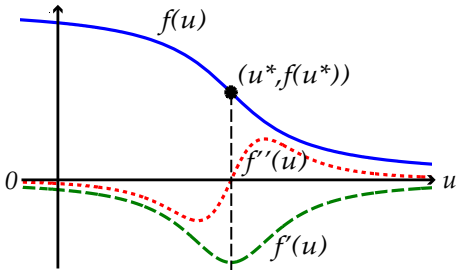

Figure 9.2: Illustration of the qualitative relationship between input and output in the static nonlinearity.

Assumption 2*: The output dynamics (described in the Laplace domain by* $F_o(s)$*) are assumed to be linear, time-invariant, and asymptotically stable. Furthermore, it is assumed that there are no zeros in the origin (equivalently at the point (1,0) on the unit circle in the discrete case).*

Maximum Slope-seeking Control Problem and Design

If a system is qualitatively defined by Assumptions 1 and 2, with unknown parameters, but where the maximum slope point $(u^*, f(u^*))$ is a good operating point, then it is proposed to use the MSS control scheme illustrated in Fig. 9.3. The objective is to make $\lim_{k\to\infty} \bar{u}(k) = u^*$ by only sampling the output y and without knowing what $(u^*, f(u^*))$ or the maximum slope is.

A perturbation signal $A_{ex}\sin(\omega_{ex}k)$ is added to the input offset $\bar{u}(k)$. The curvature of the s-shaped nonlinear map will distort the perturbation signal, which produces second (and higher) harmonics in the output. A curvature estimator is therefore applied to the sampled output y, which is implemented using a periodic FIR filter, which extracts the

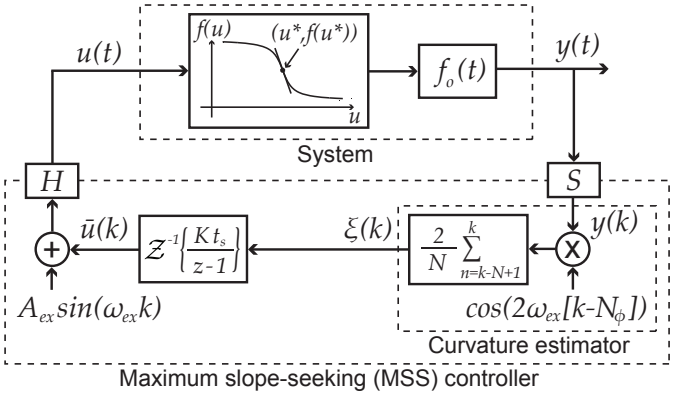

Figure 9.3: MSS control scheme.

Fourier Coefficient of the real part of the second harmonic. The output is defined as

$$\xi(k) = \frac{2}{N} \sum_{n=k-N+1}^{k} y(n) \cos\left(2\omega_{ex}\left(n - N_\phi\right)\right), \tag{9.2}$$

where $N = \frac{T_{ex}}{t_s}$ is the number of samples in one perturbation period $T_{ex} = \frac{2\pi t_s}{\omega_{ex}}$ using the sample time t_s (assumed small relative to the perturbation), and N_ϕ is an optional phase shift compensation given in samples. An additional assumption is formulated due to the necessary sampling of the system and the filter implementation.

Assumption 3*: The chosen sample time $t_s \in \mathbb{R}_{>0}$ is sufficiently small compared to the chosen perturbation period T_{ex} ($t_s << T_{ex}$) and the number of samples in one perturbation period is contained in the set of natural numbers ($N = T_{ex}/t_s \in \mathbb{N}$).*

Remark 1*: To motivate the use of the curvature filter let us first approximate the static nonlinearity under Assumption 2 with a second order Taylor series expansion in a small neighborhood around an operating point $\bar{u}$ anywhere in the set U:*

$$f(u(k)) \approx f(\bar{u}) + f'(\bar{u})(u(k) - \bar{u}) + \frac{f''(\bar{u})}{2}(u(k) - \bar{u})^2. \tag{9.3}$$

Note that the approximation includes the curvature information of the I/O-map. Inserting $u(k) = \bar{u} + A_{ex}\sin(\omega_{ex}k)$) in (9.3) and trigonometric identities gives

$$f(u(k)) \approx f(\bar{u}) + \frac{A_{ex}^2 f''(\bar{u})}{4} + A_{ex} f'(\bar{u}) \sin(\omega_{ex}k) - \frac{A_{ex}^2 f''(\bar{u})}{4} \cos(2\omega_{ex}k). \tag{9.4}$$

By including the individual gain and phase shift caused by $F_o(s)$ to each frequency in the signal one gets

$$\begin{aligned} y(k) \approx & c_o \left(f(\bar{u}) + \frac{A_{ex}^2 f''(\bar{u})}{4} \right) + c_1 A_{ex} f'(\bar{u}) \sin(\omega_{ex}(k - N_{\phi_1})) \\ & - c_2 \frac{A_{ex}^2 f''(\bar{u})}{4} \cos(2\omega_{ex}(k - N_{\phi_2})), \end{aligned} \tag{9.5}$$

where

$$c_l = |F_o(jl\omega_{ex})|\,, \tag{9.6}$$

$$N_{\phi_l} = \frac{\angle F_o(jl\omega_{ex})}{l\omega_{ex}}, \tag{9.7}$$

are the individual gain and phase shift of $F_o(s)$ on each frequency component $l = 0, 1, 2$ contained in the output from the static nonlinearity. The curvature estimator filter involves multiplication with a cosine term with the second harmonic frequency and summation over one period of ω_{ex}. This gives a filter magnitude response of zero for all harmonics and only leaves a DC term. The error signal can therefore be reduced to

$$\xi(k) \approx -\frac{c_2 A_{ex}^2 f''(\bar{u})}{4}\cos(\phi - \phi_2), \tag{9.8}$$

where the phase shifts in radians ϕ and ϕ_2 are determined by N_ϕ and N_{ϕ_2}, respectively. If Assumption 1, 2, and 3 hold and if the I/O-map is monotonic decreasing ($f'(u) < 0$ for all $u \in U$, $c_2 > 0$) and $|\phi - \phi_2| < \frac{\pi}{2}$, then

$$\xi(k) = 0 \text{ for } f''(\bar{u} = u^*), \tag{9.9}$$

$$\xi(k) > 0 \text{ for } f''(\bar{u} < u^*), \tag{9.10}$$

$$\xi(k) < 0 \text{ for } f''(\bar{u} > u^*), \tag{9.11}$$

for sufficiently small $A_{ex} > 0$ and $K > 0$. A small A_{ex} and K is needed in the analysis because of the small neighborhood assumption in the Taylor series expansion and because the closed-loop will change $\bar{u}$, which adds low frequency content to the input signal. If the low frequency content is well separated from $2\omega_{ex}$ then it will be filtered away by the periodic FIR filter defined in (9.2). The feedback integral gain K also needs to be small due to stability reasons (treated in the following subsections) and the sign should in general match the system under consideration and thus reflect the sign of the gain in the static nonlinearity (monotonic decreasing or increasing) and the sign of the gain in the linear dynamics ($c_2 > 0$ or $c_2 < 0$). Furthermore, the requirement $|\phi - \phi_2| < \frac{\pi}{2}$ can be achieved by picking ω_{ex} small compared to the dynamics in F_o and states that any uncompensated phase shift, at the second harmonic frequency, should be less than 90 degree. If the phase shift ϕ_2 is known then the optional phase shift compensation ϕ can be set equal to ϕ_2. An additional requirement is that $2\omega_{ex}$ is not a persistent frequency in the disturbance, since this will give an offset in $\xi(k)$.

The output from the curvature filter $\xi(k)$ in (9.8) becomes a good estimate of the curvature if it is scaled by $-\frac{4}{c_2 A_{ex}^2}$ and if $\phi \approx \phi_2$. However, it is only the sign change that is interesting for feedback purposes. Furthermore, the discrete integrator in the feedback loop, denoted $C(z)$, should in general match the particular system. However, $C(z)$ can be chosen to match a relatively large class of systems; experience from refrigeration systems has shown that a simple integral controller can be used here, where the assumptions are that the system is open-loop asymptotically stable and that it does not have zeros in the origin (equivalently at the point (1,0) on the unit circle in the discrete case). Finally, the error signal $\xi(k)$ should not be used before N samples of the output $y(k)$, needed to initialize the periodic FIR filter, are acquired.

Closed-Loop Convergence

Theorem 1. *Suppose that Assumptions 1, 2, and 3 hold and that the perturbed open-loop system in serial connection with the periodic FIR filter is in periodic steady state at time*

k_0 (loop opened before the integrator with zero as input and initial condition $\bar{u}(k) \in U$, see Fig. 9.3). Furthermore, assume that the closed-loop is formed at time k_0. Then, this system is asymptotically stable and there exists $\delta \in \mathbb{R}$, such that the dynamic response of the input offset $\bar{u}$ satisfies

$$\lim_{k\to\infty} \bar{u}(k) = (1-\delta)u^* \tag{9.12}$$

for sufficiently small ω_{ex}, A_{ex}, and K. Additionally, $\delta u^* < A_{ex}$.

Theorem 1 states that there exist a set of control parameters, which can ensure that the closed-loop system input $\bar{u}(k)$ converges to the point where the perturbed input experiences a zero mean curvature due to the static nonlinearity. Furthermore, the zero mean curvature point will be offset from the maximum slope point u^* by a small constant δu^*, if the nonlinear I/O-map is not symmetric around u^* (if the map is symmetric then $\delta = 0$) and the offset can not exceed the size of the perturbation. The following lemma can be used in the proof of asymptotic stability and convergence in Theorem 1.

Lemma 1. *The system described in (9.1) under Assumptions 1 and 2 followed by the periodic FIR filter defined in (9.2) is uniformly globally asymptotically stable (UGAS) and bounded for all fixed $u(t) \in U \subset \mathbb{R}$ and for all $t \geq 0$.*

A formal proof of Theorem 1 can be carried out along the lines of [11]. The proof is omitted for brevity reasons. However, the intuition for Theorem 1 is as follows. Perturbation of the system in Fig. 7.2 results in an error signal ξ with the sign properties in Remark 1. Stability and convergence can then be ensured by choosing a sufficiently small feedback gain K. In more detail, the input at the maximum slope point u^* can, without loss of generality, be assumed to be 0, since any offset does not change the analysis. A condition for asymptotic stability and convergence can then be formulated for $\bar{u}(k) > 0$ $\forall k$ as:

$$\begin{aligned} \bar{u}(k) &> \bar{u}(k+1) > 0 \Leftrightarrow \\ \bar{u}(k) &> \bar{u}(k) + Kt_s\xi(k) > 0 \Leftrightarrow \\ 0 &> Kt_s\xi(k) > -\bar{u}(k). \end{aligned} \tag{9.13}$$

An integral feedback gain K that satisfy this only exist if $\xi(k)$ is bounded, the sign of $\xi(k)$ is constant, and $\xi(k)$ goes to 0 as $\bar{u}(k)$ goes to 0. Boundedness of $\xi(k)$ follows directly from Lemma 1. The output of the nonlinear part, $f(\cdot)$ is bounded by Assumption 1. Since the dynamics is an IIR filter with kernel f_o, this has a finite $\mathcal{L}_\infty$ induced norm. Thus, also the output of this part is bounded. Forming the finite sum in the FIR filter, clearly also yields a bounded signal $\xi(k)$. The sign properties of $\xi(k)$ were shown in Remark 1 for a monotonically decreasing I/O-map and (9.8) shows that $\xi(k)$ goes to 0 as $\bar{u}(k)$ goes to 0, since f'' is continuous and bounded with a unique zero crossing (Assumption 1). Note that the assumptions made in Remark 1 only holds if higher order terms in the Taylor series expansion approximation are negligible and if low frequency content added to the input, due to changes in $\bar{u}$, is well separated from the second harmonic frequency and filtered away by the periodic FIR filter, which has zero DC gain. These assumptions therefore require that A_{ex} and K are small. The same analysis can be made for initial input offset $\bar{u}(k) < 0$. Finally, any potential asymmetry in the I/O-map does not change the continuity and boundedness of f'' or the existence of a stable K.

Upper Bound Estimate on the Integral Gain

A discrete system with state vector $\mathbf{x}(k) \in \mathbb{R}^n$ and state transition matrix $\mathbf{A} \in \mathbb{R}^{n\times n}$ defined as

$$\mathbf{x}(k+1) = \mathbf{A}\mathbf{x}(k), \tag{9.14}$$

is stable if and only if the eigenvalues of $\mathbf{A}$ are within the open unit disc. Furthermore, the monodromy matrix $\Psi_A(k) = \Phi_A(k+T,k)$ can be used to analyze stability in systems where $\mathbf{A}$ is periodic with period T. $\Phi_A(k+T,k)$ is the transition matrix for one period defined as

$$\Phi_A(k+T,k) = \mathbf{A}(k+T-1)\mathbf{A}(k+T-2)...\mathbf{A}(k). \tag{9.15}$$

The monodromy matrix eigenvalues does not depend on k and the system is stable if and only if the eigenvalues (characteristic multipliers) are contained in the open unit disc [16].

The FIR filter defined in (9.2) is periodic and the eigenvalues of (9.15) can therefore be used to analyze stability of the closed-loop system. The integral controller $C(z)$ gives a single eigenvalue at $(1,0)$. In general, marginal stability is obtained if and only if the eigenvalues are within the closed unit disc, and any eigenvalue on the unit circle is semi-simple [17]. This is satisfied if the system has a single eigenvalue with multiplicity one on the unit circle (for $z = 1$). This makes every operating point a stable equilibrium and the perturbation ensures that the system converges toward the maximum slope point. Furthermore, since the desired operating point is at the maximum slope (gain) of the system and the nonlinearity $f(\cdot)$ is assumed smooth, then it is possible to limit the analysis to this point and use $max(f'(u))\ \forall u$ as system gain. Stability here means that the closed-loop system stays at the maximum slope point $(u^*, f(u^*))\ \forall k > 0$ if $\bar{u}(0) = u^*$ with the perturbation set to zero ($A_{ex} \to 0$). Thus, by analyzing the eigenvalues of the monodromy matrix an upper bound on K can be found, where the eigenvalues are still within the unit disc. A higher K will not be stable, when the perturbation amplitude is small, and limit cycles will occur since the system gain decreases away from u^*.

Note that the gradient filter in SS control also gives periodic coefficients and the eigenvalue stability check, with the monodromy matrix, can also be applied here.

3 Motivating Example - Superheat Control

Refrigeration systems are used in a multitude of applications ranging from small fridges and freezers in our homes to larger chillers, air conditioning systems, and supermarket refrigeration systems with display cases. Refrigeration systems typically transfer heat from one place to another by continuous vaporization and compression of refrigerant in a cycle, which is basically maintained by a compressor, a valve, an evaporator, and a condenser. A full description of a refrigeration system and the required control loops are not given here (see instead references such as [18, 19]). However, in the following, more detail is provided regarding the control of the valve opening degree OD at the evaporator, in the case that an electronic expansion valve (EEV) is used.

When the refrigerant evaporates at low pressure in the evaporator it takes heat from the surroundings and thus delivers the desired cooling. The refrigerant enters the evaporator as a mixture of liquid and gas (two-phase); it is important to have as much liquid refrigerant in the evaporator as possible to maximize the heat transfer and thus the efficiency of

the system. It is also important that only gaseous refrigerant enters the compressor, since two-phase refrigerant increases the power consumption and wear of the compressor, or in the worst case damages it. When the refrigerant is fully evaporated, it starts to superheat and the level of superheat, denoted T_{sh}, is defined as

$$T_{sh} \equiv T_{e,o} - T_e = T_{e,o} - f_e(P_e), \tag{9.16}$$

where $T_{e,o}$ is the temperature at the outlet of the evaporator and T_e is the evaporation temperature. The evaporation temperature is typically calculated using refrigerant property tables and a pressure measurement P_e. It could also be approximated by measuring the evaporator inlet temperature $T_{e,i}$. A control objective is the regulation of the amount of superheat, which in most cases is done by controlling the flow of refrigerant using the expansion valve [19–21]. Fig. 9.4 shows the qualitative input/output (I/O) relationship between valve OD and temperature. The qualitative behavior of $T_{e,o}$ approximately follows an s-shaped curve when OD is slowly increased from a nearly closed position to a high position. The horizontal asymptotes are governed by the temperatures T_{amb} and T_e and the gain is highest (negative gain) at the middle temperature, which also corresponds to a good superheat or filling level of the evaporator.

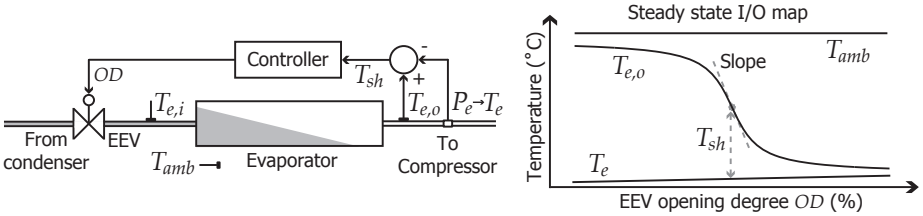

Figure 9.4: Example steady state I/O-map between valve opening degree OD and evaporator outlet temperature $T_{e,o}$ and typical superheat control using pressure and temperature transducers.

Test results from three different evaporators are shown in Fig. 9.5. These systems are not described here; further detail can be found at `http://www.es.aau.dk/projects/refrigeration/test-facilities/` and in [14]. All tests show that the outlet temperature $T_{e,o}$ approximately follows an s-shaped curve when OD is slowly increased. The nonlinear behavior has sigmoid function properties, with two horizontal asymptotes and a non-positive bell shaped first derivative. The system is therefore approximated by a Hammerstein model using a sigmoid function to describe the nonlinearity ($\arctan$ function) and then a first order plus dead time (FOPDT) model to describe the system dynamics, which is also suggested in [19, 22]. The equations are;

$$f(u) = -k_1 \arctan\left(k_2\left(u - u^*\right)\right) + f(u^*), \tag{9.17}$$

$$F_o(s) = \frac{1}{T_{sys}s + 1} e^{-sT_d}, \tag{9.18}$$

where, in the evaporator case, the input u is the OD, $f(u)$ is $T_{e,o}$, k_1 and k_2 are system specific gains, and $(u^*, f(u^*))$ denotes the offset (also the maximum slope or symmetry point). The Laplace domain transfer function for the dynamics are given by the system

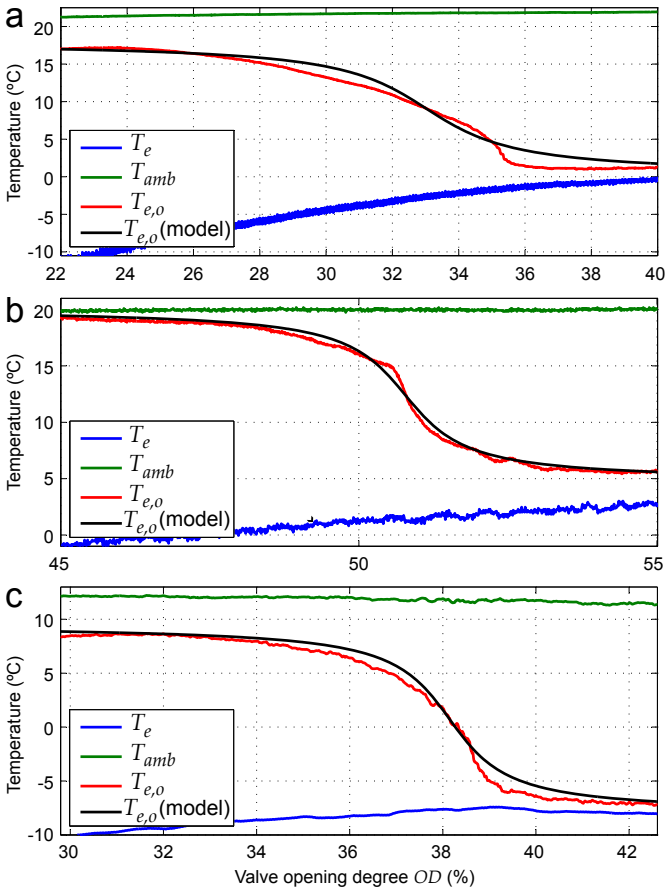

Figure 9.5: Evaporator I/O-map revealed by a slow input sweep for an air conditioning system (a), a water chiller refrigeration system (b), and a supermarket display case (c). The input is the valve OD and the output is the evaporator outlet temperature $T_{e,o}$. Ambient temperature T_{amb} and evaporation temperature T_e are also shown.

time constant T_{sys} and the delay T_d. When using a Hammerstein model it is assumed that the input dynamics are fast and thus negligible. Also note that the Hammerstein model is only an approximation of the real system for a given set of operating conditions, where the output $y = f(x, u, w, t)$ is a function of both the state x, the input u, the disturbances w, the time t, and the nonlinearity and dynamics are not separable. However, the model approximation has shown to fit well enough for simulation purposes and MSS is a non model-based control method, which can adapt to changes in system parameters as long as the qualitative shape of the I/O-map remains. The model parameters, from the tests shown in Fig. 9.5, were derived in [14] and are summarized in Table 9.1.

A known challenge in controlling the evaporator superheat temperature is that the pressure sensor can fail to function properly, which could lead to compressor malfunction and the inability to run the system. For example, dirt or oil could choke the sensor and

Parameter	Air con.	Chiller	Display
k_1	5.68	4.89	5.59
k_2	0.50	1.31	1.07
u^*	33.02	50.78	38.15
$f(u^*)$	9.08	12.41	0.71
$f'(u^*)$	-2.84	-6.41	-5.98
T_{sys}	23.07	31.51	59.52
T_d	15	26	29

Table 9.1: Evaporator model parameters for the air conditioning, water chiller, and supermarket refrigeration systems.

thus "'freeze"' the output or it could break. An alternative would be to use a temperature sensor giving $T_{e,i}$ (see Fig. 9.4), however, this sensor is not normally installed. This means that an alternative control method is needed when the pressure sensor fails. The idea is to adapt the OD to a level which gives a suitable superheat while only using the $T_{e,o}$ measurement. Another reason for using the MSS control method is that the pressure sensor is expensive and it would be possible to reduce the superheat control installation costs substantially if it could be removed. Note also that if the surrounding temperature or the evaporation temperature changes, then it will result in a change in the suitable outlet temperature; this is the main reason for avoiding the use of a fixed $T_{e,o}$ reference. The evaporator superheat control problem and the three identified models will be used in the following as examples showing the applicability of the MSS control method.

4 Simulation Examples

The air conditioning system (see Table 9.1) is investigated in the following using $t_s = 1$ second and $T_{ex} = 120$ seconds. The monodromy matrix, derived in the appendix, is used to find an upper bound estimate for K. Fig. 9.6 shows the steady state I/O-map and the simulation response in the stable simulation with convergence of $\bar{u}(k)$ to u^*. The output

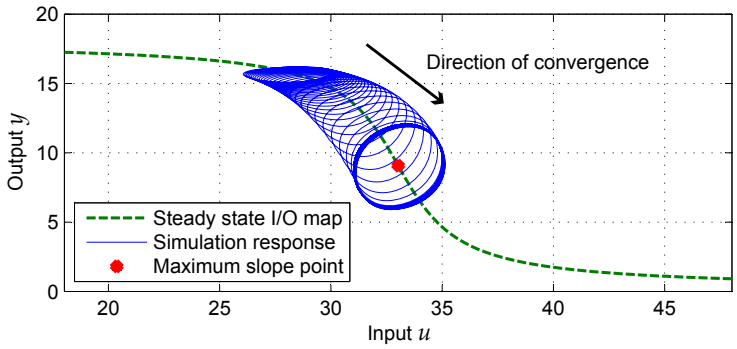

Figure 9.6: Steady state I/O-map for the air conditioning system model and convergence from $\bar{u}(0) = u^* - 5$ using perturbation amplitude $A_{ex} = 2$ and integral gain $K = 0.04$.

circles around the I/O-map due to the continuous perturbation of the input and the system dynamics, which is intentional. The simulation response would follow the I/O-map back and forth if there were no dynamics. Fig. 9.7 shows the eigenvalues using both a stable and an unstable integral gain K. The eigenvalues show that the system is unstable if K is chosen too high. Stability and instability resulting in limit cycles is also shown in Fig. 9.8. The top graph shows how the system converges to the maximum slope point $u^* = 33.02$ when a perturbation signal is added and that limit cycles occur near this point if the gain is chosen too high. The bottom graph shows the same simulation without a perturbation signal. Here the high gain drives the system away from the maximum slope point to a smaller slope and stabilizes here (it will not converge back because $A_{ex} = 0$).

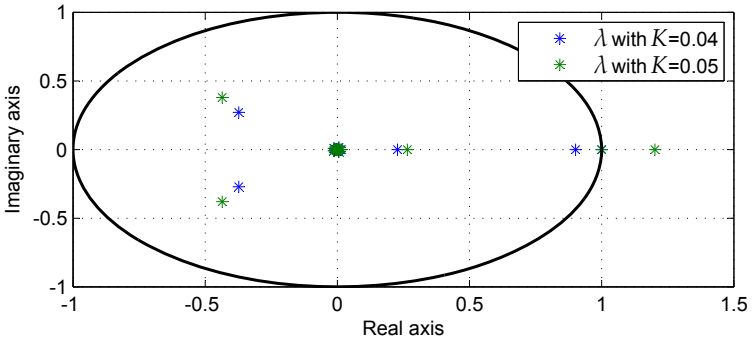

Figure 9.7: Eigenvalues of $\Psi_A(k)$ for the air conditioning system model for different integral gains K.

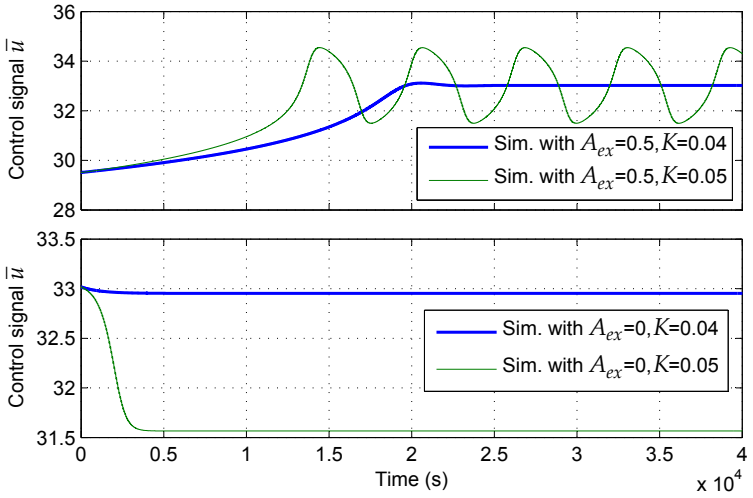

Figure 9.8: Closed-loop simulation response with different integral gain using the air conditioning system model. The top graph shows convergence from $\bar{u}(0) = u^* - 3.5$ using perturbation amplitude $A_{ex} = 0.5$ and the bottom graph show simulations starting at $\bar{u}(0) = u^*$ without perturbation ($A_{ex} = 0$).

5 Modified MSS for Systems with Dynamics

System dynamics can change the sign of the feedback error signal $\xi(k)$ if the phase shift of the second harmonic is larger than 90 degrees, which would result in divergence from the desired operating point. The phase shift can be compensated for using the parameter N_ϕ in (9.2). However, the exact phase shift is typically unknown and time-varying, which is permissible if guarantees on parameter bounds can be made or if a sufficient time scale separation between perturbation and dynamics is ensured (thereby reducing the phase shift). A disadvantage of this approach is that low frequency perturbation results in a rather slow feedback loop. A modified MSS control setup is therefore introduced and shown in Fig. 9.9. The difference is that the cross product between the first and second harmonic is now taken. The equations are

$$H_p(k) = \frac{2}{N} \sum_{n=k-N+1}^{k} \left(\cos\left(p\omega_{ex}\left(n - N_\phi\right)\right) - j\sin\left(p\omega_{ex}\left(n - N_\phi\right)\right)\right) y(n), \quad (9.19)$$

$$M(H_1, H_2) = \frac{|H_1|\,|H_2|\sin\left(\theta_{12}\right)}{\eta}, \quad (9.20)$$

where the harmonics $H_p(k)$ are found using two separate filters with $p = \{1, 2\}$ being the number of the harmonic, $\eta > 0$ is an optional normalization function, and θ_{12} is the angle from the first harmonic to the second.

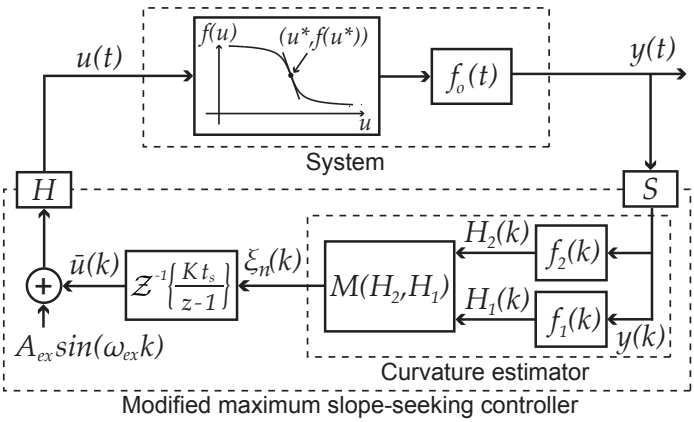

Figure 9.9: Modified MSS control scheme.

Remark 2: The same analysis as in Remark 1 can be used to motivate the modified curvature

estimator in Fig. 9.9. The normalized error signal $\xi_n(k)$ (normalized curvature estimate) is now

$$\begin{aligned}\xi_n(k) =& \frac{a_1(k)b_2(k) - a_2(k)b_1(k)}{\eta} \\ \approx& \frac{1}{\eta}\left(\left[\frac{2}{N}\sum_{n=k-N+1}^{k}\cos(\omega_{ex}(n-N_\phi))y(n)\right]\right. \\ & \left[\frac{2}{N}\sum_{n=k-N+1}^{k}\sin(2\omega_{ex}(n-N_\phi))y(n)\right] \\ & -\left[\frac{2}{N}\sum_{n=k-N+1}^{k}\cos(2\omega_{ex}(n-N_\phi))y(n)\right] \\ & \left.\left[\frac{2}{N}\sum_{n=k-N+1}^{k}\sin(\omega_{ex}(n-N_\phi))y(n)\right]\right),\end{aligned} \tag{9.21}$$

where $a_1(k)$, $b_1(k)$, $a_2(k)$, and $b_2(k)$ are the Fourier coefficients of the first and second harmonic. Using (9.5)-(9.7) and trigonometric identities it is possible to reduce (9.21) to

$$\xi_n(k) = \frac{c_1 c_2 A_{ex}^3 f'(\bar{u}) f''(\bar{u})}{4\eta}\cos(\phi_1 - \phi_2 + \phi), \tag{9.22}$$

where $\frac{1}{\eta} > 0$. If assumption 1, 2, and 3 hold and if the I/O-map is monotonic decreasing ($f'(u) < 0$ for all $u \in U$, $c_1 > 0$, $c_2 > 0$) and $|\phi_1 - \phi_2 + \phi| < \frac{\pi}{2}$, then

$$\xi_n(k) = 0 \text{ for } f''(\bar{u} = u^*), \tag{9.23}$$

$$\xi_n(k) > 0 \text{ for } f''(\bar{u} < u^*), \tag{9.24}$$

$$\xi_n(k) < 0 \text{ for } f''(\bar{u} > u^*), \tag{9.25}$$

for sufficiently small $A_{ex} > 0$ and $K > 0$. This setup is thus a more robust solution for systems with dynamics, in the sense that only the difference in phase shift between the first and second harmonic frequencies needs to be below 90 degrees. Ensuring this is easier, since there is only an octave in-between.

The optional normalization in (9.20) can help to compensate for changes in system gain. Fig. 9.10 shows different normalizations and the effect on the error signal in open-loop using the same simulation parameters as in the test shown in Fig. 9.6. In the simulations the first harmonic is used to normalize and η is here;

$$\eta_0 = 1,\ \eta_2 = |H_1(k)|^2,\ \eta_3 = |H_1(k)|^3. \tag{9.26}$$

The cubed amplitude of the first harmonic gives an almost linear relationship between input offset $\bar{u}$ and error signal ξ_n. However, tests have shown that using η_2 as normalization gives a good weighting factor on the error and it performs better in noisy systems, because the decrease in error signal far from the desired operating point corresponds to the very low amplitudes and the resulting trust that can be put in the Fourier analysis. η_2 is thus used as normalization in the following.

The design parameters are the integral gain K, the perturbation angular frequency $\omega_{ex} = 2\pi t_s / T_{ex}$, and the amplitude A_{ex}. An tuning approach was suggested in [14] and test on the three mentioned refrigeration systems showed good results. Moreover, this

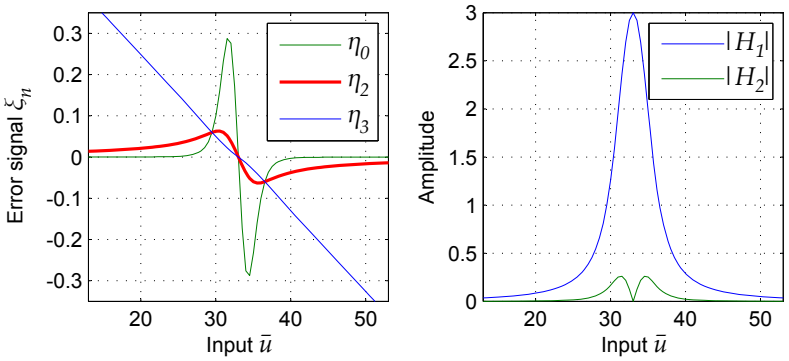

Figure 9.10: Open-loop error signal as a function of input offset $\bar{u}$ using different normalizations (right) and amplitude of harmonics (left). The maximum slope point is $u^* = 33.02$.

procedure was automated in [15]. In summary, a slow ramp test is performed in the procedure to identify the steady state nonlinear I/O-map (as was shown in Fig. 9.5), which is followed by a biased relay feedback test. The result of this is provided in Table 9.1 and gives an approximate Hammerstein model of the system, which can be used for simulation purposes. Better results could possibly be obtained using system identification for Hammerstein models (e.g., see [23]) or using the Matlab® system identification toolbox and the $nlhw$ function. If parameter bounds are known, then the worst case parameter set could also be used to give limits on the design parameters.

The dominant system time constant can then be used to find an appropriate perturbation period T_{ex}, which based on test experience should be 3-5 times the time constant for refrigeration systems. With a model it is also possible to choose T_{ex} to give a difference in phase shift less than a design criteria (should as a minimum be $<$90 degrees) and the parameter N_ϕ can also be used to compensate for phase shift. A way to choose N_ϕ is to set it equal to the estimated system delay, since delays in refrigeration systems can be large and introduce a large contribution to the phase shift difference between the two harmonics.

The perturbation amplitude A_{ex} is not highly critical. However, it should be large enough to give distinguable perturbation in the output. The model could be used to iteratively find a good amplitude. Another possibility is to limit the amount of system excitation using an Automatic Gain Controller (AGC), since the amount of excitation is measurable through the first harmonic; this approach was presented in [12].

Having the simulation model and the perturbation signal in place, then a suitable K can be identified iteratively, e.g. using a bisection algorithm search, where K is iterated until a prespecified overshoot (or some other performance criteria) is obtained in a convergence test. The upper bound estimate on K provided in Subsection 2 can also be used if the simple MSS control without the normalized cross product is employed.

Finally, standard integral control anti-windup is necessary if there are saturation limits on the input u.

6 Simulation of the Modified MSS Control

Monte Carlo simulation results are presented in this section to show the robustness of the modified MSS controller toward uncertainty in parameter values on the three identified models from Section 3.

The same MSS control parameters as were used on the real system (see [14]) are used in the Monto Carlo simulations. These parameters are listed in Table 9.2 for the air conditioning system, the water chiller, and the supermarket display case.

Parameter	Air con.	Chiller	Display
T_{ex}	120	130	180
A_{ex}	8.5	10.8	8.0
K	0.079	0.067	0.042
N_ϕ	15	26	29

Table 9.2: Chosen perturbation signal values, integral control gain, and phase shift compensation used in tests on the refrigeration systems.

It is assumed that the input dynamics are negligible. However, quantization on the input valve opening degree OD of 1% and measurement noise with standard deviation $2\sigma = 0.1\ ^\circ C$ is added to make the simulation more realistic. Furthermore, a spread on the parameters T_{sys}, T_d, k_1, and k_2 of $\pm 50\%$ with a uniform random distribution is used to simulate the uncertainty in the estimation of the system model. A spread of up to $\pm 50\%$ was also suggested in [22] for the system dynamics. Finally, the initial input offset $\bar{u}(0)$ (initial average opening degree) is chosen uniformly in the range $\pm 20\%$ from the desired value.

Fig. 9.11 shows the simulation result from 100 simulations with different system parameters using either the air conditioning system model, the water chiller system model, or the supermarket display case system model. The input offset $\bar{u}$ converges in all cases toward the desired value u^* listed in Table 9.1, even with up to $\pm 50\%$ spread in system parameters, while keeping the control parameters fixed. This indicates the robustness of the control method toward parameter uncertainty. However, the robustness depends on the severity of the nonlinearity and the specific case.

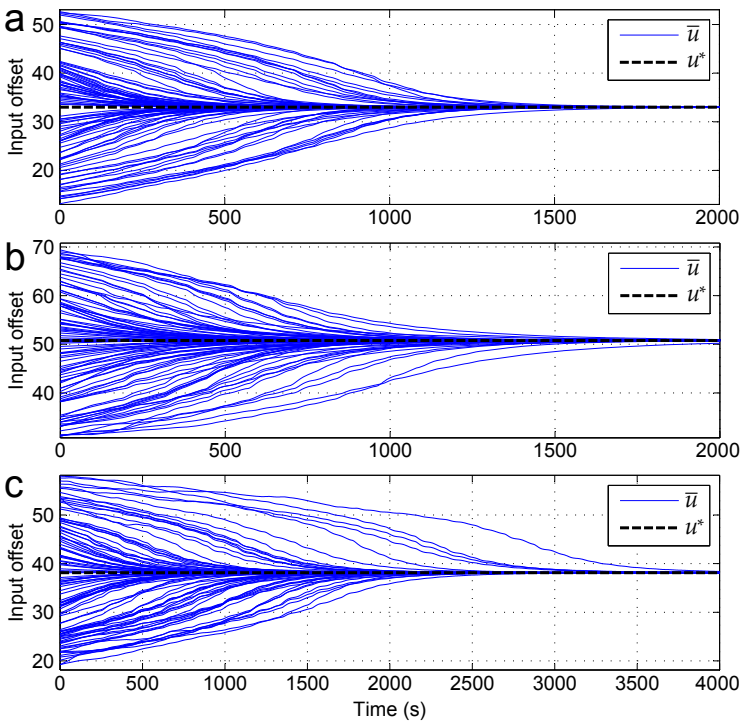

Figure 9.11: Time evolution of $\bar{u}$ in the 100 simulations using either the air conditioning system model (a), the water chiller system model (b), or the supermarket display case system model (c).

7 Evaporator Superheat Control Test Results

Results from tests on the water chiller refrigeration system, air conditioning system, and supermarket display case were presented in [14]. Zoomed graphs of some of the results are presented in Fig. 9.12-9.14 showing the performance of the MSS control.

A step in the compressor frequency gives a disturbance in the evaporation temperature T_e, which results in a change in the desirable $T_{e,o}$ and the appropriate opening degree OD. The error signal in Fig. 9.12 and 9.13 changes after the step, which results in adaptation of $\bar{u}$ to match the new operating conditions (new location of the maximum slope point). There is a small delay before the error signal changes, which can be related to the length of the FIR filter N. The delay before the control reacts is less than half a perturbation period, which is considered acceptable. The superheat defined in (9.16) reaches in average a good level using MSS control, which is achieved by only ensuring that the average $T_{e,o}$ (only available measurement) is maintained near the maximum slope point. Note that the Monte Carlo simulations in Section 6 also showed that the model parameters could easily be change up to $\pm 50\%$ while still reaching the maximum slope point, which corresponds to a suitable filling of the evaporator, where only a few more % opening of the valve will flod the compressor.

Fig. 9.14 shows the result from the supermarket refrigeration system where it was not

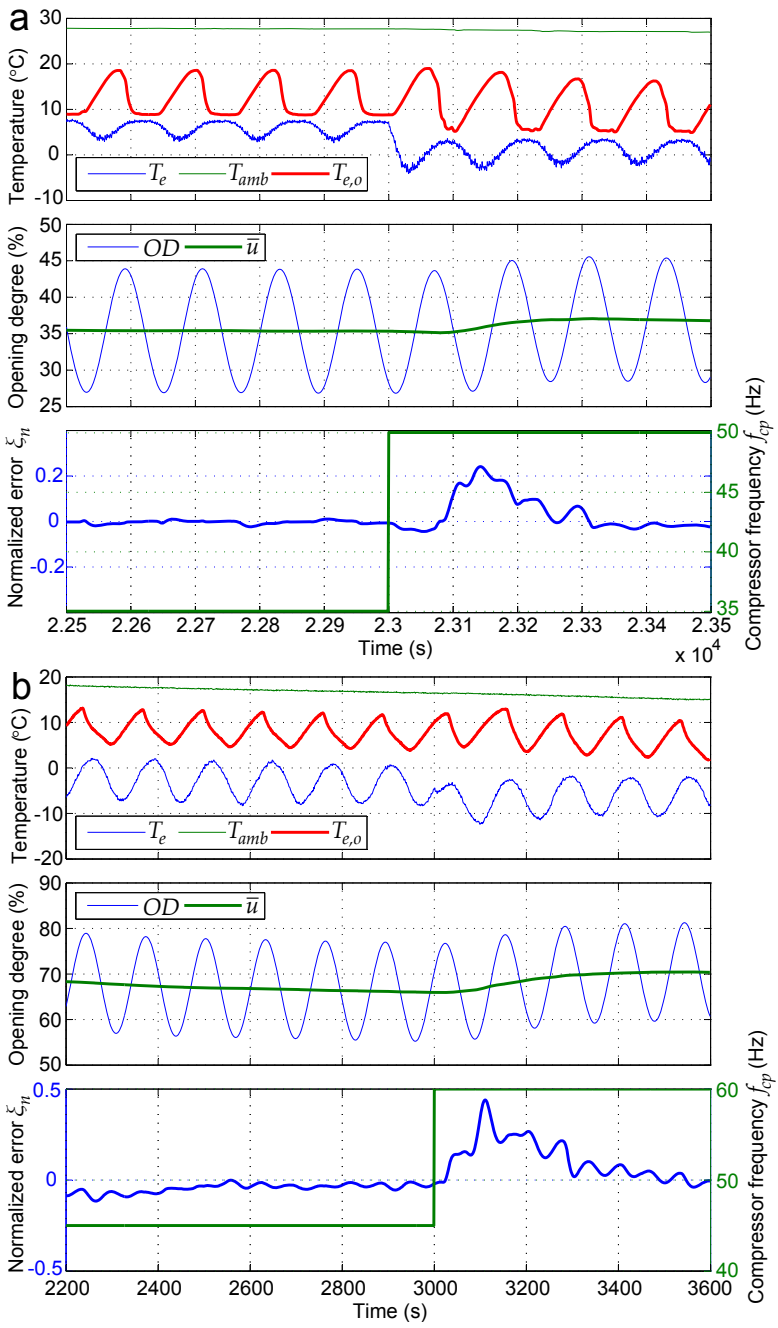

Figure 9.12: Test results showing MSS performance during a step up in compressor frequency on the air conditioning system (a) and the water chiller refrigeration system (b).

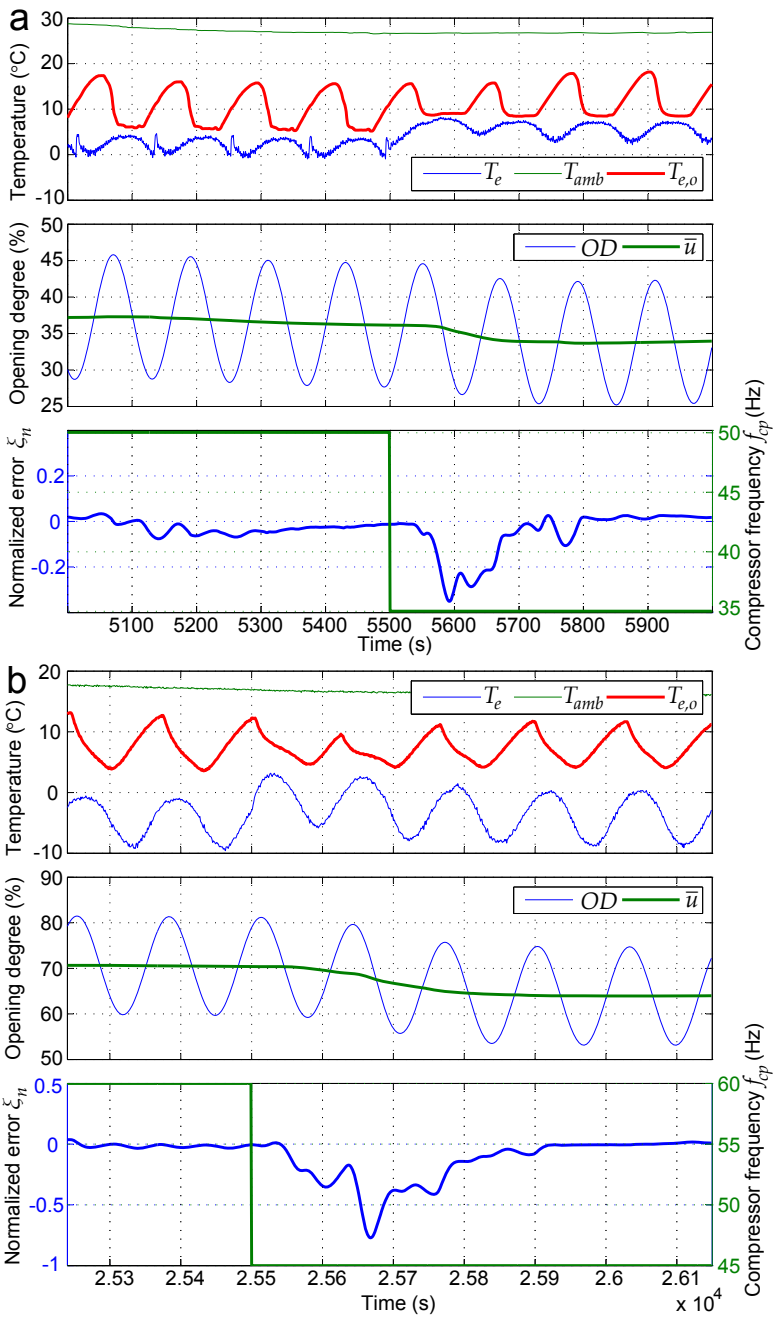

Figure 9.13: Test results showing MSS performance during a step down in compressor frequency on the air conditioning system (a) and the water chiller refrigeration system (b).

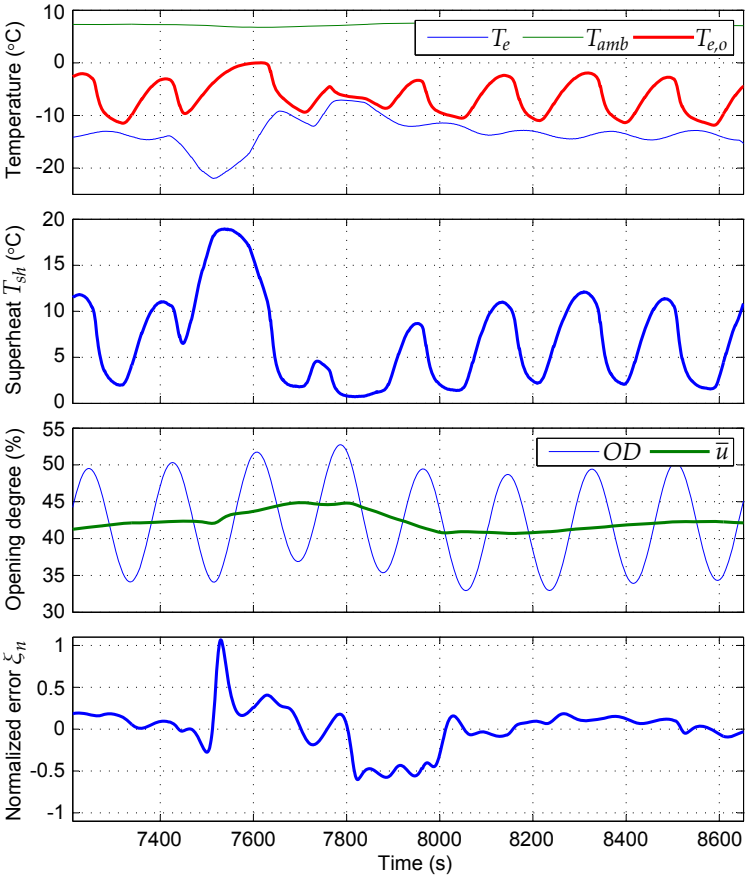

Figure 9.14: Test results showing MSS performance during large evaporation pressure disturbances on the supermarket display case.

possible to make a compressor frequency step. However, a moment with a large disturbance in T_e is captured and the result shows how the MSS controller adapts $\bar{u}$ up until the disturbance is gone and then adapts back down, in order to maintain the average $T_{e,o}$ near the maximum slope point and thus a good average superheat level. For a comparison of the obtained superheat with conventional two sensor control strategies see [14].

The test results indicate that MSS control works in the refrigeration system case and also shows that MSS control works in systems where u^* is not constant, but changed with a disturbance step, where the compressor frequency can be seen as a disturbance input to the evaporator system with OD as input and $T_{e,o}$ as output.

8 Conclusion

A maximum slope-seeking (MSS) controller has been proposed. This non model-based control method is beneficial if a suitable reference setpoint is unknown but qualitatively

located where the slope (gain) has an extremum in the I/O-map. If the system under consideration has sigmoid function properties then there is exactly one maximum slope point. The control method also has potential in systems with discontinuities and when the I/O-map is not symmetric around the maximum slope point, since the control converges toward a point with zero mean curvature. Conditions for closed-loop stability and convergence of the basic MSS scheme has been derived and an improved MSS setup has been proposed, which is more robust toward phase shift introduced by system dynamics. A way to estimate an upper bound on the feedback gain has also been provided. Furthermore, Monte Carlo simulations have shown convergence for models of three vapor-compression refrigeration systems even when all model parameters were varied up to $\pm 50\%$ and tests on these systems have shown that evaporator superheat can be controlled with MSS using a reduced set of sensors. Without a model, additional sensors are usually required to gain the same information needed for control. However, MSS control can extract more information from each sensor due to continuous perturbation of the system and by exploiting the nonlinear relationship between input and output. Refrigeration system tests also showed that the MSS controller was able to adapt when the operating conditions were changed.

Acknowledgments

The authors gratefully acknowledge financial support from the Faculty of Engineering and Science at Aalborg University, the Danish Council for Independent Research - Technology and Production Sciences, and Danfoss A/S.

References

[1] M. Leblanc, "Sur l'électrification des chemins de fer au moyen de courants alternatifs de fréquence élevée," *Revue Générale de l'Electricité*, 1922.

[2] H.-H. Wang and M. Krstić, "Extremum seeking for limit cycle minimization," *IEEE Transactions on Automatic Control*, vol. 45, no. 12, pp. 2432–Ű2437, December 2000.

[3] K. B. Ariyur and M. Krstić, *Real-Time Optimization by Extremum-Seeking Control*. Wiley-Interscience, 2003.

[4] C. Zhang and R. Ordóñez, *Extremum-Seeking Control and Applications: A Numerical Optimization-Based Approach*, ser. Advances in Industrial Control. Springer, 2012.

[5] Y. Tan, W. Moase, C. Manzie, D. Nešić, and I. Mareels, "Extremum Seeking From 1922 To 2010," in *Proceedings of the 29th Chinese Control Conference*, Beijing, China, July 2010, pp. 14–26.

[6] Y. Li, M. A. Rotea, G. T.-C. Chiu, L. G. Mongeau, and I.-S. Paek, "Extremum Seeking Control of a Tunable Thermoacoustic Cooler," *IEEE Transactions on Control Systems Technology*, vol. 13, no. 4, pp. 527–Ű536, July 2005.

[7] V. Tyagi, H. Sane, and S. Darbha, "An Extremum Seeking Algorithm for Determining the Set Point Temperature for Condensed Water in a Cooling Tower," in *American Control Conference*, Minneapolis, Minn., USA, June 2006, pp. 1127–1131.

[8] X. Li, Y. Li, J. E. Seem, and P. Li, "Extremum Seeking Control of Cooling Tower for Self-Optimizing Efficient Operation of Chilled Water Systems," in *American Control Conference*, Montreal, Canada, June 2012, pp. 3396–3401.

[9] P. Li, Y. Li, and J. E. Seem, "Efficient Operation of Air-Side Economizer Using Extremum Seeking Control," *Journal of Dynamic Systems, Measurement, and Control*, vol. 132, no. 3, p. 031009 (10 pages), April 2010.

[10] D. J. Burns and C. Laughman, "Extremum Seeking Control for Energy Optimization of Vapor Compression Systems," in *International Refrigeration and Air Conditioning Conference*, Purdue, USA, 2012.

[11] M. Haring, N. van de Wouw, and D. Nešić, "Extremum-seeking control for nonlinear systems with periodic steady-state outputs," *Automatica*, vol. 49, no. 6, pp. 1883–1891, June 2013.

[12] K. Vinther, H. Rasmussen, R. Izadi-Zamanabadi, and J. Stoustrup, "Utilization of Excitation Signal Harmonics for Control of Nonlinear Systems," in *IEEE Multi-Conference on Systems and Control*, Dubrovnik, Croatia, October 2012, pp. 1627–1632.

[13] ——, "Single Temperature Sensor based Evaporator Filling Control using Excitation Signal Harmonics," in *IEEE Multi-Conference on Systems and Control*, Dubrovnik, Croatia, October 2012, pp. 757–763.

[14] ——, "Single temperature sensor superheat control using a novel maximum slope-seeking method," *International Journal of Refrigeration*, vol. 36, no. 3, pp. 1118–1129, May 2013.

[15] ——, "A Fault Tolerant Superheat Control Strategy for Supermarket Refrigeration Systems," in *International Conference on Control and Fault-Tolerant Systems (SysTol)*, Nice, France, October 2013, pp. 426–431.

[16] S. Bittanti and P. Colaneri, "Invariant representations of discrete-time periodic systems," *Automatica*, vol. 36, no. 12, pp. 1777–1793, December 2000.

[17] R. A. Horn and C. R. Johnson, *Matrix Analysis*. Cambridge University Press, 1985.

[18] I. Dincer and M. Kanoglu, *Refrigeration Systems and Applications*, 2nd ed. Wiley, 2010.

[19] B. P. Rasmussen, "Dynamic modeling for vapor compression systems - Part I: Literature review," *HVAC&R Research*, vol. 18, no. 5, pp. 934–955, September 2012.

[20] D. P. Finn and C. J. Doyle, "Control and optimization issues associated with algorithm-controlled refrigerant throttling devices," *ASHRAE Transactions*, vol. 106, no. 1, pp. 524–533, 2000.

[21] M. S. Elliott and B. P. Rasmussen, "On reducing evaporator superheat nonlinearity with control architecture," *International Journal of Refrigeration*, vol. 33, no. 3, pp. 607–614, May 2010.

[22] R. Izadi-Zamanabadi, K. Vinther, H. Mojallali, H. Rasmussen, and J. Stoustrup, "Evaporator unit as a benchmark for Plug and Play and fault tolerant control," in *8th IFAC Symposium on Fault Detection, Supervision and Safety of Technical Processes*, Mexico City, Mexico, August 2012, pp. 701–706.

[23] E. Eskinat, S. H. Johnson, and W. L. Luyben, "Use of Hammerstein Models in Identification of Nonlinear Systems," *AIChE Journal*, vol. 37, no. 2, pp. 255–268, February 1991.

A Derivation of Monodromy Matrix for Periodic Systems

The monodromy matrix $\Psi_A(k)$ is derived here for illustrative purposes for a system with linear FOPDT dynamics (P_{sys}), a FIR filter, and integral feedback control (C). The system is shown in Fig. 9.15 using the discrete time notation and it is assumed that the sample time t_s is small (good approximation of continuous system). The equations are

$$P_{sys}(z) = z^{-N_d} \frac{b_{sys}}{z + a_{sys}} \tag{9.27}$$

$$\xi(k) = \frac{2}{N} \sum_{n=k-N+1}^{k} y(n) \cos\left(p \frac{2\pi}{N}(n - N_\phi)\right) \tag{9.28}$$

$$C(z) = \frac{K t_s}{z - 1}, \tag{9.29}$$

where N_d, a_{sys} and b_{sys} are given by the system, $N = T_{ex}/t_s$ is the number of samples used in the filter, $p = 1, 2, ...$ is the harmonic of interest, N_ϕ is phase shift compensation, $\Xi(z)$ is the z-transform of (9.28), and K is the integral gain. Using the one step back in time shift operator q^{-1}, the system can be redrawn as shown in Fig. 9.16. The update of the state vector $\mathbf{x}(k) = [x_1(k), x_2(k), .., x_{N+1+N_d}(k)]^T$ is given as

$$\mathbf{x}(k+1) = \mathbf{A}(k)\mathbf{x}(k), \tag{9.30}$$

where the periodic matrix $\mathbf{A}(k)$ can be derived from Fig. 9.16. An example with a dead time delay $N_d = 2$ gives the matrix in (9.31).

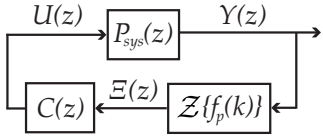

Figure 9.15: Example system.

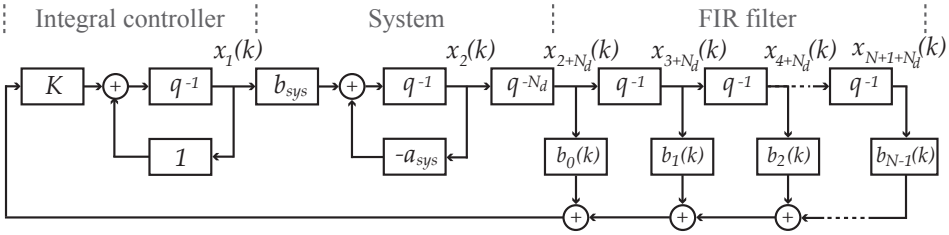

Figure 9.16: Discretized example system with two IIR filters ($C(z)$ and $F_o(z)$) and a periodic FIR filter.

$$\mathbf{A}(k) = \begin{bmatrix} 1 & 0 & 0 & Kb_0(k) & Kb_1(k) & \cdots & Kb_{N-2}(k) & Kb_{N-1}(k) \\ b_{sys} & -a_{sys} & 0 & 0 & 0 & \cdots & 0 & 0 \\ 0 & 1 & 0 & 0 & 0 & \cdots & 0 & 0 \\ 0 & 0 & 1 & 0 & 0 & \cdots & 0 & 0 \\ \vdots & \vdots & \vdots & \vdots & \vdots & \ddots & \vdots & \vdots \\ 0 & 0 & 0 & 0 & 0 & \cdots & 1 & 0 \end{bmatrix} \tag{9.31}$$

The diagonal from $A_{3,2}$ to $A_{N+3,N+2}$ contain ones (due to the FIR filter) and the periodic coefficients $b_i(k)$ in the FIR filter for $i = [0, 1, .., N-1]$ are

$$b_i(k) = \frac{2}{N} \cos\left(2\frac{2\pi}{N}(N - i + k - N_\phi)\right). \tag{9.32}$$

The monodromy matrix for one period T is then

$$\Psi_A(k) = \mathbf{A}(k+T-1)\mathbf{A}(k+T-2)...\mathbf{A}(k). \tag{9.33}$$

Paper G

Learning/Repetitive Control for Building Systems with Nearly Periodic Disturbances

Kasper Vinther, Vikas Chandan, and Andrew G. Alleyne

This appendix is based on a paper published in:
The proceedings of the European Control Conference (ECC), July 2013

Abstract

In this paper, learning/repetitive control is proposed for improvement of existing feedback control loops for temperature regulation in buildings. A single zone office building is used as an example, with real weather data for Phoenix Arizona and realistic occupancy load schedules. Simulations have shown a decrease in the average setpoint tracking error of more than 50%, even without additional energy consumption. This can be achieved in situations where the load disturbances have enough repeatability and a repeatable-to-nonrepeatable ratio can be computed to determine if learning should be used and at which frequencies. Furthermore, the increased tightness in reference tracking could be used to lower energy consumption by moving the reference setpoint closer to the boundaries of the allowable temperature range.

1 Introduction

Temperature control in buildings is important for various reasons. It could be used to improve occupancy comfort in commercial and residential spaces, to maintain good quality of products in cold storage rooms or for safety reasons in pharmaceutical processing facilities. The temperature is often controlled with a heating ventilation and air-conditioning (HVAC) system using either on/off type hysteresis control or variations of PI/PID control due to their simple implementations [1, 2]. However, they seldom perform well at all possible operating conditions because the control is typically tuned only for a selected nominal situation; also the control might not be tuned properly in the first place [2–4].

Model-based control can improve the performance over on-off or PID control, but obtaining a sufficiently accurate model of the building and the HVAC system is a time consuming and costly process and the uncertainty of these models can be quite severe due to several reasons. Firstly, certain parameters are expected to be time-varying, such as the thermal capacities, and therefore are hard to obtain. Secondly, there will be uncertainty in the estimation of load disturbances, which are dictated by several factors such as weather conditions, occupancy, appliances, lighting, etc. Although weather can be included in the control [5], the exact contribution of factors such as occupants, appliances, and thermal infiltration is difficult to predict accurately.

This paper investigates the use of learning type control such as iterative learning control (ILC) and repetitive control (RC) for improvement of existing feedback controllers in buildings such as the ones mentioned above. A survey on ILC is provided in [6] and RC is covered in references such as [7, 8], which also show the similarity of these methods. The basic concept of these types of learning control methodologies is that feedforward signals are generated and updated based on previous errors and they do not require the costly process of identifying system models. However, they do need repetitiveness in the tracking error and disturbances.

Buildings experience repetitiveness in load disturbances on a daily and a seasonal basis due to the weather. A good prediction of the weather tomorrow is that it will most likely be close to what it was today. Also, the occupancy and appliance loads will often repeat themselves on a daily basis governed by actions such as people going to work, having lunch, supermarkets opening and closing, etc. The assumptions about the repetitiveness of various disturbances will not always hold true, but the idea in learning is that the control adapts to changes based on past experience. This means that we only need

nearly periodic disturbances, in the sense that they are allowed to change, but on average they will show periodicity. The authors in [9] have provided a way to calculate the Repeatable-to-Nonrepeatable Ratio (RNR), which can be used to determine if the repeatable part of the tracking error or disturbance is larger than the nonrepeatable part for each frequency. A ratio above zero means that there is potential for applying learning type control.

A single zone office building is provided as an example case study to show the possible tracking performance improvement with learning/repetitive control. A MATLAB Simulink model of this building is derived using lumped parameter modeling with resistive-capacitive networks and quasi periodic disturbances such as real weather data and occupancy load schedules are used. This model allows us to simulate an entire year or even longer and makes it possible to compare different control strategies, which would not be possible in a real building. The proposed steps to improve tracking performance in an already existing stable feedback system are to: (i) Collect error data for an appropriate time window. (ii) Calculate RNR. (iii) Use RC or ILC to design a learning filter that corresponds to the RNR findings and thus improve tracking performance at appropriate frequencies.

This paper first introduces a simple modeling framework for buildings and provides a description of the model of a single zone office building. A temperature controller is then designed in Section 3, which provides a comparative case for analysis. Then, the learning/repetitive control design is described in Section 4, followed by results in Section 5, from simulations on the single zone building spanning an entire year. Finally, conclusions are drawn in Section 6.

2 Modeling

Lumped Parameter Modeling of Buildings Using Resistive-Capacitive Networks

A commonly used method of modeling the thermal dynamics of buildings is using lumped resistive-capacitive networks [10–12]. In this paper, each room (zone) is considered as a single capacitance and each wall is represented with 3 resistors and 2 capacitors also referred to as the 3R2C modeling approach [11]. Fig. 10.1 illustrates the 3R2C network, where $R_{wo,i}$ is the thermal resistance between the outer wall surface of wall i and ambient, $R_{wi,i}$ is the resistance between the inner wall surface and ambient, and $R_{ww,i}$ is the resistance between the inner and outer wall surfaces. The states in the model are

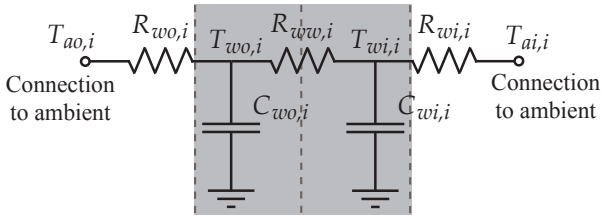

Figure 10.1: 3R2C network model of a wall.

the temperatures of the inner wall surfaces $T_{wi,i}$, the outer wall surfaces $T_{wo,i}$, and the room/zone temperatures. The ambient temperatures $T_{ao,i}$ and $T_{ai,i}$ could be zone temperature, outside air temperature, or ground temperature, where outside air ($T_{air,o}$) and ground (T_{gnd}) temperatures are considered inputs to the system.

The zones have controllable inputs, which are the heat transfer rates $\dot{\mathbf{Q}}_{hvac}$ supplied by the HVAC system (positive when heating and negative when cooling). A discrete state space model representation of this system is shown in (10.1).

$$\begin{bmatrix}\mathbf{T}_w\\ \mathbf{T}_z\end{bmatrix}(k+1) = \begin{bmatrix}\mathbf{A}_{ww} & \mathbf{A}_{wz}\\ \mathbf{A}_{zw} & \mathbf{A}_{zz}\end{bmatrix}\begin{bmatrix}\mathbf{T}_w\\ \mathbf{T}_z\end{bmatrix}(k) + \begin{bmatrix}\mathbf{0}\\ \mathbf{B}_z\end{bmatrix}\dot{\mathbf{Q}}_{hvac}(k) + \begin{bmatrix}\mathbf{B}_{air} & \mathbf{B}_{gnd} & \mathbf{B}_{dw} & \mathbf{0}\\ \mathbf{0} & \mathbf{0} & \mathbf{0} & \mathbf{B}_{dz}\end{bmatrix}\begin{bmatrix}T_{air,o}\\ T_{gnd}\\ \mathbf{d}_w\\ \mathbf{d}_z\end{bmatrix}(k) \tag{10.1}$$

The vector $\mathbf{T}_w$ contains all the wall surface temperatures (both inside and outside) and the vector $\mathbf{T}_z$ contains all the zone temperatures. $T_{air,o}$, T_{gnd}, $\mathbf{d}_w$, and $\mathbf{d}_z$ are considered as disturbances to the system, where $\mathbf{d}_w$ is a vector of lumped Long Wave Radiation (LWR) and Short Wave Radiation (SWR) heat transfers affecting each wall and $\mathbf{d}_z$ is a vector of the thermal load applied directly on each zone (e.g. occupants, appliances, and lighting). These are further described in Subsection 2.

Single Zone Office Model

In this paper, we use a single zone office building with four walls, a ceiling, and a floor as an example, which is assumed to be located in Phoenix, Arizona. Using a standard medium office building construction template provided in the OpenStudio tool [13] developed by the National Renewable Energy Laboratory (NREL) an EnergyPlus [14] model of this building was created, which uses a weather file for Phoenix, Arizona. A Google SketchUp illustration of the building is shown in Fig. 10.2.

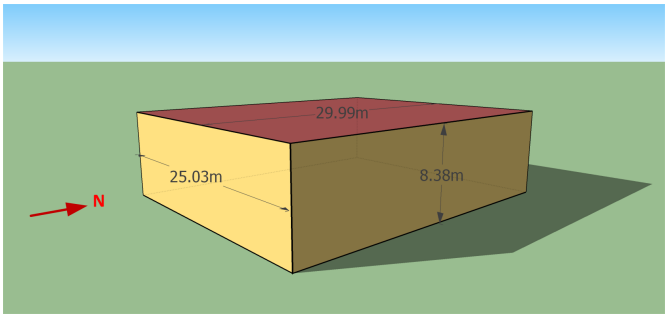

Figure 10.2: Google SketchUp illustration of single zone EnergyPlus model created in OpenStudio.

The 3R2C framework described in Subsection 2 was used to construct a simplified resistive-capacitive network model in MATLAB. This model is based on the EnergyPlus

model, where the resistances corresponding to the heat transfer between the zone and wall surfaces, and the zone capacitance were obtained using a least squares based system identification procedure applied on data generated using EnergyPlus. The capacitances for the inner and outer wall surfaces, and the resistances between them were computed based on physical properties of the wall construction layers. The resistances corresponding to thermal interactions of the wall surfaces with the ground and ambient air were obtained by averaging the corresponding heat transfer coefficient data obtained from a yearlong EnergyPlus simulation. The floor is modeled with only one state $T_{wi,6}$ as the ground temperature under the floor ($T_{wo,6}$) is considered constant.

The thermal load disturbances acting on the eleven wall surfaces are collected in a single vector $\mathbf{d}_w(t) = [d_{wi,1}(t), d_{wo,1}(t), ..., d_{wi,5}(t), d_{wo,5}(t), d_{wi,6}(t)]^T$ consisting of the disturbance on the inner wall surfaces ($i \in 1, 2, ..., 6$)

$$d_{wi,i}(t) = \underbrace{\sigma A_i \sum_{j=1}^{6} \mathbf{F}_{i,j} \left(T_{wi,j}^4(t) - T_{wi,i}^4(t)\right)}_{LWR\ from\ wall\ surfaces}, \tag{10.2}$$

and the outer wall surfaces ($i \in 1, 2, ..., 5$)

$$\begin{aligned} d_{wo,i}(t) = &\underbrace{\epsilon_i \sigma A_i F_{gnd,i} \left(T_{gnd}^4(t) - T_{wo,i}^4(t)\right)}_{LWR\ from\ ground} \\ &+ \underbrace{\epsilon_i \sigma A_i F_{sky,i} \left(T_{sky}^4(t) - T_{wo,i}^4(t)\right)}_{LWR\ from\ sky} \\ &+ \underbrace{\epsilon_i \sigma A_i F_{air,i} \left(T_{air,o}^4(t) - T_{wo,i}^4(t)\right)}_{LWR\ from\ air} + \underbrace{\alpha_i A_i q_{SWR,i}(t)}_{SWR}, \end{aligned} \tag{10.3}$$

where i is the wall number, σ is the Stefan-Boltzmann constant, A_i is the surface area, $\mathbf{F} \in \mathbb{R}^{6x6}$ is a matrix of Script-F factors [15], $F_{gnd,i}$, $F_{sky,i}$, and $F_{air,i}$ are view factors for the outer surface of wall i, T_{sky} is the sky temperature, ϵ_i is the thermal absorbtance of wall i, α_i is the solar absorbtance of wall i, and q_{SWR} is the incident solar radiation per unit area on wall i. These values, together with $T_{air,o}$ and T_{gnd}, can be obtained directly from EnergyPlus for an entire year and (10.2) and (10.3) emulate how EnergyPlus calculates the disturbances (short and long wave radiation).

The zone load d_z is pseudo randomly generated for each day for an entire year. Each day we assume that five Gaussian probability density functions (PDF) govern how many people arrive for work, how many hours each person works, when each person work (midpoint of working hours), when each person has lunch (midpoint), and how long that person's lunch is. The PDF parameters are mean $\bar{x} = \{$ 45 people, 9 hours, 13:00 hours, 12:30 hours, 0.75 hours $\}$ and standard deviation $\sigma_{std} = \{$ 3 people, 1 hour, 0.5 hours, 0.25 hours, 0.1 hours $\}$. Each occupant in the office corresponds to 0.6 kW (0.1 kW body heat, 0.4 kW appliances, 0.1 kW lighting) and 0.3 kW when they are at lunch (0.2 kW appliances, 0.1 kW lighting). For simplicity there is no distinction of weekends, however, one could just turn the learning off during weekends or even have different learning controllers for weekdays and weekends.

In this case study, the controllable heat transfer rate to the zone $\dot{Q}_{hvac}$ is assumed to be bounded between -35 and 17.5 kW. This will result in controller saturation during

some hot summer days and thus requirement for integrator anti-windup. Furthermore, the zone temperature reference $T_{z,r}$ is set to 22.5°C. A reference that varies during the day could also be used, as long as it repeats itself daily.

3 Office Building Temperature Control

The air temperature in office buildings can be controlled in different ways, e.g. with simple on/off hysteresis-based control, PI/PID control, or more advanced model-based control. In most cases one of the first two methods is used [1–4], primarily due to their simple implementations and relatively simple tuning procedures. Fig. 10.3 shows the closed-loop feedback system, where the zone air temperature T_z tracks a reference temperature $T_{z,r}$. The system is denoted by G and has the heat transfer rate provided by an HVAC system, $\dot{Q}_{hvac}$, as input. The disturbances to the system are the thermal loads on the walls $\mathbf{d}_w$ and the thermal load on the zone air d_z. The system model and disturbances in the single zone building case study are defined in Subsection 2 and are assumed to be unknown to the feedback controller.

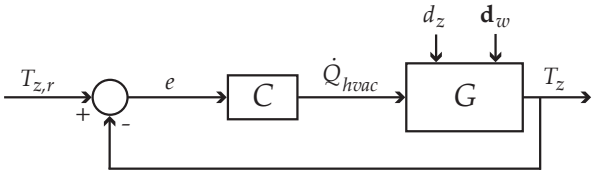

Figure 10.3: Closed-loop feedback control structure for temperature control.

Sensing of the zone air temperature with a digital sensor (thermostat) and its communication with the controller C is performed in discrete time. A realistic sample time for buildings is somewhere between 1 to 15 minutes depending on the size of the zones among other factors. Here a 5 minute sample time t_s is used. This sampling rate is faster than that of the underlying system dynamics and slow enough to allow the HVAC system to meet the desired $\dot{Q}_{hvac}$ before the demand is changed again. For comparison, the open-loop zone temperature time constant is about 27 minutes and the wall surface temperature time constants are much larger.

PI control is used in the feedback loop in this case study, since it performs better than just having hysteresis-based control and because it is commonly used as mentioned earlier. There exist various different PI tuning methods ranging from step response analysis, relay feedback, robust synthesis, etc. However, robust control methods require a nominal model of the system and uncertainty models, which can be difficult to obtain as mentioned earlier, and are usually not available to the control engineer. The step response method is therefore proposed, which gives different results depending on the particular load on the system. Critical regions of operation correspond to high and low load situations, which should be considered in order to design a robust PI controller. Fig. 10.4 shows closed-loop step responses using three different discrete-time test controllers C_1, C_2, and C_3 (10.4) for a high load situation (Fig. 10.4(a) and 10.4(b)) and a low load situation (Fig. 10.4(c) and 10.4(d)). The high load situation is generated based on the air

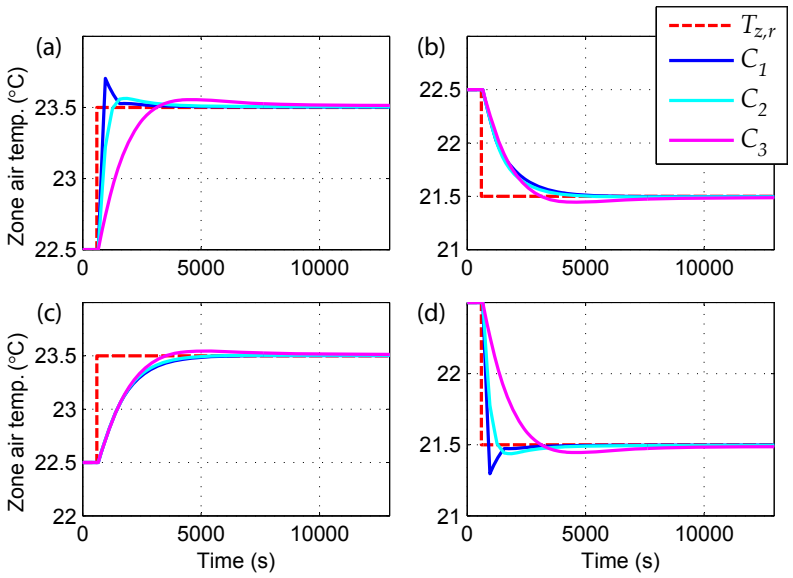

Figure 10.4: Closed-loop step response with different controllers C_n during high load (a,b) and low load (c,d).

and sky temperature at 1 pm July 1 with zone load $d_z = 25$ kW and the low load situation is generated based on conditions at midnight on January 1 and with zone load $d_z = 0$ kW.

$$C_n = K_{p,n} + K_{i,n} t_s \frac{z}{z-1},\ n \in \{1,2,3\}, \tag{10.4}$$

where $K_{p,1} = 25, K_{i,1} = 0.025,$

$K_{p,2} = 15, K_{i,2} = 0.015,$

$K_{p,3} = 5, K_{i,3} = 0.005.$

The step up in reference at high load and the step down at low load determines how fast a controller we can design. In these situations, the controller C_1 is too aggressive, giving a large overshoot in just one time step. Controller C_3 on the other hand is too conservative, whereas C_2 provides a good balance with a maximum overshoot of 6% and a minimum rise time of approximately one time step (300 seconds). This corresponds to Fig. 10.4(a) and 10.4(d). The slowest responses are observed in Fig. 10.4(b) and 10.4(c), where the rise time is between 900-1200 seconds. This confirms that a fixed gain PI control is not ideal under all operating conditions and therefore motivates the development of a learning/repetitive type control for improvement of tracking performance.

4 Learning/Repetitive Control for Improved Reference Tracking

Fig. 10.5 illustrates the proposed addition of RC to the feedback control loop shown in Fig. 10.3. The RC block modifies the original temperature reference $T_{z,r}$ based on the

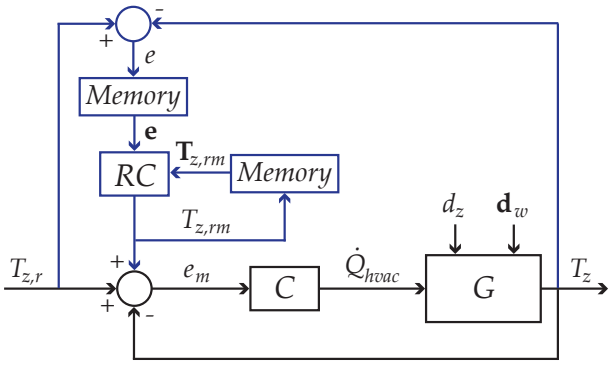

Figure 10.5: Existing feedback loop (black) with additional RC (blue).

tracking error one trial back in time e (one trial is a repetitive cycle, e.g. 24 hours), which will lower e as the number of trials goes to infinity, if the load pattern is repetitive enough.

Collecting past errors e and reference modifiers $T_{z,rm}$ in vectors, $\mathbf{T}_{z,rm} = [T_{z,rm}(k-2N+1), ..., T_{z,rm}(k-2), T_{z,rm}(k-1)]$ and $\mathbf{e} = [e(k-2N+2), ..., e(k-1), e(k)]$, where k is the current time step, and using buffers (memory blocks in Fig. 10.5) of size $2N-1$, where N is the number of discrete samples in one repetitive trial, we can define a repetitive controller as

$$\hat{\mathbf{T}}_{z,rm} = Q(\mathbf{T}_{z,rm} + L\mathbf{e}). \tag{10.5}$$

The vector $\hat{\mathbf{T}}_{z,rm} = [\hat{T}_{z,rm}(1), \hat{T}_{z,rm}(2), ..., \hat{T}_{z,rm}(2N-1)]$ is the output of the learning algorithm and it contains updated reference modifiers. However, we are only interested in $\hat{T}_{z,rm}(N+1)$ since this is the updated version of the reference modifier during the last trial (N samples back in time) to be applied in the next time step $k+1$. Therefore, the reference modifier for the next time step is

$$T_{z,rm}(k+1) = \hat{T}_{z,rm}(N+1). \tag{10.6}$$

The calculations are repeated at each time step and L and Q can be causal/non-causal filters with low-pass, band-pass or high-pass characteristics depending on the frequencies of the repetitive part of the error. Choosing L and Q as filters is also the reason why vectors are used in (10.5).

The proposed RC is similar to a serial structure ILC implementation, with the only difference being that the reference modifier is calculated in real-time at each time step k, whereas in ILC, all reference modifiers are calculated after a trial has ended for the entire subsequent trial. The benefit of RC is that it does not require the same initial condition each trial. For more detail on discrete RC see [7, 16, 17].

In order to determine the cutoff frequencies for the learning filter L we propose to calculate the Repeatable-to-Nonrepeatable Ratio (RNR) for all frequencies. This method is shown in [9] and calculated as

$$RNR = 20log\left(\frac{|FFT[\bar{\mathbf{e}}]|^2}{\frac{1}{N_t}\sum_{j=1}^{N_t}|FFT[\bar{\mathbf{e}} - \mathbf{e}_j]|^2}\right), \tag{10.7}$$

where N_t is the number of trials used in the analysis, FFT is the Fast Fourier Transform, and the repeatable error is

$$\bar{\mathbf{e}} = \frac{1}{N_t} \sum_{j=1}^{N_t} \mathbf{e}_j, \tag{10.8}$$

where $\mathbf{e}_j$ is a vector of all the errors in trial j. Equation (10.7) calculates the power of the repeatable signal versus the power of the nonrepeatable signal and converts it to dB. If this number is larger than 0 dB for a particular frequency it means that there is more repetitiveness in the error than nonrepetitiveness. The learning filter L should then be applied only on these frequencies, which can be achieved by picking appropriate cutoff frequencies for a band-pass filter or an upper cutoff frequency for a low pass filter. The filter Q can then e.g. have cutoff frequency above L in the low-pass case and is there to ensure that the condition for stability is met. Stability can be checked using (10.9) (derivation in [7]), which must be satisfied for all frequencies.

$$\|Q(1 - zLP)\|_\infty < 1 \tag{10.9}$$

The transfer function P is the complementary sensitivity transfer function from reference to output defined as

$$P = \frac{GC}{1 + GC}. \tag{10.10}$$

5 Case Study - One Year Simulation

The previously described single zone office building is used here as a case study, to show the reference tracking performance improvement of RC when applied to a system with nearly periodic load disturbance. The repetitive trial length is identified as one day starting from midnight, where the occupancy load is small.

Fig. 10.6(a) shows the tracking error for each day in January (blue) for the feedback control without RC and the corresponding repeatable error (red), calculated using (10.8), where $N_t = 30$. Furthermore, for comparison, the error for each day in an entire year is also shown (cyan). Based on the tracking error, the RNR is calculated for January and also for an entire year. However, we assume that only data from January was available as training set for the design of the learning filter L. The uncertainty of not having each month in the year will get assigned to the nonrepeatable part of the signal. More data could be used if available.

The RNR in Fig. 10.6(b) indicates that L should be a low-pass filter in this particular case study and the cutoff frequency was set to 0.000223 Hz. The MATLAB command $butter$ was used to design a first order Butterworth low-pass filter and the command $filtfilt$ was then used to make a non-causal zero phase filter. The Q filter was also chosen to be a non-causal zero phase filter with a cutoff frequency of two times 0.000223 Hz. This satisfies the stability condition in (10.9). Additionally, the reference modifier $T_{z,rm}$ was limited between -1 and 1. This means that in worst case, if today does not look like yesterday, we will only end up following a reference of minimum 21.5 or maximum 23.5 degrees, which should still be acceptable for the occupants. Tighter constraints can be used if necessary.

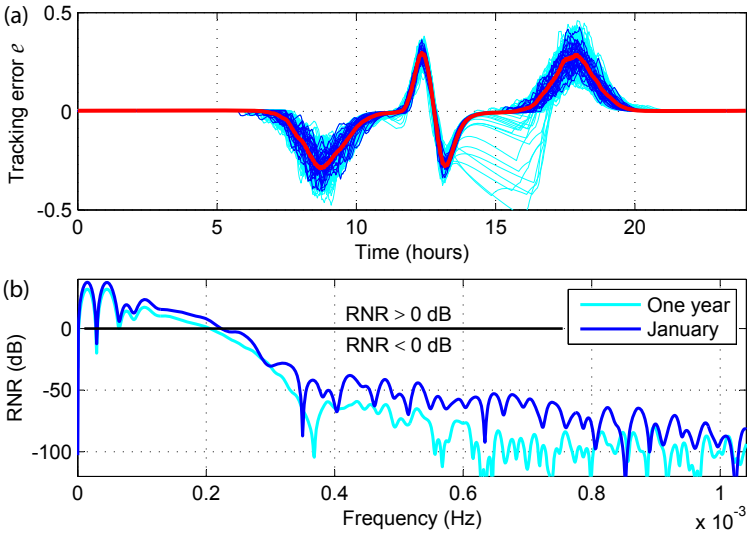

Figure 10.6: The top graph (a) shows the daily tracking error e during January (blue), the repeatable error (red), and the daily error for an entire year (cyan). The bottom graph (b) shows the RNR at different frequencies based on the January errors (blue) and the entire year (cyan).

After the training period, RC can be added to the system. Fig. 10.7 shows the infinity-norm, 2-norm, and 1-norm of the error for each day from the 1st of February to the 31st of December plotted in a histogram. The same simulation is repeated without RC for comparison. All error norms show that RC improves the reference tracking performance. This is also indicated in Fig. 10.8 where the 2-norm is plotted for May, June, and July. However, there are a few days where the RC performs worse (e.g. trial 152). These outliers are caused by hot summer days where the HVAC system is saturated, which is also visible in Fig. 10.6 with larger errors around the hot hours of the day between 1-5pm. If there is saturation one day (e.g. trial 151), the RC will learn a reference that compensates for this effect, but the next day might be colder resulting in worse tracking that following day. However, the control has converged again the day after (trial 153). The outliers, both with and without RC, can potentially be avoided by increasing the systems saturation bounds.

Fig. 10.9 shows the reference signal and the modified reference signal for two consecutive trials, indicating the continuous modifications to the reference signal for the inner PI control, which results in better tracking of the original reference $T_{z,r}$. The modified reference goes down during the morning hours when people arrive for work and increases after they leave in the afternoon. Furthermore, the lunch break causes a modification of the reference starting at around 11 am until 2 pm. This also correlates with the repeatable error shown in Fig. 10.6(a), when RC is not applied.

Fig. 10.10 shows the energy charge in U.S. dollars for each month of the year with and without RC using a time-of-use tariff effective in 2010 from the Arizona Public Service Company [18]. The expected energy consumption was estimated by assuming a

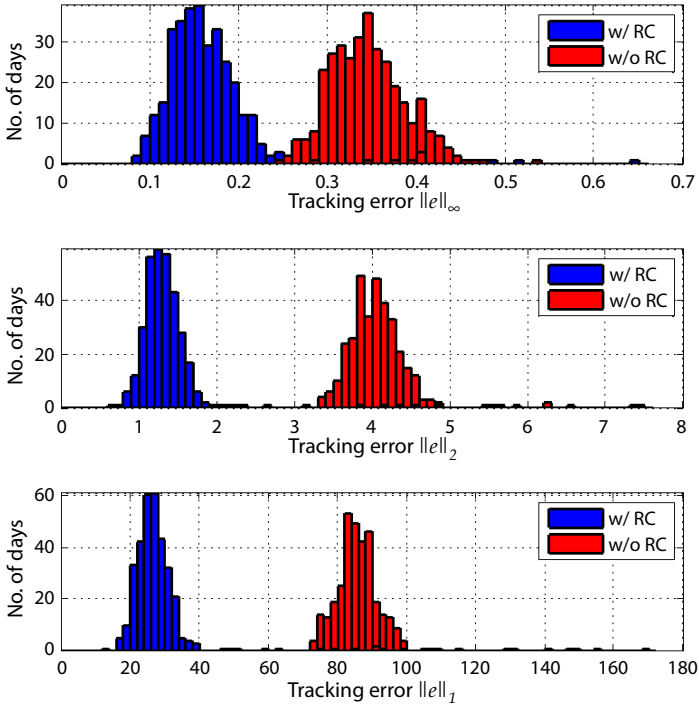

Figure 10.7: Histogram of the ∞-norm, 2-norm, and 1-norm of the error for each day between 1st of Feb. to the 31st of Dec. with and without RC.

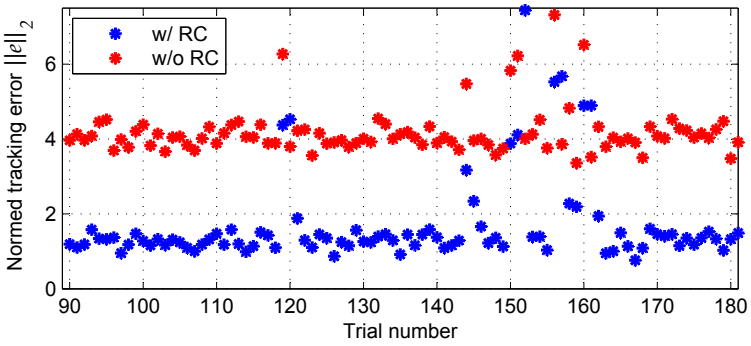

Figure 10.8: 2-normed error for the days (trials) in May, June, and July with and without RC.

constant heating efficiency of 1 and cooling efficiency of 2. The figure shows that there is negligible difference in energy charge with and without RC. Although there may be some uncertainty in the estimation of total consumed power since constant efficiencies are used, the importance is not in estimating the correct bill amount, but rather in comparing the control with and without RC under the same tariff schedule.

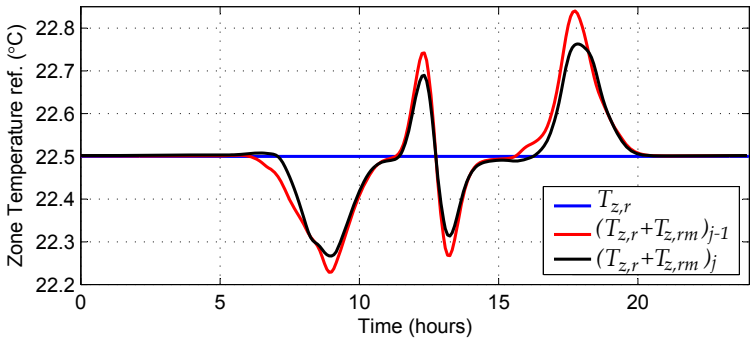

Figure 10.9: Reference signal $T_{z,r}$ and modified reference signal for December 30th (red) and 31st (black) with $j = 334$ indicating the trial number.

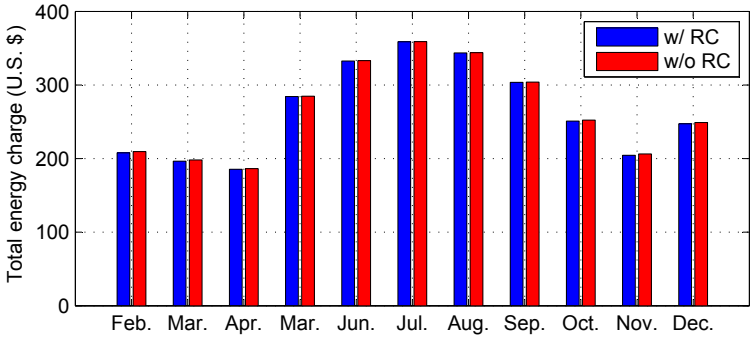

Figure 10.10: Total energy charge each month with and without RC.

Table 10.1 summarizes the results and gives percentage improvements. We can conclude that the reference tracking performance was significantly improved with RC and this performance improvement came at no increase in energy consumption or spending cost. The tracking performance improvement could also be used to change the temperature reference setpoint to a value that requires less energy in terms of cooling or heating, while still staying within tolerable temperature bounds. This could be used in applications

Table 10.1: Summary of case study results for simulation from 1st of February to the 31st of December.

quantity	without RC	with RC	% improvement
$\sum_{j=1}^{334} \|\mathbf{e}_j\|_\infty$	115.28	55.43	51.91
$\sum_{j=1}^{334} \|\mathbf{e}_j\|_2$	1357.70	475.87	64.95
$\sum_{j=1}^{334} \|\mathbf{e}_j\|_1$	29037.42	9584.77	66.99
Total energy (kWh)	50612	50450	0.32
Total cost (U.S. $)	2926.31	2915.54	0.37

where we are mostly concerned with staying below a certain upper temperature bound, e.g. a food processing/storage facility or in a pharmaceutical processing facility. As a result, this could provide significant electricity savings.

6 Conclusion

In this paper, the use of repetitive control is studied in the context of building temperature regulation. Improvements of more than 50% in setpoint tracking performance were achieved with no additional energy consumption, when the proposed RC procedure was applied to an existing feedback controller in a single zone office building simulation. No extra hardware is required and the proposed procedure is to use closed-loop data from an appropriate time window, such as the previous year or month, and use that to calculate the repeatable-to-nonrepeatable ratio of the tracking error for each frequency. This is then used to design a repetitive controller with a learning filter that improves performance at frequencies where the repeatable part of the error is larger than the nonrepeatable part. The single zone case study used as an example is a simplified version of a true system, but detailed enough to give a realistic picture of the potential of learning control in building systems. Furthermore, the lumped parameter resistive-capacitive network modeling framework is applicable on larger buildings as well.

References

[1] C. P. Underwood, *HVAC Control Systems: Modelling, Analysis and Design*. Spon Press, 1999.

[2] J. E. Seem, "A New Pattern Recognition Adaptive Controller with Application to HVAC Systems," *Automatica*, vol. 34, no. 8, pp. 969–982, August 1998.

[3] Q. Bi, W. Cai, Q. Wang, C. Hang, E. Lee, Y. Sun, K. Liu, Y. Zhang, and B. Zou, "Advanced controller auto-tuning and its application in HVAC systems," *Control Engineering Practice*, vol. 8, no. 6, pp. 633–644, June 2000.

[4] D. Lim, B. P. Rasmussen, and D. Swaroop, "Selecting PID Control Gains for Nonlinear HVAC&R Systems," *HVAC&R Research*, vol. 15, no. 6, pp. 991–1019, 2009.

[5] F. Oldewurtel, A. Parisio, C. N. Jones, D. Gyalistras, M. Gwerder, V. Stauch, B. Lehmann, and M. Morari, "Use of model predictive control and weather forecasts for energy efficient building climate control," *Energy and Buildings*, vol. 45, pp. 15–27, February 2012.

[6] D. A. Bristow, M. Tharayil, and A. G. Alleyne, "A survey of iterative learning control," *IEEE Control Systems Magazine*, vol. 26, no. 3, pp. 96–114, June 2006.

[7] R. W. Longman, "Iterative learning control and repetitive control for engineering practice," *International Journal of Control*, vol. 73, no. 10, pp. 930–954, 2000.

[8] Y. Wang, F. Gao, and F. J. Doyle, "Survey on iterative learning control, repetitive control, and run-to-run control," *Journal of Process Control*, vol. 19, no. 10, pp. 1589–1600, December 2009.

[9] B. E. Helfrich, C. Lee, D. A. Bristow, X. H. Xiao, J. Dong, A. G. Alleyne, S. M. Salapaka, and P. M. Ferreira, "Combined H_∞-Feedback and Iterative Learning Control Design with Application to Nanopositioning Systems," in *American Control Conference*, Seattle, Washington, USA, June 2008, pp. 3983–3900.

[10] F. Lorenz and G. Masy, "Méthode d'évaluation de l'économie d'énergie apportée par l'intermittence de chauffage dans les bâtiments," *Traitement par differences finies d'un model a deux constantes de temps, Report No. GM820130-01. Faculte des Sciences Appliquees, University de Liege, Liege, Belgium*, 1982, (in French).

[11] M. Gouda, S. Danaher, and C. Underwood, "Building thermal model reduction using nonlinear constrained optimization," *Building and Environment*, vol. 37, no. 12, pp. 1255–1265, December 2002.

[12] G. Hudson and C. P. Underwood, "A simple building modelling procedure for MATLAB/SIMULINK," in *IBPSA Building Simulation Conference*, Kyoto, Japan, September 1999, pp. 776–783.

[13] National Renewable Energy Laboratory. (2013) Openstudio. http://openstudio.nrel.gov/.

[14] U.S. Department of Energy. (2013) Energyplus energy simulation software. http://apps1.eere.energy.gov/buildings/energyplus/.

[15] H. C. Hottel and A. F. Sarofim, *Radiative transfer*. McGraw-Hill New York, 1967.

[16] M. Tomizuka, T. Tsao, and K. Chew, "Analysis and Synthesis of Discrete-Time Repetitive Controllers," *Journal of Dynamic Systems, Measurement, and Control*, vol. 111, pp. 353–358, September 1989.

[17] C. Kempf, W. Messner, M. Tomizuka, and R. Horowitz, "Comparison of Four Discrete-Time Repetitive Control Algorithms," *IEEE Control Systems*, vol. 13, no. 6, pp. 48–54, December 1993.

[18] APS, "Rate Schedule E-32TOU S - Small General Service (21 kW - 100 kW) - Time of Use," Arizona Public Service Company, Tech. Rep., 2010. [Online]. Available: http://www.aps.com/_files/rates/e-32TOUS.pdf

Paper H

A Learning Based Precool Algorithm for Utilization of Foodstuff as Thermal Energy Storage

Kasper Vinther, Henrik Rasmussen, Roozbeh Izadi-Zamanabadi, Jakob Stoustrup, and Andrew G. Alleyne

This appendix is based on a paper published in:
The Proceedings of the IEEE Multi-conference on Systems and Control (MSC), October 2013

Abstract

Maintaining foodstuff within predefined temperature thresholds is important due to legislative requirements and to sustain high foodstuff quality. This is achieved using a refrigeration system. However, these systems might not be dimensioned for hot summer days or possible component performance degradation. A learning-based algorithm is proposed in this paper, which precools the foodstuff in an anticipatory manner based on the saturation level in the system on recent days. The method is evaluated using a simulation model of a supermarket refrigeration system and simulations show that thermal energy can be stored in foodstuff to cope with saturation in refrigeration equipment. Additional hardware or a system model is not required, making it easy to implement the method in existing systems.

1 Introduction

Cooling equipment is installed in many places to preserve foodstuff/goods and to maintain room temperatures within desired bounds on hot days. Usually foodstuff must be maintained at temperatures determined by legislative requirements and divergence of room temperatures from a setpoint leads to discomfort for occupants. Saturation in the cooling equipment can result in violation of the predefined temperature bounds and can occur if e.g. the installed system is too small to deal with very hot outside temperatures, if a component fails (e.g. a compressor in a compressor rack), if the refrigerant charge in the system changes, or due to component wear leading to degradation of performance.

Sizing up equipment in order to have spare capacity to deal with any thinkable outside temperature and possible component malfunction is costly. Also, more extreme weather due to global warming could make a perfectly sized system inadequate in the future. Finally, higher peak power demand is costly and could require expansion of transmission lines and transformers for large systems such as supermarket refrigeration systems, warehouses, and office buildings. Thermal storage tanks could be installed to overcome this problem and to utilize changes in utility price, which provides the possibility of shifting loads to off peak hours where energy is cheaper and outside temperatures are lower.

In [1–4], to reference a few, building thermal capacity and/or thermal storage tanks are used to store energy for later use. However, adding a thermal storage tank adds an additional capital investment.

Research has also been invested in precooling of foodstuff and the use of foodstuff as thermal storage. Load shifting strategies are investigated for four different low temperature warehouses in [5], where the authors show significant cost savings, possible due to the relatively large thermal capacity of these buildings and the large quantity of foodstuff. The use of Model Predictive Control (MPC) for precooling of foodstuff in supermarkets is investigated in [6] and [7]. They showed the potential of storing energy in the individual display cases in order to cope with high loads on hot summer days, but also to provide ancillary services to the Smart Grid. Furthermore, [6] and [8] have looked at food quality loss as a function of temperature and the thermal storage potential of different foodstuffs.

All references, known to the authors, either use a MPC approach, due to its ability to handle constraints, or just a predefined schedule. However, deriving a suitable model and parameters for prediction purposes can be cumbersome and costly, especially since each refrigeration system is often composed of different components and has different sizes.

As with the heuristically chosen schedule, a model-based MPC approach is often tailored to a specific system and lack modularity, flexibility, and robustness towards changes. These changes can be large changes in operating conditions, changes in load patterns, changes in system parameters due to e.g. component wear or reduction in refrigerant charge, and faulty components. Furthermore, the amount and type of foodstuff changes the storage capacity for each individual display case and could change during the year.

Instead, we have investigated the possibility of using a learning-based control method to precool, with the objective of reducing the risk of having to discard refrigerated foodstuff on hot days due to system saturation, which can be very costly. A certain amount of precooling might even be favorable cost-wise when the system is not saturated, because energy consumption can be shifted to a time with lower outdoor temperature and energy price. However, there will also be a higher heat loss from the precooled foodstuff and the general practice today is not to precool. This paper therefore only considers avoiding system saturation.

Iterative Learning Control (ILC) and Repetitive Control (RC) are two examples of learning-based control, see e.g. [9–11] for more details. These methods are often used in batch processes where the same task is repeated, which makes it possible to learn a performance improving feedforward signal or a reference modifying signal for the next repetition of the same task referred to as a trial (see parallel and serial ILC in [10]). The relation to refrigeration systems is that there is a certain amount of repeatability on a daily basis, e.g. a good estimate of the weather tomorrow is the weather today and the load from customers in a supermarket or occupants in an office will also be similar. The repeatability can be checked by calculating the repeatable-to-nonrepeatable ratio for different frequencies as done in e.g. [12, 13]. However, this is not included in this paper.

Changing the reference signal to force the refrigeration system to precool when the system is already saturated does not help. An optimization based constrained ILC is proposed in [14] to handle constrained linear systems. However, this method does not try to reduce the saturation by precooling, it only ensured that the ILC converges. In this paper we propose a precool algorithm inspired by ILC, which learns how much precool is needed and when it is needed based on previous experience and does not require extra hardware or system model knowledge as MPC. The method is tested on a realistic simulation model of a supermarket refrigeration system, where it is possible to change the air temperature thresholds for the display cases controlled by on/off relay feedback on the refrigerant inlet valve. In other words, precooling is performed by lowering the temperature thresholds for a while. This also ensures that we will never precool the foodstuff to a temperature lower than what we allow.

The paper is organized in the following way. Section 2 describes the learning-based precool algorithm and provides a simple simulation example. A simulation model of a supermarket refrigeration system is then presented in Section 3. Automatic tuning procedures for refrigeration systems are then provided in Section 4 followed by simulation results without precooling, with constant precooling and with the proposed precool algorithm in Section 5. Finally, conclusions are drawn in Section 6.

2 Learning-Based Precool Algorithm

We have a system controlled with the relay feedback

$$u(k) = \begin{cases} \overline{u} & \text{if } y(k) > \overline{y}(k) \\ \underline{u} & \text{if } y(k) < \underline{y}(k) \\ u(k-1) & \text{otherwise,} \end{cases} \tag{11.1}$$

where $u(k)$ is the control input at time k in the discrete time-domain taking the value $\overline{u}$ if the system output $y(k)$ reaches an upper threshold $\overline{y}(k)$ and $\underline{u}$ if the output reaches a lower threshold $\underline{y}(k)$. This is a very simple controller and also a widely used method of maintaining the temperature of a medium within predefined bounds.

We will in the following assume that both thresholds can be modified by a learning controller, which at the end of each trial updates a vector of threshold modifying values to be used in the next trial allowing us to precool if necessary. The threshold vectors are given as

$$\overline{\mathbf{y}}_j = \overline{\mathbf{y}}_0 + \overline{\mathbf{y}}_{m,j} \tag{11.2}$$

$$\underline{\mathbf{y}}_j = \underline{\mathbf{y}}_0 + \underline{\mathbf{y}}_{m,j}, \tag{11.3}$$

where $\overline{\mathbf{y}}_0$ and $\underline{\mathbf{y}}_0$ are the initial time-invariant thresholds and $\overline{\mathbf{y}}_{m,j}$ and $\underline{\mathbf{y}}_{m,j}$ are the threshold modifying vectors for the trial denoted by j. The modifiers are generated based on the length of the current precool period Δ_j and the specified end-time for the precool period t_{end}. For simplicity it is assumed that each $y_m(k)$ can only take the value 0 (do not precool) or α (precool) and that the end-time t_{end} is chosen manually. An automatic way of determining t_{end} for each trial is proposed later in Section 4. The controlled system in the trial domain is shown in Fig. 11.1.

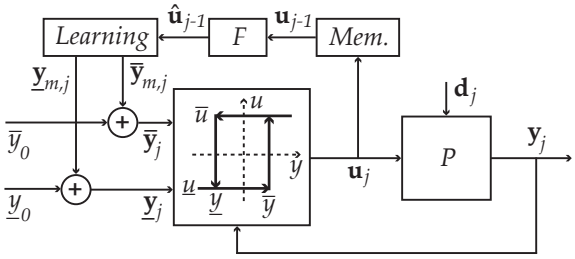

Figure 11.1: Trial domain representation of a relay feedback controlled system P with learning-based adaptation of the thresholds.

The length of the precool period at trial j is determined based on an ILC inspired learning algorithm given as

$$\Delta_j = \Delta_{j-1} + \delta_{j-1}, \tag{11.4}$$

where Δ_{j-1} is the length of the previous precool period and δ_{j-1} is the update. This update is determined by

$$\delta_{j-1} = \begin{cases} l_1\overline{\Delta} & \text{if } ||\hat{\mathbf{u}}_{j-1}||_\infty \geq \overline{\hat{u}} \\ l_2\overline{\Delta} & \text{otherwise,} \end{cases} \tag{11.5}$$

where $\hat{\mathbf{u}}_{j-1}$ is the estimated capacity of the control input (or duty cycle) during the previous trial $j-1$ and $\overline{\hat{u}}$ is a threshold that indicates if precooling is needed or not. l_1 and l_2 are the learning and de-learning gains, respectively. A gain $l_1 < 1$ means that the full precool period $\overline{\Delta}$ (maximum allowed precool time) is not reached in one trial and low values gives slower convergence.

The estimated capacity $\hat{\mathbf{u}}_{j-1}$ can be calculated by filtering the control input;

$$\hat{\mathbf{u}}_{j-1} = F\mathbf{u}_{j-1}, \tag{11.6}$$

where F can be a zero phase low pass filter that provides a mean value or duty cycle of the on/off based input vector $\mathbf{u}_{j-1}$ during the previous trial.

If the system output settles between the new modified thresholds within the precool period, then it does not make sense to extend the precool period anymore, as it will only increase the power consumption. The precool period is therefore limited by a predefined maximum length $\overline{\Delta}$;

$$\Delta_j = \begin{cases} \overline{\Delta} & \text{if } \Delta_j > \overline{\Delta} \\ 0 & \text{if } \Delta_j < 0 \\ \Delta_j & \text{otherwise.} \end{cases} \tag{11.7}$$

The maximum length should depend on the storage potential of the system and is therefore further treated in Section 4.

In the serial ILC the error in the previous trial is used to update the reference. The proposed precool algorithm instead uses the saturation level of the input to determine how long to precool the system and consequently how much energy to store in the system before the saturation.

Simple Thermal Storage Example

The learning-based precool algorithm is demonstrated using a simple thermal storage example. Assume that the temperature T_{goods} of a lumped mass of foodstuff has to be controlled indirectly by controlling the heat transfer rate $\dot{Q}_e$ out of an air volume surrounding the foodstuff. $\dot{Q}_e$ is controlled with relay feedback between $\underline{\dot{Q}_e}$ if the air temperature $T_{dc} < 2^{\circ}C$ and $\overline{\dot{Q}_e}$ if $T_{dc} > 5^{\circ}C$. The load on the system $\dot{Q}_{air,i-dc}$ is a square signal which repeats itself on a daily basis and has a maximum value above $\overline{\dot{Q}_e}$. This means that the system goes into saturation and the temperature of the foodstuff will go above $5^{\circ}C$ if energy in the form of coldness is not stored in the foodstuff before the saturation occurs.

The system is illustrated in Fig. 11.2. The governing differential equations for the temperature of the goods T_{goods} and the air T_{dc} are

$$\frac{dT_{goods}}{dt} = \frac{\dot{Q}_{dc-goods}}{m_{goods}C_{p,goods}}, \tag{11.8}$$

$$\frac{dT_{dc}}{dt} = \frac{\dot{Q}_{air,i-dc} - \dot{Q}_{dc-goods} - \dot{Q}_e}{m_{dc}C_{p,dc}}, \tag{11.9}$$

$$\dot{Q}_{dc-goods} = UA_{dc-goods}(T_{dc} - T_{goods}) \tag{11.10}$$

where $UA_{dc-goods}$ is the overall heat transfer coefficient between the air and the goods, m_{dc} is the mass of the air, m_{goods} is the mass of goods, $C_{p,dc}$ is the specific heat of the

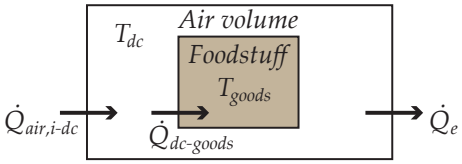

Figure 11.2: Example system with goods surrounded by an air volume. The controllable input to the system is the heat transfer rate out of the system $\dot{Q}_e$ and the disturbance load is the heat transfer rate into the system $\dot{Q}_{air,i-dc}$.

air, and $C_{p,goods}$ is the specific heat of the goods. These equations can be formulated in state space as

$$\begin{bmatrix} \dot{T}_{dc} \\ \dot{T}_{goods} \end{bmatrix} = \begin{bmatrix} \frac{-UA_{dc-goods}}{m_{dc}C_{p,dc}} & \frac{UA_{dc-goods}}{m_{dc}C_{p,dc}} \\ \frac{UA_{dc-goods}}{m_{goods}C_{p,goods}} & \frac{-UA_{dc-goods}}{m_{goods}C_{p,goods}} \end{bmatrix} \begin{bmatrix} T_{dc} \\ T_{goods} \end{bmatrix} + \begin{bmatrix} \frac{-1}{m_{dc}C_{p,dc}} \\ 0 \end{bmatrix} \dot{Q}_e + \begin{bmatrix} \frac{1}{m_{dc}C_{p,dc}} \\ 0 \end{bmatrix} \dot{Q}_{air,i-dc}. \tag{11.11}$$

For simplicity the load $\dot{Q}_{air,i-dc}$ is assumed to be state independent. However, in a more elaborate model it should be a function of the temperature difference between the ambient and the air. Table 11.1 shows the system and control parameters used in the simulation. The filter F is implemented as a zero phase Butterworth low pass filter with the Matlab commands `butter` and `filtfilt` and a cutoff frequency $\omega_F = 8.7e^{-4}\ rads^{-1}$. This gives an estimate of the required cooling $\hat{\dot{Q}}_e$ and the precool period is increased when $\hat{\dot{Q}}_e > 0.99\overline{\dot{Q}}_e$ and decreased otherwise.

Table 11.1: Parameter values used in thermal storage example.

System par.	Value	Ctrl par.	Value
$UA_{dc-goods}$	300 ($\frac{W}{K}$)	$\overline{\Delta}$	4 ($hours$)
m_{dc}	50 (kg)	l_1	$\frac{1}{4}$ (-)
$C_{p,dc}$	1 ($\frac{kJ}{kgK}$)	l_2	$-\frac{1}{12}$ (-)
m_{goods}	500 (kg)	ω_F	$8.7e^{-4}$ ($\frac{rad}{s}$)
$C_{p,goods}$	4 ($\frac{kJ}{kgK}$)	$\overline{\hat{\dot{Q}}}_e$	$0.99\overline{\dot{Q}}_e$ (W)
$\overline{\dot{Q}}_e$	2850 (W)	t_{end}	9 ($hours$)
$\underline{\dot{Q}}_e$	0 (W)	$\overline{y}_m$	-3 ($^\circ C$)
		$\underline{y}_m$	-2 ($^\circ C$)

Fig. 11.3 shows the simulation results with a max load of 3000 W. Without precooling the temperature increases to $6.6^\circ C$ because of the saturation kicking in at 9 in the morning every day. With precooling the maximum temperature is lowered to $4.5^\circ C$ after four days, which is the time it takes to reach the maximum allowed precool period with the chosen learning gain l_1.

Fig. 11.4 shows the simulation results with a max load of 2800 W. The algorithm

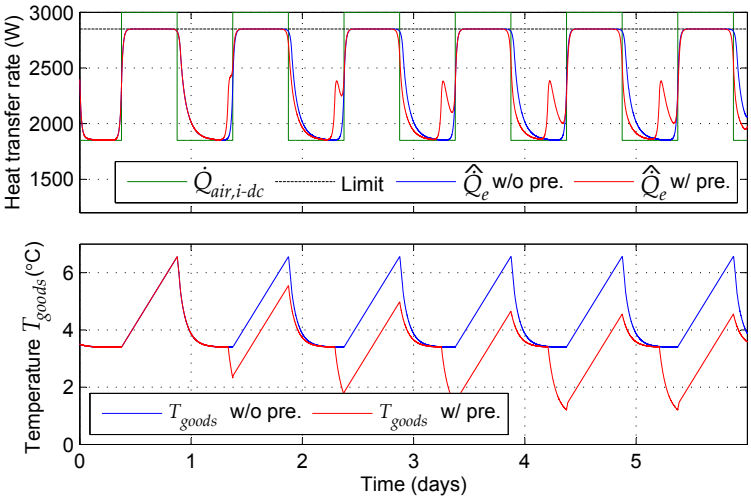

Figure 11.3: Heat transfer rates and goods temperature with and without precool algorithm applied. Limit is the upper bound on the controllable input.

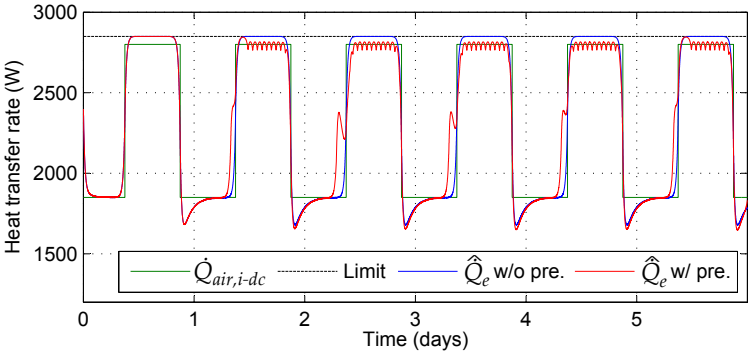

Figure 11.4: Heat transfer rates with precool algorithm applied. Cool limit is the upper bound on the controllable input.

shifts between $\Delta = \{0, 60, 120, \ \ 100, 80, 60, 120, 100, 80, 60, ...\}$ minutes of precool time in this second simulation with smaller saturation. The precool time that eliminates saturation in the simulation is approximately 70 minutes.

Convergence of Δ in the Trial Domain

Fig. 11.4 showed that the precool algorithm will cycle between levels of precool time. These levels are determined by l_1 and l_2. If we decrease the learning and de-learning rates then the jump between levels will be smaller, but we will also converge slower. Let the repeatability between trials be perfect and Δ^* be the smallest possible precool time that avoids saturation, i.e. $\Delta^* = \inf\left\{\Delta : ||\hat{\mathbf{u}}||_\infty < \overline{\hat{u}}\right\}$, then the precool time Δ_j at trial

j will converge to the interval

$$\Delta^* + l_2\overline{\Delta} < \Delta_j \leq \Delta^* + l_1\overline{\Delta}, \tag{11.12}$$

when $\Delta^* + l_2\overline{\Delta} \geq 0$ and $\Delta^* + l_1\overline{\Delta} \leq \overline{\Delta}$. If $\Delta^* \leq 0$ then $\Delta_j \to 0$ (no precooling) and if $\Delta^* > \overline{\Delta}$ then $\Delta_j \to \overline{\Delta}$ (max precooling). Furthermore, increasing l_1 and decreasing l_2 numerically improves robustness towards hot days. On the other hand, decreasing l_1 and increasing l_2 optimizes the cost of running the system (assuming that no precool is cheapest).

3 Supermarket Refrigeration System Model and Control

A supermarket refrigeration system model with control is presented in this section and illustrated in Fig. 11.5. The purpose of this model is to provide a realistic simulation to be able to evaluate the performance of the precool algorithm and compare it with other control strategies under the same conditions, which would not be possible on a real system. The first version of the model was derived in [15] and has been slightly modified in [16–18]. The model presented in this paper is again a slightly modified version that also takes into account the effect of changes in outside air temperature and corresponding condenser pressure, which can saturate the system on hot days due to higher required com-

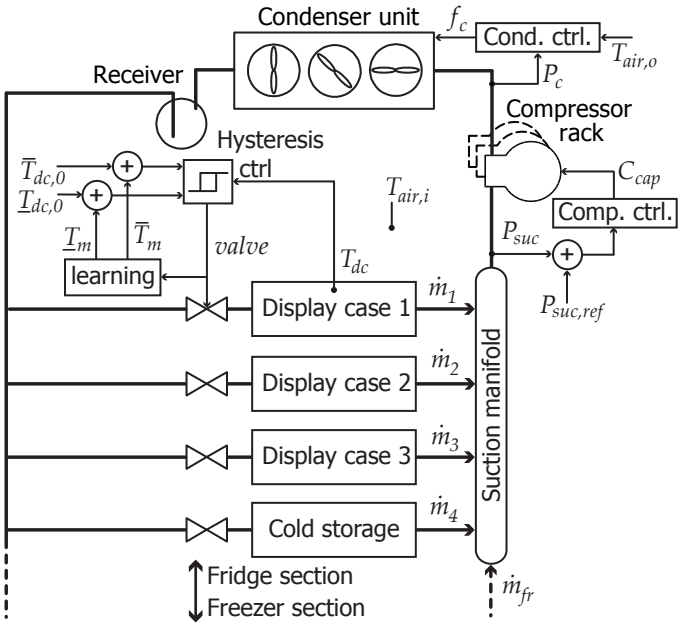

Figure 11.5: Supermarket refrigeration system with multiple fridge display cases, a cold storage room, and additional mass flow from freezers $\dot{m}_{fr}$. The compressor rack controls the suction pressure P_{suc}, the condenser fan controls the condenser pressure P_c, and finally the temperature of the display cases are controlled with hysteresis control and learning-based adaptation of the thresholds.

pressor work. The model is implemented in Matlab Simulink® and available for download at `www.es.aau.dk/projects/refrigeration/simulation-tools`.

Simplified Supermarket Refrigeration System model with Display Cases

The display cases are assumed to be of the open shelf type with night covers as shown in Fig. 11.6. A lumped temperature model is used and the constant circulation of air provides the heat transfer rates between the air and the evaporator wall $\dot{Q}_{dc-wall}$ and the air and the goods $\dot{Q}_{dc-goods}$. Furthermore, heat is transferred between the evaporator wall and the refrigerant $\dot{Q}_e$ and between the ambient air and the air inside the display case $\dot{Q}_{air,i-dc}$. Heat transfer from infiltration of air is assumed to be included in $\dot{Q}_{air,i-dc}$ by choosing a higher overall heat transfer coefficient.

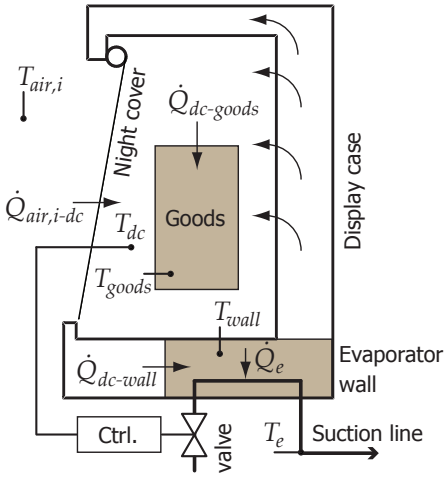

Figure 11.6: Model of an open shelf type display case with night cover.

The differential equations for the temperatures are

$$\frac{dT_{goods}}{dt} = \frac{\dot{Q}_{dc-goods}}{m_{goods}C_{p,goods}}, \tag{11.13}$$

$$\frac{dT_{wall}}{dt} = \frac{\dot{Q}_{dc-wall} - \dot{Q}_e}{m_{wall}C_{p,wall}}, \tag{11.14}$$

$$\frac{dT_{dc}}{dt} = \frac{\dot{Q}_{air,i-dc} - \dot{Q}_{dc-goods} - \dot{Q}_{dc-wall}}{m_{dc}C_{p,dc}}, \tag{11.15}$$

where m and C_p denotes mass and specific heat capacity, respectively. The heat transfer rates are

$$\dot{Q}_{dc-goods} = UA_{dc-goods}(T_{dc} - T_{goods}), \tag{11.16}$$

$$\dot{Q}_{dc-wall} = UA_{dc-wall}(T_{dc} - T_{wall}), \tag{11.17}$$

$$\dot{Q}_e = UA_{wall-re}(T_{wall} - T_e), \tag{11.18}$$

$$\dot{Q}_{air,i-dc} = UA_{air,i-dc}(T_{air,i} - T_{dc}). \tag{11.19}$$

The heat transfer coefficient between the wall and the refrigerant $UA_{wall-re}$ is a function of the amount of liquid refrigerant in the evaporator m_{re} given as

$$UA_{wall-re} = \overline{UA}_{wall-re} \frac{m_{re}}{\overline{m}_{re}}. \tag{11.20}$$

where $\overline{UA}_{wall-re}$ is the maximum value of the heat transfer coefficient when the evaporator is fully filled (it is assumed that the superheat is controlled separately and maintained at an average value of $T_{sh} = 10K$) and $\overline{m}_{re}$ is the maximum mass of the liquid refrigerant. The rate of change of the mass of the refrigerant m_{re} is

$$\frac{dm_{re}}{dt} = \begin{cases} \frac{\overline{m}_{re} - m_{re}}{\tau_{fill}} & \text{if } valve = 1, \\ -\frac{\dot{Q}_e}{\Delta h_{lg}} & \text{if } valve = 0 \text{ and } m_{re} > 0, \\ 0 & \text{otherwise.} \end{cases} \tag{11.21}$$

where Δh_{lg} is the specific latent heat of the remaining refrigerant, τ_{fill} is the time it takes to fill the evaporator from empty, and $valve$ is the control signal to the valve (either on or off).

The flow of refrigerant out of the evaporator of display case i into the suction manifold is approximated by

$$\dot{m}_i = \frac{\dot{Q}_e}{\Delta h_{lg}}. \tag{11.22}$$

Since the suction pressure P_{suc} should be a state in the model to enable suction pressure control, we define the time derivative of the suction pressure as

$$\frac{dP_{suc}}{dt} = \frac{\sum_{i=1}^{n} \dot{m}_i + \dot{m}_{fr} - \dot{V}_{cp} \rho_{suc}}{V_{suc} \frac{d\rho_{suc}}{dP_{suc}}}, \tag{11.23}$$

where $\dot{m}_{fr}$ is additional unmodeled mass flow from freezers, $\dot{V}_{cp}$ is the volume flow out of the suction manifold due to the compressor work, V_{suc} is the volume of the manifold, and ρ_{suc} is the density in the manifold.

The compressor power $\dot{W}_{cp}$ is approximated by

$$\dot{W}_{cp} = \frac{C_{cap}}{100} \overline{\dot{W}}_{cp} = \frac{\dot{V}_{cp} \rho_{suc} \left(h_{is} - h_{e,o}\right)}{\eta} \tag{11.24}$$

where C_{cap} is the requested capacity in %, $\overline{\dot{W}}_{cp}$ is the power consumed when the compressor runs at maximum capacity, h_{is} is the specific enthalpy out of the compressor with isentropic efficiency, $h_{e,o}$ is the specific enthalpy out of the evaporator, and η is the efficiency from an isentropic process to the electrical power consumed by the compressor.

In order to solve the above equations a set of refrigerant specific relations are needed. They can be computed using e.g. the software RefEqns [19]. However, (11.25)-(11.29) are polynomial and regression fits to the tables provided in RefEqns for the refrigerant R404A (all-round refrigerant good for both fridge and freezer) and the toolbox is therefore

not needed.

$$\begin{aligned}
\rho_{suc} =& 4.669 P_{suc} + 0.3672, && (11.25)\\
\frac{d\rho_{suc}}{dP_{suc}} =& 4.669, && (11.26)\\
h_{is} =& (3.6436 - 0.00968 P_{suc} + 0.0343 P_c \\
& - 0.0000495 P_{suc} P_c + 0.000373 P_{suc}^2 \\
& - 0.000629 P_c^2) 10^5, && (11.27)\\
h_{e,o} =& (0.000332 P_{suc}^3 - 0.00853 P_{suc}^2 + 0.0953 P_{suc} \\
& + 3.3467) 10^5 + \Delta h_{T_{sh}}, && (11.28)\\
\Delta h_{T_{sh}} =& 9 \ (T_{sh} = 10K \text{ assumption}), \\
P_c =& 0.00307 T_c^2 + 0.1839 T_c + 6.0826, && (11.29)\\
T_c =& T_{air,o} + 5.
\end{aligned}$$

The condenser unit and the condenser control dynamics are assumed stable and fast compared to the rest. They are therefore approximated by the static relation given in (11.29), where the condensation pressure P_c is held at a reference corresponding to a temperature T_c which is $5°C$ above the outside air temperature $T_{air,o}$.

On/Off Hysteresis Based Temperature Control of Refrigerated Display Cases

The temperature in each display case is controlled with an on/off valve and the relay feedback control is given as

$$valve(k) = \begin{cases} 1 & \text{if } T_{dc}(k) > \overline{T}_{dc}, \\ 0 & \text{if } T_{dc}(k) < \underline{T}_{dc}, \\ valve(k-1) & \text{otherwise,} \end{cases} \qquad (11.30)$$

where $\overline{T}_{dc}$ and $\underline{T}_{dc}$ are the upper and lower thresholds for the temperature of the air in the display case.

Compressor Rack Control

The suction pressure typically track a reference pressure $P_{suc,ref}$ with a PI controller on the compressor rack. The control equations with anti-windup and dead-band DB are

provided in (11.31)-(11.36) (see also [16]).

$$e(k) = P_{suc,ref} - P_{suc}(k), \tag{11.31}$$

$$e_{DB}(k) = \begin{cases} e(k) & \text{if } |e(k)| > DB, \\ 0 & \text{otherwise,} \end{cases} \tag{11.32}$$

$$I(k) = I(k-1) + \frac{K_{p,cp} t_s}{\tau_{i,cp}} e_{DB}(k) + w(k), \tag{11.33}$$

$$C_{cap}(k) = K_{p,cp} e_{DB}(k) + I(k), \tag{11.34}$$

$$C_{cap,s}(k) = \begin{cases} \overline{C}_{cap} & \text{if } C_{cap}(k) > \overline{C}_{cap}, \\ \underline{C}_{cap} & \text{if } C_{cap}(k) < \underline{C}_{cap}, \\ C_{cap}(k) & \text{otherwise,} \end{cases} \tag{11.35}$$

$$w(k+1) = \frac{t_s}{\tau_{i,cp}} (C_{cap,s}(k) - C_{cap}(k)). \tag{11.36}$$

Weather Data

A yearlong weather data file for Phoenix, Arizona with 1 minute samples is used to simulate real outdoor temperatures. Fig. 11.7 shows the seasonal change in temperature.

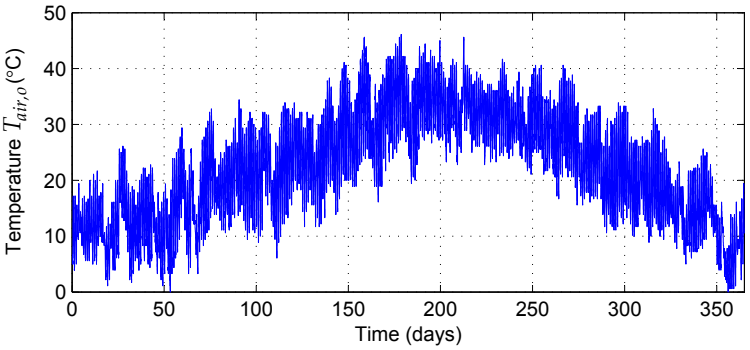

Figure 11.7: Outdoor air temperature $T_{air,o}$ from 1st of January to 31st of December in Phoenix Arizona based on typical meteorological year (TMY) 2 weather data.

Foodstuff Storage Potential Considerations

Refrigerated foodstuff has different thermal storage potential mainly determined by the overall heat transfer coefficient, total surface area, mass, and specific heat capacity of the product. Another important quantity is the Biot number, which indicates if a lumped or nonlumped temperature analysis is appropriate. The Biot number B is the ratio of internal temperature difference required to move energy within a product to temperature difference required at the surface to add or remove the same energy given as [20]

$$B = \frac{U \frac{V}{A}}{k}, \tag{11.37}$$

where U is the surface heat transfer coefficient, V is the volume, A is the surface area exposed to convective heat transfer, and k is the products thermal conductivity. A small number (< 0.1) means that the temperature will not vary significantly in space inside the body [20]. However, a nonlumped analysis would be more appropriate if it is large.

Biot numbers for different foodstuffs are provided based on experiments in [8]. Even though they in general are above 0.1, a lumped analysis is often performed, because it does not require solving complex multidimensional partial differential equations. The lumped approach is also taken here. However, it is possible to activate the entire mass of the foodstuff during precooling and the system also gradually becomes more saturated, due to increasing outside temperature, which means that the average air temperature in the display case only changes slowly over several hours.

Due to the night cover in open shelf type display cases there will be a large increase in the overall heat transfer coefficient between the ambient air and the air inside the display case during the opening hours of the supermarket. This is also when there is customer activity and it gives a high increase in heat load and will be modeled in the simulations conducted in Section 5. Furthermore, in order to evaluate the thermal storage potential of different foodstuffs, different combinations of mass times specific heat mC_p and overall heat transfer coefficient times surface area UA are used in the simulated display cases. These parameters determine the main time constant for the foodstuff temperature and a step in air temperature is made from $3.5°C$ to $1°C$ using (11.13) to determine how long it takes to precool the foodstuff from the initial value to 90% of the step size. The time is 166 min for Display Case 1, 250 min for Display Case 2, 500 min for Display Case 3, and 300 min for the cold storage room.

4 Precool Algorithm Tuning Guideline for Refrigeration Systems

Learning gains l_1 and l_2: These are tuning parameters with a value between 0 and 1 (-1 for l_2) and they are also discussed in Subsection 2. The choice should be relative to how changeable the weather is expected to be. The safest option is $l_1 = 1$ and l_2 small. However, this will also result in more precooling than necessary. Simulations have shown that $l_1 = \frac{1}{4}$ and $l_2 = -\frac{1}{12}$ are suitable with the representative weather data presented in Subsection 3.

Filter parameters ω_F and $\overline{\widehat{valve}}$: The low pass filter that converts the on/off signal to the valve to a duty cycle (utilized capacity) will depend on the switching times. The switching period usually lie somewhere between 5-15 minutes for display cases and the cutoff frequency $\omega_F = 8.7e^{-4}\ \frac{rad}{s}$ is chosen, which correspond to a frequency period of about two hours. The threshold duty cycle $\overline{\widehat{valve}}$ is set to 0.99, which means that if the utilized capacity of the display case reaches 99% of maximum we will start to precool.

Max precool time $\overline{\Delta}$: This value is individual for each display case and should correspond to the time it takes to cool the foodstuff from an initial temperature using normal temperature thresholds to the steady state temperature using precool thresholds, see Subsection 3. It can either be chosen based on experience or experiments. In cases where the foodstuff temperature is not measured, a step down in the air temperature thresholds can reveal the time constant of the foodstuff. This can be achieved by monitoring how long it takes the valve duty cycle to settle again after the step, which happens when the foodstuff temperature has settled (longer precool will not store any additional thermal energy). The

experiment could potentially be performed automatically during the night or once just after the controller is installed.

Precool end-time t_{end}: This could be set manually based on supermarket opening hours, energy tariff, experience, etc. It can also be set and updated automatically based on the estimated duty cycle output from the filter F, which indicates when the system went into saturation on the previous day. The precooling should take place before this saturation. In the simulation results presented in Section 5, t_{end} is determined as the time when the longest saturation period started the day before. The low thresholds in the precool period are also extended beyond t_{end} to include the saturation period. This ensures that the stored thermal energy is not lost immediately but kept for as long as possible.

5 Simulation Results

Table 11.2 shows the parameter values used in the simulation. The compressor size is dimensioned so that the foodstuff temperature stays below $5°C$ the whole year with the

Table 11.2: Parameter values used in supermarket system simulation. Subscript $1-3$ denotes display cases and cs is cold storage.

System par.	Value	Ctrl par.	Value
$UA_{air,i-dc,l}$	75 ($\frac{W}{K}$)	$\overline{\Delta}_1$	166+60 (min)
$UA_{air,i-dc,h}$	150 ($\frac{W}{K}$)	$\overline{\Delta}_2$	250+60 (min)
$UA_{air,i-dc,cs}$	110 ($\frac{W}{K}$)	$\overline{\Delta}_3$	500+60 (min)
$UA_{dc-goods,1}$	450 ($\frac{W}{K}$)	$\overline{\Delta}_{cs}$	300+60 (min)
$UA_{dc-goods,2}$	300 ($\frac{W}{K}$)	ω_F	$8.7e^{-4}$ ($\frac{rad}{s}$)
$UA_{dc-goods,3}$	150 ($\frac{W}{K}$)	$\overline{\widehat{valve}}$	0.99 ($-$)
$UA_{dc-goods,cs}$	600 ($\frac{W}{K}$)	l_1	$\frac{1}{4}$ ($-$)
$UA_{dc-wall}$	500 ($\frac{W}{K}$)	l_2	$-\frac{1}{12}$ ($-$)
$\overline{UA}_{wall-re}$	900 ($\frac{W}{K}$)	$\overline{T}_m$	-3 ($°C$)
$C_{p,goods}$	3917 ($\frac{J}{kgK}$)	$\underline{T}_m$	-2 ($°C$)
$C_{p,dc}$	1000 ($\frac{J}{kgK}$)	$\overline{T}_{dc,0}$	5 ($°C$)
$C_{p,wall}$	385 ($\frac{J}{kgK}$)	$\underline{T}_{dc,0}$	2 ($°C$)
m_{wall}	180 (kg)	$P_{suc,ref,l}$	4.4 (bar)
$m_{dc,1-3}$	50 (kg)	$P_{suc,ref,h}$	4.1 (bar)
$m_{dc,cs}$	125 (kg)	DB	0.1 (bar)
$\overline{m}_{re}$	0.6 (kg)	K_p	-10 ($-$)
$m_{goods,1-3}$	500 (kg)	T_i	220 (s)
$m_{goods,cs}$	1200 (kg)	$t_{s,cp}$	60 (s)
τ_{fill}	40 (s)	$t_{s,ilc}$	5 (s)
$T_{air,i}$	22 ($°C$)		
$\overline{\eta}$	0.5 ($-$)		
$\overline{\dot{W}}_{cp}$	7985 (W)		
$\dot{m}_{fr}$	0.05 ($\frac{kg}{s}$)		

representative weather data, if the thresholds are constantly kept on low settings. No precool would result in some days where the foodstuff goes above $5°C$, which is used as a benchmark and precooling all the time is expensive energy wise. The precool algorithm is therefore compared with these two extremes in terms of energy consumption and temperature. The heat transfer coefficient $UA_{air,i-dc,l}$ is used for the display cases when the night cover is on when the supermarket is closed and $UA_{air,i-dc,h}$ is used when the night cover is off in the opening hours from 9 am to 9 pm. A variation with a factor of two is used and this also includes the extra load due to exchange of foodstuff during the day. Zero mean Gaussian noise is also added to the simulation. The standard deviation for the noise added to $UA_{air,i-dc,l}$, $UA_{air,i-dc,h}$, and $UA_{air,i-dc,cs}$ during the opening hours is 5 and 1 during closed hours. Noise is also added to the mass flow from freezers $\dot{m}_{fr}$ with a standard deviation of 0.0032. It is assumed that the supermarket is open the same hours all week and all year and that the customer load is even during the day. Individual learning controllers could be activated for each day or maybe for weekdays and weekends, if some days look different. Finally, note that one hour is added to $\overline{\Delta}$ to account for uncertainties and the sample time for the precool algorithm $t_{s,ilc}$ is set to 5 seconds.

Fig. 11.8 shows the simulation result with and without precool algorithm activated for four days during the summer period out of the 365 day long simulation. The compresser capacity C_{cap} saturates during the supermarket opening hours. This results in an increase in the suction pressure, which gets worse as the outside temperature increases. The valve duty cycle also saturates and the air and foodstuff temperature goes up. The foodstuff temperature goes beyond $5°C$ during day 177 and 178, if precooling is not performed.

Fig. 11.9 shows the precool time for each day during the simulation with the precool algorithm. Precool is mostly activated during the hot summer period as expected and goes to $\overline{\Delta}$ for each of the storages. By defining the accumulated errors in temperature constraint satisfaction γ_{con} as

$$\gamma_{con} = \sum_{i=1}^{n} \epsilon_{T_i} t_s \tag{11.38}$$

$$\epsilon_{T_i} = \begin{cases} T_i - \overline{T}_i & \text{if } T_i > \overline{T}_i \\ \underline{T}_i - T_i & \text{if } T_i < \underline{T}_i \\ 0 & \text{otherwise,} \end{cases}$$

we get a measure of how much the constraints 0 and $5°C$ for the foodstuff are violated during the simulations. Furthermore, the energy charge is calculated based on a 2010 time-of-use tariff for Phoenix, Arizona [21]. Table 11.3 sums up the results. The temperature threshold is violated in Display Case 1 in five days and in Display Case 2 in four days when precooling is not used. The cost increase from no precool to constant precool is 4.24% and 1.21% from no precool to variable precool, which shows the advantage of the precool algorithm. Even though the precool algorithm costs 1.21% more to run, it also approximately maintains a $0.3°C$ lower average foodstuff temperature, which will result in a small decrease in bacteria growth.

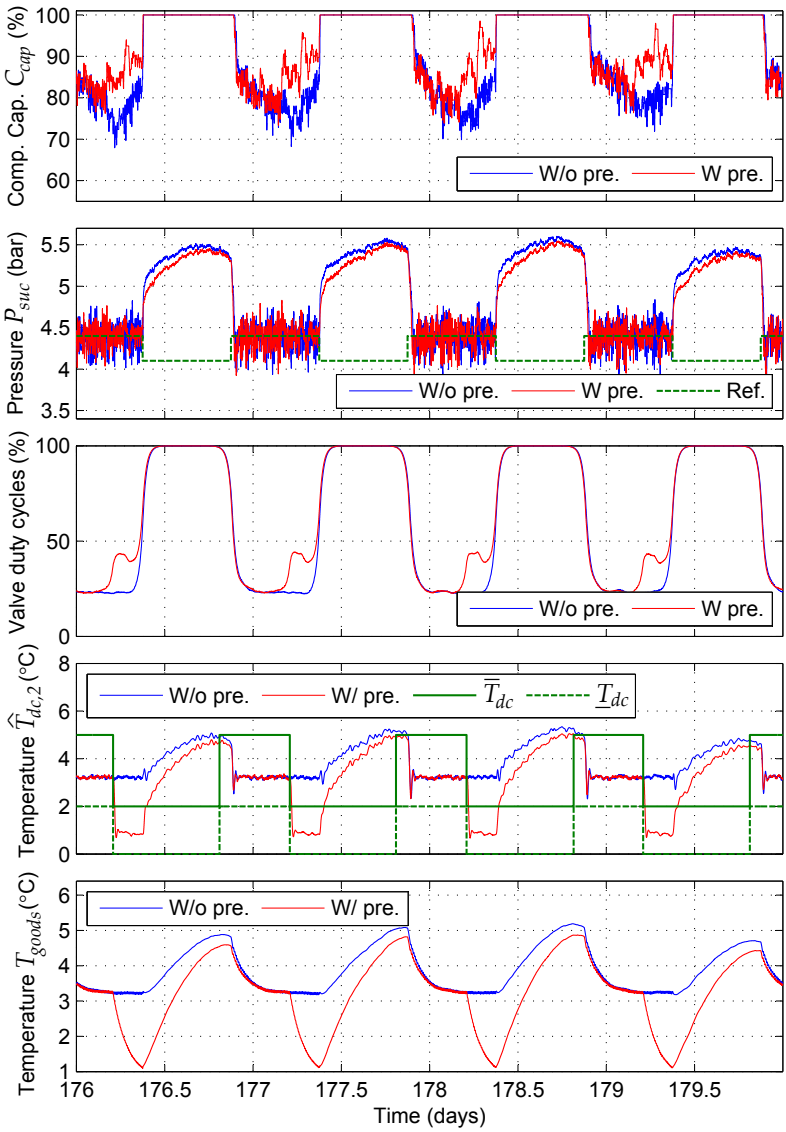

Figure 11.8: Compressor capacity, suction pressure, valve duty cycle (approximated), air temperature (filtered), and foodstuff temperature in Display Case 2 with and without precool algorithm applied for selected days.

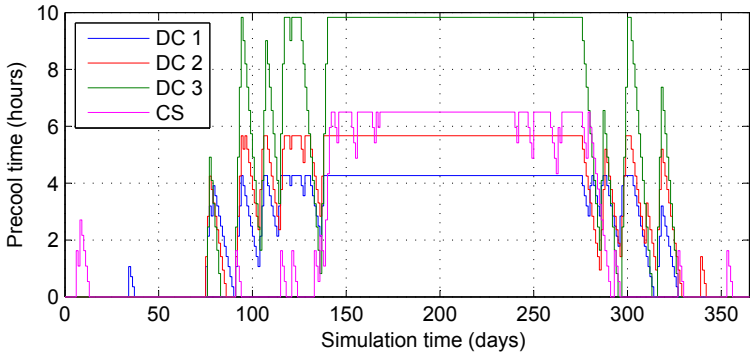

Figure 11.9: Precool time in hours for each day in the simulation with precool.

Table 11.3: Summary of case study results for simulation from 1st of January to the 31st of December.

Quantity	No precool	Variable precool	Constant precool
γ_{con} $(T_{goods,1})$	7481	0	0
γ_{con} $(T_{goods,2})$	3679	0	0
γ_{con} $(T_{goods,3})$	0	0	0
γ_{con} $(T_{goods,cs})$	0	0	0
Avg. $T_{goods,1}$ $(^{\circ}C)$	3.44	3.12	1.33
Avg. $T_{goods,2}$ $(^{\circ}C)$	3.35	2.97	1.31
Avg. $T_{goods,3}$ $(^{\circ}C)$	3.24	2.68	1.31
Avg. $T_{goods,3}$ $(^{\circ}C)$	3.26	2.93	0.88
$T_{goods,1}$ above lim. (days)	5	0	0
$T_{goods,2}$ above lim. (days)	4	0	0
$T_{goods,3}$ above lim. (days)	0	0	0
$T_{goods,cs}$ above lim. (days)	0	0	0
Total energy (kWh)	54742	55401	57235
Energy charge (U.S. $)	3089	3126	3220

6 Conclusion

Foodstuff has thermal storage capabilities. A learning-based algorithm has been proposed that automatically starts to precool the foodstuff at the appropriate time if the refrigeration system becomes saturated during hot days or because of component performance degradation and can thus help prevent deterioration of foodstuff. A model of a supermarket refrigeration system with multiple display cases was derived and simulations for an entire year showed that precooling could prevent violation of an upper temperature threshold during the hottest days. The cost of running the algorithm was also less than if precool was applied all the time.

The learning-based algorithm does not require any additional hardware nor a system model. Furthermore, the experience based approach ensures that the precool control

adapts to load changes, e.g. due to the seasonal temperature differences and to system changes, e.g. component wear. This means that it can easily be plugged into existing systems and thus provides an interesting alternative to model-based approaches such as MPC and precooling based on fixed schedules. The method could potentially be used in other applications as well such as warehouses, refrigerated transports, freezers, ice production, building air conditioning, etc. The only requirement is that there is enough repeatability in the load pattern to allow the learning to converge. The precool might not last all day, but it is considerably better than doing nothing.

References

[1] G. P. Henze and M. Krati, "Ice Storage System Controls for the Reduction of Operating Cost and Energy Use," *Journal of Solar Energy Enginering*, vol. 120, no. 4, pp. 275–281, November 1998.

[2] J. E. Braun, "Load Control Using Building Thermal Mass," *Journal of Solar Energy Enginering*, vol. 125, no. 3, pp. 292–301, August 2003.

[3] G. Zhou, M. Krati, and G. P. Henze, "Parametric Analysis of Active and Passive Building Thermal Storage Utilization," *Journal of Solar Energy Enginering*, vol. 127, no. 1, pp. 37–46, February 2005.

[4] Y. Ma, A. Kelman, A. Daly, and F. Borrelli, "Predictive Control for Energy Efficient Buildings with Thermal Storage: Modeling, Simulation, and Experiments," *IEEE Control Systems Magazine*, vol. 32, no. 1, pp. 44–64, February 2012.

[5] J. E. Altwies and D. T. Reindl, "Passive thermal energy storage in refrigerated warehouses," *International Journal of refrigeration*, vol. 25, no. 1, pp. 149–157, January 2002.

[6] J. Cai, "Control of Refrigeration Systems for Trade-off between Energy Consumption and Food Quality Loss," Ph.D. dissertation, Section of Automation and Control, Department of Electronic Systems, Aalborg University, 2007.

[7] T. G. Hovgaard, L. F. S. Larsen, and J. B. Jørgensen, "Flexible and Cost Efficient Power Consumption using Economic MPC - A Supermarket Refrigeration Benchmark," in *IEEE Conference on Decision and Control and European Control Conference*, Orlando, Florida, December 2011, pp. 848–854.

[8] T. G. Hovgaard, L. F. S. Larsen, and M. J. Skovrup, "Analyzing Control Challenges for Thermal Energy Storage in Foodstuffs," in *IEEE Multi-conference on Systems and Control*, Dubrovnik, Croatia, October 2012, pp. 956–961.

[9] R. W. Longman, "Iterative learning control and repetitive control for engineering practice," *International Journal of Control*, vol. 73, no. 10, pp. 930–954, 2000.

[10] D. A. Bristow, M. Tharayil, and A. G. Alleyne, "A survey of iterative learning control," *IEEE Control Systems Magazine*, vol. 26, no. 3, pp. 96–114, June 2006.

[11] Y. Wang, F. Gao, and F. J. Doyle, "Survey on iterative learning control, repetitive control, and run-to-run control," *Journal of Process Control*, vol. 19, no. 10, pp. 1589–1600, December 2009.

[12] B. E. Helfrich, C. Lee, D. A. Bristow, X. H. Xiao, J. Dong, A. G. Alleyne, S. M. Salapaka, and P. M. Ferreira, "Combined H_∞-Feedback and Iterative Learning Control Design with Application to Nanopositioning Systems," in *American Control Conference*, Seattle, Washington, USA, June 2008, pp. 3983–3900.

[13] K. Vinther, V. Chandan, and A. G. Alleyne, "Learning/Repetitive Control for Building Systems with Nearly Periodic Disturbances," in *European Control Conference*, Zürich, Switzerland, July 2013, pp. 1198–1203.

[14] S. Mishra, U. Topcu, and M. Tomizuka, "Optimization-Based Constrained Iterative Learning Control," *IEEE Transactions on Control Systems Technology*, vol. 19, no. 6, pp. 1613–1621, 2011.

[15] L. F. S. Larsen, "Model Based Control of Refrigeration Systems," Ph.D. dissertation, Section of Automation and Control, Department of Electronic Systems, Aalborg University, 2005.

[16] L. F. S. Larsen, R. Izadi-Zamanabadi, and R. Wisniewski, "Supermarket Refrigeration System - Benchmark for Hybrid System Control," in *European Control Conference*, Kos, Greece, July 2007.

[17] C. Sonntag, A. Devanathan, and S. Engell, "Hybrid NMPC of a Supermarket Refrigeration System using Sequential Optimization," in *17th IFAC World Congress*, Seoul, Korea, July 2008, pp. 13 901–13 906.

[18] Z. Yang, K. B. Rasmussen, A. T. Kieu, and R. Izadi-Zamanabadi, "Fault Detection and Isolation for a Supermarket Refrigeration System - Part One: Kalman-Filter-Based," in *18th IFAC World Congress*, Milano, Italy, September 2011, pp. 13 233–13 238.

[19] M. Skovrup, "Thermodynamic and thermophysical properties of refrigerants - software package in borland delphi," Technical University of Denmark, Tech. Rep., 2000.

[20] *ASHRAE Handbook - Fundamentals (SI Edition)*. American Society of Heating, Refrigeration and Air-conditioning Engineers, Inc., 2005.

[21] APS, "Rate Schedule E-32TOU S - Small General Service (21 kW - 100 kW) - Time of Use," Arizona Public Service Company, Tech. Rep., 2010. [Online]. Available: http://www.aps.com/_files/rates/e-32TOUS.pdf

Paper I

Learning-Based Precool Algorithms for Exploiting Foodstuff as Thermal Energy Reserve on Hot Days

Kasper Vinther, Henrik Rasmussen, Roozbeh Izadi-Zamanabadi, Jakob Stoustrup, and Andrew G. Alleyne

This appendix is based on a paper submitted for journal publication

Abstract

Refrigeration is important to sustain high foodstuff quality and lifetime. Keeping the foodstuff within temperature thresholds in supermarkets is also important due to legislative requirements. Failure to do so can result in discarded foodstuff, a penalty fine to the shop owner, and health issues. However, the refrigeration system might not be dimensioned to cope with hot summer days or performance degradation over time. Two learning-based algorithms are therefore proposed for thermostatically controlled loads, which precools the foodstuff in display cases in an anticipatory manner based on how saturated the system has been in recent days. A simulation model of a supermarket refrigeration system is provided and evaluation of the precool strategies shows that negative thermal energy can be stored in foodstuff to cope with saturation. A system model or additional hardware is not required, which makes the algorithms easy to implement in existing systems.

1 Introduction

Supermarkets require refrigeration systems in order to maintain a high quality and lifetime of foodstuff, which is achieved by keeping the food at low temperatures. These refrigeration systems have multiple fridge and freezer display cases each equipped with local control of the air temperature inside the display case. A refrigerant is used to ensure transport of heat, which is achieved by proper control of pressures and mass flows inside the refrigeration system using compressors, valves, and fans. Further description of refrigeration systems is given later and examples of modeling of such systems can be found in [1–6].

Depending on the type of foodstuff there will be different legislative temperature thresholds, that must be maintained. In Denmark the Danish Veterinary and Food Administration (DVFA) conducts yearly checks of the supermarkets to ensure that regulations are met and that the legally required self-checks have been performed. The thresholds and inspection rules can be found in [7, 8] and depending on the type of food the fridges should typically be operated below $5°C$ and freezers should be operated below -18$°C$. If the DVFA inspects the supermarket and some of the foodstuff is maintained outside the limits, then that could result in discarded foodstuff and possibly a fine depending on the severity. Apart from regulatory requirements, proper temperature control avoids bacteria growth and resulting food safety risk, which is very important to the overall society.

The main contributors to changes in the load on supermarket refrigeration systems are the outside air temperature, which determines the high pressure setpoint for the condenser unit, and the daily opening and closing of the supermarket, which changes the load on the individual display cases. Refrigeration systems are therefore usually dimensioned to cope with all weather conditions and loads in order to guarantee that the foodstuff can be maintained within the prescribed temperature bounds independent of the ambient temperature. A negative aspect of over-dimensioning a system is higher peak power demand, which is costly and could require larger transformers or extensions of transmission lines for large systems such as warehouses and supermarkets. An interesting alternative to over-dimensioning the system is to store energy in terms of "coldness" for later use. It is possible to use the refrigerated food to store energy during the lightly loaded hours of the day; e.g. at night or early morning. In other words, precooling of foodstuff can

be used to temporally shift some of the load on the refrigeration system to reduce the peak loads. Precooling can also help if the refrigeration system capacity changes such as becoming less efficient due to component wear or changes in refrigerant charge. The number of display cases might also have increased since the commissioning phase which puts further stress on the system.

Installation of thermal energy storage tanks can help solve capacity problems and provides a way to shift loads to off peak hours with cheaper energy and to hours where the outside temperature is lower. Examples of utilization of thermal storage tanks and/or building thermal capacity is given in [9–11]. However, a considerable additional capital investment is also associated with installation of thermal storage tanks.

Research has been invested in the use of foodstuff as thermal storage. The authors in [12] showed significant cost savings in four low temperature warehouses using load shifting strategies, where the foodstuff and building was cooled more during the night and less during the day. Model Predictive Control (MPC) has also been investigated as control strategy for predicting when precooling of foodstuff in supermarkets is required. MPC was e.g. used in [13] to store energy in the display case to cope with capacity problems during hot summer days and in [14–16] to provide ancillary services to the Smart Grid. Further, thermal storage potential of different foodstuffs has been investigated in [17].

To the knowledge of the authors, previous work has used either a predefined precool schedule or a MPC approach, due to its constraint handling capabilities. In Denmark, with a population of 5.6 million, there are roughly 4500 supermarkets and the refrigeration systems in these supermarkets are seldom completely similar. This potentially gives thousands of different systems and, as with the heuristically chosen schedule, a model-based MPC approach is often tailored to a specific system where deriving a suitable model can be cumbersome and costly. Changes in load patterns, operating conditions, and storage capacity will also occur during the year. Finally, system parameters also change due to e.g. reduction in refrigerant charge, faulty components, or component wear. These approaches therefore often lack flexibility, modularity and robustness towards changes.

Two alternative model-free precool strategies are investigated in this paper in order to reduce the effect of system saturation on hot days. The first precool strategy was first introduced in [18], where precooling is applied individually to each fridge display case. The second strategy applies the precooling to the freezer section, since the freezers have slower dynamics and a wider dynamic range and thus higher storage potential. The strategies are inspired by learning-based control methods, where Repetitive Control (RC) and Iterative Learning Control (ILC) are two examples of such methods. These methods are well covered in the literature (see e.g. [19–21]) and are often used in batch processes where a task is repeated. This makes it possible to learn a performance improving reference modifying signal (Serial ILC/RC) or a feedforward signal (parallel ILC/RC) for the next repetition of that task. Analysis of data from a Danish medium size supermarket system have shown that there is also a certain amount of daily repeatability in the operation of refrigeration systems. The proposed strategies are therefore devised to learn how much precool is needed and when it is needed based on data from previous days. The precooling can then be applied in the next day by temporarily lowering the air temperature thresholds within permissible bounds for the display cases controlled by on/off hysteretic control. The solutions do not require system model knowledge as MPC. They can be applied directly to existing lower level control without additional hardware, and they are tested on a realistic simulation model of a supermarket refrigeration system.

Data from a Danish supermarket is analyzed in Section 2 and a simulation model of a supermarket refrigeration system with typical control loops is provided in Section 3. The precool strategies are then derived in Section 4 and simulation results are presented in Section 5. Finally, concluding remarks are given in Section 6.

2 Analysis of Medium Size Supermarket Refrigeration System Data

Data from a Danish medium size supermarket refrigeration system has been available through the ESO2 project [22]. The supermarket is open every day between 8 am and 9 pm and the main components of the refrigeration system are seven medium temperature (MT) storage evaporators, four low temperature (LT) storage evaporators, two compressors for the MT storages, two compressors for the LT storages, a bypass valve (BP), a gas cooler/condenser, and a receiver. The refrigerant in the system is CO_2 (R744) and data are logged with a sample time of 60 seconds. A schematic of the system is shown in Fig. 12.1. The work done by each of the two compressor racks can be estimated from the

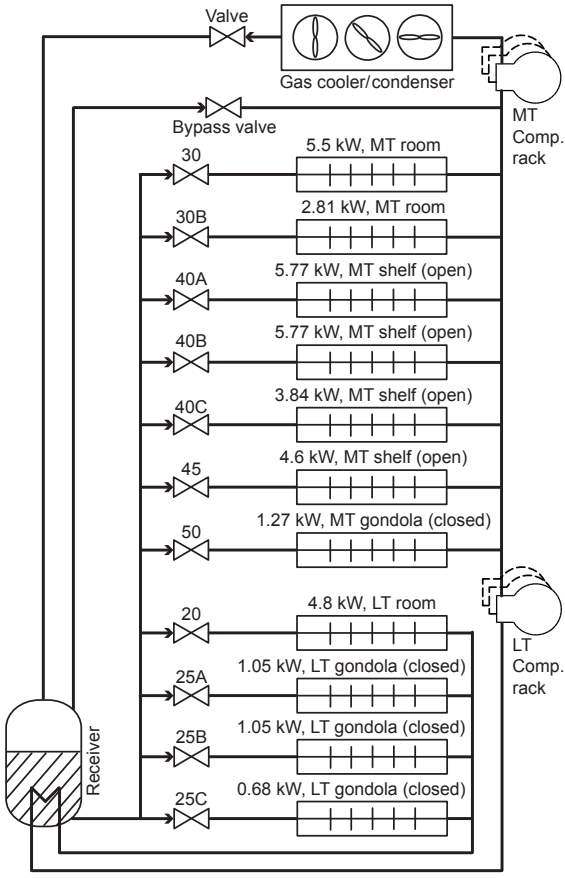

Figure 12.1: Simplified schematic of the medium size supermarket refrigeration system. The numbers on the valves are used as reference.

available data by

$$\dot{W}_{cp} = \frac{C_{cap}}{100} \overline{\dot{V}}_{cp} \rho_{suc} \left(h_{cp,o} - h_{cp,i} \right), \tag{12.1}$$

where C_{cap} is the requested capacity and $\overline{\dot{V}}_{cp}$ is the volumetric flow rate at maximum capacity, which is approximated by a constant value. The refrigerant density in the suction line ρ_{suc}, specific enthalpy out of the compressor rack $h_{cp,o}$, and the specific enthalpy into the compressor rack $h_{cp,i}$ is determined based on temperature and pressure measurements and refrigerant property tables (Software package RefEqns is used [23]). The collected cooling loads from the MT section, the LT section, and the BP valve are estimated as

$$\dot{Q} = \dot{m}_{re} \Delta h, \tag{12.2}$$

where $\dot{Q}$ is the heat transfer rate (cooling load), $\dot{m}_{re}$ is the refrigerant mass flow rate (measured by mass flow meters individually for the MT section, the LT section, and the BP valve), and Δh is the specific enthalpy difference between the refrigerant at the receiver and either the outlet of the evaporators or the BP valve. The enthalpies are again based on temperature and pressure measurements.

The compressor works, cooling loads, and valve opening degrees OD for a fridge and a freezer display case are shown for six consecutive days from 18. of September 2011 in Fig. 12.2. The variation in the data is large and Matlab's `smooth` function has therefore

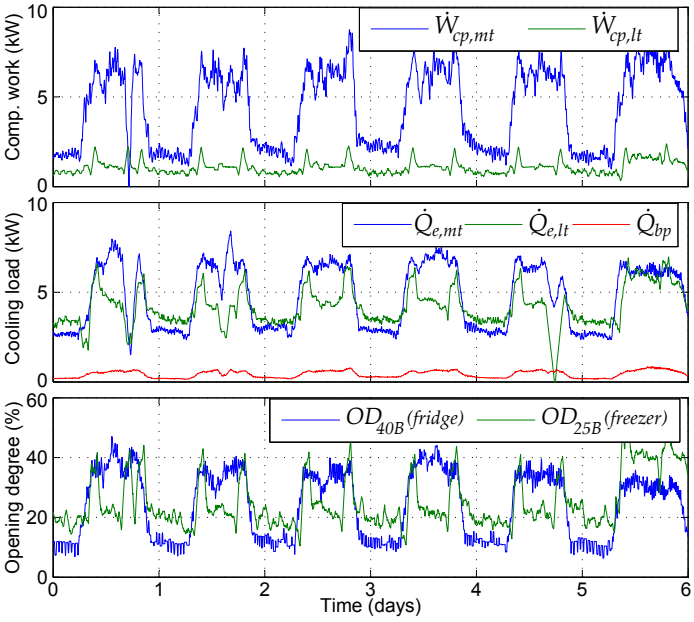

Figure 12.2: Filtered supermarket data for six consecutive days in September 2011. The top graph shows the estimated work of the compressor racks. The middle graph shows the estimated cooling loads. The bottom graph shows the opening degree OD of a fridge and a freezer display case.

been used to filter the data to reveal the average tendency during the day. 60 samples are used to filter the compressor work and 120 samples are used to filter the cooling loads and the valve opening degree. Fig. 12.3 shows the mean and standard deviation for 20 days. The graphs only indicate the spread in the mean value between days, since the data is filtered. A high degree of repeatability is seen and there is an increase in the load in the opening hours during the daytime, which is not surprising. The repeatability is mostly visible in the MT section and in open shelf type display cases. The refrigeration system does not saturate. However, if saturation would occur it would most likely be mid day, mid opening hours, and on hot summer days.

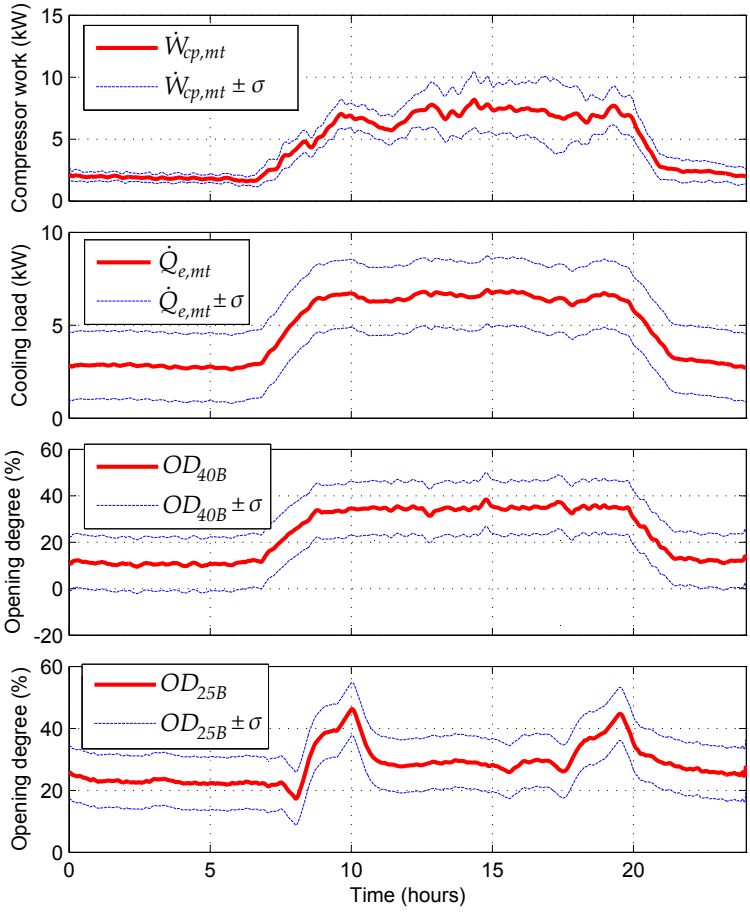

Figure 12.3: Mean and standard deviation of filtered supermarket data based on 20 days of data from September and November 2011. The top graph shows the estimated work of the MT compressor rack. The second graph shows the estimated MT cooling load. The third graph shows the opening degree OD of a fridge display case and the last graph shows the OD for a freezer.

3 Supermarket Refrigeration System Model and a Standard Control Approach

Making yearlong tests and introducing saturation on the refrigeration system in an operating supermarket is not practically feasible. A benchmark model of a typical supermarket refrigeration system is therefore derived for simulation purposes with a focus on simulating air and foodstuff temperature. The typical control of such systems is also implemented and an overview of the simulation environment is provided in Fig. 12.4. This model makes it possible to evaluate the performance of different precool strategies and compare them under the same conditions, which would also not be possible with a real system. The model was first presented in [18] and represents a slightly modified version of a benchmark model widely studied in the literature, see [1, 2, 24, 25]. The major modification made is that the effect of changes in the outside air temperature can now result in saturation of the system on hot days due to a higher required compressor work. The model implemented in Matlab Simulink is available at `www.es.aau.dk/projects/refrigeration/simulation-tools`.

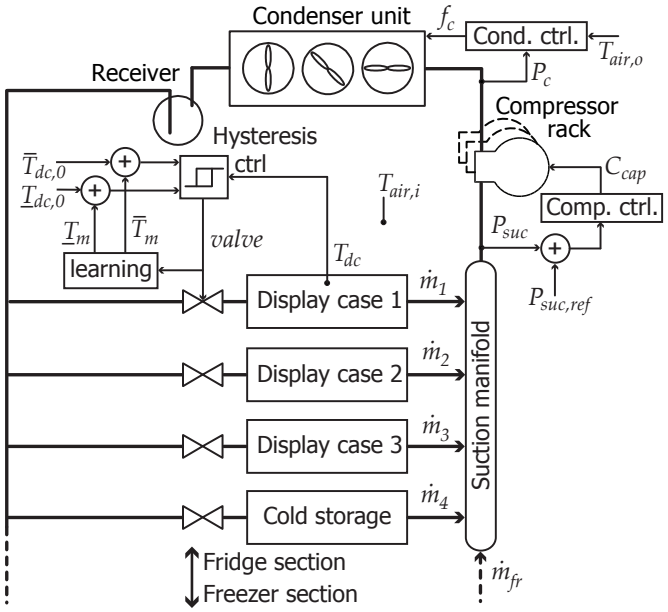

Figure 12.4: Overview of supermarket refrigeration system model with multiple display cases and a cold storage room. The freezer section is simulated by an additional mass flow $\dot{m}_{fr}$ and controllers are used to regulate pressures and temperatures as indicated. Only one of the valve hysteresis controllers are shown in the figure.

Fridge Display Case model

A model of an open shelf type display case with night cover is illustrated in Fig. 12.5 with indication of heat transfer paths. The heat transfer rates are between the evaporator

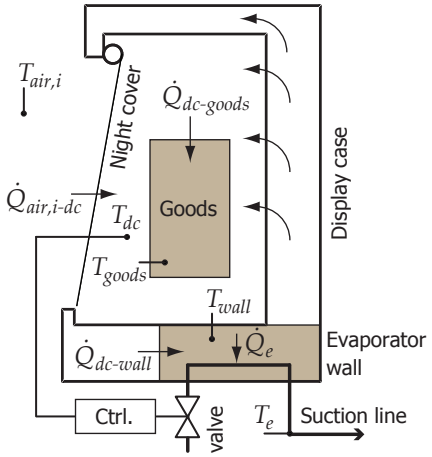

Figure 12.5: Open shelf type display case model with night cover.

wall and the refrigerant $\dot{Q}_e$, between the air that circulates over the evaporator and the evaporator wall $\dot{Q}_{dc-wall}$, between the air and the foodstuff $\dot{Q}_{dc-goods}$, and between the ambient air and the air in the display case $\dot{Q}_{air,i-dc}$. Heat transfer caused by infiltration of air into the display case is assumed to be included in $\dot{Q}_{air,i-dc}$ and a lumped temperature model is used for simplicity. This gives the following differential equations for the temperatures:

$$\frac{dT_{goods}}{dt} = \frac{\dot{Q}_{dc-goods}}{m_{goods}C_{p,goods}}, \tag{12.3}$$

$$\frac{dT_{wall}}{dt} = \frac{\dot{Q}_{dc-wall} - \dot{Q}_e}{m_{wall}C_{p,wall}}, \tag{12.4}$$

$$\frac{dT_{dc}}{dt} = \frac{\dot{Q}_{air,i-dc} - \dot{Q}_{dc-goods} - \dot{Q}_{dc-wall}}{m_{dc}C_{p,dc}}, \tag{12.5}$$

where m is mass, C_p is the specific heat capacity, and the heat transfer rates are given as

$$\dot{Q}_{dc-goods} = UA_{dc-goods}(T_{dc} - T_{goods}), \tag{12.6}$$

$$\dot{Q}_{dc-wall} = UA_{dc-wall}(T_{dc} - T_{wall}), \tag{12.7}$$

$$\dot{Q}_e = UA_{wall-re}(T_{wall} - T_e), \tag{12.8}$$

$$\dot{Q}_{air,i-dc} = UA_{air,i-dc}(T_{air,i} - T_{dc}). \tag{12.9}$$

Here, T_e is the evaporation temperature of the refrigerant and UA denotes the overall heat transfer coefficient.

The heat transfer coefficient $UA_{wall-re}$, between the evaporator wall and the refrigerant, is predominantly a function of the mass of liquid refrigerant m_{re} in the evaporator given as

$$UA_{wall-re} = \overline{UA}_{wall-re}\frac{m_{re}}{\overline{m}_{re}}, \tag{12.10}$$

where $\overline{m}_{re}$ is the maximum mass of liquid refrigerant and $\overline{UA}_{wall-re}$ is the heat transfer coefficient when the evaporator is fully filled and maintained at a superheat level of $T_{sh} = 10K$ (it is assumed that the superheat is controlled to this level when the valve is on). The rate of change of the mass of the refrigerant $\frac{dm_{re}}{dt}$ is simulated as

$$\frac{dm_{re}}{dt} = \begin{cases} \frac{\overline{m}_{re} - m_{re}}{\tau_{fill}} & \text{if } valve = 1, \\ -\frac{\dot{Q}_e}{\Delta h_{lg}} & \text{if } valve = 0 \text{ and } m_{re} > 0, \\ 0 & \text{otherwise.} \end{cases} \tag{12.11}$$

where $valve$ is the control signal to the valve (either on or off), τ_{fill} is the time it takes to fill the evaporator from empty to full, and the specific latent heat of the remaining refrigerant is denoted Δh_{lg}.

Supermarket Refrigeration System Model

The mass flow from each display case, the suction pressure, and the compressor power is simulated to observe the effect of system saturation and precooling.

The dynamics of the condenser unit and the control on the condenser are assumed stable and fast compared to the rest of the system. A static relation is therefore used for the condensation temperature $T_c = T_{air,o} + 5$, where it is kept at a reference $5°C$ above the outside temperature $T_{air,o}$.

The mass flow of refrigerant from each display case i into the suction manifold can be formulated as

$$\dot{m}_i = \frac{\dot{Q}_e}{\Delta h_{lg}}. \tag{12.12}$$

The time derivative of the suction pressure is then defined as

$$\frac{dP_{suc}}{dt} = \frac{\sum_{i=1}^{n} \dot{m}_i + \dot{m}_{fr} - \dot{V}_{cp}\rho_{suc}}{V_{suc}\frac{d\rho_{suc}}{dP_{suc}}}, \tag{12.13}$$

where V_{suc} is the volume of the suction manifold, ρ_{suc} is the density, $\dot{V}_{cp}$ is the volume flow out of the manifold caused by the compressor work, and $\dot{m}_{fr}$ is additional mass flow from the freezer section.

The electrical power consumed by the compressor $\dot{W}_{cp}$ is finally approximated by

$$\dot{W}_{cp} = \frac{C_{cap}}{100}\overline{\dot{W}}_{cp} = \frac{\dot{V}_{cp}\rho_{suc}\left(h_{is} - h_{cp,i}\right)}{\eta}, \tag{12.14}$$

where the controllable input C_{cap} is the requested capacity in %, $\overline{\dot{W}}_{cp}$ is the power consumption at maximum capacity, $h_{cp,i}$ and h_{is} are the specific enthalpies in and out of the compressor assuming an isentropic compression, and η is the efficiency from an isentropic process to the actual electrical power consumed.

A set of refrigerant specific relations are needed in order to solve the above equations. Software packages such as RefEqns [23] can be used for this purpose. However, to make the simulation independent of this package, a set of polynomial and regression fits

to the refrigerant tables in RefEqns are provided here for refrigerant R404A (all-round refrigerant good for both fridges and freezers):

$$\rho_{suc} = 4.669 P_{suc} + 0.3672, \tag{12.15}$$

$$\frac{d\rho_{suc}}{dP_{suc}} = 4.669, \tag{12.16}$$

$$\Delta h_{lg} = (0.00184 P_{suc}^2 - 0.0683 P_{suc} + 2.0339) 10^5, \tag{12.17}$$

$$\begin{aligned} h_{is} = &(3.6436 - 0.00968 P_{suc} + 0.0343 P_c \\ &- 0.0000495 P_{suc} P_c + 0.000373 P_{suc}^2 \\ &- 0.000629 P_c^2) 10^5, \end{aligned} \tag{12.18}$$

$$\begin{aligned} h_{cp,i} = &(0.000332 P_{suc}^3 - 0.00853 P_{suc}^2 + 0.0953 P_{suc} \\ &+ 3.3467) 10^5 + \Delta h_{T_{sh}}, \end{aligned} \tag{12.19}$$

$$\Delta h_{T_{sh}} = 9 \text{ } (T_{sh} = 10K \text{ assumption}),$$

$$P_c = 0.00307 T_c^2 + 0.1839 T_c + 6.0826. \tag{12.20}$$

The specific enthalpy $\Delta h_{T_{sh}}$ is the average increase in enthalpy when the refrigerant is superheated 10 degree and P_c is the condensation pressure. The fits are made for the operating ranges used in the simulations.

Suction Pressure Control

A PI controller with anti-windup is typically used to maintain the suction pressure at a specified reference $P_{suc,ref}$. This is achieved by changing the capacity C_{cap} of the compressor rack to meet the mass flow demand and a dead-band DB and a slow update time $t_{s,cp}$ is often used to reduce the mechanical stress on the compressors by reducing the number speed changes required. It is assumed that C_{cap} can be changed in a continuous fashion, i.e. the compressor rack has at least one variable speed compressor. The control equations are given in (12.21)-(12.26) and also provided in e.g. [2].

$$e(k) = P_{suc,ref} - P_{suc}(k), \tag{12.21}$$

$$e_{DB}(k) = \begin{cases} e(k) & \text{if } |e(k)| > DB, \\ 0 & \text{otherwise,} \end{cases} \tag{12.22}$$

$$I(k) = I(k-1) + \frac{K_{p,cp} t_{s,cp}}{\tau_{i,cp}} e_{DB}(k) + w(k), \tag{12.23}$$

$$C_{cap,s}(k) = K_{p,cp} e_{DB}(k) + I(k), \tag{12.24}$$

$$C_{cap}(k) = \begin{cases} \overline{C}_{cap} & \text{if } C_{cap,s}(k) > \overline{C}_{cap}, \\ \underline{C}_{cap} & \text{if } C_{cap,s}(k) < \underline{C}_{cap}, \\ C_{cap,s}(k) & \text{otherwise,} \end{cases} \tag{12.25}$$

$$w(k+1) = \frac{t_{s,cp}}{\tau_{i,cp}} (C_{cap}(k) - C_{cap,s}(k)). \tag{12.26}$$

The tunable PI control parameters are $K_{p,cp}$ and $\tau_{i,cp}$ and k is the discrete time index.

Relay Feedback Control of Display Case Air Temperature

Refrigerated air is circulated over the foodstuff to cool it down and the air temperature T_{dc} in each display cases is controlled with an on/off valve and relay feedback control (hysteretic control) given as

$$valve(k) = \begin{cases} 1 & \text{if } T_{dc}(k) > \overline{T}_{dc}, \\ 0 & \text{if } T_{dc}(k) < \underline{T}_{dc}, \\ valve(k-1) & \text{otherwise,} \end{cases} \tag{12.27}$$

where $\overline{T}_{dc}$ and $\underline{T}_{dc}$ define the upper and lower thresholds for the temperature and 0 and 1 corresponds to a fully closed or fully open valve, respectively. This type of control is very simple and a commonly used control method for regulating the temperature of a medium within bounds. The foodstuff temperature is usually not measured in supermarkets.

Representative Weather Data

A weather file for Phoenix, Arizona is used to simulate realistic high outdoor temperatures and load profiles on the refrigeration system. This data is based on typical meteorological year 2 (TMY2) weather data and shown in Fig. 12.6 for a year, which reveals the seasonal changes in temperature. The higher outdoor temperature during the summer period will also result in a higher load on the refrigeration system as the difference in condenser and suction pressure needs to be higher.

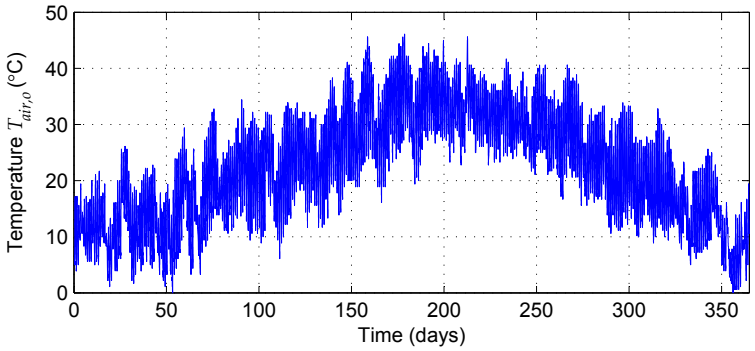

Figure 12.6: Outdoor air temperature $T_{air,o}$ in Phoenix Arizona based on TMY2 weather data from 1st of January to 31st of December.

4 Precool of Refrigerated Foodstuff

The potential for precooling of refrigerated foodstuff in supermarkets is investigated in this section, to be able to handle capacity saturation problems better. As stated in Subsection 3, relay feedback (hysteretic control) is used as temperature control. In the following it is assumed that the thresholds on the output T_{dc} can be shifted up or down within some legislative hard constraints. This is also the only possible way to apply precooling, if assuming that the foodstuff temperature T_{goods} is unknown and that the precool control

should not change the original setup, but only modify the references/thresholds to the lower level controllers. Two precool algorithms are outlined at the end of the section, which are both based on a general learning-based precool concept.

Learning-Based Precool

A general way to apply precooling to thermostatically controlled systems is shown in Fig. 12.7, which illustrates the proposed solution using a trial domain notation, where the input and output vectors contain all the discrete samples in one trial j (for trial domain notation see e.g. [20]). The system is denoted P and it is disturbed by unknown disturbances $\mathbf{d}_j$ during trial j. These disturbances have some repeatable part from trial to trial (e.g. day to day). This repeatability was also presented in Section 2. A memory block is used to save previous valve input signals $\mathbf{valve}_{j-1}$ and an estimate of the load on the system is obtained by filtering this signal giving the vector $\widehat{\mathbf{valve}}_{j-1}$. The idea is then to use this data to modify the initial air temperature threshold vectors $\overline{\mathbf{T}}_{dc,0}$ and $\underline{\mathbf{T}}_{dc,0}$ with the reference modifying vectors $\overline{\mathbf{T}}_{m,j}$ and $\underline{\mathbf{T}}_{m,j}$;

$$\overline{\mathbf{T}}_{dc,j} = \overline{\mathbf{T}}_{dc,0} + \overline{\mathbf{T}}_{m,j} \tag{12.28}$$

$$\underline{\mathbf{T}}_{dc,j} = \underline{\mathbf{T}}_{dc,0} + \underline{\mathbf{T}}_{m,j}. \tag{12.29}$$

By lowering the thresholds for a period of time it is possible to precool the foodstuff, since the air flowing across the foodstuff is colder in this period. Note that F can have zero phase shift properties and by low pass filtering the on/off signal a mean value or duty cycle is obtained. If this duty cycle reaches an upper limit during the trial $j-1$ it is likely to assume that it will happen again in trial j and preemptive action is taken by precooling in advance.

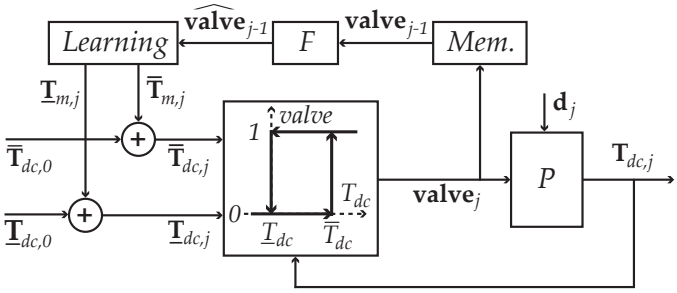

Figure 12.7: Relay feedback controlled system P with adaptation of the thresholds using a learning-based approach. The trial domain is denoted j.

The reference modifying vectors are recalculated each trial and contain zeros except for the precool period where the values are set to $\overline{T}_m$ or $\underline{T}_m$, which are the allowed modification of the upper and lower thresholds. The precool period is determined by a length Δ and an end-time t_{end}. The end-time could either be based on when the duty cycle went into saturation in the previous trial, when it came out of saturation, or based on some known schedule like the opening hours of the supermarket. The length of the

precool period is determined based on a serial ILC inspired learning algorithm;

$$\Delta_j = \Delta_{j-1} + \delta_{j-1} \tag{12.30}$$

$$\delta_{j-1} = \begin{cases} l_1\overline{\Delta} & \text{if } \left|\left|\widehat{\mathbf{valve}}_{j-1}\right|\right|_\infty \geq \overline{\widehat{valve}} \\ l_2\overline{\Delta} & \text{otherwise,} \end{cases} \tag{12.31}$$

where δ_{j-1} is the update and $\overline{\widehat{valve}}$ is the upper threshold on the duty cycle, which indicates if the system was saturated in the previous trial and if more or less precooling is required. The gains $l_1 \in]0, 1]$ and $l_2 \in [-1, 0[$ are the learning and de-learning gains, where e.g. $l_1 = 1$ means that the maximum allowed precool time $\overline{\Delta}$ is reached in one trial and lower values mean slower convergence.

The upper limit on the precool time $\overline{\Delta}$ should approximately correspond with the time it takes to precool the foodstuff, since a longer precool time only results in an increase in power consumption. The precool time is therefore limited as

$$\Delta_j = \begin{cases} \overline{\Delta} & \text{if } \Delta_j > \overline{\Delta} \\ 0 & \text{if } \Delta_j < 0 \\ \Delta_j & \text{otherwise.} \end{cases} \tag{12.32}$$

Potential ways of determining a suitable maximum precool time is further discussed in Subsection 4.

Remark that the reference update is based on the error in the previous trial in serial ILC, whereas it is based on the saturation of the input in previous trials in the proposed solution. This strategy is chosen, because it does not help to change the reference signal to force precooling in the refrigeration system when the system is already saturated. Note also that $valve$ and T_{dc} could be replaced by other inputs and outputs in other types of storage control problems, e.g. buffer tank level control or building indoor temperature control.

Simple Thermal Storage Example

A simple thermal storage example is presented in the following, to demonstrate the precool algorithm under perfect repeatability in load pattern and without multiple display cases. Fig. 12.8 shows a model of the system, which is essentially a very simplified refrigeration system. Relay feedback control was applied on the air temperature T_{dc} with the heat transfer going out of the system $\dot{Q}_e$ as an on/off type input with $\overline{\dot{Q}}_e$ and $\underline{\dot{Q}}_e$ as

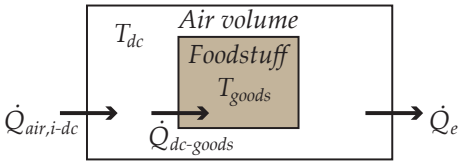

Figure 12.8: Simple thermal example system model. The load disturbance is the heat transfer from the surroundings $\dot{Q}_{air,i-dc}$ and the controllable input is the heat transfer $\dot{Q}_e$.

the on and off signals, respectively. The load on the system $\dot{Q}_{air,i-dc}$ was simulated as a square signal that repeats itself daily. The upper value is higher than the possible cooling $\overline{\dot{Q}}_e$, which will result in input saturation and thus temperature deviation. The objective is to keep the foodstuff temperature T_{goods} below $5°C$.

A state space representation of the system illustrated in Fig. 12.8 can be derived from (12.3), (12.5), and (12.6) giving

$$\begin{bmatrix} \dot{T}_{dc} \\ \dot{T}_{goods} \end{bmatrix} = \begin{bmatrix} \frac{-UA_{dc-goods}}{m_{dc}C_{p,dc}} & \frac{UA_{dc-goods}}{m_{dc}C_{p,dc}} \\ \frac{UA_{dc-goods}}{m_{goods}C_{p,goods}} & \frac{-UA_{dc-goods}}{m_{goods}C_{p,goods}} \end{bmatrix} \begin{bmatrix} T_{dc} \\ T_{goods} \end{bmatrix} + \begin{bmatrix} \frac{-1}{m_{dc}C_{p,dc}} \\ 0 \end{bmatrix} \dot{Q}_e + \begin{bmatrix} \frac{1}{m_{dc}C_{p,dc}} \\ 0 \end{bmatrix} \dot{Q}_{air,i-dc}, \tag{12.33}$$

and system and control parameters used in the simulation are collected in Table 12.1. The low pass filter F is implemented using the Matlab command `butter` with a cutoff frequency $\omega_F = 8.7E^{-4}$ radians/s. Furthermore, `filtfilt` is used to make the filter have zero phase shift properties and this gives a good estimate of the average load $\widehat{\dot{Q}}_e$. The precool time is then increased if $\widehat{\dot{Q}}_e > 0.99\overline{\dot{Q}}_e$ (99% of maximum capacity).

Table 12.1: Parameter values used in the simple thermal storage example.

System par.	Value	Ctrl par.	Value
$UA_{dc-goods}$	300 ($\frac{W}{K}$)	$\overline{\Delta}$	4 ($hours$)
m_{dc}	50 (kg)	l_1	$\frac{1}{4}$ (-)
$C_{p,dc}$	1 ($\frac{kJ}{kg \cdot K}$)	l_2	$-\frac{1}{12}$ (-)
m_{goods}	500 (kg)	ω_F	$8.7E^{-4}$ ($\frac{rad}{s}$)
$C_{p,goods}$	4 ($\frac{kJ}{kg \cdot K}$)	$\overline{\widehat{\dot{Q}}}_e$	$0.99\overline{\dot{Q}}_e$ (W)
$\overline{\dot{Q}}_e$	2850 (W)	t_{end}	9 ($hours$)
$\underline{\dot{Q}}_e$	0 (W)	$\overline{T}_m$	-3 ($°C$)
		$\underline{T}_m$	-2 ($°C$)

The results using a maximum load of 3 kW is shown in Fig. 12.9. The foodstuff temperature increased to $6.6°C$ without precooling, because the load became too large at 9 in the morning each day. This was lowered to $4.5°C$ after four days, when precooling was applied with the chosen learning gain.

A similar simulation was performed with a maximum load on the air of 2.8 kW and the results are shown in Fig. 12.10. The algorithm cycled between different values of precool time on a four day basis. The precool times are $\Delta_j = \{0, 60, 120, 100, 80, 60, 120, 100, 80, 60, ...\}$ minutes of precool and the required precool time that just exactly removes the saturation is approximately 70 minutes. This value can not be reached with the chosen learning gains, since the they discretize the obtainable precool times.

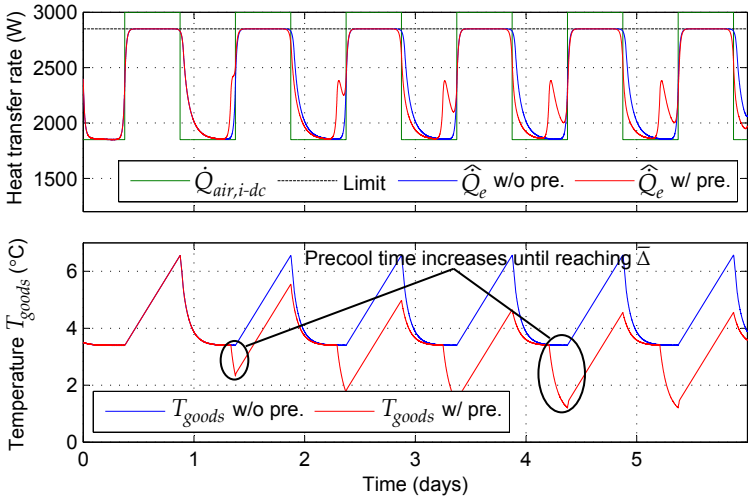

Figure 12.9: Simulation results without and with variable precool using the simple example model with a max load of 3 kW and an upper limit on $\dot{Q}_e$ of 2.85 kW.

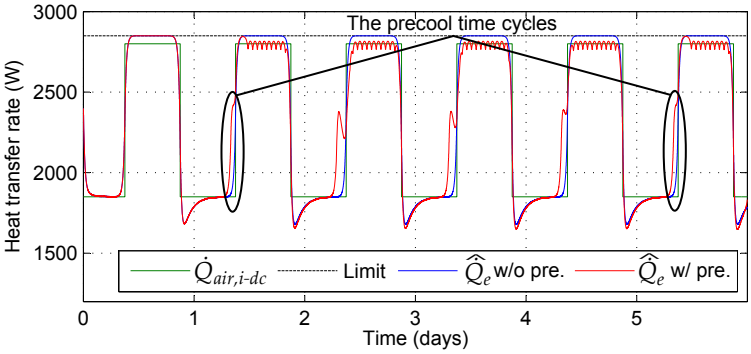

Figure 12.10: Simulation results without and with variable precool using the simple example model with a max load of 2.8 kW and an upper limit on $\dot{Q}_e$ of 2.85 kW.

Convergence of the Precool Time in the Trial Domain

The precool period will cycle between levels of precool time as indicated in Fig. 12.10 and the levels are determined by l_1 and l_2. The jump between levels can be made smaller by decreasing the learning and de-learning rates (l_1 and l_2), but that will also result in slower convergence.

If there is total repeatability between trials and if Δ^* denotes the smallest possible precool time that avoids input saturation, i.e. $\Delta^* = \inf\left\{\Delta : \left|\left|\widehat{\mathbf{valve}}\right|\right|_\infty < \overline{\widehat{valve}}\right\}$, then the precool time Δ_j will converge to the interval

$$\Delta^* + l_2\overline{\Delta} < \Delta_j \leq \Delta^* + l_1\overline{\Delta}, \tag{12.34}$$

when $\Delta^* + l_2\overline{\Delta} \geq 0$ and $\Delta^* + l_1\overline{\Delta} \leq \overline{\Delta}$. Furthermore, if no precooling is required ($\Delta^* \leq 0$) then $\Delta_j \to 0$ and if maximum precooling is required ($\Delta^* > \overline{\Delta}$) then $\Delta_j \to \overline{\Delta}$.

Since no precool is cheapest in terms of energy, then l_1 should be small and l_2 should be large numerically (removes precool quickly again). However, if robustness towards hot days is more important, then it should be the opposite.

Foodstuff Storage Potential Considerations

The temporal thermal storage potential of different refrigerated foodstuffs is predominantly determined by the foods total surface area, mass, overall heat transfer coefficient, and specific heat capacity. The Biot number B is also an important factor and it is the ratio of internal temperature difference required to move energy within a product compared to the difference required at the surface to add or remove the same energy. The Biot number therefore gives an indication of the appropriateness of a lumped versus a non-lumped temperature analysis and defined as [26]

$$B = \frac{U\frac{V}{A}}{k}, \tag{12.35}$$

where A is the exposed surface area of the product, V is the volume, U is the surface heat transfer coefficient, and k is the thermal conductivity. A lumped analysis can be applied if the Biot number is small ($B < 0.1$), which means that the temperature will not vary significantly inside the product and a non-lumped analysis is more appropriate if B is large.

[17] provides experimentally obtained Biot numbers for different type of foods, which indicate that they are generally above 0.1. However, a lumped analysis is often performed despite of this, because it does not involve solving complex multidimensional partial differential equations. The lumped approach is also taken here for two additional reasons; because the entire mass of the foodstuff can be activated during precooling and because the system only gradually becomes more saturated, due to a slowly changing average air temperature, caused by the increasing outside temperature, which changes slowly over several hours.

A large increase is seen, in the overall heat transfer coefficient between the air in the store and the air inside the display case, when the supermarket is open, since the insulating night cover in open shelf type display cases has to be removed in this period. This also coincides with customer activity, which gives an increased heat load and the behavior is included in the simulations presented in Section 5. The constant flow of foodstuff from store to display cases to the customers (out of the store) is therefore included in the behavior of the overall heat transfer coefficient, since no specific data was available on how much food is moved during the day due to confidentiality. Additionally, since foods have different thermal storage potential, different combinations of UA values and mass times specific heat mC_p is used in each display case. This gives different time constants and a step in the air temperature from 3.5 to $1^{\circ}C$ using (12.3) is performed in order to determine how long it takes to precool the food. The time is measured as the time from the step to when 90% of the step is reached and the result is shown in Fig. 12.11. This gives 166 minutes for Display case 1, 250 minutes for Display Case 2, 500 minutes for Display Case 3, and 300 minutes for the cold storage room. They therefore represent different time constants and storing potentials.

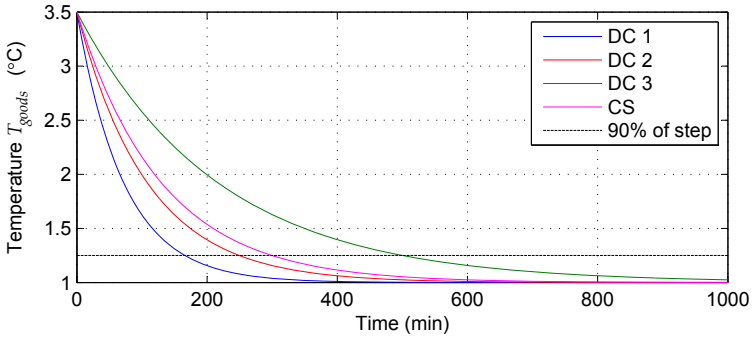

Figure 12.11: Food temperature during a step in the air temperature.

Precool Algorithms and Tuning Guideline

Ad hoc tuning guidelines are provided here based on simulations and experience with supermarket refrigeration systems. The parameters can also be tuned after installation if needed.

Learning gains l_1 and l_2

Tuning of these parameters was discussed in Subsection 4 and they should have a value in the intervals $l_1 \in]0, 1]$ and $l_2 \in [-1, 0[$. Setting $l_1 = 1$ and l_2 small gives the safest option, but will often result in more precooling than necessary. The choice should reflect how changeable the weather can be expected to be. Simulations with the weather data presented in Fig. 12.6 have shown that $l_1 = \frac{1}{4}$ and $l_2 = -\frac{1}{12}$ gives a good tradeoff between ensuring precooling when needed and energy consumption.

Filter parameters ω_F and $\overline{\widehat{valve}}$

A zero phase shift low pass filter is used to convert the valve on/off signal to a duty cycle (utilized capacity). The filter therefore depends on the approximate switching period of the valves, which is usually between 5-15 minutes in display cases. A cutoff frequency of $\omega_F = 8.7E^{-4}$ radians/s is used in the following, which corresponds to a period of two hours. The duty cycle threshold $\overline{\widehat{valve}}$ is set to 0.99. Precooling is thus activated when the utilized capacity reaches 99% of maximum on previous days.

Maximum precool time $\overline{\Delta}$

The maximum precool time is individual for each display case and could either be based on experiments or experience. It should approximately be the time it takes to cool the foodstuff down from the normal steady state temperature to the steady state value using the precool thresholds, see also Subsection 4. A potential way to reveal the time constant of the foodstuff temperature, when this temperature is not measured, could be to make a step down in the air temperature thresholds and then monitor how long it takes the valve duty cycle to settle after the step. This is possible because the valve duty cycle

settles when the foodstuff temperature has settled. The test could either be performed during initial startup, as part of an automatic night procedure, or it could be based on the previous precool cycle.

Precool end-time t_{end}

The placement of the precool period could be based on supermarket opening hours, energy tariffs if they are known in advance, experience, etc. An alternative is to update it automatically, since the estimated duty cycle also gives an indication of when the system was saturated on the previous day. The precool period should then be placed before this period and should be extended into the saturation period to ensure that the stored thermal energy is kept for as long as possible in the local fridges. The automatic approach is used in the simulation in Subsection 5 and a fixed t_{end} corresponding to the opening of the supermarket is used in the simulation in Subsection 5.

The two precool strategies are outlined in the pseudocode denoted algorithm 1 and 2. The first algorithm applies precool individually in each fridge display case and finds t_{end} automatically. An algorithm is needed for each of the fridges:

Initialize $\Delta = 0$, $n = 0$, $\overline{\mathbf{T}}_m = \mathbf{0}$, $\underline{\mathbf{T}}_m = \mathbf{0}$, $t_{end} = 0$
Wait until midnight (start of new trial)
function ALGORITHM_1($valve$)
    if n has reached 24 hours of data **then**
        Reset n
        Filter **valve** to get $\widehat{\textbf{valve}}$
        Find longest saturation period in $\widehat{\textbf{valve}}$
        if system is saturated **then**
            Set t_{end} at start of long saturation period
        end if
        Update Δ according to (12.30), (12.31), and (12.32)
        Set $\overline{\mathbf{T}}_m = \mathbf{0}$ and $\underline{\mathbf{T}}_m = \mathbf{0}$
        Insert precool in $\overline{\mathbf{T}}_m$, $\underline{\mathbf{T}}_m$ using Δ, t_{end}, $\overline{T}_m$, $\underline{T}_m$
        Extend precool to include saturation period
    else
        Increment n
    end if
    Set new temperature thresholds in fridge display case: $\overline{T}_{dc} = \overline{\mathbf{T}}_{dc,0}(n) + \overline{\mathbf{T}}_m(n)$, $\overline{T}_{dc} = \overline{\mathbf{T}}_{dc,0}(n) + \overline{\mathbf{T}}_m(n)$
    Save **valve**$(n) = valve$
end function

The second algorithm determines if any of the m number of fridges are saturated and then applies precooling in the freezer section instead and uses a fixed t_{end}. An algorithm is needed for each individual freezer display case or room:

Initialize $\Delta = 0$, $n = 0$, $\overline{\mathbf{T}}_m = \mathbf{0}$, $\underline{\mathbf{T}}_m = \mathbf{0}$, $t_{end} = 0$
Wait until midnight (start of new trial)
function ALGORITHM_2($valve_1$,$valve_2$,...,$valve_m$)
    if n has reached 24 hours of data **then**
        Reset n

for $i = 1, m$ **do**
Filter **valve**$_i$ to get $\widehat{\textbf{valve}}_i$
end for
Update Δ according to (12.30), (12.31), and (12.32)
Set $\overline{\mathbf{T}}_m = \mathbf{0}$ and $\underline{\mathbf{T}}_m = \mathbf{0}$
Insert precool in $\overline{\mathbf{T}}_m$, $\underline{\mathbf{T}}_m$ using Δ, t_{end}, $\overline{T}_m$, $\underline{T}_m$
else
Increment n
end if
Set new temperature thresholds in freezer: $\overline{T}_{dc} = \overline{\mathbf{T}}_{dc,0}(n) + \overline{\mathbf{T}}_m(n)$, $\overline{T}_{dc} = \overline{\mathbf{T}}_{dc,0}(n) + \overline{\mathbf{T}}_m(n)$
Save **valve**$(n) = valve$
end function

Both Algorithm 1 and 2 should run with the same sample time as the $valve$ signal being updated.

5 Simulation Results

First, Algorithm 1 is simulated, for an entire year starting from 1st of January using the weather data shown in Fig. 12.6. The size of the compressor is dimensioned so that the temperature of the foodstuff stays below 5°C in all display cases and in the cold storage room even during the hottest day in the year, if the air temperature thresholds are kept on the low settings constantly (constant precool). This is the most costly scenario in terms of energy and if there is no precool, then there will be some days where the temperature of the foodstuff exceeds 5°C. The precool algorithm is therefore compared with these two extremes in terms of both keeping the energy consumption and the temperature low.

Algorithm 2 is also simulated for a year. The difference here is that precooling is applied to the freezer section. A small extension of the model presented in Section 3 is therefore required. All freezer section foodstuff is lumped together and represented by the temperature of the foodstuff $T_{goods,fr}$ and simulated using (12.3). The load heat transfer rate is calculated as in (12.6) and the cooling heat transfer rate is calculated using (12.12), where the specific latent heat $\Delta h_{lg,fr}$ is approximated with a constant, since it is assumed that the low temperature pressure can be maintained at a constant level. The controllable input is the mass flow from the freezer section, which is allowed to vary $\pm 30\%$ around the nominal value $\dot{m}_{fr} = 0.05$ kg/s. The nominal value is the value used in the first simulation and corresponds to the required mass flow for keeping $T_{goods,fr}$ at the setpoint -18°C in steady state. This makes the simulations comparable and does not require modeling and simulation of multiple freezer display cases and an additional compressor rack. A simple PI temperature controller is used to control the mass flow to make the freezer food temperature follow the setpoint reference and has control parameters $K_{p,fr}$ and $T_{i,fr}$.

All simulation parameters are shown in Table 12.2 and the system parameters are in the same range as values used in the benchmark models presented in [1, 2, 24, 25]. The supermarket is assumed to be open from 9 am to 9 pm all days in the year and the customer load is evenly distributed during the day. Although not incorporated here, individual learning algorithms could be activated for weekdays and weekends, if there is a

Table 12.2: Parameter values used in supermarket system simulations. Subscript $1-3$ denotes display cases, cs is cold storage, and fr is freezer section.

System par.	Value	Ctrl par.	Value
$UA_{air,i-dc,l}$	75 ($\frac{W}{K}$)	$\overline{\Delta}_1$	226 (min)
$UA_{air,i-dc,h}$	150 ($\frac{W}{K}$)	$\overline{\Delta}_2$	310 (min)
$UA_{air,i-dc,cs}$	110 ($\frac{W}{K}$)	$\overline{\Delta}_3$	560 (min)
$UA_{dc-goods,1}$	450 ($\frac{W}{K}$)	$\overline{\Delta}_{cs}$	360 (min)
$UA_{dc-goods,2}$	300 ($\frac{W}{K}$)	$\overline{\Delta}_{fr}$	480 (min)
$UA_{dc-goods,3}$	150 ($\frac{W}{K}$)	ω_F	$8.7E^{-4}$ ($\frac{rad}{s}$)
$UA_{dc-goods,cs}$	600 ($\frac{W}{K}$)	$\widehat{valve}$	0.99 ($-$)
$UA_{dc-wall}$	500 ($\frac{W}{K}$)	l_1	$\frac{1}{4}$ ($-$)
$\overline{UA}_{wall-re}$	900 ($\frac{W}{K}$)	l_2	$-\frac{1}{12}$ ($-$)
UA_{fr}	137.5 ($\frac{W}{K}$)	$\overline{T}_m$	-3 ($^\circ C$)
$C_{p,goods}$	3917 ($\frac{J}{kg \cdot K}$)	$\underline{T}_m$	-2 ($^\circ C$)
$C_{p,dc}$	1000 ($\frac{J}{kg \cdot K}$)	$\overline{T}_{dc,0}$	5 ($^\circ C$)
$C_{p,wall}$	385 ($\frac{J}{kg \cdot K}$)	$\underline{T}_{dc,0}$	2 ($^\circ C$)
$C_{p,fr}$	2000 ($\frac{J}{kg \cdot K}$)	$P_{suc,ref,l}$	4.4 (bar)
m_{wall}	180 (kg)	$P_{suc,ref,h}$	4.1 (bar)
$m_{dc,1-3}$	50 (kg)	DB	0.1 (bar)
$m_{dc,cs}$	125 (kg)	$K_{p,cp}$	-10 ($-$)
$\overline{m}_{re}$	0.6 (kg)	$T_{i,cp}$	220 (s)
$m_{goods,1-3}$	500 (kg)	$t_{s,cp}$	60 (s)
$m_{goods,cs}$	1200 (kg)	$t_{s,ilc}$	5 (s)
$m_{goods,fr}$	4000 (kg)	$K_{p,fr}$	-0.2 ($-$)
τ_{fill}	40 (s)	$T_{i,fr}$	1800 (s)
$T_{air,i}$	22 ($^\circ C$)		
η	0.5 ($-$)		
$\overline{\dot{W}}_{cp}$	7985 (W)		
$\overline{\dot{m}}_{fr}$	0.065 ($\frac{kg}{s}$)		
$\underline{\dot{m}}_{fr}$	0.035 ($\frac{kg}{s}$)		
$\Delta h_{lg,fr}$	110 ($\frac{kJ}{kg}$)		

discrepancy in loading patterns. $UA_{air,i-dc,h}$ is used in the open period and $UA_{air,i-dc,l}$ is used when the night cover is down during the closed hours. The factor two variation includes the extra load due to exchange of foodstuff during the day and correspond to the supermarket data shown in Section 2. Gaussian noise is also added to $UA_{air,i-dc,l}$, $UA_{air,i-dc,h}$, and $UA_{air,i-dc,cs}$ with a standard deviation of 5 W/K during the opening hours and 1 W/K during the closed hours, which gives realistic variations in the load disturbances. Furthermore, noise with a standard deviation of 0.0032 kg/s is added to the freezer mass flow, the precool algorithm sample time $t_{s,ilc}$ is set to 5 seconds (sampling of the valve signal), and $\overline{\Delta}$ is extended by one hour to account for uncertainties.

Local Precool Control in Fridge Display Cases

Simulation results with and without the precool algorithm are shown for four summer days in Fig. 12.12. The compressor capacity goes into saturation when the supermarket is open due to the high condenser pressure (hot outside temperature). The result is that the suction pressure control can not keep the suction pressure at the reference and the largest deviation is during the hottest hours of the day. This also means that the valve duty cycle for the display cases saturates at 100%, which gives an increase in the average air temperature $\widehat{T}_{dc}$ (low pass filtered). Finally, this makes the foodstuff temperature exceed $5^{\circ}C$ during day 177 and 178 without precooling. The precool time is shown in Fig. 12.13. Precooling is mostly applied in the hot summer months as expected and limited by the individual $\overline{\Delta}$ for the storages.

The total energy charge can be calculated based on the simulated compressor power combined with an energy tariff. Here a 2010 time-of-use tariff [27] is applied for Phoenix, Arizona, which corresponds with the weather data file.

The simulation results are compared in Table 12.3. Display cases 1 and 2 violate the $5^{\circ}C$ threshold in five and four days, respectively, if precooling is not applied. The precool algorithm increases the energy charge cost by only 1.21% compared to 4.24% if the display cases are precooled all the time, showing the advantage of the precool learning algorithm.

Table 12.3: Summary of case study results for simulation from 1st of January to the 31st of December with and without precool locally in each fridge.

Quantity	No precool	Variable precool	Constant precool
$T_{goods,1}$ above lim. (days)	5	0	0
$T_{goods,2}$ above lim. (days)	4	0	0
$T_{goods,3}$ above lim. (days)	0	0	0
$T_{goods,cs}$ above lim. (days)	0	0	0
Total energy (kWh)	54742	55401	57235
Energy charge (U.S. $)	3089	3126	3220

Note that the proposed algorithm does not guarantee the temperatures will be held

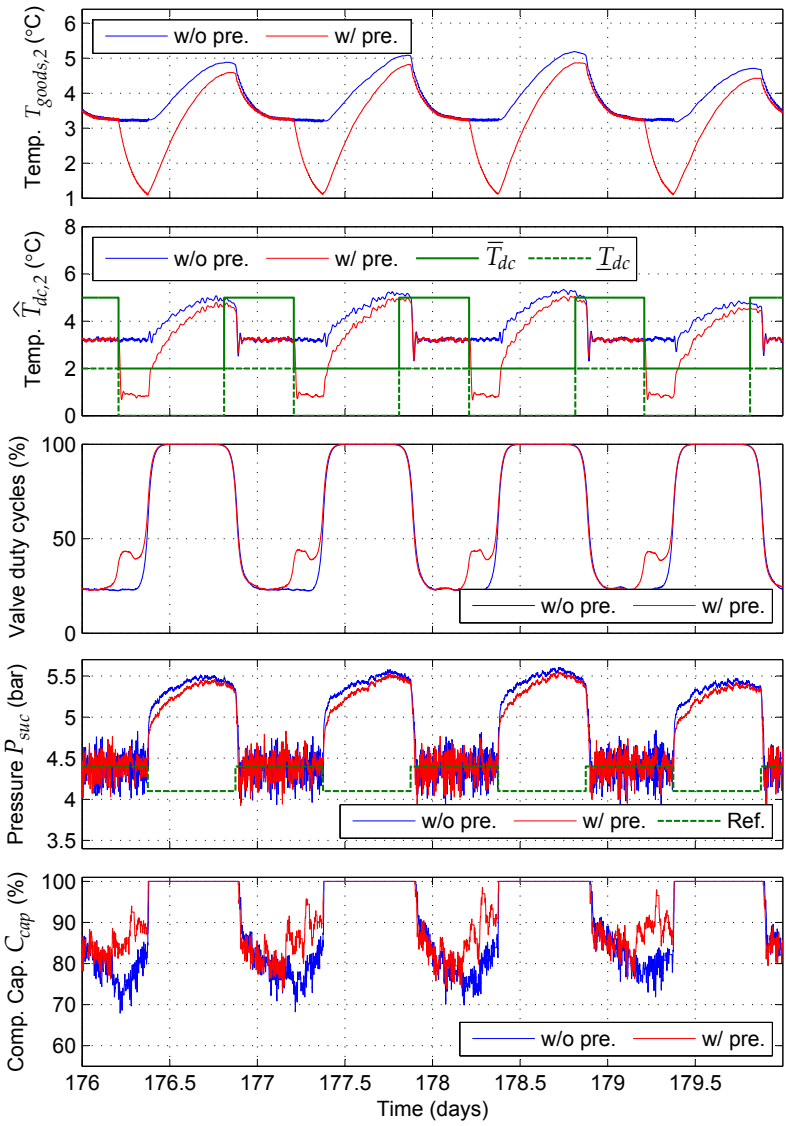

Figure 12.12: Simulation results with and without precool in each fridge for selected days during the summer period. The air temperature (filtered) and foodstuff temperature are shown for display case 2.

within the constraints, but only keeps the foodstuff temperatures as low as possible when the system saturates and thus increases the robustness of the system. The limit of $5°C$ for some fridge products might be different elsewhere, but most bacterial growth stops below this temperature [7].

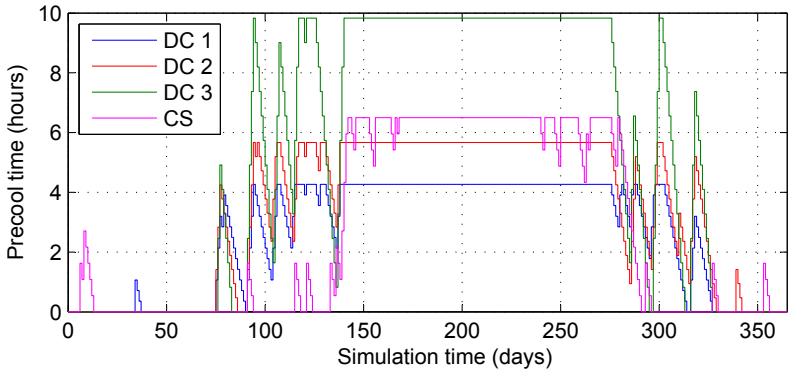

Figure 12.13: Precool time used in the three display cases and in the cold storage room for each day in the simulation starting from 1st of January.

Precool in the Freezer Section

Simulation results with and without the precool in the freezer section are shown for four summer days in Fig. 12.14. The saturation in the display case valve duty cycle is much less when compared with the result presented in Fig. 12.12. The suction pressure is also kept at the reference much longer and the compressor works more during the non-saturated period resulting in an overall higher power consumption. This is due to the increased refrigerant mass flow in the freezer section during the precool period until 9 am, where the foodstuff temperature $T_{goods,fr}$ reaches the lower reference at $-23°C$ and the lower mass flow after when the temperature increases to $-18°C$ again. The freezer section parameters used in the simulation gives a relatively fast time constant compared to an average freezer display case. However, approximately the same performance is achieved in terms of keeping the maximum foodstuff temperature in the fridge display cases below $5°C$ and no days went above the limit. This indicates that there could be a high potential in placing the precool in the freezers instead. The precool time applied to the freezer section is shown in Fig. 12.15.

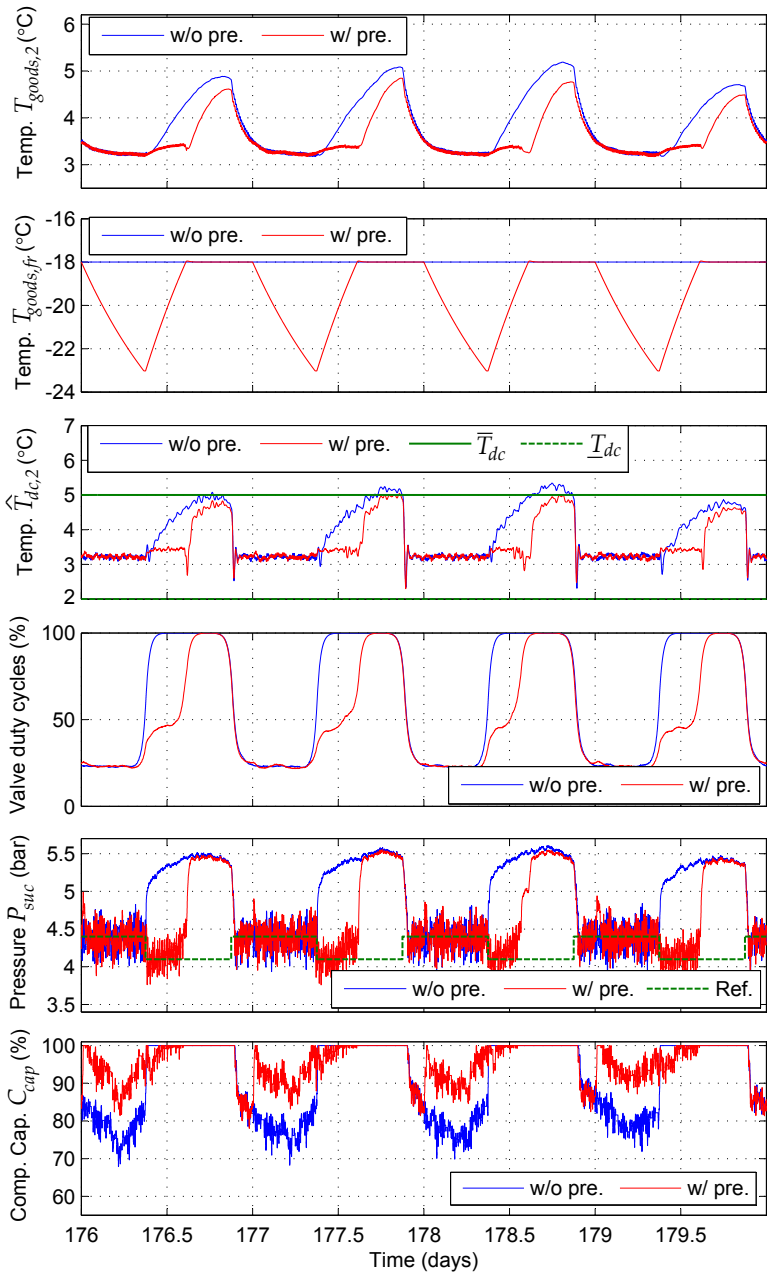

Figure 12.14: Simulation results with and without precool in the freezer section for selected days during the summer period. The air temperature (filtered) and foodstuff temperature are shown for display case 2 along with the freezer foodstuff temperature $T_{goods,fr}$.

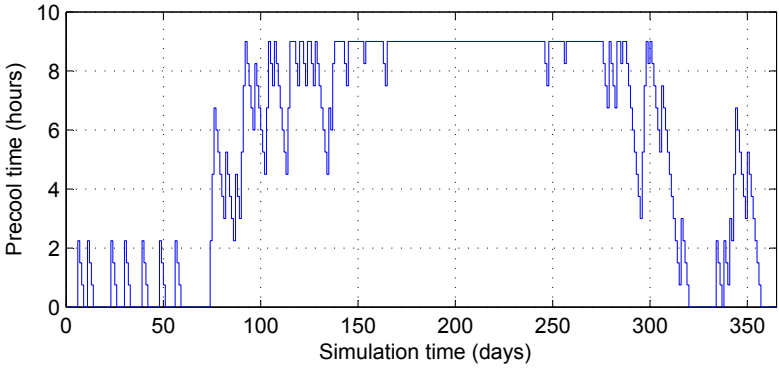

Figure 12.15: Precool time used in the freezer section for each day in the simulation starting from 1st of January.

6 Conclusion

Two learning-based algorithms have been proposed for storage of thermal energy in foodstuff. They automatically find the appropriate amount of precool time to be applied and when the precooling should be started in the current day. The first method applies the precooling directly to the individual fridge display cases and the second method instead applies it to the freezer section to lower the total system load later in the day. A supermarket refrigeration system model with multiple display cases has been derived and yearlong simulations showed that precooling of the foodstuff could prevent upper temperature thresholds from being violated during the hottest days of the year with both algorithms. Precooling the fridge display cases constantly demonstrated that intelligent precooling was less costly. Additionally, there could be a high potential in combining precooling in fridges with precooling in freezers, if coordinated correctly. Finally, the methodology presented could easily be extended to handle operation of ice storages for supermarkets, which is currently being introduced in some larger supermarket chains.

The proposed precool algorithms provide interesting alternatives to MPC and fixed precool schedules, since no system model is required and because the learning-based approach ensures adaptation to changes in load patterns. Furthermore, no additional hardware is required and the algorithms can easily be plugged into existing systems. The primary additional effort would be tuning but good initial guidelines are given in Section IV. Potential uses of this approach could also extend to ice production, warehouses, refrigerated transports, building air conditioning, etc. The primary requirement is that there is sufficient repeatability in the load pattern.

Acknowledgment

The authors would like to thank Danfoss Refrigeration & Air Conditioning for providing valuable data from a Danish supermarket through the ESO2 research project.

References

[1] L. F. S. Larsen, "Model Based Control of Refrigeration Systems," Ph.D. dissertation, Section of Automation and Control, Department of Electronic Systems, Aalborg University, 2005.

[2] L. F. S. Larsen, R. Izadi-Zamanabadi, and R. Wisniewski, "Supermarket Refrigeration System - Benchmark for Hybrid System Control," in *European Control Conference*, Kos, Greece, July 2007.

[3] B. Li and A. G. Alleyne, "A dynamic model of a vapor compression cycle with shut-down and start-up operations," *International Journal of Refrigeration*, vol. 3, no. 33, pp. 538–552, May 2010.

[4] B. P. Rasmussen, "Dynamic modeling for vapor compression systems - Part I: Literature review," *HVAC&R Research*, vol. 18, no. 5, pp. 934–955, September 2012.

[5] ——, "Dynamic modeling for vapor compression systems - Part II: Simulation tutorial," *HVAC&R Research*, vol. 18, no. 5, pp. 956–973, September 2012.

[6] S. E. Shafiei, H. Rasmussen, and J. Stoustrup, "Modeling Supermarket Refrigeration Systems for Demand-Side Management," *Energies*, vol. 6, no. 2, pp. 900–920, February 2013.

[7] Danish Veterinary and Food Administration, "Fakta om fødevarehygiejne - Tilberedning," Ministry of Food, Agriculture and Fisheries, Tech. Rep., 2005, in Danish.

[8] ——. (2013) How we control. http://www.foedevarestyrelsen.dk/english/Inspection/.

[9] G. P. Henze and M. Krati, "Ice Storage System Controls for the Reduction of Operating Cost and Energy Use," *Journal of Solar Energy Enginering*, vol. 120, no. 4, pp. 275–281, November 1998.

[10] Y. Ma, A. Kelman, A. Daly, and F. Borrelli, "Predictive Control for Energy Efficient Buildings with Thermal Storage: Modeling, Simulation, and Experiments," *IEEE Control Systems Magazine*, vol. 32, no. 1, pp. 44–64, February 2012.

[11] K. M. Powell, W. J. Cole, U. F. Ekarika, and T. F. Edgar, "Dynamic Optimization of a Campus Cooling System with Thermal Storage," in *European Control Conference*, Zürich, Switzerland, July 2013, pp. 4077–4082.

[12] J. E. Altwies and D. T. Reindl, "Passive thermal energy storage in refrigerated warehouses," *International Journal of refrigeration*, vol. 25, no. 1, pp. 149–157, January 2002.

[13] J. Cai, J. Stoustrup, and J. B. Joergensen, "Preventing Refrigerated Foodstuffs in Supermarkets from Being Discarded on Hot Days by MPC," in *17th IFAC World Congr.*, Seoul, Korea, July 2008, pp. 11 092–11 097.

[14] T. G. Hovgaard, L. F. S. Larsen, and J. B. Jørgensen, "Flexible and Cost Efficient Power Consumption using Economic MPC - A Supermarket Refrigeration Benchmark," in *IEEE Conference on Decision and Control and European Control Conference*, Orlando, Florida, December 2011, pp. 848–854.

[15] R. Pedersen, J. Schwensen, S. Sivabalan, C. Corazzol, S. E. Shafiei, K. Vinther, and J. Stoustrup, "Direct Control Implementation of a Refrigeration System in Smart Grid," in *American Control Conference*, Washington, USA, June 2013.

[16] S. E. Shafiei, H. Rasmussen, and J. Stoustrup, "Model Predictive Control for a Thermostatic Controlled System," in *European Control Conference*, Zürich, Switzerland, July 2013, pp. 1559–1564.

[17] T. G. Hovgaard, L. F. S. Larsen, and M. J. Skovrup, "Analyzing Control Challenges for Thermal Energy Storage in Foodstuffs," in *IEEE Multi-conference on Systems and Control*, Dubrovnik, Croatia, October 2012, pp. 956–961.

[18] K. Vinther, H. Rasmussen, R. Izadi-Zamanabadi, J. Stoustrup, and A. G. Alleyne, "A Learning Based Precool Algorithm for Utilization of Foodstuff as Thermal Energy Storage," in *IEEE Multi-Conference on Systems and Control*, Hyderabad, India, August 2013, pp. 314–321.

[19] R. W. Longman, "Iterative learning control and repetitive control for engineering practice," *International Journal of Control*, vol. 73, no. 10, pp. 930–954, 2000.

[20] D. A. Bristow, M. Tharayil, and A. G. Alleyne, "A survey of iterative learning control," *IEEE Control Systems Magazine*, vol. 26, no. 3, pp. 96–114, June 2006.

[21] Y. Wang, F. Gao, and F. J. Doyle, "Survey on iterative learning control, repetitive control, and run-to-run control," *Journal of Process Control*, vol. 19, no. 10, pp. 1589–1600, December 2009.

[22] L. N. Petersen, H. Madsen, and C. Heerup, "ESO2 Optimization of Supermarket Refrigeration Systems : Mixed Integer MPC and System Performance," Tech. University of Denmark, Tech. Rep., 2012.

[23] M. Skovrup, "Thermodynamic and thermophysical properties of refrigerants - software package in borland delphi," Technical University of Denmark, Tech. Rep., 2000.

[24] C. Sonntag, A. Devanathan, and S. Engell, "Hybrid NMPC of a Supermarket Refrigeration System using Sequential Optimization," in *17th IFAC World Congress*, Seoul, Korea, July 2008, pp. 13 901–13 906.

[25] Z. Yang, K. B. Rasmussen, A. T. Kieu, and R. Izadi-Zamanabadi, "Fault Detection and Isolation for a Supermarket Refrigeration System - Part One: Kalman-Filter-Based," in *18th IFAC World Congress*, Milano, Italy, September 2011, pp. 13 233–13 238.

[26] *ASHRAE Handbook - Fundamentals (SI Edition)*. American Society of Heating, Refrigeration and Air-conditioning Engineers, Inc., 2005.

[27] APS, “Rate Schedule E-32TOU S - Small General Service (21 kW - 100 kW) - Time of Use,” Arizona Public Service Company, Tech. Rep., 2010. [Online]. Available: http://www.aps.com/_files/rates/e-32TOUS.pdf